A STUDY ON CO-FREE HYDROGEN PRODUCTION AND ADSORBENT DESIGN FOR SELECTIVE CARBON DIOXIDE REMOVAL

by

Melek Selcen Başar

B.S., Chemical Engineering, Boğaziçi University, 2008

M.S., Chemical Engineering, Boğaziçi University, 2010

Submitted to the Institute for Graduate Studies in
Science and Engineering in partial fulfillment of
the requirements for the degree of
Doctor of Philosophy

Graduate Program in Chemical Engineering

Boğaziçi University

2016

to my brother

ACKNOWLEDGEMENTS

First of all, I would like to express my gratitude to my thesis supervisor Prof. Ahmet Erhan Aksoylu for his guidance, encouragement and trust in me. I also want to thank my thesis co-supervisor Assoc. Prof. Hasan Bedir for his support and wisdom in modeling and related research. It was a great honor for me to work with them, where I learned from their great expertise and experiences in catalysis, reaction engineering and modeling.

Very special thanks to Burcu Selen Çağlayan for her everlasting help and guidance throughout my work. I also would like to thank for her wisdom in adsorption studies.

I am very grateful to Prof. Hüsnü Atakül, Prof. Zeynep İlsen Önsan, Prof. Ramazan Yıldırım and Assoc. Prof. Alper Uzun for accepting to be a member of the thesis committee, sparing their valuable time for reading and commenting on my thesis.

I would like to thank my dearest and lovely friends Aybüke Leba, Aysun İpek Paksoy, Belkız Merve Eropak, Ali Uzun and Elif Erdinç. Their intimate friendship was the most valuable gain of my PhD years.

Burcu Acar, Coşar Doğa Demirhan, Feyza Gökaliler, Metin Irmak, Bahar Kesim, Özgü Özer, Ufuk Özgen, Cihat Öztepe and Çağla Uzunoğlu deserve special and heartfelt thanks for their contribution and help in writing my thesis.

I also wish to express my gratitude to all former members of KB 403. I was very lucky to work with the CATREL team and thus I would like to thank all team members and my colleagues in ChE Department for their support and friendship.

Cordial thanks for Bilgi Dedeoğlu, Nurettin Bektaş, Yakup Bal, Murat Düzgünoğlu, Melike Gürbüz and Başak Ünen for their technical assistance and help.

I should also thank Bilge Gedik Uluocak for her significant effort in SEM analyses and Erkan Karabekmez for his help in XRD analyses that were conducted at Boğaziçi University Advanced Technologies Research and Development Center.

I wish to thank my family for their continuous support all these years in any possible way. Finally, very special thanks for my brother, not being here around anymore, but I believe that he is watching me all the time. All his successes and accomplishments have been guidance for me. This work is especially dedicated to my brother, without whom it would have never been possible.

The graduate scholarship provided by TÜBİTAK through program 2211 for my PhD studies deserves thankful recognition. Financial support provided by TÜBİTAK through projects 113M263 and 215M312, by Boğaziçi University through project BAP 09HA505D, and by State Planning Organization of Turkey through project DPT 07K120630 are gratefully acknowledged.

ABSTRACT

A STUDY ON CO-FREE HYDROGEN PRODUCTION AND ADSORBENT DESIGN FOR SELECTIVE CARBON DIOXIDE REMOVAL

The aim of this research study was to design and construct a fuel processor prototype (FPP), to determine its optimum steady state operation conditions, to model its dynamic performance, and to design and develop high performance AC based adsorbents for selective CO_2 capture in order to reduce its CO_2 emission. In this context, an FPP consisting of OSR, WGS and PROX units was designed and constructed; propane/methane individual and serial reaction tests were performed on Pt-Ni/δ-Al_2O_3 (OSR), Au-Re/ZrO_2, Au-Re/CeO_2 and Pt-Re-V/CeO_2 (WGS), and Pt-Sn/AC (PROX) catalysts. In propane reaction tests, simultaneous use of high temperature (723 K) and S/C feed ratio (5) led to increased H_2 (70%) and decreased CO concentrations (0.58%) in accordance with the fuel processing targets. The stability of the catalysts were confirmed during 75 hours TOS test. C_3H_8 and O_2 were totally consumed, whereas the new WGS catalyst Pt-Re-V/CeO_2 gave higher CO conversions (55-60%) than Au-Re/ZrO_2 (45-50%). In methane reaction tests, O_2 was totally consumed, whereas CH_4 conversions were 73%, CO and H_2 concentrations were obtained as 0.66% and 66%, respectively. The experimental product distributions/trends were consistent with the thermodynamics. Comparison of the conversions obtained through the kinetic experiments and modeling by the use of formerly obtained power law type kinetics gave the average error as 16.3%. Sensing time of a step change by the MS was 4.5 minutes at the FPP exit, and 36 minutes were required for reaching a new steady state. CO_2 and CH_4 concentrations were the most reliable parameters during real operation of the FPP (~0.6 L). 1.46, 2.19 and -0.60 combination as C_3H_8, O_2 and H_2O rate orders gave the min error in the correction of the OSR rate expression. A new methodology for the determination of selective adsorption capacity of the adsorbent under multicomponent gas mixture flow. The highest CO_2 adsorption capacity was measured on AC1-N-600 sample (10.4%) and the best data fit was obtained in Dubinin-Radushkevich isotherm model with correlation coefficients > 0.999.

ÖZET

KARBON MONOKSİT İÇERMEYEN HİDROJEN ÜRETİMİ VE SEÇİMLİ KARBON DİOKSİT GİDERİMİ İÇİN ADSORBAN TASARIMI ÜZERİNE BİR ÇALIŞMA

Bu çalışmanın amacı; bir yakıt işlemcisi prototipi tasarlamak ve üretmek, optimum durağan koşullarını belirlemek, dinamik performansını modellemek ve seçimli CO_2 tutumu için yüksek performanslı aktif karbon bazlı adsorban tasarlamak ve geliştirmektir. Bu bağlamda, oksidatif buhar reformlama (OBR), su gaz değişim (SGD) ve seçimli oksidasyon (SO) ünitelerinden oluşan bir yakıt işlemcisi prototipi tasarlanmış ve üretilmiş; propan ya da metan tekli ve seri reaksiyon testleri Pt-Ni/δ-Al_2O_3 (OBR), Au-Re/ZrO_2, Au-Re/CeO_2 ve Pt-Re-V/CeO_2 (SGD) ve Pt-Sn/AC (SO) katalizörleri ile gerçekleştirilmiştir. Propan reaksiyon testlerinde yüksek sıcaklık (723 K) ve yüksek buhar/karbon besleme oranı (5) yakıt işleme amacı olan yüksek H_2 (%70) ve düşük CO (%0.58) konsantrasyonlarını sağlamıştır. Katalizörlerin kararlılığı 75 saatlik reaksiyon testi ile teyit edilmiştir. Propan ve oksijenin tamamen harcanmış, yeni SGD katalizörünün (Pt-Re-V/CeO_2) CO çevrimi (%55-60), Au-Re/ZrO_2 katalizörüne (%45-50) göre daha yüksek çıkmıştır. Metan reaksiyon testlerinde de oksijen tamamen harcanmış, metan çevrimleri %73, CO ve H_2 konsantrasyonları sırasıyla %0.66 ve %66 olarak ölçülmüştür. Deneysel ürün dağılım ve eğilimleri termodinamikle örtüşmüştür. Kinetik deney çevrimlerinin önceden elde edilen hız denklemleriyle modellenen çevrimlerle kıyaslamasında ortalama hata %16 bulunmuştur. Beslemedeki pertürbasyonların yakıt işlemcisi çıkışında algılanması 4.5 dakika sürmüş ve durağan koşula 36 dakikada ulaşılmıştır. Gerçek deney şartlarında yakıt işlemcisinin (~0.6 L) en güvenilir parametreleri CO_2 ve CH_4 konsantrasyonları olmuştur. C_3H_8-(1.46), O_2-(2.19), H_2O-(-0.60) hız derece kombinasyonu SGD hız denklemi geliştirilmesinde en düşük hatayı vermiştir. Bir adsorbanın çok gazlı bir akış altındaki seçimli adsorpsiyon kapasitesini belirleyen yeni bir metot geliştirilmiştir. En yüksek CO_2 adsorpsiyon kapasitesi AC1-N-600 (%10.4) örneğinde ölçülmüş ve verilerle en iyi uyum Dubinin-Radushkevich izoterm modelinde 0.999'dan yüksek korelasyon katsayıları ile elde edilmiştir.

TABLE OF CONTENTS

LIST OF FIGURES

LIST OF TABLES

LIST OF SYMBOLS

a	Rate order of CO in WGS reaction
b	Rate order of H_2O in WGS reaction
c	Rate order of CO_2 in WGS reaction
C	Concentration
d	Rate order of H_2 in WGS reaction
E	Error
E_A	Activation energy
F	Molar flow rate
k_0	Pre-exponential factor
k	Specific rate constant
K_{eq}	Equilibrium constant
n	Number of moles
n_s	Number of sampling time
P	Pressure
r	Reaction rate
R	Universal gas constant
t	Time
T	Temperature
x	Mole fraction
X	Conversion
V	Volume
W	Catalyst weight
wt	Weight
α	Rate order of C_3H_8 or CO in OSR or PROX reactions, respectively
β	Rate order of O_2 in OSR or PROX reactions, respectively
γ	Rate order of H_2O in OSR reaction
ΔH°_{298}	Standard enthalpy of reaction
δ	Change in total number of moles per A reacted

ε	Change in total number of moles for complete conversion/total moles fed
v_0	Volumetric flow rate in the feed stream
v	Volumetric flow rate in the product stream
ξ	Extent of a reaction
φ	Stoichiometric coefficient
i	Species
j	Reactions

LIST OF ACRONYMS/ABBREVIATIONS

AC	Activated Carbon
ATR	Autothermal Reforming
CATREL	Catalysis and Reaction Engineering Laboratory
DI	Deionized
EDX	Energy Dispersive X-Ray
FC	Fuel Cell
FP	Fuel Processor
FPP	Fuel Processor Prototype
GHSV	Gas Hourly Space Velocity
HPLC	High Performance Liquid Chromatography
HTS	High Temperature Shift
HTWGS	High Temperature Water Gas Shift
ID	Inner Diameter
IGA	Intelligent Gravimetric Analyzer
IPOX	Indirect Partial Oxidation
LPG	Liquefied Petroleum Gas
LTWGS	Low Temperature Water Gas Shift
MFC	Mass Flow Controller
MS	Mass Spectrometer
MW	Molecular Weight
OD	Outer Diameter
OSR	Oxidative Steam Reforming
PEMFC	Proton Exchange Membrane Fuel Cell
POX	Partial Oxidation
PROX	Preferential Oxidation
RSS	Residual Sum of Squares
RT	Room Temperature
RWGS	Reverse Water Gas Shift
SEM	Scanning Electron Microscopy

SR	Steam Reforming
TC	Thermocouple
TOS	Time on Stream
TOX	Total Oxidation
WGS	Water Gas Shift
WHSV	Weight Hourly Space Velocity
XRD	X-Ray Diffraction

1. INTRODUCTION

Most of the current world energy requirement is met through coal/gas, nuclear, solar and hydropower in centralized facilities having large production capacities. Unfortunately, the combustion of coal and hydrocarbon fuels releases large amounts of air pollutants and contributes over half of all greenhouse gas emissions. Increasing energy demand and existence of limited energy supplies force the transformation in energy production and distribution from central production with unidirectional flow to decentralized or distributed energy production with bidirectional flow. This transformation makes on-board power production in the range of 2-5 kW through the use of combined fuel processor (FP) and proton exchange membrane fuel cell (PEMFC) systems in small stationary units, like houses and small scale businesses, an attractive research area.

Hydrogen is the ideal fuel in power generation due to its high reactivity and zero emission characteristics for a clean and sustainable energy future. As non-pressurized hydrogen storage has technological barriers, which have not been overcome yet, and establishing wide hydrogen distribution network is not economically feasible; energy production by PEMFC fed by CO-free hydrogen, which is catalytically produced from hydrocarbons having suitable storage properties and/or well established network via an *on-board* FP, is a very promising solution (Kolb, 2008; Lee *et al.*, 2011; Specchia, 2011).

In FP-PEMFC systems, hydrogen stream having maximum 40 ppm CO, guaranteeing stable operation of PEMFC, is produced from easy-to-store and/or distribute hydrocarbon or alcohol fuels such as methane, methanol, propane, butane, gasoline and diesel through the use of FPs (Gupta, 2009; Hordeski, 2009; Vadlamudi and Palanki, 2011). Propane, which is the primary constituent of LPG (76%-99%), is a sulfur-free hydrocarbon. Amongst all the fossil fuels, it serves the highest amount of hydrogen on a gravimetric basis (Hordeski, 2008; Kolb, 2008; Wang *et al*., 2011).

A typical fuel processor consists of three units, in which reforming, water gas shift (WGS) and preferential oxidation (PROX) reactions are conducted in series. Commonly used process technologies for reforming of hydrocarbons involve steam reforming (SR),

partial oxidation (POX), oxidative steam reforming (OSR) and thermo-neutral OSR called auto-thermal reforming (ATR). In the reformer, the hydrocarbon or alcohol fuel is broken down while producing a gas rich in hydrogen, but the product stream contains side products like CO and CO_2. In the following WGS unit of conventional FPs, hydrogen yield is increased, while CO concentration is reduced down to 1-1.5% (Gonzales *et al.*, 2010; Siddle *et al.*, 2003). Since WGS is a reversible exothermic reaction, CO conversion is limited at high temperatures by thermodynamic equilibrium (Sammes, 2006). In the following PROX unit, which is the simplest and most cost effective unit available for CO removal, the remaining CO is oxidized to CO_2 with air/O_2 (Recupero *et al.*, 2005). However, the reaction is accompanied by the undesired side reaction, in which some of the hydrogen present in the reaction mixture is oxidized to water.

On-board hydrogen generation led researchers to develop efficient, robust and easy-to-use FPPs for the fuel cell industry. Testing the effect of the changes in feed and operating conditions on the FPP performance is necessary in order to determine the best possible fuel processor design and control scheme, to optimize steady state and dynamic operation performance of the FP and to evaluate whole system performance (Boehme *et al*., 2008; Lin *et al*., 2006; Ramaswamy *et al*., 2000; Tang *et al*., 2010).

During the last ten years, high performance in house catalysts, namely; Pt-Ni/δ-Al_2O_3 for OSR unit (Çağlayan *et al.*, 2005a; Gökaliler *et al*., 2008; Gökaliler *et al*., 2012), Au-Re/ZrO_2 (Güven, 2009), Au-Re/CeO_2 (Çağlayan and Aksoylu, 2011; Gökaliler *et al*., 2013) and Pt-Re-V/CeO_2 (Özer, 2016; Kesim, 2016) for WGS unit, and Pt-Sn/AC (Aksoylu *et al.*, 2000; Özkara and Aksoylu, 2003; Çağlayan *et al*., 2011b; Eropak and Aksoylu, 2016) for PROX unit have been designed, developed, tested and optimized, and power-law type kinetic expressions for each reaction have been obtained by our group.

Carbon dioxide, which is a by-product of fuel processing reactions and mainly released from fossil fuel combustion processes and industrial power plants, is the main reason for global warming and climate change. Although combined FP-PEMFC systems emit ‘smaller CO_2 per unit energy produced’ compared to conventional systems, even such systems need a CO_2 capturing unit for CO_2-free energy production. Therefore, capture and storage of CO_2 is another important task and one of the most challenging issues of CO_2 mitigation. Various

CO_2 capture and removal technologies, including sequestration, absorption, adsorption, and membranes, have been studied. Among them, adsorption is the most promising technology in terms of its low cost, low energy demand, and reusability after many processes. The ideal candidates for CO_2 adsorption are carbonaceous materials, especially, activated carbon (AC) due to its high surface area, big pore volume and high CO_2 adsorption capacity at ambient pressure and temperature. Thus, design and development of high performance adsorbents by chemical and thermal modification of AC has been a great interest for researchers aiming to enhance effectiveness of its specific properties in capturing CO_2.

Most of the published papers include overviews of the fuel processing technology, especially reforming technology; steady state performances, simulations and dynamic performance analysis of FPs, which were mostly made over mathematical models. The very limited availability of experimental data presented in the literature for FP systems, and even when available, the fact that most of those data belong to the experiments using commercial catalysts is our motivation for the current study, which utilizes novel catalysts in an integrated system, and presents steady state and dynamic data obtained from individual and serial fuel processing reactions.

The aim of this research study is to design and construct a fuel processor prototype (FPP), to determine its optimum steady state operation conditions, to model its dynamic or transient performance, and to design and develop high performance AC based adsorbents for selective CO_2 capture in order to reduce its CO_2 emission.

In this context, a fuel processor prototype (FPP) consisting of OSR, WGS and PROX units was designed and constructed; individual (OSR, WGS, PROX) and serial (OSR-WGS-PROX) performance tests were performed by using propane/methane as the hydrocarbon fuel over novel OSR, WGS and PROX catalysts by utilizing Pt-Ni/δ-Al_2O_3 as OSR, Au-Re/ZrO_2, Au-Re/CeO_2 and Pt-Re-V/CeO_2 as WGS, and Pt-Sn/AC as PROX catalysts in order to determine the optimum steady state operation conditions of each individual units and the FPP as a whole through in the tests having temperature combination(s) of the units, steam/carbon and oxygen/carbon ratio of the OSR feed, and absence/presence and flow rate of additional O_2 stream to the PROX unit as the experimental parameters; the dynamic/transient performance of the FPP was modeled through the use of formerly

obtained power-law type kinetics of reactions, which were corrected further based on the response of the units/FPP to step changes in process variables, in order to determine the most reliable and consistent control parameters and to construct a suitable control-oriented full system dynamic model for the FPP; and high performance AC based, chemically modified adsorbents for selective CO_2 capture were designed and developed through an experimental design procedure having AC pretreatment types, type and loading of additives, temperature and adsorbate gas composition as the parameters.

Chapter 2 contains a comprehensive and up-to-date literature survey related to the theoretical background and information about decentralized energy systems, fuel processor and fuel cell technologies, followed by detailed information about fuel processing reactions as well as CO_2 adsorption and activated carbon adsorbents. The experimental systems and procedures used in catalyst and adsorbent preparation in the current study are presented in Chapter 3. The results obtained in the steady state and dynamic experiments, modeling calculations, and adsorption tests and related discussions can be found in Chapter 4. Finally, the conclusions that are drawn from this research and the recommendations for future studies are summarized in Chapter 5.

2. LITERATURE SURVEY

2.1. Decentralized Energy Production

Centralized generation facilities are very common in industrialized countries, and a major portion of the electricity is generated by coal-fired, natural gas, oil, nuclear, and hydropower plants providing energy for an entire region. While centralized plants have good economies with high efficiencies, they transmit electricity long distances and confront transmission and distribution losses.

Distributed generation, also called on-site or decentralized generation, is the term used for generation of electricity *at* or *near* the point of consumption from renewable sources such as hydro power, biomass, solar power (photovoltaic/thermal), wind turbines, and geothermal power or electrochemical devices such as fuel cells. This energy generation method is environmentally friendly by reducing the energy lost in transmission and distribution, which improves the power quality and the reliability, by addressing actual local demand for energy (Aslanzadeh *et al*., 2014), and especially by providing access to remote areas.

2.2. Fuel Cell and Fuel Processor Technology

Fuel cells are electrochemical devices converting the energy of a fuel (usually hydrogen) directly into efficient, clean and on site electricity without combustion or thermal cycles. All fuel cells consist of an electrolyte layer in contact with an anode and a cathode on either side. Oxygen enters through the catalytic cathode and hydrogen diffuses to the anode catalyst where it later dissociates into protons and electrons. The oxidation reaction occurs on the anode side of the fuel cell, while reduction takes place on the cathode side (Sammes, 2006; Lee *et al*., 2007). The oxygen for the fuel cell is normally supplied using air, which is readily available. However, there is not any available hydrogen distribution infrastructure and therefore many fuel cell systems include an incorporated fuel processing system (Avcı, 2003).

Fuel cells are classified according to the type of electrolyte used and also to the operating temperature. The most known types are proton exchange/polymer electrolyte membrane fuel cells (PEMFCs), molten carbonate fuel cells (MCFCs) and solid oxide fuel cells (SOFCs) (Gou *et al*., 2010). Each type has its own advantage. SOFCs do not need pure hydrogen to generate electricity, because they can internally reform carbon monoxide and light hydrocarbons in the anode material (Yoon and Bae, 2010). High temperature PEMFCs require CO concentrations of around 1 vol.%. On the other hand low temperature PEMFCs, which are the most widely accepted technology for portable and small scale immobile applications, are more sensitive to CO and cannot tolerate a CO concentration exceeding 40 ppm during fuel processing (Hessel *et al*., 2005; Kolb *et al*., 2008b). Fuel cell temperatures should be kept higher than 333 K and less than 373 K, in order to sustain reaction kinetics and to humidify the electrolyte to conduct protons (Avcı, 2003).

Fuel processors can be considered as little chemical factories, in which conventional fossil fuels or renewable fuels are catalytically converted into carbon monoxide-free hydrogen rich fuel to be used as a feed in PEM fuel cells. The processing sequence of hydrocarbon fuels in hydrogen production may involve several steps including fuel desulfurization, reforming (steam reforming, partial oxidation, oxidative steam reforming, autothermal reforming), WGS (high temperature shift, low temperature shift) and CO clean-up (preferential CO oxidation, CO methanation) depending on the needs of the purity of hydrogen and the impacts of impurities for the specific applications (Brandon and Thompsett, 2005). These units can be either separate units operating in series or integrated.

During the conversion process in a fuel processor, various by-products are formed such as carbon dioxide, carbon monoxide or methane, depending on the type of the hydrocarbon fuel and operating conditions of the reactions. Among the by-products, carbon monoxide is the most important one, since it poisons the catalysts and the Pt anode of the PEM type fuel cells, when its concentration is greater than 40 ppm. Thus, besides increasing hydrogen yield, minimizing carbon monoxide yield is a crucial target in developing fuel processing technologies (Chan and Wang, 2001; Hessel *et al*., 2005).

2.3. Reactions in Reformer Unit of a Fuel Processor

Reforming process is breaking down of the hydrocarbon fuel by applying heat, simultaneously producing a gas rich in hydrogen but containing other reaction side products like CO and CO_2. There are three types of reforming reactions, which are steam reforming (SR), partial oxidation (POX)/total oxidation (POX) and oxidative steam reforming (OSR)/autohermal reforming (ATR). The most important parameters in reforming are steam to carbon and oxygen to carbon ratios in the feed mixture depending on the reaction type. Consequently, the function of all these reactions is to produce hydrogen-rich synthesis gas (Kolb, 2008; Momirlan and Veziroğlu, 2005).

2.3.1. Steam Reforming

It is the most important and widely used process for the industrial manufacture of hydrogen, most notably in the production of ammonia. Nickel and noble metals are known to be catalytically active metals in the steam reforming process. Although Ni is less active than some noble metals and more prone to deactivation (e.g., by coking), steam reforming (Equation 2.1) of hydrocarbons on Ni promoted catalysts is the conventional, cheapest and highly efficient process for providing synthesis gas (H_2 + CO) and for large scale hydrogen production (Çağlayan *et al.*, 2005a; Gupta, 2009; Schadel *et al*., 2009).

Steam reforming has several advantages, including a high hydrogen concentration (over 70% on a dry basis) and long term stability at a steady state. However, requirement of large amounts of energy input and high volume reactor because of the high endothermicity of the reaction and the presence of catalyst deactivation due to coke deposition possibility turn out to be major disadvantages of steam reforming reaction. It is difficult to start steam reforming reaction quickly because of its slow response. This reaction is preferred only for large scale hydrogen production and should be designed to accommodate the desired heat transfer (Avcı *et al*., 2001; Kang and Bae, 2006).

The general equations of CO and CO_2 producing SR reactions are given in Equation 2.1 and 2.2, respectively. Propane SR reactions (Equation 2.3 and 2.4) ad methane SR reactions (Equation 2.5 and 2.6) with their reaction enthalpies are given below:

$$C_mH_{2n} + mH_2O \rightarrow mCO + (m+n)H_2 \qquad \Delta H^{\circ}_{298K} > 0 \qquad (2.1)$$

$$C_mH_{2n} + 2mH_2O \rightarrow mCO_2 + (2m+n)H_2 \qquad \Delta H^{\circ}_{298K} > 0 \qquad (2.2)$$

$$C_3H_8 + 3H_2O \rightarrow 3CO + 7H_2 \qquad \Delta H^{\circ}_{298K} = 497\ kJ/mol \qquad (2.3)$$

$$C_3H_8 + 6H_2O \rightarrow 3CO_2 + 10H_2 \qquad \Delta H^{\circ}_{298K} = 376\ kJ/mol \qquad (2.4)$$

$$CH_4 + H_2O \rightarrow CO + 3H_2 \qquad \Delta H^{\circ}_{298K} = 206\ kJ/mol \qquad (2.5)$$

$$CH_4 + 2H_2O \rightarrow CO_2 + 4H_2 \qquad \Delta H^{\circ}_{298K} = 165\ kJ/mol \qquad (2.6)$$

Steam to carbon ratio and temperature become important parameters to prevent coke deposition. Commonly, excess of steam is used to overcome carbon deposition on the catalyst surface (Gupta, 2009). Methanation may also occur at low temperatures by consuming considerable amounts hydrogen and producing methane (Equation 2.7 and 2.8).

$$CO_2 + 4H_2 \leftrightarrow CH_4 + 2H_2O \qquad \Delta H^{\circ}_{298K} = -165\ kJ/mol \qquad (2.7)$$

$$CO + 3H_2 \leftrightarrow CH_4 + H_2O \qquad \Delta H^{\circ}_{298K} = -206\ kJ/mol \qquad (2.8)$$

2.3.2. Partial Oxidation and Total Oxidation

Since steam reforming is an endothermic reaction, sufficient heat should be introduced into the reactor in order to initiate the reaction. Exothermic combustion of the unconverted hydrocarbon is the most suitable reaction to be coupled with the endothermic SR in order to supply the energy necessary for the continuation of SR reaction. In partial oxidation (POX) reaction (Equation 2.9), the oxygen to carbon ratio and temperature are adjusted such that the hydrocarbon fuel is converted into a mixture of H_2 and CO, instead of CO_2 and H_2O as in total oxidation (TOX) reaction (Equation 2.10). POX reaction is a rapid reaction with quick response and higher reaction rates than SR reaction and can be conducted in the presence or absence of catalyst. The non-catalytic process operates at high temperatures (1100-1500 °C), whereas the catalytic one at much lower range of temperatures (600-900

°C). The catalyst should be very active also in SR reaction to ensure complete conversion of the hydrocarbon fuel. Most commonly used catalysts are refractory supported Ni and noble metal based (e.g., Rh, Pt, Pd, Ir, Ru, and Re) catalysts in the form of pellets and monoliths (Hu and Ruckenstein, 2004; Reuse *et al*., 2004; Vita *et al*., 2010).

Unlike total oxidation, partial oxidation reaction uses lower stoichiometric oxygen with respect to the hydrocarbon fuel to produce hydrogen. However, the concentration of the hydrogen produced using POX is lower than that using SR. In addition, conducting PX reaction at high temperatures create difficulties with regard to catalyst selection. Moreover, the high possibility of coke formation is another disadvantage of using POX (Kang and Bae, 2006). Oxidation reactions for propane (Equation 2.11 and 2.12) ad methane (Equation 2.13 and 2.14) with their reaction enthalpies are given below:

$$C_mH_{2n} + \left(\frac{1}{2}m\right)O_2 \leftrightarrow mCO + nH_2 \qquad \Delta H^{\circ}_{298K} < 0 \qquad (2.9)$$

$$C_mH_{2n} + \left(m + \frac{1}{2}n\right)O_2 \leftrightarrow mCO_2 + nH_2O \qquad \Delta H^{\circ}_{298K} < 0 \qquad (2.10)$$

$$C_3H_8 + \frac{3}{2}O_2 \leftrightarrow 3CO + 4H_2 \qquad \Delta H^{\circ}_{298K} = -229\ kJ/mol \qquad (2.11)$$

$$C_3H_8 + 5O_2 \leftrightarrow 3CO_2 + 4H_2O \qquad \Delta H^{\circ}_{298K} = -2046\ kJ/mol \qquad (2.12)$$

$$CH_4 + \frac{1}{2}O_2 \leftrightarrow CO + 2H_2 \qquad \Delta H^{\circ}_{298K} = -38\ kJ/mol \qquad (2.13)$$

$$CH_4 + 2O_2 \leftrightarrow CO_2 + 2H_2O \qquad \Delta H^{\circ}_{298K} = -803\ kJ/mol \qquad (2.14)$$

2.3.3. Oxidative Steam Reforming and Autothermal Reforming

Combining simultaneously endothermic steam reforming (Equation 2.1) and exothermic partial oxidation (Equation 2.9) of hydrocarbon fuels results in oxidative steam reforming. Depending on the amount of steam used, CO_2 may also be produced during an

alternative steam reforming reaction besides H_2 and CO products. Coupling and adjusting the scales of these two reactions by carefully calculating the amounts of hydrocarbon fuel, steam and oxygen/air in the feed stream results in lower reaction temperatures and higher efficiencies in an ideally thermally balanced system, which is a special case of OSR called as autothermal reforming (ATR) (Kolb *et al*., 2008a). ATR is conducted at thermo-neutral conditions, where the net heat of reaction is "0" at the reformer temperature, without using any external heat source. The amount of air or oxygen addition should be very well calculated in order to prevent carbon deposition (Kolb, 2008). The concentration of hydrogen produced by the ATR reaction is higher than that produced using POX (Kang and Bae, 2006).

The previous studies revealed that carbon deposition on the catalyst surface and the catalyst stability are major problems in the production of hydrogen, which result in activity loss and active metal degradation. There are few studies on oxidative steam reforming or autothermal reforming of propane concerning the development of Al_2O_3 or CeO_2 supported transition metal based (Ni, Co and Fe) catalysts having improved activity, yield and stability characteristics by the addition of nobel metals such as Pd, Pt, Ru, and Rh (Lee *et al*., 2009). The studies on precious metal supported catalysts proved their superiority in the catalyst activity and stability, however, because of their high costs; optimization efforts are made in order to develop Ni-based catalysts with improved resistance to coke formation through very small additions of noble metals (Lim *et al*., 2009; Vita *et al*., 2010; Zhang *et al*., 2009).

The catalyst activities with different nickel and ceria loadings on propane OSR were tested in a quartz reactor with a reactant ratio of $H_2O/C_3H_8/O_2$=8.96/1.0/1.1 at a velocity of 9600 ml/gcat.h. The highest propane conversion was observed on the Ni(15)-Ce(5)/$LaAl_2O_3$ catalyst at reforming temperatures ranging from 300 to 700 °C up to 100% (Lim *et al*., 2009).

Ceria supported platinum catalysts have demonstrated high performance in hydrocarbon reforming. In previous papers Ni/CeO_2 and Pt/CeO_2 (80-100% conversion at 650-750 °C O_2/C_3H_8=1.5-2, H_2O/C_3H_8=2-3.6) catalysts have shown high activity in C_3H_8 oxidative steam reforming (Pino *et al.*, 2006; Pino *et al.*, 2008).

The propane autothermal reforming was studied in supported CeO_2/Al_2O_3 based Pd catalysts prepared with different Pd precursors. High production of hydrogen was obtained by autothermal reforming of propane on $Pd/CeO_2/\gamma\text{-}Al_2O_3$ catalysts under substoichiometric O_2/C_3H_8 ratio in presence and absence of water. The maximum propane conversions at reforming temperatures ranging from 450 to 750 K and O_2/C_3H_8 ratios of 1.5-5 were observed around 40% (Faria et al., 2008).

The effect of promoting a 15 wt.% Ni/Al_2O_3 catalyst with small amounts of Mo (0.1 and 0.5 wt.%) to produce H_2 via propane oxidative steam reforming was recently investigated. The results of propane OSR at 450 °C with S/C=3, O_2/C=0.3 and GHSV=339,800 ml/h.gcat demonstrated that the addition of small amounts of Mo (0.1 wt.%) had a significant effect on the stability and activity (propane conversion 66%→83%) of the Ni-based alumina catalyst (Malaibari *et al*., 2015).

Ayabe performed ATR of propane reaction on monometallic Ni/Al_2O_3 catalyst and reported a propane conversion of 100%. However, use of propane as hydrocarbon fuel caused a large amount of carbon deposition, which resulted in lower values of hydrogen concentration than the equilibrium values for low steam contents (Ayabe *et al*., 2003).

Indirect partial oxidation of propane on bimetallic $Pt\text{-}Ni/\delta\text{-}Al_2O_3$ catalyst prepared by sequential impregnation was studied for the first time in the literature by CATREL group in the temperature range of 623-743 K. The results showed the superior performance characteristics of bimetallic catalysts compared to monometallic catalysts. Çağlayan et al. explained these characteristics by the high energy efficiency of the bimetallic catalyst led by the transfer of energy from Pt sites which catalyzes exothermic TOX, to the Ni sites which catalyzes endothermic SR. Based on this study; she concluded that catalyst particles were acting like micro heat exchangers during OSR (Çağlayan *et al*., 2005a).

In another study conducted by Gökaliler and her coworkers, OSR of propane was carried out and the effect of Ni:Pt ratio on the performance of $Pt\text{-}Ni/\delta\text{-}Al_2O_3$ catalyst was investigated. Also, a trimetallic $Pt\text{-}Ni\text{-}Au/\delta\text{-}Al_2O_3$ catalyst was additionally tested to observe the effect of Au addition in reforming catalysts. The results showed that catalysts prepared with 0.2wt.%Pt-10wt.%Ni and 0.3wt.%Pt-15wt.%Ni loadings have suppressed methanation

reactions, enhanced H_2 production and increased WGS performance. It was also concluded that Au promotion as a third metal caused poor activity and selectivity to those of the bimetallic catalysts (Gökaliler *et al*., 2008).

2.4. Carbon Monoxide Removal Techniques

Reforming step is followed by a series of catalytic steps suitable for both increasing hydrogen and decreasing carbon monoxide. Considering the tolerable limit of low temperature PEM type fuel cells, CO concentration in the reformer outlet should be decreased to ppm levels.

2.4.1. Water Gas Shift Reaction

CO concentration at the outlet stream of reforming reactor is usually in the range of 6-10%. The reformate has to be purified from CO in order to be used as a high quality feedstock in fuel cell applications. The role of water gas shift reaction (Equation 2.15) in a fuel processor is to provide a main CO cleanup step, by eliminating most of the CO and at the same time, to act as a second reactor to produce hydrogen after reforming step. WGS increases H_2 yield, and simultaneously reduces the CO concentration from 10% to 0.5-1% (Gonzales *et al*., 2010; Luengnaruemitchai *et al*., 2003; Siddle *et al*., 2003).

$$CO + H_2O \leftrightarrow CO_2 + H_2 \qquad \Delta H^{\circ}_{298K} = -41\ kJ/mol \qquad (2.15)$$

The reaction is moderately exothermic, and since it is an equilibrium reaction, it is thermodynamically limited. CO cannot be totally converted into CO_2, therefore, water is commonly added to the reformate to shift the equilibrium of the reaction in the desired direction at favored low temperatures. Conventionally, the reaction is carried out in two steps, namely, high temperature WGS reaction and low temperature WGS reaction. The one at high temperature is conducted over Fe_2O_3/Cr_2O_3 catalysts in the temperature range of 400-500 °C to reduce the CO content to around 2-5%, whereas the latter one over Cu/ZnO catalysts between 200 and 400 °C to reduce the CO concentration further down to 1% depending on the feed composition (Hessel *et al*., 2005; Luengnaruemitchai *et al*., 2003; Sammes, 2006).

Conventional high temperature (Fe-Cr oxide) and low temperature (Cu-Zn-Al_2O_3) WGS catalysts are not applicable for portable and vehicular applications because of their insufficient durabilities and activities. Because of the slow kinetics observed at low temperatures, the WGS unit is expected to be the largest component of a fuel processor and the strong necessity to reduce the volume and weight of the whole processor has driven the researchers to develop more active WGS catalysts with properties fundamentally different from those in the industrial use (Boaro *et al.,* 2009). WGS catalysts for fuel cell applications should be sufficiently active in the temperature range of 200-280 °C, thermally stable, resistant to coke deposition and highly selective for high H_2O/CO ratios with no side reactions, especially methanation, consuming valuable hydrogen (Panagiotopoulou and Kondarides, 2007).

In WGS reaction, both the support and the metal play essential roles in the activity and stability of the catalyst. The most active formulations are based on noble and transition metals supported on reducible oxides. Noble metal catalysts supported on CeO_2, ZrO_2 and TiO_2 are the most promising catalysts for WGS reaction.

Ceria is known as an oxygen-storage material, having high redox properties, while maintaining high dispersion for metal nanoparticles, hence giving high activity for CO oxidation at low temperature and high WGS activity. Additionally, the oxidation of ceria by water to give hydrogen is thermodynamically favorable (El-Moemen *et al*., 2009; Hurtado-Juan *et al*., 2008; Luengnaruemitchai *et al*., 2003).

A comparative study of water gas shift reaction over ceria-supported metallic catalysts was conducted by Hilaire and his co-workers. Pd, Ni, Fe and Co metals were used as transition metals. This study showed that ceria-supported transition metals were active catalysts for the water gas shift reaction. Pd/ceria and Ni/ceria showed essentially the same activities and were much more active than either Co/ceria or Fe/ceria (Hilaire *et al*., 2004).

Gold-based catalysts received great attention, since Haruta and Date (2001) discovered that gold exhibited high catalytic activity for CO oxidation at temperature as low as 200 K, when it was deposited as nanoparticles on metal oxides (Tabakova *et al*., 2004). Recently, Au/CeO_2 catalysts turned out to be very active catalysts for the low temperature WGS

reaction, as gold promoter particularly showed to possess higher activity than other noble metals (Fu *et al*., 2005).

Extraordinary activities of Au/CeO_2 catalysts led scientists to make extensive researches on the addition of a second active metal to gold catalysts. In a study conducted by Yu, the activities of bimetallic Au-M (M=Ni, Cu, Ag, Pt, and Pd) catalysts supported on CeO_2 were investigated. WGS reaction activities over these catalysts decreased as the following order: $Au\text{-}Pt/CeO_2 > Au\text{-}Ni/CeO_2 > Au/CeO_2 > Au\text{-}Cu/CeO_2 > Au\text{-}Ag/CeO_2 > Au\text{-}Pd/CeO_2$. A CO conversion of 78% was achieved with $Au\text{-}Pt/CeO_2$ catalyst at 250 °C (Yu *et al*., 2010).

Çağlayan carried out a study on WGS activity of Au-Re/ceria, Au/ceria and Re/ceria catalysts. The objective of this study was to investigate the effect of Re incorporation, metal addition sequence, space velocity and H_2O/CO ratio on the catalytic performance. Her study revealed that the novel Au-Re/ceria catalysts showed high activity in WGS reaction, especially at high H_2O/CO ratios (Çağlayan *et al*., 2011a).

The effect of Re addition as a second metal beside a precious metal has also been studied by Sato and his coworkers. They conducted WGS reaction over Ir/TiO_2 and $Ir\text{-}Re/TiO_2$ catalysts and concluded that addition of Re clearly increased the WGS activity, as is in their previous study over Pt/TiO_2 and Pd/TiO_2 catalysts (Sato *et al.*, 2005; Sato *et al.*, 2006).

Beside ceria supported Au catalysts, ZrO_2 supported catalysts also showed exceptionally high activities for WGS reaction (Li *et al*., 2008). In recent years noble metal catalysts supported on CeO_2 and Ce-Zr mixed oxides have been intensely investigated as promising next generation WGS catalysts, which exhibited much faster high temperature kinetics than conventional ferrochrome catalysts and were not inhibited by CO_2 (Bi *et al*., 2009). Ceria-zirconia mixed oxides supported WGS catalysts were also studied by Radhakrishnan. In there, the effect of addition of rhenium metal to platinum/ceria-zirconia catalysts was investigated. It was found that rhenium nearly doubled the reaction rate of the supported platinum catalyst and that rhenium carbonyl was the optimal precursor for the deposition of the promoter on the catalyst surface (Radhakrishnan *et al*., 2006).

Güven designed and developed an Au-based, bimetallic WGS catalyst to be used in a fuel processor. The catalyst composition and preparation method were the experimental parameters studied in the catalyst design and testing. The effect of Re addition to Au-based zirconia supported catalysts was also investigated. It was concluded that Re addition improved the catalytic activity significantly, suggesting that rhenium is a good promoter for bimetallic gold based WGS catalysts. The optimum catalyst composition for WGS reaction was found to be 1 wt.%%Re-2 wt.%%Au/ZrO_2, prepared by impregnation of Re on ZrO_2 followed by deposition precipitation of Au (Güven, 2009).

The low temperature WGS reaction has been studied over AC supported nickel catalysts promoted by ceria under ideal and realistic conditions for different ceria loadings (10, 20, 30 and 40 wt.%). CO conversion greater than 40% was obtained in a stability test after 150 h of reaction at 493 K with the promotion of 10 wt.% CeO_2. With the feed mixture containing the main components of a post-reforming stream (1.75% CO, 35.92% H_2O, 34.45% H_2, 1.12% CO_2 and He balance) CO conversions around 60% at 493 K and above 95% at 513 K were observed over Ni10CeO_2/C catalyst (Pastor-Perez *et al*., 2014).

A trimetallic WGS catalyst (Pt-Re-V/CeO_2) was recently designed, developed and tested by Özer and Kesim in CATREL group. The WGS performance of Pt-Re-V/CeO_2 catalysts with different metal loadings were investigated at 300, 350 and 400 °C for two ideal and two real feed compositions. The experiments were performed using 75 mg freshly reduced catalyst with 120,000 ml $g_{cat}^{-1}h^{-1}$ GHSV for 6 hour TOS. High CO conversion levels (max 65%) and positive net H_2 production values with no methanation activity were observed at 350 C. 1Pt-1Re-0.5V/CeO_2 and 1Pt-1Re-1V/CeO_2 catalysts showed best performance with fixed loadings of Pt and Re (Özer, 2016; Kesim, 2016).

2.4.2. Preferential Oxidation Reaction

In order to decrease CO concentration from 0.5-1% at the WGS exit to ppm levels at the exit of the fuel processor is achieved by preferential oxidation (PROX) reaction of CO with air/O_2, which is also referred to as selective catalytic oxidation of CO in the presence of H_2. This step is necessary, since even 0.5-1% CO levels are too high for the low temperature PEM fuel cells. Therefore, preferential oxidation is performed to reduce the CO in the feed

to 40 ppm or less. Unfortunately, the reaction (Equation 2.16) may be accompanied by the undesired H_2 oxidation side reaction (Equation 2.17). The amount of air/O_2 in the feed to PROX reactor has to be calculated carefully to avoid oxidizing H_2 and/or producing an explosive mixture (Hessel *et al*., 2005; Lee and Chu, 2003; Sammes, 2006):

$$CO + \frac{1}{2}O_2 \rightarrow CO_2 \qquad \Delta H^{\circ}_{298K} = -283\ kJ/mol \qquad (2.16)$$

$$H_2 + \frac{1}{2}O_2 \rightarrow H_2O \qquad \Delta H^{\circ}_{298K} = -242\ kJ/mol \qquad (2.17)$$

The O/CO ratio in the feed stream should be between 1.5 and 2.0, i.e. the oxygen should be minimized in order to suppress the hydrogen oxidation side reaction (Kolb, 2008). Therefore, a PROX catalyst should exhibit high activity and selectivity towards CO oxidation especially in the presence of H_2. It also has to be active in the presence of CO_2 and H_2O, which are the products of PROX and H_2 oxidation reactions, respectively.

Low temperature WGS reactions are conducted at temperatures ranging from 250-350 °C and low temperature PEMFCs are operated below 100 °C, therefore the PROX catalyst should work between these temperatures. Since preferential oxidation is exothermic, the increase in reaction temperature results in lower CO conversion levels. Consequently, temperature and O/CO feed ratio play vital role in the final concentration of CO at the exit of the PROX.

The reported promising catalysts for PROX reaction are: Metal oxide supported nobel metal catalysts like Ir/CeO_2, Ru/SiO_2-Al_2O_3, Pt/CeO_2, gold-based catalysts like Au/Al_2O_3, Au/CeO_2, Au/ZrO_2, Au/TiO_2, and several transition metal (Co, Cr, Cu, Fe, Ni, Zn) catalysts supported on base metal oxides (MgO, La_2O_3, SiO_2-Al_2O_3, CeO_2) such as CuO-CeO_2/γ-Al_2O_3 (Gosavi and Biniwale, 2013; Mishra and Prasad, 2011).

Recently, there is a growing interest in using activated carbon as the support material of PROX catalysts. Its high surface and pore area, withstanding high pressure and temperature and serving as an inert makes it a highly effective catalyst support. Aksoylu and his coworkers studied PROX reaction on Pt-Sn/AC catalyst and reported that there is a high

correlation between surface chemistry of the AC supports, the Pt:Sn ratio, the pretreatment procedure and CO oxidation activities of the catalysts (Aksoylu *et al.*, 2000).

In another study, Özkara et al. conducted PROX reaction in H_2-rich gas streams over Pt-Ce and Pt-Sn catalysts supported on activated carbon. Three types of activated carbon were used depending on the preparation method; grinded and HCl washed activated carbon (AC1), and air-oxidized form of AC1, and HNO_3 oxidized forms of AC1. She came to a conclusion that the activities of AC supported catalysts were directly proportional with the reduction temperature. Higher conversion levels were observed on catalysts supported on oxidized AC with respect to non-oxidized support. The highest activity with an 80% CO conversion is obtained on air-oxidized AC having 0.25% and 1% loading of SnO_x and Pt, respectively (Özkara and Aksoylu, 2003).

PROX reaction on activated carbon supports have also been investigated by Şimşek. He also performed PROX reaction on Pt-SnO_x supported AC catalysts and found that PROX over 1% Pt-0.25% SnO_x supported on HNO_3-oxidized AC catalyst yielded 100% CO conversion under realistic feed conditions. The study represents the successful development of catalyst design meaning use of this catalyst as a potential candidate for commercial use in PROX (Şimşek *et al*., 2007). There are also several other studies that utilize Pt-SnO_x system over activated carbon supports (Çağlayan *et al.*, 2011b; Eropak and Aksoylu, 2016).

2.5. Steady State and Transient Performance Analysis of Fuel Processors

On-board hydrogen generation as an alternative to hydrogen transport and storage, both of which still have technological problems and barriers, led researchers to develop efficient, robust and easy-to-use fuel processor prototypes for the fuel cell industry to be used in portable, automobile, or residential applications (Lee and Chu, 2003). Many studies have been conducted about the steady state performances of combined fuel processor/fuel cell systems with different hydrocarbon or alcohol fuels such as methane (Lin *et al*., 2005), ethanol (Aicher *et al*., 2009), isooctane (Kolb *et al*., 2008a; Kolb *et al*., 2008b) and gasoline (Papadias *et al*., 2006).

Dynamic response, i.e. the ability to quickly change the processing rate, is an important feature of the on-board fuel processor. A fuel processor is expected to go through often and rapid changes in processing rates. The dependence of the temperature profiles in a catalytic reaction system to the processing rates became important, considering that the changes in temperature profiles affect the product quality in the intermediate steps and at the fuel processor exit as well. Besides the operation temperature of its reactors, a fuel processor's processing rates and response times depend only on the feed rates of the components, type of fuel, air/oxygen feed ratio and water flow rate (Ahmed *et al*., 2006).

Start-up time and transient behavior are the key requirements for the success of fuel cells, since a fuel processor's response time is important for the overall power plant response. Testing of dynamic performance of a fuel processor is necessary in order to determine the best possible fuel processor design, control scheme and overall operating strategy. By investigating the effect of various operating parameters, it is possible to get information on possible operating strategy and to optimize steady state operation performance.

Ramaswamy developed a computer program based on system analysis, and performed simulations using this computer program to demonstrate the effects of various system parameters on the dynamics, transient response and efficiency of a combined on-board fuel processor/fuel cell system. His simulations showed expected steady state efficiencies with respect to the control parameters and operating conditions (Ramaswamy *et al*., 2000).

Dokupil and his team carried out thermodynamic simulations of a LPG fuel processor in combination with a fuel cell for theoretical investigation of the dynamic and steady state system performance in response to operation parameters. A compact propane FP was also designed and developed. The fuel processor consisted of a reformer/burner module and a CO-purification module, employing water-gas shift and single-stage preferential oxidation reactors. The performance was tested by measuring the concentration of hydrogen and carbon monoxide at the outlet of the PROX reactor. Fast transient responses of the FP with negligible fluctuation of reformate gas composition were measured (Dokupil *et al*., 2006).

In another study conducted by Chen and his colleagues, an experimental methane fuel processor consisting of series of combined reformer, three water-gas-shift-reactors and a

preferential reactor was constructed. According to Chen, CO concentration level should be taken into consideration in order to explore start-up strategy. Without changing process configuration, sensitivity analysis was carried out in order to see the effects of three manipulated variables, namely, methane feed flow, steam feed flow, and air feed rate, on rapid start-up of the fuel processor and on its dynamic modeling (Chen *et al*., 2006).

Beckhaus carried out a study on dynamics of H_2 production by steam reforming. The main focus of his work was to calculate the dynamic step response of a methane steam reformer under load change conditions by using a simulative approach. He concluded that simulative results were close to the experimental data of the manufactured prototype (Beckhaus *et al.*, 2004).

Sommer reported a study on modeling and dynamic simulation of a fuel cell system with an autothermal gasoline reformer using Matlab simulink. A system configuration was developed with the steady state simulations of Aspen Plus. The system was composed of an autothermal reformer, high temperature shift reactor, low temperature shift reactor, preferential oxidation reactor and a fuel cell. The study aims to calculate composition of the gas streams at the exit of each reactor and observe their dynamic response on load changes (Sommer *et al.*, 2004).

Tang and his team experimentally investigated the dynamic performance and transient responses of a kW-class PEM fuel cell stack under various load changes. He performed the dynamic tests on a commercial PEM fuel cell in five categories, which are start-up, shut-down, step-up load, regular load variation and irregular load variation and aimed to find out the influential factors on the performance of fuel cell. He concluded that the dynamic performance of PEM fuel cells are highly dependent on operating conditions such as temperature, pressure, gas flow rate and load changes (Tang *et al.*, 2010).

There are many research papers examining various aspects of the fuel processors and/or fuel cell systems. Some include overviews of the fuel processing technology, especially reforming technology; some include steady state performances and simulations of fuel processors, etc. Unfortunately, there are very few studies focusing on the system dynamics and transient response of the fuel processors (Lin *et al*., 2006). The published

papers on dynamics of fuel processors/fuel cell systems usually include simulation models of developed fuel processors or single unit such as reformer using commercial catalysts. The experimental set up and data are usually hindered.

2.6. Carbon Dioxide Removal Techniques

The removal and recovery of carbon dioxide from power plant fuel gases as a post-combustion separation of is considered to be one of the effective approaches for reducing the total carbon dioxide emissions (Yong *et al*., 2002). Post-combustion capture requires removing CO_2 from flue gas, comprised mainly of N_2 and CO_2, before emission into the atmosphere. CO_2 is a major impurity in fuel gas, which reduces the energy content and heating value of fuel gas, and together with water it corrupts the transportation and storage system (Fenrong *et al*., 2009, Rong Li *et al*., 2011).

Commercial CO_2 capture technologies, such as monoethanolamine chemical absorption and cryogenic separation, are based on cooling and condensation in order to operate below room temperature (RT), and therefore are energy intensive applications with high cost (Rong Li *et al*., 2011). Improved technologies for CO_2 capture are necessary to achieve low energy requirements. There, adsorption becomes a viable alternative because of the reusable nature of the adsorbents used. Pressure swing adsorption, temperature swing adsorption, vacuum swing adsorption and their combinations are also intensively studied for capturing CO_2 from post-combustion (Shen *et al*., 2010). Among these, PSA technology has gained interest due to low energy requirements and low capital investment costs. In PSA, CO_2 is removed from any hot fuel gas at high pressures, and when the pressure is decreased, the gas is desorbed from the porous sorbent and the sorbent can be reused for subsequent adsorption.

Current potential candidate adsorbent materials available are carbonaceous materials, zeolite molecular sieves (Zhao *et al*., 2007), metal organic framework materials (Chen *et al*., 2011), amine-functionalized porous materials (Dantas *et al*., 2010), hydrotalcite-like compounds (Aschenbrenner *et al.*, 2011), limestone, and other metal oxides materials (Baltrusaitis *et al.*, 2011). Development of regenerable adsorbents that have high adsorption capacity, high selectivity for CO_2, adequate adsorption/desorption kinetics at operating

conditions and stable adsorption capacity and adequate mechanical strength after repeated adsorption/desorption cycles is critical for the success of the adsorption process. (Shen *et al*., 2010; Yong *et al*., 2002)

2.6.1. Activated Carbon

Activated carbon is a black, solid substance resembling granular or powdered charcoal having strongest physical adsorption forces of the highest volume of adsorbing porosity of any material known to mankind. The term activation is used for AC's with enhanced adsorption capacities obtained by some chemical and physical treatments. AC consists mainly of carbon (87 to 97%) and other elements such as hydrogen, oxygen, sulfur and nitrogen. Activated carbon can be produced from different raw materials and each type AC exhibits different characteristics depending upon the raw material, surface chemistry and activation method used in their production (Dali *et al.*, 2012).

Activated carbon is crude form of graphite with a random or amorphous structure, which is highly porous over a broad range of pore sizes. Activated carbon is manufactured from different raw materials. The main characteristics of the raw material should be having high carbon content. Coal, wood, coconut shells (Fenrong *et al*., 2010), peat and petroleum coke are the mostly used raw materials (Calgon Carbon Cooperation, 2007).

Activated carbon is extensively used in applications such as separation of gases, recovery of solvent and removal of organic pollutants from drinking water, and also used as a catalyst support. It is the most widely used adsorbent owing to its large adsorption capacity and low cost. Activated carbons are important adsorbents in various industrial sectors such as the food, pharmaceutical and chemical industries. It is also used as an adsorbent in the desulphurization process (Guo *et al.*, 2006).

Activated carbon with its microcrystalline structure is the most promising adsorbent due to its high surface area (up to more than 1000 m^2/g), big pore volume, good CO_2 adsorption capacity at ambient pressure and temperature and water tolerance among carbonaceous materials. It can be produced with different novel morphologies such as monolith, bead, fiber and granular (Shen *et al.*, 2010).

It should be known that carbon monoxide is not well adsorbed by activated carbon. This should be of particular concern to those using the material in filters for respirators, fume hoods or other gas control systems as the gas is undetectable to the human senses, toxic to metabolism and neurotoxic.

2.6.2. Pure and Selective Carbon Dioxide Adsorption on Activated Carbon

There is an extensive research on developing adsorbents from agricultural or industrial wastes to obtain low cost and highly porous adsorbents. In the study conducted by Aroua, palm shell-based activated carbon prepared by polyethyleneimine impregnation method was used. The study aimed to investigate the effects of amount of PEI impregnated on activated carbon on CO_2, O_2, N_2 and CH_4 adsorption capacities of carbon molecular basket. Adsorption capacities of CO_2, O_2, N_2 and CH_4 were enhanced by factors up to 4.7, 16.3, 4.9 and 5.2, respectively with increasing PEI impregnation from virgin AC to 0.26 wt.% PEI/AC (Aroua *et al.*, 2008).

The capture/recovery of CO_2 by adsorptive technology is mainly based on preferential adsorption of the objective adsorbates on a porous adsorbent. The study conducted by Shen focused on a new adsorbent synthesized as pitch-based AC beads. The study investigated the fundamental adsorption properties of this adsorbent. Adsorption equilibrium for CO_2 and N_2 were gravimetrically measured between 30-150 °C and at 100 kPa and 4000 kPa. The data were well fitted with the Virial isotherm model both at low and high pressures, whereas the Langmuir model only fitted well with low pressure data. The adsorption capacities were found to be 1.918 mol/kg for CO_2 and 0.270 mol/kg for N_2 at 303K and 100 kPa. CO_2 is *preferentially* adsorbed making it a promising candidate for CO_2 separation from flue gas (Shen *et al*., 2010).

Selective CO_2 adsorption on activated carbon has also been studied by Ning. In the study, the adsorption of CH_4 and CO_2 on two microwave activated carbon samples at different temperatures from 25 to 50 °C have been investigated using a vacuum adsorption apparatus. He came to a conclusion that the activated carbon modified by K_2CO_3 sample has the higher equilibrium selectivity for CO_2 over CH_4. The adsorption equilibrium data of CO_2 and CH_4 were fitted to Langmuir and Langmuir-Freundlich isotherm models, where the

former one fitted Langmuir model better of the adsorption of CH_4 than CO_2 and the latter one was more suitable for description of the two gases adsorption process (Ning *et al.*, 2012).

In the study performed by Goetz pure and binary adsorption equilibria of CO_2 and CH_4 on AC at 273 and 298 K were investigated. The pressure range studied were 0-3.5 MPa for pure gases and 0-0.1 MPa for mixtures. Pure gas isotherms were analyzed with Dubinin-Astakhov equation. Binary CO_2/CH_4 mixture adsorption equilibria on AC are predicted by Myers-Prausnitz-Dubinin model (Goetz *et al*., 2006).

Ben and his team investigated selective CO_2 adsorption on carbonized porous aromatic framework for binary mixtures of N_2, CH_4 and H_2. The highest adsorption capacity was obtained as 4.5 mmol/g CO_2 at 273 K and 1 bar. The dual-site Langmuir-Freundlich adsorption model-based ideal adsorption solution theory predicts the CO_2/N_2 adsorption selectivity as high as 209 at a 15/85 CO_2/N_2 ratio, the CO_2/CH_4 adsorption selectivity in the range of 7.8-9.8 at a 15/85 CO_2/CH_4 ratio at pressures up to 40 bar, and the CO_2/H_2 adsorption selectivity as 392 at 273 K and 1 bar at a 20/80 CO_2/H_2 ratio (Ben *et al*., 2012).

Pires conducted selective adsorption experiments of carbon dioxide for binary mixtures of methane and ethane on porous clays heterostructures, which presented specific surface areas up to 634 m^2/g. The selectivity of the binary mixtures such as CO_2/CH_4, CO_2/C_2H_6 and C_2H_6/CH_4, were estimated by a methodology based on the determination of the Gibbs free energy. The highest selectivity was obtained for the CO_2/CH_4 binary mixture, when the sample was prepared with tetraethoxysilane. In case of phenyltriethoxysilane, the highest selectivity was obtained for the C_2H_6/CH_4 binary mixture (Pires *et al*., 2008).

In another study carried out by Vaduva and Stanciu, selective CO_2 adsorption from N_2-CH_4-CO_2 mixture experiments were conducted on carbon molecular sieves. They came to a conclusion that high dynamic absorption capacity and CO_2 selectivity indicate adsorbents' suitability for packing Pressure Swing Adsorption columns for recovery of CO_2 and CH_4, from landfill gases (Vaduva and Stanciu, 2007).

Investigators have examined the CO_2 adsorption capacities of activated carbon based adsorbents for many decades. Recent studies have reported CO_2 uptake values of 7-9.5

mmol/g adsorbent at 2.3 MPa and at 303 K for activated carbon pellets based on olive stones (Djeridi *et al*., 2016).

In another study conducted by Hosseini et al. the adsorption of CO_2 was carried out in a flow rate of 240 cm^3/min, concentrations of 5-35%, temperature from 30 to 50 °C, and pressures of 100-300 kPa. The adsorption capacity increased from 0.184 to 1.139 mmol/g, when CO_2 concentration increased from 5 to 35%. The adsorption capacity enhanced from 0.52 to 1.633 mmol/g with increasing pressure from 100 to 300 kPa (Hosseini *et al*., 2015).

The adsorption of CO_2 on ammonia-modified and untreated carbon were investigated at temperatures of 30, 45 and 60 °C and at pressures up to 1 atm. The ranges for temperature and pressure were chosen on the basis that a typical post-combustion flue gas contains approximately 10-15% CO_2 at a total pressure of 1 bar and a temperature range of 40-60 °C. The maximum observed CO_2 adsorption capacities were measured as 1.8 and 1.2 mol/kg adsorbent for ammonia-modified and untreated carbon, respectively (Shafeeyan *et al*., 2015)

Different CO_2 adsorption capacities were reported in literature depending on the type of the AC, pretreatment and feed conditions, temperature, etc. CO_2 adsorption capacity of N-enriched porous carbon adsorbents was found to be 0.676 mmol/g at 30 °C under 12.5% inlet CO_2 concentration. Adsorption capacity decreased from 0.68 to 0.192 mmol/g with increase in temperature from 30 to 100 °C, whereas increased from 0.36 to 0.676 mmol/g with increase in CO_2 feed concentration from 5 to 12.5% (Goel *et al*., 2016). Similarly, adsorption capacity as high as 67 mg CO_2/g was achieved by N-enriched activated fibers at exposure to CO_2 flow twice higher than that observed for the N-free fibers (Diez *et al*., 2015).

The influence of surface modification of AC through amination and ammoxidation on adsorption properties toward pure and selective CO_2 adsorption was reviewed. CO_2 adsorption capacity of activated carbon can be increased by the introduction of basic nitrogen functionalities into the carbon surface. Amination treatments, which were carried out in the temperature range of 400-800 °C and ammoxidation treatments, which were carried out in the temperature range of 300-350 °C at a NH_3:air ratio of 1:3 resulted in highest CO_2 adsorption capacities (Shafeeyan *et al*., 2010; Adelodun *et al*., 2015).

3. EXPERIMENTAL WORK

3.1. Materials

3.1.1. Gases

All of the gases used in this research were supplied by the Linde Group, Gebze, Turkey. The specifications and uses of the gases in this study are listed in Table 3.1.

Table 3.1. Specifications and applications of the gases used.

Gas	Formula	Specification	Application
Ammonia	NH_3	99.98%	Adsorbate
Carbon dioxide	CO_2	99.995%	MS calibration/Adsorbate
Carbon monoxide	CO	99.998%	MS calibration
Helium	He	99.999%	MS calibration/Inert
Hydrogen	H_2	99.998%	MS calibration/Reducing agent
Methane	CH_4	99.5%	MS calibration/Adsorbate/Reactant
Nitrogen	N_2	99.998%	Air treatment/Inert
Oxygen	O_2	99.998%	MS calibration/Reactant
Propane	C_3H_8	99.998%	MS calibration/Reactant

3.1.2. Chemicals

All solid and liquid chemicals used for catalyst and adsorbent preparation are listed in Table 3.2.

Table 3.2. Chemicals used for catalyst and adsorbent preparation.

Chemical	**Formula**	**Specification**	**Source**	**MW (g/gmol)**
Activated carbon	C	ROX 0.8	Norit	12.01
Aluminum oxide	γ-Al_2O_3	Catalyst support, high surface area	Alfa Aesar	101.96
Ammonium carbonate	$CH_6N_2O_2$. CH_5NO_3 (1:1)	30+% NH_3	Merck	157.13
Ammonium hydroxide	NH_4OH	25% aq. solution for analysis	Merck	35.04
Ammonium metavanadate	NH_4VO_3	99%	Riedel-de Haën	116.98
Ammonium perrhenate	NH_4ReO_4	99.999%	Sigma-Aldrich	268.24
Cerium (III) nitrate hexahydrate	$Ce(NO_3)_3.6H_2O$	99.99%	Sigma-Aldrich	434.23
Gold (III) chloride trihydrate	$HAuCl_4.3H_2O$	99.9+%	Sigma-Aldrich	393.83
Hexachloroplatinic (IV) acid hexahydrate	$H_2PtCl_6.6H_2O$	~40% Pt	Merck	517.94
Hydrochloric acid	HCl	37% aq. solution	Merck	36.46
Nickel (II) nitrate hexahydrate	$Ni(NO_3)_2.6H_2O$	99+%	Merck	290.81
Nitric acid	HNO_3	65% aq. solution	Merck	63.01
Oxalic acid dihydrate	$C_2H_2O_4.2H_2O$	98%	Alfa Aesar	126.07
Sodium carbonate	Na_2CO_3	99.9+%	Merck	105.99
Tetraammine platinum (II) nitrate	$Pt(NH_3)_4(NO_3)_2$	99.995%	Sigma-Aldrich	387.22
Tin (IV) chloride pentahydrate	$SnCl_4.5H_2O$	98+%	Riedel-de Haën	350.58
Water	H_2O	Deionized	-	18.02
Zirconium oxide	ZrO_2	Catalyst support	Alfa Aesar	123.22

3.2. Experimental Systems

The experimental systems used in this study can be divided mainly into four groups; which are catalyst/adsorbent preparation systems, catalyst characterization systems, catalytic reaction system and gravimetric gas sorption analysis system.

3.2.1. Catalyst and Adsorbent Preparation Systems

The system used for catalyst preparation by *incipient-to-wetness impregnation method* includes a Retsch UR1 ultrasonic mixer providing uniform mixing, a Büchner flask, a KNF Neuberger vacuum pump, a Masterflex computerized-drive peristaltic pump used for contacting the precursor solution to be impregnated with the support material, a beaker containing the precursor solution and silicone tubing (Figure 3.1).

In this method, specified amount of support (2-5 g) was placed in the Büchner flask and kept under vacuum both before and after the addition of precursor solution. Since trapped air in the pores of the support could prevent penetration of the solutions, vacuum pump was used to remove the trapped air, i.e. to evacuate the support and to give a uniform distribution of the active component. Before impregnating the solution, the support material was mixed with the ultrasonic mixer for 30 minutes under vacuum. The peristaltic pump was used to feed the precursor solution at a rate of 0.5 ml/min via silicone tubing to the support material in the Büchner flask. The slurry was mixed in the ultrasonic mixer during the impregnation in order to maintain uniform distribution of the precursor solution. After the addition of precursor solution, the slurry was ultrasonically mixed for an additional 90 minutes under vacuum. The obtained thick slurry was dried overnight in the oven at the specified temperature.

The system used for catalyst preparation by *homogeneous deposition precipitation method* includes a Retsch UR1 ultrasonic mixer or a Julabo ED-13 water bath circulator, a beaker, a Heidolph RZR 2021 overhead stirrer and a Mettler Toledo FE20 pH meter (Figure 3.2). The details about both methods and procedures specific to the catalyst are given in Section 3.3.

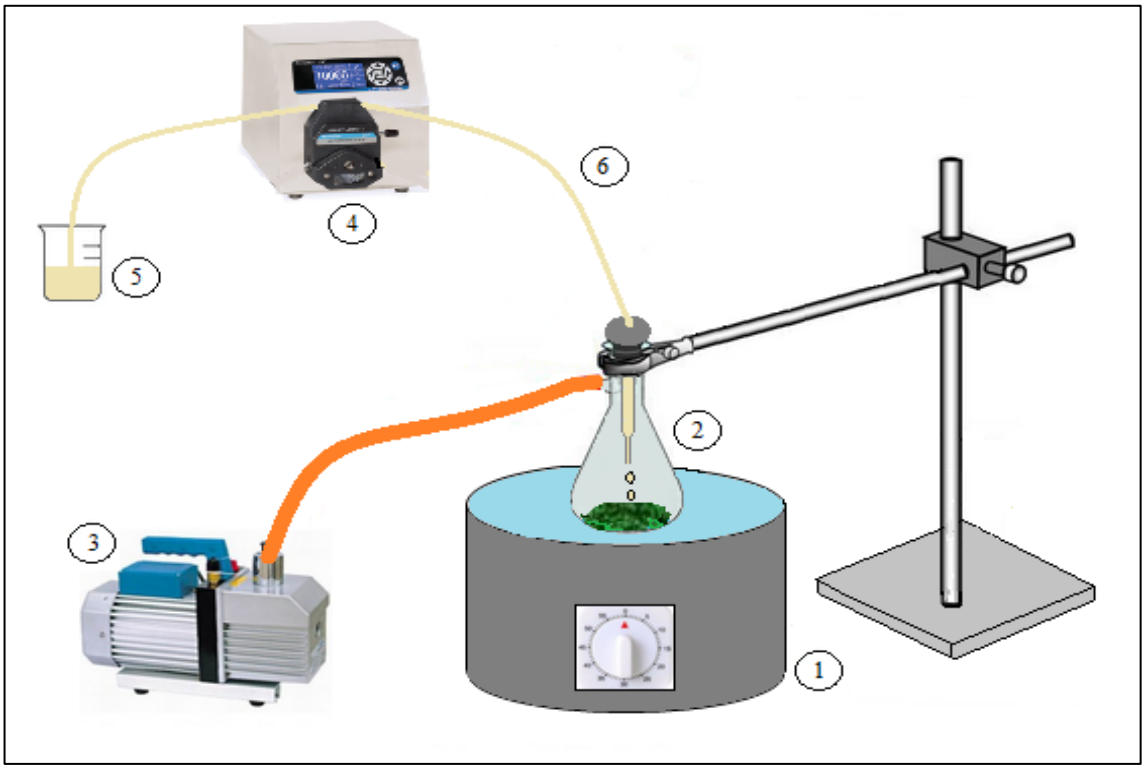

Figure 3.1. Schematic diagram of the impregnation system (1. Ultrasonic mixer, 2. Büchner flask, 3. Vacuum pump, 4. Peristaltic pump, 5. Beaker, 6. Silicone tubing).

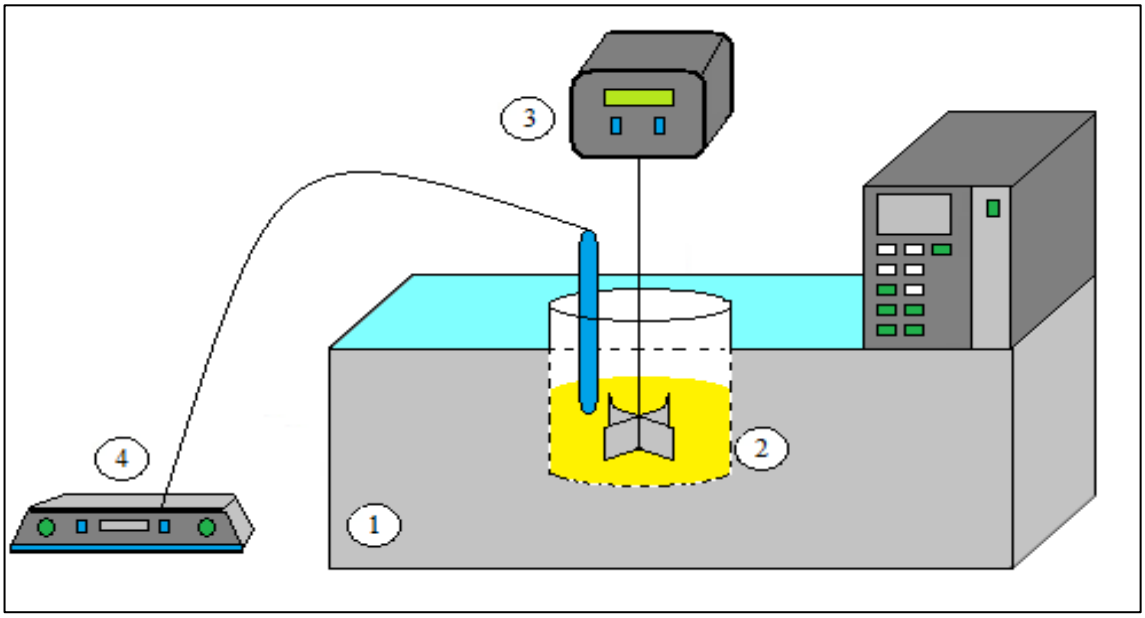

Figure 3.2. Schematic diagram of the deposition precipitation system (1. Ultrasonic mixer or water bath circulator, 2. Beaker, 3. Overhead stirrer, 4. pH meter).

The adsorbent preparation and modification system, which was used for HCl, HNO_3 and DI water treatments of activated carbons, includes an Electro-mag heating mantle, a soxhlet apparatus, a thimble, a condenser, a round bottom flask, a 2 L beaker and a Heidolph MR 3001 magnetic stirrer depending on the treatment type (Figure 3.3).

The air oxidation, amination, ammoxidation and calcination treatments of the activated carbon samples were carried out in a Lenton tube furnace (max. temperature: 1473 K) equipped with a Eurotherm 91e controller; the N_2, O_2, He and NH_3 gases were supplied from pressurized cylinders by gas regulators and Brooks/Aalborg mass flow controllers.

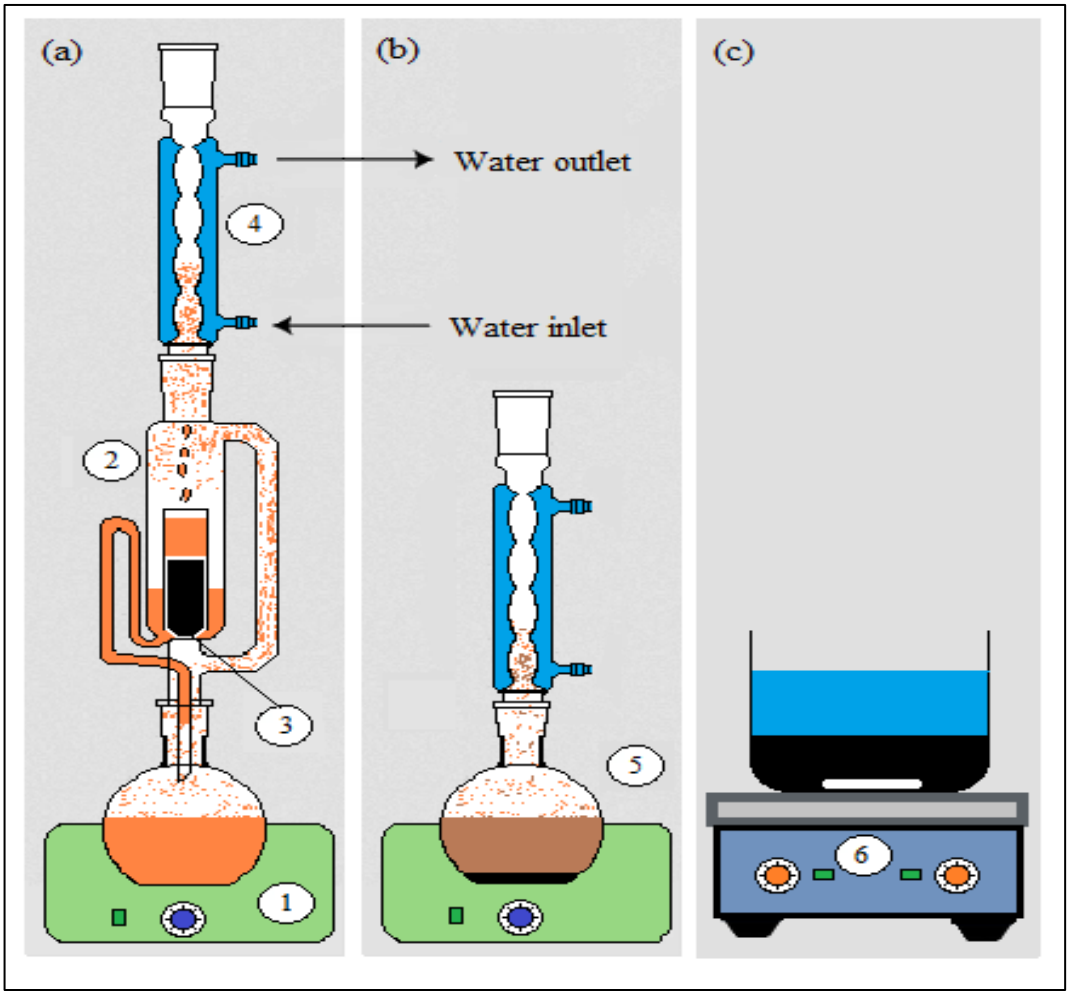

Figure 3.3. Schematic diagram of the system used for (a) HCl, (b) HNO_3 and (c) DI water treatments of activated carbons (1. Heater, 2. Soxhlet apparatus, 3. Thimble, 4. Condenser, 5. Flask, 6. Magnetic stirrer).

3.2.2. Catalytic Reaction System

The FPP system, shown in Figures 3.4 and 3.5, was designed, constructed and tested in our laboratories. The system consists of feed, reaction and analysis sections. The feed section includes Brooks model 5850E mass flow controllers (MFCs) for controlled flow of the inlet gases, i.e. C_3H_8, CH_4, O_2, H_2 and He, which were supplied by pressurized gas cylinders, a Jasco PU-2089 Plus HPLC pump for water feed and a mixing zone. K-type sheathed thermocouple was placed in the water transfer line and connected to the temperature controller (Shimaden SR91) with ±0.1 K sensitivity to keep the temperature at 413 K and to enable complete vaporization of water before contacting the gas mixture in the mixing zone. On-off valves were placed at the exit of mass flow controllers to protect them from possible back pressure.

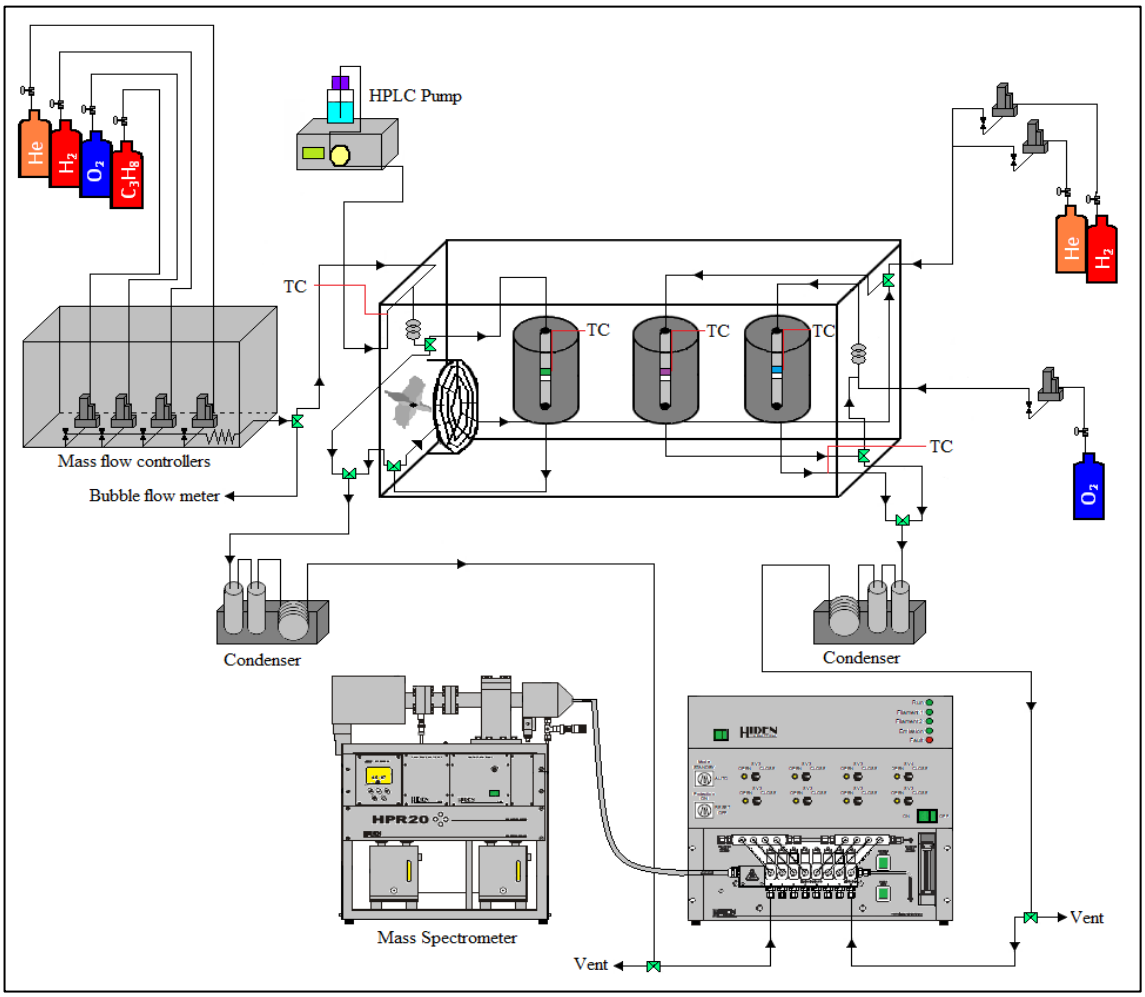

Figure 3.4. Schematic diagram of the FPP with its feed, reaction and analysis sections.

The reaction section includes a main oven (100 cm x 30 cm x 60 cm) and three vertical cylindrical reactor ovens (25 cm x 20 cm OD x 4 cm ID) inside the main oven (Figure 3.4). There is a stainless steel fixed bed microreactor (37 cm x 4.5 mm ID) inside each vertical oven. The catalyst bed, which was hold in a fixed position using silane treated glass wool, was placed at the center of the stainless steel reactor to coincide with the constant-temperature zone of the vertical ovens. K-type sheathed thermocouple was placed inside each vertical oven and connected to the temperature controller (Shimaden FP23) with ±0.1 K sensitivity. Instead of wrapping the thermocouple around the reactor, the thermocouple was attached to an L-shaped 1/8" stainless steel tubing and fastened. The tubing was attached to the reactor such that curled end of the thermocouple pointed exactly the center of the catalyst bed (Figure 3.6). Ceramic glass wool insulations were placed in top and bottom ends of the reactor ovens to prevent heat loss and to provide a stable temperature profile. The main oven has a circulating fan with a heater resistance for keeping liquid reactant, e.g. water and products, in vapor phase, for guaranteeing homogeneous temperature distribution inside the main oven, around the reactor ovens, at all transfer lines between the serial reactors and transfer lines to the analysis block, as well. K-type sheathed thermocouple was placed in the main oven and connected to the temperature controller (Shimaden SR91) with ±0.1 K sensitivity to keep the temperature of the main oven at 413 K.

Figure 3.5. Photograph of the fuel processor prototype.

The analysis section, where the concentrations of the reactant and product gases were determined, has a Hiden Analytical HPR-20 Quartz Inert Capillary Mass Spectrometer equipped with a Faraday/SEM detector and 8-way manifold/diverter system connected to a computer employing MASsoft software enabling simultaneous on line and real time analysis of all feed and product streams - total of 6 lines incoming to/outgoing from the reactors.

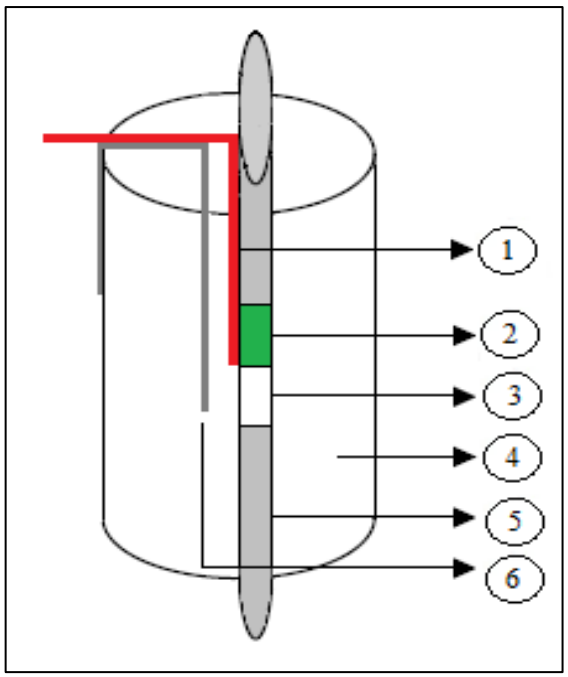

Figure 3.6. Schematic diagram of the reactor and oven system (1. Thermocouple, 2. Catalyst, 3. Catalyst bed, 4. Oven, 5. 1/4" reactor, 6. 1/8" stainless steel tubing).

Material of construction of all ovens is stainless steel and 1/4", 1/8" and 1/16" Swagelok stainless steel tubings, valves and fittings are used in the construction of transfer lines. Lids of the main oven can be opened upwards and/or frontwards. Lids and walls of the main oven were constructed by sandwiching glass wool and rock wool between two stainless steel plates, providing efficient thermal insulation, less energy consumption and limited temperature fluctuation. Cold traps, which guarantee complete condensation of remaining water vapor prior to the MS analysis, were placed before the first reactor for feed analysis, after the first and last reactors for product analysis. The cold trap consists of an ice box, two serially connected stainless steel cylinders and one coiled tubing to increase contact time between the gas flow and cold environment. The prototype enables to perform three

reactions at different temperatures in a serial operation. The system can be used for different combinations of reactions; not only for OSR, WGS and PROX in a serial operation, but also for any reactions in series such as HTWGS, LTWGS and PROX; for serial operations of two reactors or for individual tests in a parallel fashion under different reaction conditions, as well.

3.2.3. Catalyst Characterization Systems

This group involves the analytical and spectroscopic techniques and systems, which are used to characterize the physical, microstructural and electronic properties of the catalyst samples prepared and to examine the changes during and/or after reaction of the freshly reduced catalyst samples. The analyses were performed at the Advanced Technologies Research and Development Center of Boğaziçi University.

3.2.3.1. Scanning Electron Microscopy and Energy Dispersive X-Ray. Micrographs of the freshly reduced and spent catalyst samples as well as the adsorbent samples were taken by SEM and SEM-EDX to analyze their microstructure and morphology, to clarify their quantitative/qualitative elemental analysis and to obtain information on the dispersion of the metals on the catalyst surface. The tests were conducted in a Philips XL 30 ESEM-FEG system having a maximum resolution of 2 nm.

3.2.3.2. X-Ray Diffraction. The crystalline phases of the catalyst samples were identified by using a Rigaku D/MAX-Ultima+/PC X-ray diffraction equipment having an X-ray generator with Cu target and scan speed of 2°/min.

3.2.3.3. Raman Spectroscopy. The possible coke formations on spent catalyst samples were examined with Raman spectroscopy. Raman spectra of the freshly reduced and spent catalyst samples were obtained by using a Renishaw inVia Raman microscope with the following operation parameters: 514 nm 20 mW Ar^+ laser as the excitation source, laser intensity of ~10 mW, 5 s acquisition time; a total of 20 accumulation/spectrum. Before measurements, Raman spectrum was calibrated by using a silicon wafer peak at 520 cm^{-1}.

3.2.4. Gravimetric Gas Sorption Analysis System

The gravimetric gas sorption analysis system includes a Hiden Isochema Intelligent Gravimetric Analyzer IGA-003 Dynamic Mixed Gas Sorption Analyzer (Figure 3.7) and a Hiden Analytical Dynamic Sampling Mass Spectrometer (DSMS). It is designed to study the single/mixed gas sorption equilibrium isotherms and sorption kinetics on materials such as activated carbons, zeolites, polymers and catalysts from vacuum to high pressures (up to 20 bar) in the temperature range from -190 °C to 1000 °C by using gravimetric technique with a resolution of 0.1 µg. The system enables a broad range of experiments to be performed by using several accessories including vacuum pump, standard furnace, cryofurnace, humidifier, pressurizer, etc. In sorption tests, pressure is changed ramp-wise and then held constant during sorption at the set point. Weight data are acquired and analyzed in real time to determine kinetic parameters and to predict the exact point of equilibrium mass uptake. Equilibrium points (pressure vs. weight data) are collected and plotted as an isotherm. The combination of gravimetric sorption measurement and unadsorbed/evolved gas analysis provides a reliable tool for material characterization, thermal decomposition and desorption processes and also temperature programmed (TPO-TPR) techniques.

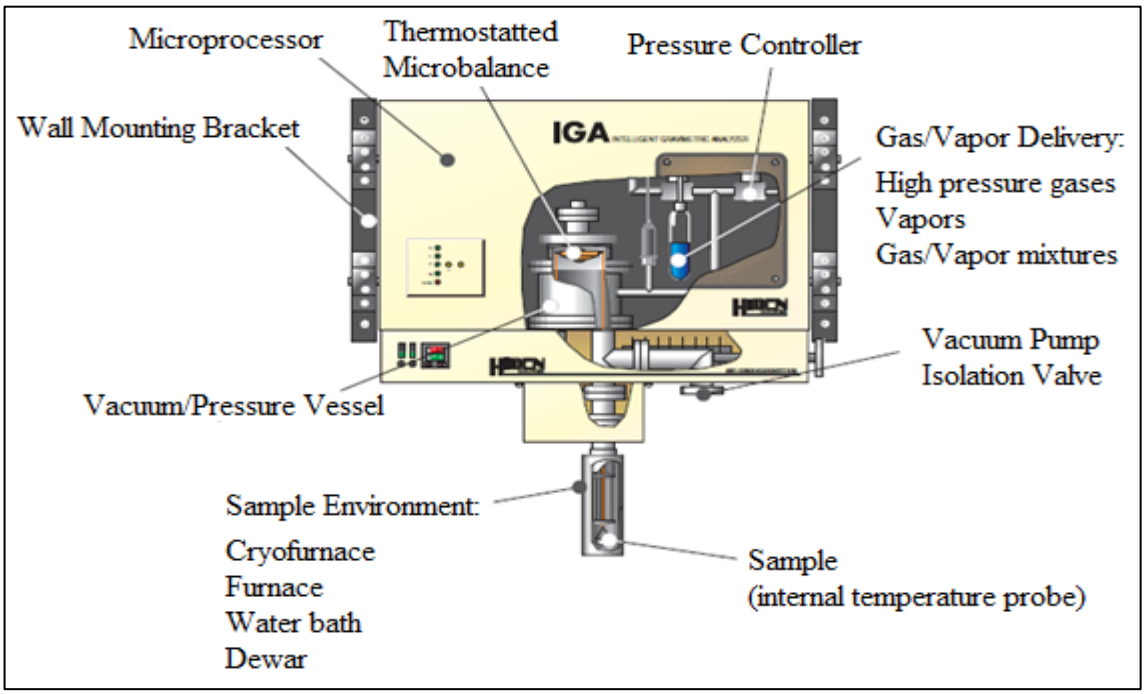

Figure 3.7. Schematic diagram of the Intelligent Gravimetric Analyzer.

IGA is designed and programmed to work in two pressure/control modes; which are static (Figure 3.8) and dynamic pressure modes (Figure 3.9). In static mode, a single component gas is supplied by pressurized cylinder through a gas pressure regulator and sent directly to IGA chamber without controlling the flow via MFC. In dynamic pressure mode, one or more gases are supplied by pressurized cylinders through gas pressure regulators and MFCs at constant pressure and at constant flow rate to IGA chamber (e.g. multicomponent sorption). There is always some flow of gas into or out of the IGA chamber to maintain constant pressure inside.

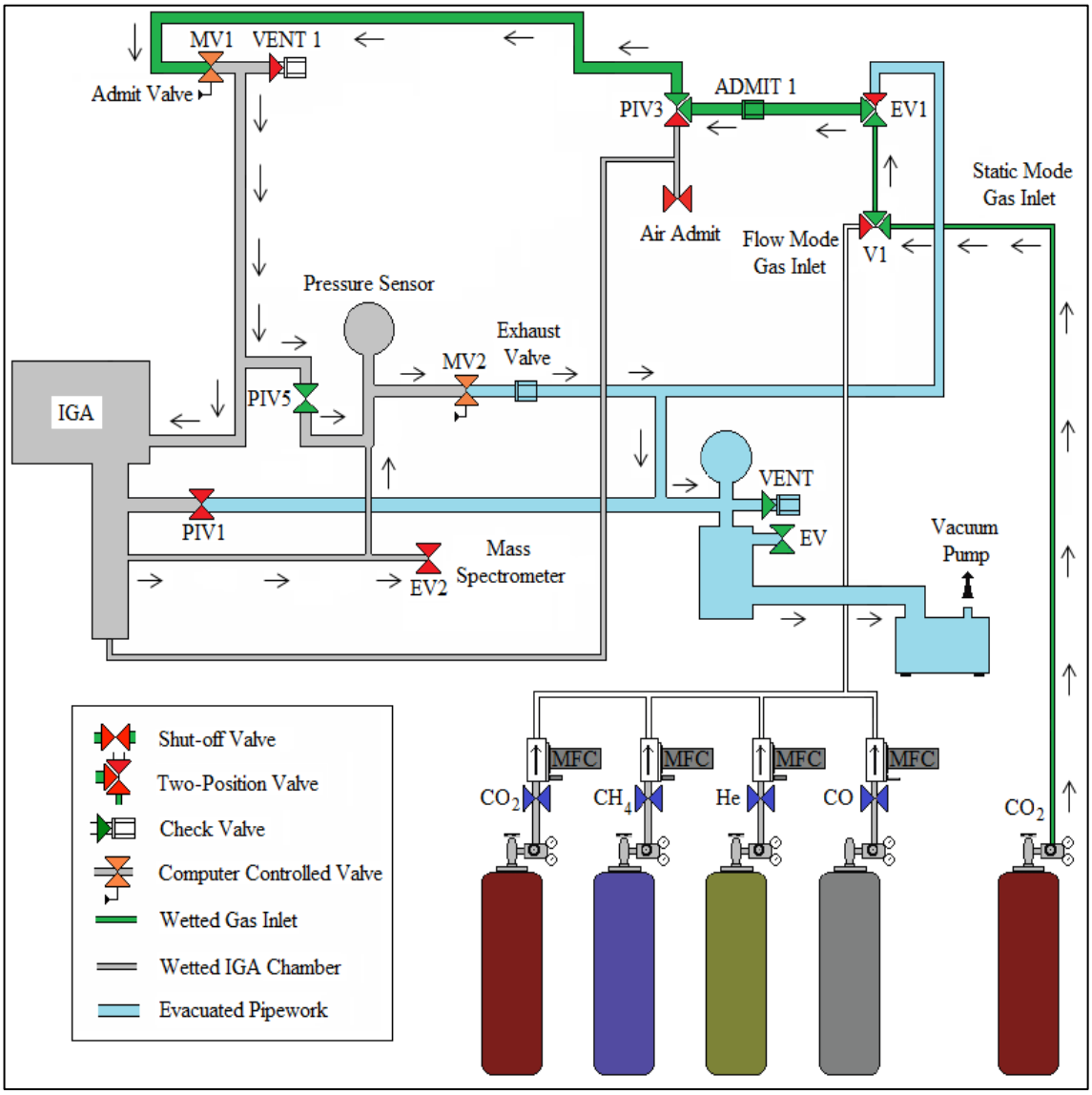

Figure 3.8. IGA static pressure mode flow chart.

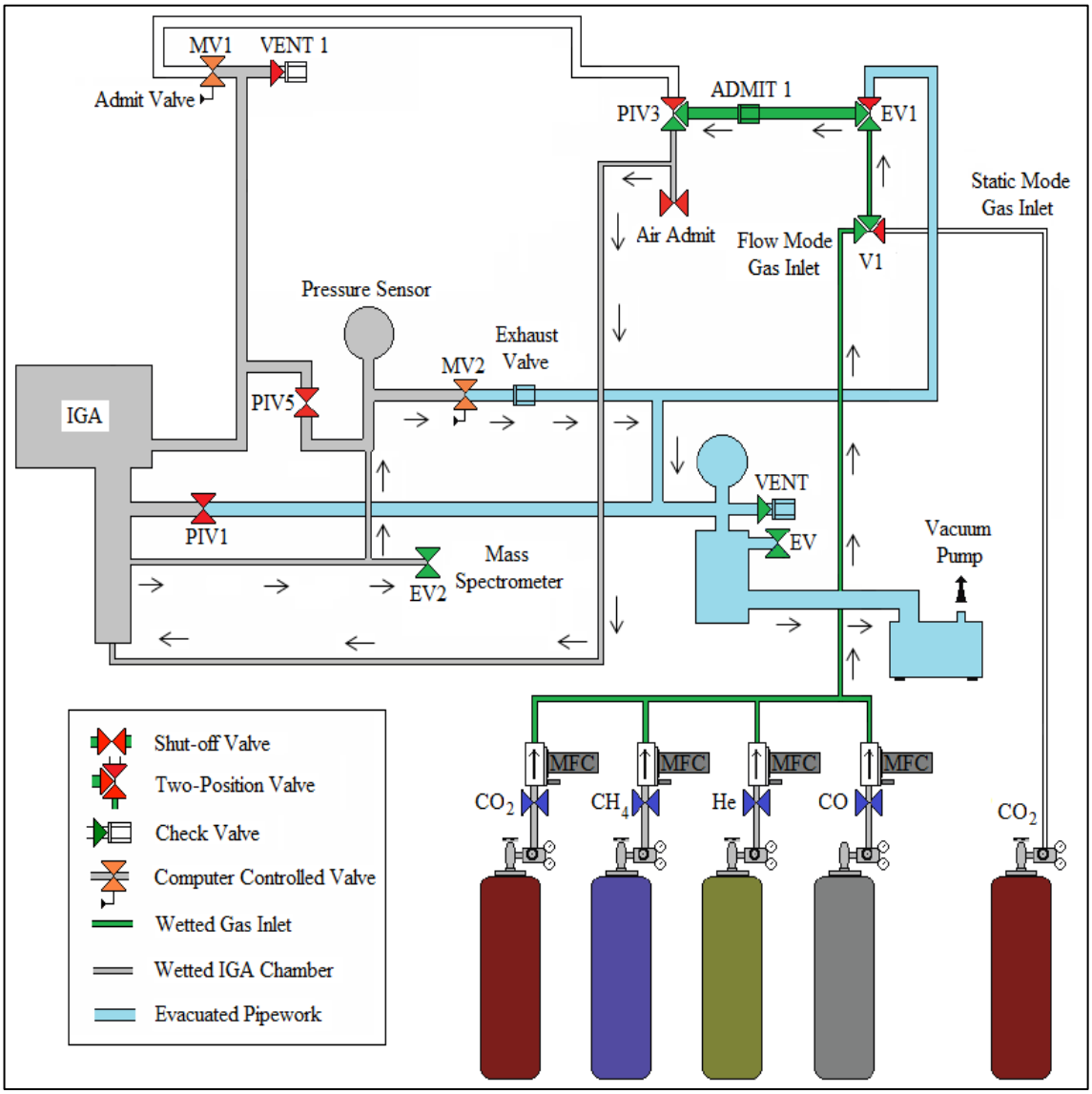

Figure 3.9. IGA dynamic pressure mode flow chart.

The feed section of the gravimetric gas sorption analysis system includes Brooks model 5850E MFCs for controlled flow of the inlet gases, i.e. CO_2, CH_4, CO and He, which were supplied by pressurized cylinders, an Agilent 1200 series HPLC pump for water feed, a TRL Gas Conditioning Unit for heating/mixing zone and 1/4", 1/8" and 1/16" Swagelok stainless steel tubings, valves and fittings (Figures 3.10 and 3.11). On-off valves were placed at the exit of mass flow controllers to protect them from possible back pressure. K-type sheathed thermocouple was placed inside the water transfer line and connected to the temperature controller (Shimaden SR91) with ±0.1 K sensitivity. TRL Gas Conditioning Unit includes Ordel SC441 temperature controller with ±0.1 K sensitivity. The combination

of HPLC pump and gas conditioning unit enables to perform the adsorption tests in the presence of moisture. The system configuration combining pressurizer (stainless steel vessel), Parker ABP1 series back pressure regulator (BPR) and Keller LEO1 digital manometer allows to conduct the tests in dynamic pressure mode up to ~8 bar. In order to conduct the tests e.g. at 5 bar, the gases are sent at 7 bar from the gas pressure regulators first to the mass flow controllers then to the pressurizer, whose high volume enables to prepare homogeneous and pressurized gas mixture, the BPR opening is adjusted in such a way that the digital manometer displays a constant value of 5 bar and the extra gas mixture is purged from the other outlet of the BPR (Figures 3.10 and 3.11).

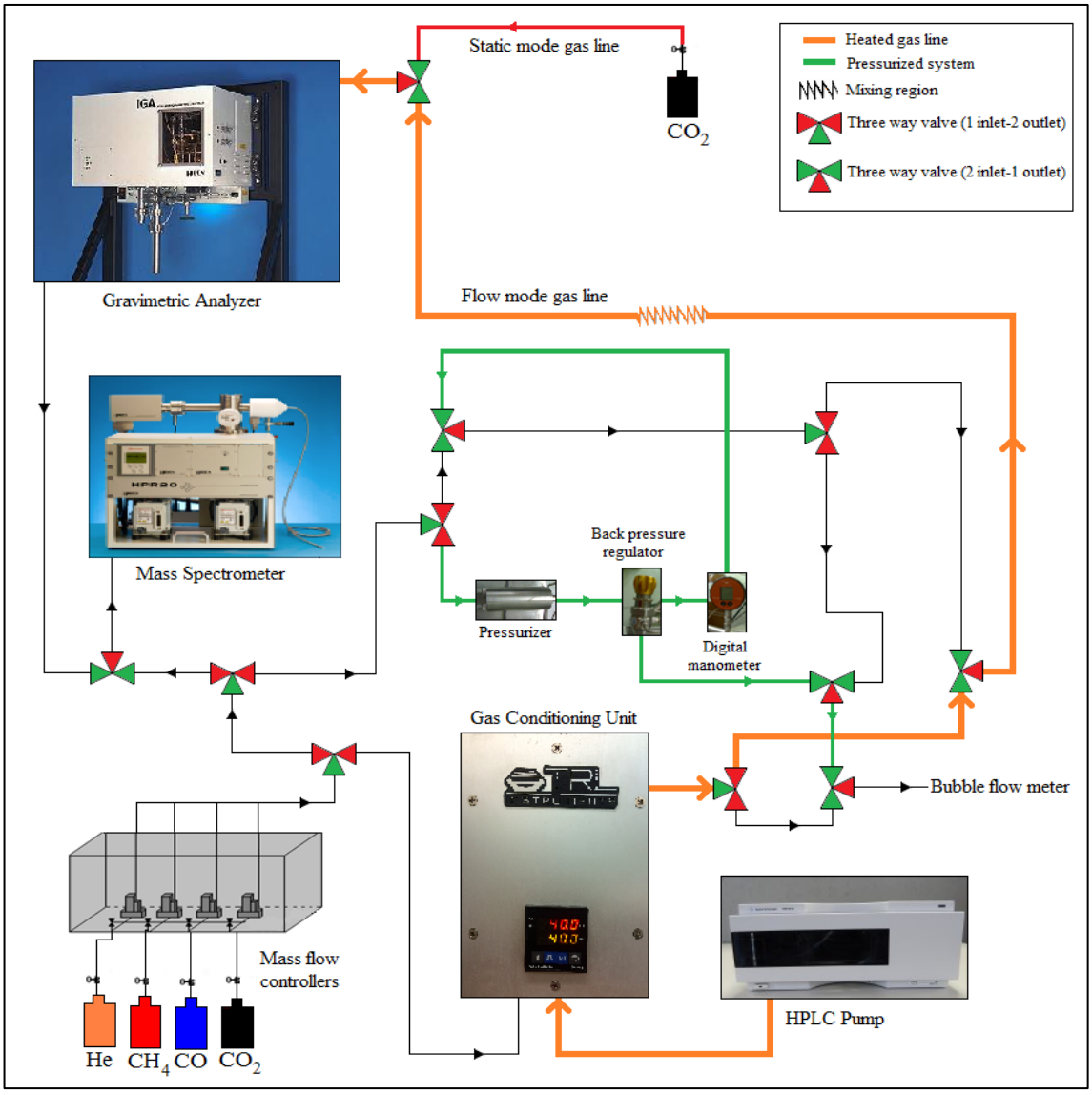

Figure 3.10. Schematic diagram of the gravimetric gas sorption analysis system.

Figure 3.11. Photograph of the gravimetric gas sorption analysis system.

3.3. Catalyst/Adsorbent Preparation and Pretreatment

Five sets of catalysts were prepared to be used in oxidative steam reforming (OSR), water gas shift (WGS) and preferential oxidation (PROX) reactions, which are:

- Platinum and nickel loaded bimetallic OSR catalyst supported on alumina
- Gold and rhenium loaded bimetallic WGS catalyst supported on zirconia
- Gold and rhenium loaded bimetallic WGS catalyst supported on ceria
- Platinum, rhenium and vanadium loaded trimetallic WGS catalyst supported on ceria
- Platinum and tin loaded bimetallic PROX catalyst supported on activated carbon

3.3.1. Oxidative Steam Reforming Catalyst (Pt-Ni/δ-Al_2O_3)

The catalytic oxidation and steam reforming of hydrocarbons are known to be high-temperature reactions. Therefore, the catalyst supports should not only have high surface

areas, but also must possess high thermal stabilities. γ-Al_2O_3 is a commonly used support material due to its high surface area. However, it is reported to have low stability at temperatures higher than 873 K and tend to facilitate carbon formation in the presence of steam due to its high acidity (Ma, 1995). The most thermally stable version of alumina is obtained when γ-phase is transformed into α-phase at temperatures higher than 1400 K (Doesburg *et al*., 1999). However, its low surface area being less than 5 m^2/g, is likely to end up with poor catalytic activities due to the low dispersion of active metals. Hence, using a support such as δ-alumina, an intermediate phase between γ and α, having relatively high thermal stability and an acceptable surface area is optimum in terms of obtaining efficient catalytic performance (Ma, 1995).

The support preparation procedure used in this study involves crushing and sieving γ-Al_2O_3 pellets into 354-250 μm (45-60 mesh) particle size and drying at 423 K for 2 hours followed by calcination at 1173 K for 4 hours in a muffle furnace. The bimetallic Pt-Ni/δ-Al_2O_3 catalyst (0.2wt.%Pt-10wt.%Ni) was prepared by a sequential route in which Pt solution was impregnated over initially prepared and calcined NiO/δ-Al_2O_3 catalyst, which was prepared by the incipient-to-wetness impregnation method using aqueous solution of nickel (II) nitrate hexahydrate (ca. 1.1 ml DI water/g support) as explained in Section 3.2.1. The obtained thick slurry formed after ultrasonic mixing of the aqueous solution of the precursor salt and the support was dried overnight at 393 K and calcined at 873 K for 4 hours to obtain NiO/δ-Al_2O_3. Similarly, aqueous solution of tetraammineplatinum (II) nitrate (ca. 1.1 ml DI water/g support) was impregnated over NiO/δ-Al_2O_3 as explained in Section 3.2.1. The resulting slurry involving two metals was dried overnight at 393 K and finally calcined at 773 K for 4 hours.

In order to obtain high catalytic activities, a pretreatment involving the reduction of the active metals from the oxide state, which is formed during the calcinations, to the metallic state is required prior to the reaction, since catalysts in their oxide forms are usually inactive for the reactions.

Temperature programmed reduction studies have shown that reduction using pure H_2 flow at 773 K for 4 hours is a suitable procedure for pretreating the bimetallic Pt-Ni catalyst (Ma, 1995). Ma has also reported that during reduction, the water in the catalyst may cause

premature sintering, which may lead to deactivation before the reaction. Considering these issues, the following stepwise pretreatment and reduction procedure was followed for the bimetallic OSR catalyst.

After placing the catalyst into the constant temperature zone of the microreactor, He was allowed to flow at 50 ml/min for 7 minutes to remove O_2 from the system at RT. The gas flow was then switched from H_2 and it was set to flow at 20 ml/min. Reduction was started by heating the catalyst from RT to 423 K at a rate of 10 K/min. The temperature was kept constant at 423 K for 30 minutes for the removal of adsorbed water. Third step involved heating the sample from 423 K to 573 K at a rate of 5 K/min, followed by an isothermal segment of 30 minutes at 573 K for the removal of crystalline water. The temperature was then increased from 573 K to 773 K at a rate of 2 K/min and finally kept constant at 773 K for 4 hours. After reduction, the system was allowed to cool down to ca. 423 K under H_2 flow. Below this temperature, the gas flow was switched to He and it was allowed to flow at 5 ml/min overnight to sweep H_2 from the system prior to the catalytic tests (Figure 3.12).

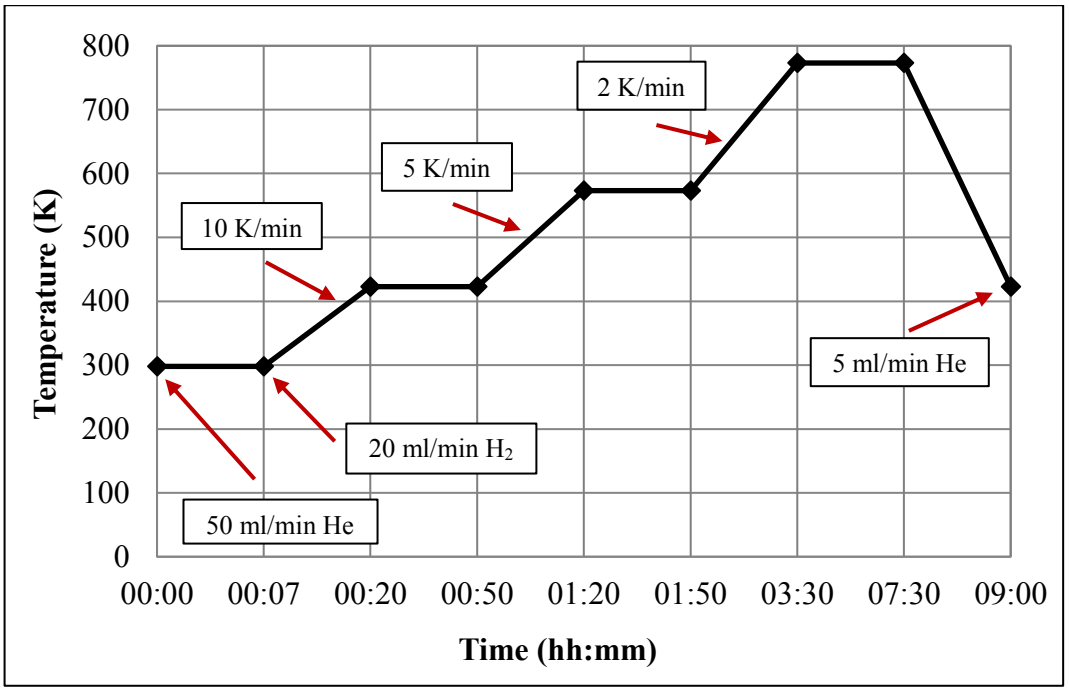

Figure 3.12. Pretreatment and reduction procedure for Pt-Ni/δ-Al_2O_3 catalyst.

3.3.2. Water Gas Shift Catalysts

3.3.2.1. Au-Re/ZrO_2. The support preparation procedure used in this study involved crushing and sieving zirconia pellets into 354-250 μm (45-60 mesh) particle size and calcination at 923 K for 3 hours in a muffle furnace. The bimetallic Au-Re/ZrO_2 catalyst (2wt.%Au-1wt.%Re) was prepared by a sequential route in which Re precursor solution was added by impregnation method followed by the addition of Au precursor solution by deposition precipitation method. Re/ZrO_2 catalyst was prepared by the incipient-to-wetness impregnation method using aqueous solution of ammonium perrhenate (ca. 0.75 ml DI water/g support) as explained in Section 3.2.1. The obtained thick slurry formed after ultrasonic mixing of the aqueous solution of the precursor salt and the support was dried overnight at 383 K and calcined at 523 K for 1 hour in a muffle furnace.

Re-impregnated support was put in a beaker along with DI water to obtain a suspension, and the suspension's pH was adjusted around 8 using a solution of ammonium carbonate. The beaker containing the suspension was placed in an ultrasonic bath to carry out the procedure in continuous agitation in the system as given in Figure 3.2. Gold (III) chloride trihydrate was dissolved in DI water to obtain a 10^{-3} M solution and this solution was added to the support suspension dropwise. The resulting mixture was left in the ultrasonic bath for 1 more hour and then filtered. The sample was washed with DI water several times, dried overnight at 383 K and calcined at 523 K for 1 hour in a muffle furnace.

After placing the catalyst into the constant temperature zone of the microreactor, the sample was heated from RT to the reduction temperature of 453 K at a rate of 7.5 K/min under 95 ml/min He flow and then 5 ml/min H_2 was introduced to the reactor to clear the catalyst surface from oxygen, which was present in the metal oxide form, for 1 hour. After reduction, the gas flow was switched to He and it was allowed to flow at 5 ml/min overnight to sweep H_2 from the system prior to the catalytic tests or to flow at 50 ml/min to heat the microreactor up to the reaction temperature (Figure 3.13).

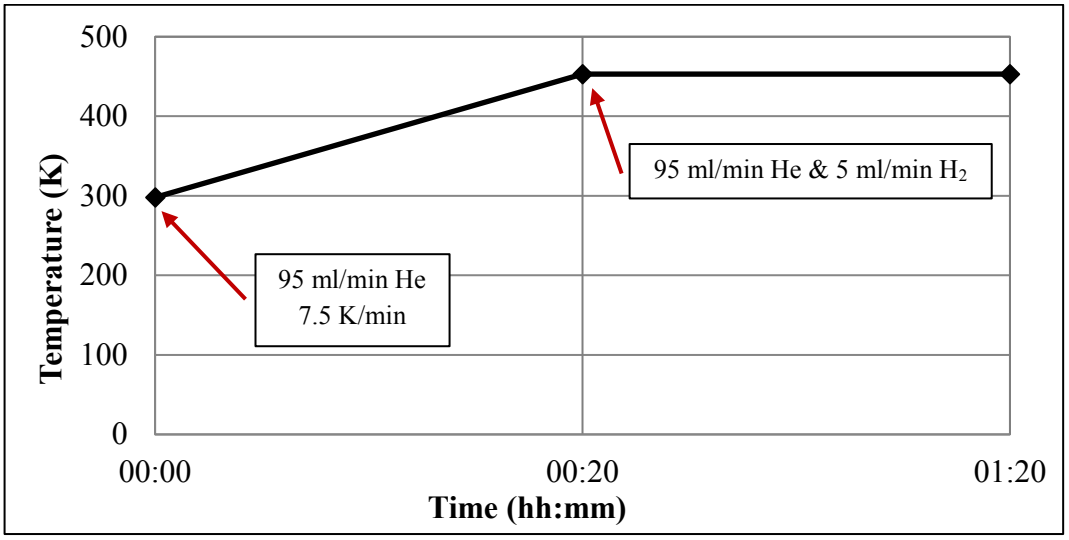

Figure 3.13. Pretreatment and reduction procedure for Au-Re/ZrO_2 catalyst.

3.3.2.2. Au-Re/CeO_2. Ceria support was prepared by homogenous precipitation of cerium nitrate using sodium carbonate. About 20 g of cerium (III) nitrate hexahydrate was mixed with 100 ml DI water to obtain a suspension. The pH of the solution was adjusted to 8 with vigorous stirring in a water bath at 333 K with the controlled addition of aqueous sodium carbonate solution in the system as given in Figure 3.2. When the pH value of 8 was obtained, the resulting suspension was allowed to mix for 1 more hour under controlled temperature and pH. It was then filtered and washed with DI water several times. Finally, it was dried overnight at 383 K and calcined at 673 K for 4 hours in a muffle furnace.

The bimetallic Au-Re/CeO_2 catalyst (1wt.%Au-0.5wt.%Re) was prepared by a sequential route in which Re precursor solution was added by impregnation method followed by the addition of Au precursor solution by deposition precipitation method. Re/CeO_2 catalyst was prepared by the incipient-to-wetness impregnation method using aqueous solution of ammonium perrhenate (ca. 1.1 ml DI water/g support) as explained in Section 3.2.1. The obtained thick slurry formed after ultrasonic mixing of the aqueous solution of the precursor salt and the support was dried overnight at 383 K in an oven. No calcination procedure was required at this step.

Re-impregnated support was put in a beaker along with 100 ml of DI water in an ultrasonic bath to obtain a suspension, and the suspension's pH was adjusted around 8 by

dropwise addition of aqueous ammonium carbonate solution (10 g salt in 100 ml DI water). Subsequently, the calculated amount of gold precursor dissolved in 100 ml DI water was added dropwise, which was carried out under fully controlled pH, stirring speed and RT to obtain highly dispersed Au particles in the system as given in Figure 3.2. The precipitate was aged for 1 more hour, filtered and washed with DI water at 338 K several times. In order to avoid any possible photochemical reaction, gold loading was performed in the absence of light. The filtrate was then dried overnight at 348 K under vacuum and calcined at 673 K for 4 hours in a muffle furnace.

Preliminary tests have shown that reduction under flow of 5% H_2/balance He mixture for 1 hour at 473 K was the optimum reduction procedure for Au monometallic and Au-Re bimetallic catalysts to be tested for WGS performances. After placing the catalyst into the constant temperature zone of the microreactor, the sample was heated from RT to the reduction temperature of 473 K at a rate of 7.5 K/min under 95 ml/min He flow and then 5 ml/min H_2 was introduced to the reactor to clear the catalyst surface from oxygen, which was present in the metal oxide form, for 1 hour. After reduction, the gas flow was switched to He and it was allowed to flow at 5 ml/min overnight to sweep H_2 from the system prior to the catalytic tests or to flow at 50 ml/min to heat the microreactor up to the reaction temperature (Figure 3.14).

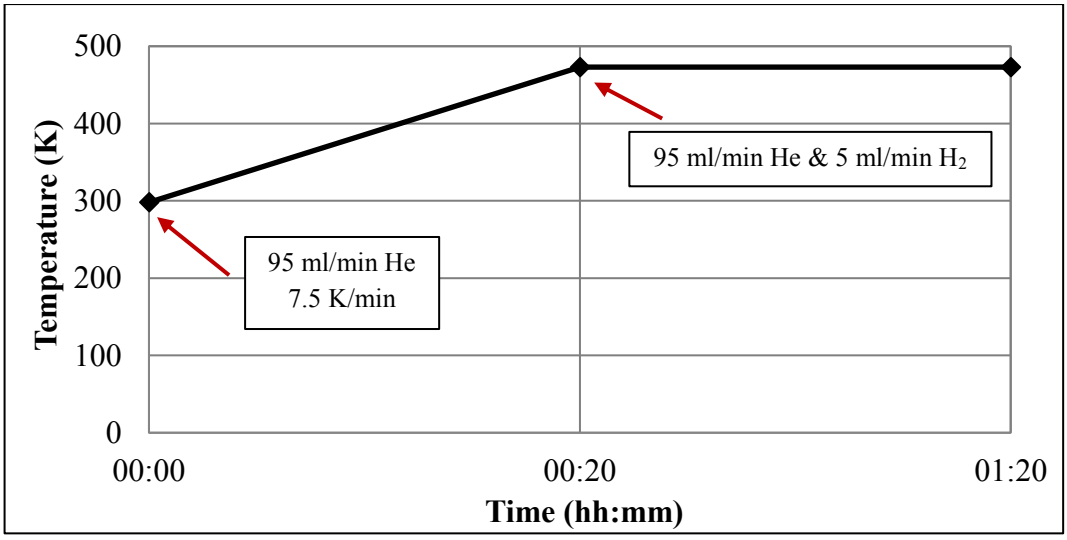

Figure 3.14. Pretreatment and reduction procedure for Au-Re/CeO_2 catalyst.

3.3.2.3. Pt-Re-V/CeO_2. Ceria support was prepared by homogenous precipitation of cerium nitrate using sodium carbonate. About 20 g of cerium (III) nitrate hexahydrate was mixed with 100 ml DI water to obtain a suspension. The pH of the solution was adjusted to 8 with vigorous stirring in a water bath of 333 K with the controlled addition of aqueous sodium carbonate solution. When the pH value of 8 was obtained, the resulting suspension was allowed to mix for 1 more hour under controlled temperature and pH in the system as given in Figure 3.2. It was then filtered and washed with DI water several times. Finally, it was dried overnight at 383 K and calcined at 673 K for 4 hours in a muffle furnace.

The trimetallic Pt-Re-V/CeO_2 catalyst (1wt.%Pt-0.5wt.%Re-1wt.%V) was prepared by a sequential route in which V precursor, Re precursor and Pt precursor solutions were added by impregnation method, respectively. V/CeO_2 catalyst was prepared by the incipient-to-wetness impregnation method using aqueous solution of ammonium metavanadate and oxalic acid dihydrate with a 1:1.5 molar ratio (ca. 1.25 ml DI water/g support) as explained in Section 3.2.1. The obtained thick slurry formed after ultrasonic mixing of the aqueous solution of the precursor salt and the support was dried overnight at 383 K and calcined at 673 K for 2 hours in a muffle furnace.

Re-V/CeO_2 catalyst was prepared by the incipient-to-wetness impregnation method using aqueous solution of ammonium perrhenate (ca. 1.1 ml DI water/g support) as explained in Section 3.2.1. The obtained thick slurry formed after ultrasonic mixing of the aqueous solution of the precursor salt and the support was dried overnight at 383 K and calcined at 673 K for 2 hours in a muffle furnace.

Pt-Re-V/CeO_2 catalyst was prepared by the incipient-to-wetness impregnation method using aqueous solution of tetraammineplatinum (II) nitrate (ca. 1.1 ml DI water/g support) as explained in Section 3.2.1. The obtained thick slurry formed after ultrasonic mixing of the aqueous solution of the precursor salt and the support was dried overnight at 383 K and calcined at 673 K for 4 hours in a muffle furnace.

After placing the catalyst into the constant temperature zone of the microreactor, the sample was heated from RT to the reduction temperature of 648 K at a rate of 8.75 K/min under 85 ml/min He flow and then 15 ml/min H_2 was introduced to the reactor to clear the

catalyst surface from oxygen, which was present in the metal oxide form, for 2 hours. After reduction, the gas flow was switched to He and it was allowed to flow at 5 ml/min overnight to sweep H_2 from the system prior to the catalytic tests or to flow at 50 ml/min to heat the microreactor up to the reaction temperature (Figure 3.15).

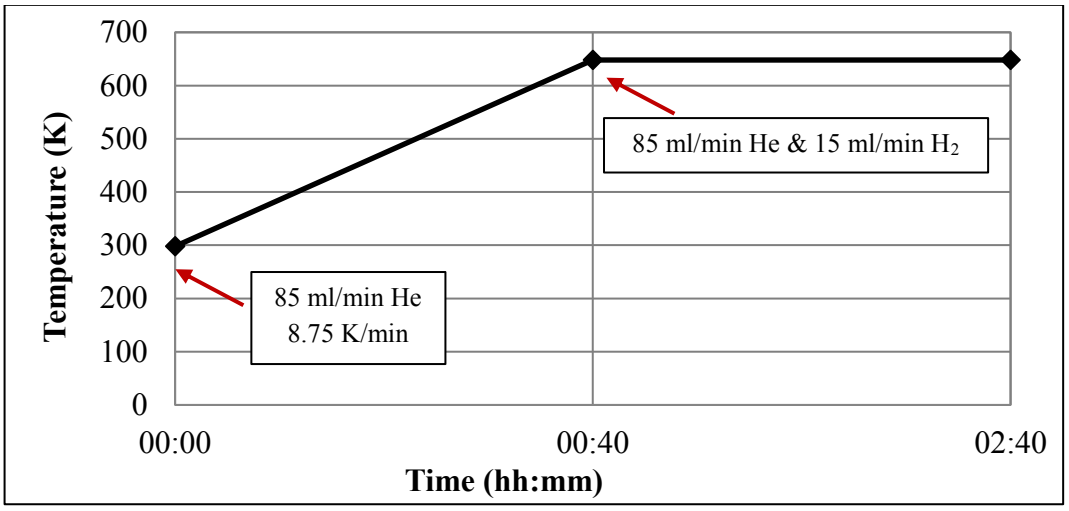

Figure 3.15. Pretreatment and reduction procedure for Pt-Re-V/CeO_2 catalyst.

3.3.3. Preferential Oxidation Catalyst (Pt-Sn/AC3)

Commercial activated carbon pellets (NORIT ROX 0.8) were crushed and sieved into 354-250 μm (45-60 mesh) particle size and exposed to different thermal and chemical pretreatments prior to being used as support. As the initial step, AC was treated with 2 N hydrochloric acid solution in a Soxhlet apparatus under total reflux for 12 hours to remove some ash content and accompanying sulfur. The slurry was then rinsed and washed with DI water for 6 hours to remove hydrochloric acid remaining on the support surface in the system given in Figure 3.3a. Finally, the slurry was dried at 383 K overnight. Then, AC was treated with 5 N nitric acid solution under total reflux for 3 hours in the system given in Figure 3.3b. The rinsing procedure with DI water was repeated several times (Figure 3.3c), and then the slurry was dried at 383 K overnight. The obtained support is called AC3. Details on AC treatments are explained in Section 3.3.4.

The bimetallic Pt-Sn/AC3 catalyst (1wt.%Pt-0.25wt.%Sn) was prepared by a sequential route in which Pt solution was impregnated over initially prepared and calcined

Sn/AC3 catalyst, which was prepared by the incipient-to-wetness impregnation method using aqueous solution of tin (IV) chloride pentahydrate (ca. 1.9 ml DI water and 0.2 ml HCl (37wt.%) solution/g support) as explained in Section 3.2.1. The obtained thick slurry formed after ultrasonic mixing of the aqueous solution of the precursor salt and the support was dried overnight at 383 K and calcined under 50 ml/min He flow at 673 K for 2 hours. Similarly, aqueous solution of hexachloroplatinic (IV) acid hexahydrate (ca. 2.1 ml DI water/g support) was impregnated over monometallic Sn/AC3 catalyst as explained in Section 3.2.1. The resulting slurry involving two metals was dried overnight at 383 K.

After placing the catalyst into the constant temperature zone of the microreactor, the pretreatment was started by heating the catalyst from RT to 398 K with a heating rate of 10 K/min under 50 ml/min He flow. Then, He was allowed to flow at 398 K for 20 minutes. Next step involved heating the sample from 398 K to 573 K with a heating rate of 10 K/min, followed by an isothermal segment of 20 minutes at 573 K. The temperature was then increased from 573 K to 673 K with a heating rate of 10 K/min. The bimetallic catalyst was calcined *in situ* under 50 ml/min He flow at 673 K for 2 hours, then reduced under 50 ml/min H_2 flow at 673 K for 10 hours and finally flushed/swept under 50 ml/min He flow at 673 K for 1 hour prior to the catalytic tests in order to enable surface stabilization (Figure 3.16).

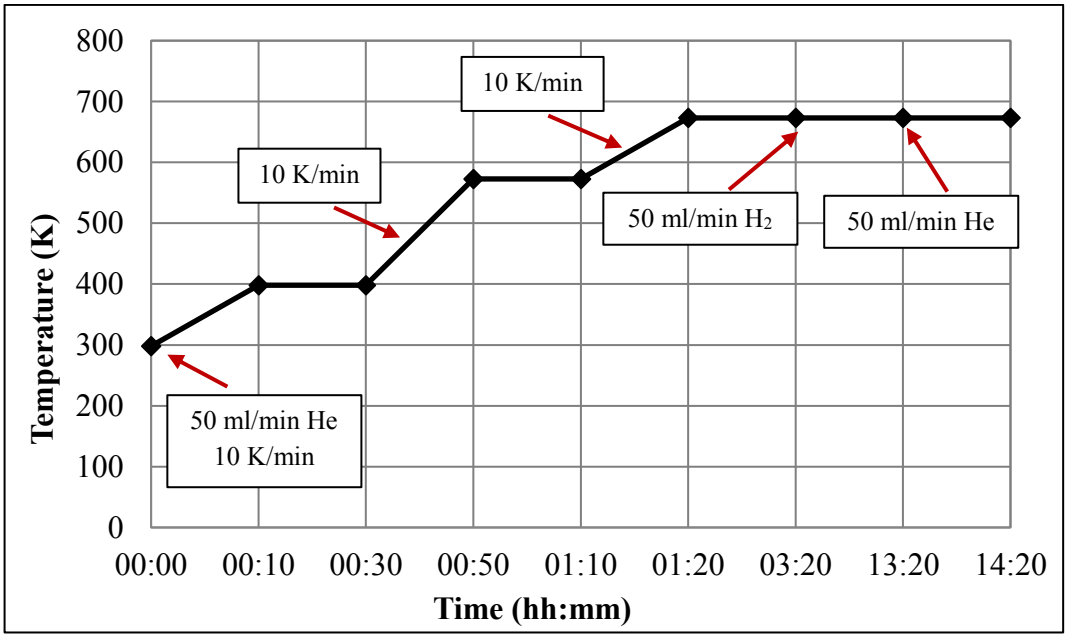

Figure 3.16. Pretreatment and reduction procedure for Pt-Sn/AC3 catalyst.

3.3.4. Activated Carbon Based Adsorbents

The modified activated carbon adsorbents used in this study were prepared by subjecting the commercial activated carbon to different oxidative, alkali, thermal, amination and ammoxidation treatments as described below:

Commercial activated carbon pellets (NORIT ROX 0.8) were crushed and sieved into 354-250 μm (45-60 mesh) particle size referred to as AC0. Then, approximately 20 g of AC0 was placed in an extraction thimble and was washed at 448 K with 200 ml of 2 N HCl solution for 12 hours in a Soxhlet apparatus system to remove some ash and sulfur content. After the extraction process was completed, the slurry was then rinsed and washed with 250 ml DI water for 6 hours to remove HCl remaining from the activated carbon surface (Figure 3.3a). Finally, the slurry was dried at 383 K overnight. This support is referred to as AC1.

10-15 g of AC1 was oxidized in a quartz down flow reactor in a tube furnace under the flow of 10 ml/min O_2-190 ml/min N_2 (5% O_2-95% N_2) mixture for 10 hours at 723 K in the system as described in Section 3.2.1. Heating the activated carbon up to the oxidation temperature and cooling down to the RT processes were done under the flow of 150 ml/min N_2. The air oxidized AC material obtained through this procedure is referred to as AC2.

10-15 g of AC1 was put into a round bottom flask containing 350 ml of 5 N HNO_3 solution and washed at 448 K under total reflux for 3 hours (Figure 3.3b). The suspension was allowed to precipitate through the night. The resulting precipitate was put in a 2 L beaker with 1.5 L DI water. The mixture was boiled at 523 K at 250 rpm, until 300 ml of the DI water (ca. 4 hours) evaporated (Figure 3.3c) and was again allowed to precipitate through the night. The rinsing procedure with DI water was repeated several times until there was no precipitation (i.e. the solution had a homogeneous appearance). Then the solution was filtrated using vacuum filtration. Obtained AC was dried at 383 K overnight. The nitric acid oxidized AC material obtained through this procedure is referred to as AC3.

Current experimental procedures on wet NH_3 treatment methods were based on the former studies of ammonia-modified AC-based adsorption (Zhang *et al.*, 2010; Shaarani *et al.*, 2011; Przepiorski *et al.*, 2004). 2 g of AC1 samples were placed in 150 ml of 10 wt.%

and 25 wt.% NH_3 solutions and left for 48 hours at RT. After this time, the solutions were washed with DI water and vacuum-filtered, until the filtrate showed a pH value of 7. These supports were referred to as AC1-10NH3w and AC1-25NH3w. Finally, the samples were dried at 383 K for 24 hours. Another NH_3 treatment technique is incipient-to-wetness-impregnation method. 2 g of AC1 samples were placed in Büchner flasks and impregnated with 10 wt.% and 25 wt.% NH_3 solutions (2.1 ml solution/g AC) and were dried at 383 K for 24 hours. Finally, the samples were calcined under 150 ml/min N_2 flow at 523 K for 2 hours and named according to the calcination temperatures as AC1-10NH3i-250 and AC1-25NH3i-250. AC1-25NH3w sample was subjected to thermal treatment under 50 ml/min He flow for 2 hours at 873 K and this support is denoted as AC1-25NH3w-600He.

Gaseous ammonia treatments were carried out either in pure ammonia flow (amination) or in a mixture of ammonia and oxygen (ammoxidation). In determination of treatment conditions, the flammability limits of ammonia in air (16-27% by vol.) and ammonia in oxygen (15-79% by vol.) at room temperature and atmospheric pressure were considered. It should be noted that elevated temperatures result in wider flammability limits, and for this reason the flammability limits of air-ammonia mixture (11-37%) at 400 °C was also considered (Nielsen, 1995).

In order to avoid combustion of the activated carbon, ammoxidation treatments were applied at lower temperatures than amination. As the initial step of the ammoxidation treatment, 2 g AC1 sample was introduced into the quartz reactor and ramped up to 300 °C under 50 ml/min N_2 flow. After the temperature reached the desired point, NH_3 and O_2 gases were introduced into the reactor. Finally, ammoxidation was conducted at 300 °C for 2 hours by a mixture of NH_3 and air at the ratio of 1:2 for a total flow rate of 50 ml/min. This adsorbent is denoted as AC1-X-300. As the initial step of the amination treatment, 2 g AC1 sample was introduced into the quartz reactor and similarly ramped up to 600 °C or 800 °C under 50 ml/min N_2 flow. Then, the inert flow was replaced with 50 ml/min NH_3 flow and the sample was held for 2 hours. These samples were referred to as AC1-N-600 and AC1-N-800. Introducing additional basic groups by 10% Na_2CO_3 solution (ca. 2.1 ml DI water/g AC) impregnation on the aminated sample (AC1-N-600) was also tested and the sample was shown as AC1-N-600i-250, where the calcination was carried out at 250 °C under the flow of 5% O_2-95% N_2 mixture for 2 hours. Amination and amination followed by impregnation

and calcination methods were also applied to AC0 samples, which were referred to as AC0-N-600 and AC0-N-600i-250. The adsorbents used in this study are given in Table 3.3.

Table 3.3. List of modified activated carbon adsorbents.

Name	Treatment Type
AC0	NORIT ROX
AC1	HCl washed AC0
AC2	Air oxidized AC1
AC3	HNO_3 oxidized AC1
AC1-10NH3w	10% NH_3 washed AC1
AC1-25NH3w	25% NH_3 washed AC1
AC1-10NH3i-250	10% NH_3 impregnated and calcined (250 °C) AC1
AC1-25NH3i-250	25% NH_3 impregnated and calcined (250 °C) AC1
AC1-25NH3w-600He	Thermally treated (600 °C) AC1-25NH3w
AC1-X-300	Ammoxidized AC1 (300 °C & NH_3:Air = 1:2)
AC1-N-600	Aminated AC1 (600 °C)
AC1-N-800	Aminated AC1 (800 °C)
AC1-N-600i-250	Aminated (600 °C), Na_2CO_3 impregnated and calcined (250 °C) AC1
AC0-N-600	Aminated AC0 (600 °C)

3.4. Catalytic Reaction and Adsorption Tests

3.4.1. Propane OSR and Serial OSR-WGS Reaction Tests over Pt-Ni/δ-Al_2O_3 and Au-Re/ZrO_2 Catalysts

In this section, the fuel processor prototype is used for both individual OSR and serial OSR-WGS reaction tests. The reaction conditions as well as the catalyst types were based on the former studies conducted by our group for OSR reaction (Çağlayan *et al*., 2005a) and for WGS reaction (Güven, 2009). Çağlayan investigated OSR of propane over bimetallic Pt-

Ni/δ-Al_2O_3 catalyst. The experiments were conducted according to the assigned C/O_2, S/C and W/F ratios; i.e. $1.50 < C/O_2 < 2.70$; $2 < S/C < 3$; $0.51 <$ W/F (mg-cat.min/ml) < 1.37, for the temperature range of 623-743 K and for a total feed flow in the range of 110-293 ml/min. Optimum activity and selectivity was obtained with S/C of 3, C/O_2 of 2.7 and W/F ratio of 0.51. Helium was used as the balance gas in order to use a total inflow of 100 ml/min for different feed compositions. Güven studied several Au-based bimetallic catalysts and investigated the effect of temperature (523-623 K), W/F (0.012-0.060 mg-cat.h/ml), H_2O/CO ratio (5, 6 and 7), and also Re impregnation and the Au:Re loading ratio on the WGS performance. The highest CO conversion (~50%) was obtained on 2wt.%Au-1wt.%Re/ZrO_2 catalyst.

18 individual OSR reaction tests for three temperature levels and 30 serial OSR-WGS reaction tests for five temperature combinations of OSR-WGS reactors were conducted; the experimental conditions are listed in Table 3.4 and Table 3.5 for individual OSR and serial OSR-WGS reaction tests, respectively. Randomly selected 9 individual OSR and 15 combined OSR-WGS tests were repeated; the comparative analysis confirmed the repeatability of the tests and reliability of the test system. In the tests, 150 mg of fresh OSR catalyst (0.2wt.%Pt-10wt.%Ni/δ-Al_2O_3) and 170 mg of fresh WGS catalyst (2wt.%Au-1wt.%Re/ZrO_2) were placed into the constant temperature zones of OSR and WGS microreactors, respectively. In individual OSR and serial OSR-WGS tests, OSR catalyst type and weight were the same. The OSR catalyst was pretreated through reduction under 20 ml/min pure H_2 flow at 773 K for 4 hours (Figure 3.12). The WGS catalyst was pretreated through reduction under 5% H_2-He flow at 453 K for 1 hour (Figure 3.13). In the performance tests, product analysis was performed for the given experimental conditions, as given in Table 3.4 and Table 3.5 in terms of S/C and O/C ratios, for two hours time-on-stream (TOS) guaranteeing that steady state product composition was achieved. C_3H_8, O_2 and H_2O flow rates were kept in the ranges of 5.1-7.3 ml/min, 7.3-10.3 ml/min and 44.7-59.6 ml/min, respectively. Helium was used as a balance for keeping the total feed flow fixed at 100 ml/min, corresponding to a space velocity (GHSV) of 40000 ml/(h.g-cat) and a weight hourly space velocity (WHSV) of 28 h^{-1} based on OSR catalyst/reactor.

Table 3.4. Experimental conditions used in individual OSR reaction tests.

Exp. #	T_{OSR} (K)	C_3H_8 (%)	O_2 (%)	H_2O (%)	S/C	O/C
O1	623	6.6	7.3	59.6	3.01	0.74
O2	623	6.6	8.4	59.6	3.01	0.85
O3	623	6.6	10.3	59.6	3.01	1.04
O4	623	5.1	7.3	59.6	3.89	0.95
O5	623	7.3	7.3	59.6	2.72	0.67
O6	623	6.6	7.3	44.7	2.26	0.74
O7	673	6.6	7.3	59.6	3.01	0.74
O8	673	6.6	8.4	59.6	3.01	0.85
O9	673	6.6	10.3	59.6	3.01	1.04
O10	673	5.1	7.3	59.6	3.89	0.95
O11	673	7.3	7.3	59.6	2.72	0.67
O12	673	6.6	7.3	44.7	2.26	0.74
O13	723	6.6	7.3	59.6	3.01	0.74
O14	723	6.6	8.4	59.6	3.01	0.85
O15	723	6.6	10.3	59.6	3.01	1.04
O16	723	5.1	7.3	59.6	3.89	0.95
O17	723	7.3	7.3	59.6	2.72	0.67
O18	723	6.6	7.3	44.7	2.26	0.74

Table 3.5. Experimental conditions used in serial OSR-WGS reaction tests.

Exp. #	T_{OSR} (K)	T_{WGS} (K)	C_3H_8 (%)	O_2 (%)	H_2O (%)	S/C	O/C
S1	673	573	6.6	7.3	59.6	3.01	0.74
S2	673	573	6.6	8.4	59.6	3.01	0.85
S3	673	573	6.6	10.3	59.6	3.01	1.04
S4	673	573	5.1	7.3	59.6	3.89	0.95
S5	673	573	7.3	7.3	59.6	2.72	0.67
S6	673	573	6.6	7.3	44.7	2.26	0.74
S7	673	623	6.6	7.3	59.6	3.01	0.74
S8	673	623	6.6	8.4	59.6	3.01	0.85
S9	673	623	6.6	10.3	59.6	3.01	1.04
S10	673	623	5.1	7.3	59.6	3.89	0.95
S11	673	623	7.3	7.3	59.6	2.72	0.67
S12	673	623	6.6	7.3	44.7	2.26	0.74
S13	723	523	6.6	7.3	59.6	3.01	0.74
S14	723	523	6.6	8.4	59.6	3.01	0.85
S15	723	523	6.6	10.3	59.6	3.01	1.04
S16	723	523	5.1	7.3	59.6	3.89	0.95
S17	723	523	7.3	7.3	59.6	2.72	0.67
S18	723	523	6.6	7.3	44.7	2.26	0.74
S19	723	573	6.6	7.3	59.6	3.01	0.74
S20	723	573	6.6	8.4	59.6	3.01	0.85
S21	723	573	6.6	10.3	59.6	3.01	1.04
S22	723	573	5.1	7.3	59.6	3.89	0.95
S23	723	573	7.3	7.3	59.6	2.72	0.67
S24	723	573	6.6	7.3	44.7	2.26	0.74
S25	723	623	6.6	7.3	59.6	3.01	0.74
S26	723	623	6.6	8.4	59.6	3.01	0.85
S27	723	623	6.6	10.3	59.6	3.01	1.04
S28	723	623	5.1	7.3	59.6	3.89	0.95
S29	723	623	7.3	7.3	59.6	2.72	0.67
S30	723	623	6.6	7.3	44.7	2.26	0.74

3.4.2. Propane OSR, Serial OSR-WGS, OSR-PROX and OSR-WGS-PROX Reaction Tests over Pt-Ni/δ-Al_2O_3, Pt-Re-V/CeO_2 and Pt-Sn/AC3 Catalysts

In this section, the FPP was used for individual OSR, serial OSR-WGS, OSR-PROX and OSR-WGS-PROX reaction tests. The reaction conditions and catalysts were based on the former studies conducted by our group for propane OSR (Çağlayan *et al*., 2005a), WGS (Özer, 2016; Kesim, 2016) and PROX reactions (Çağlayan *et al*., 2011b; Eropak and Aksoylu, 2016).

16 individual propane OSR reaction tests, 12 serial OSR-WGS reaction tests, 10 serial OSR-PROX reaction tests and 7 serial OSR-WGS-PROX reaction tests for four S/C ratios and for different temperature combinations of the serial reactors were conducted; the experimental conditions are listed in Table 3.6, Table 3.7, Table 3.8 and Table 3.9, respectively. In all catalytic performance tests, the feed stream included fixed volumetric flow rates of O_2 (7.3 ml/min), C_3H_8 (6.6 ml/min) and He (26.5 ml/min). Changes were made in steam flow rate and reaction temperatures in order to investigate the product composition via the changes in the extent of the contributing reactions. In the tests, O/C ratio was fixed at 0.74 and S/C ratio was selected as 2.25, 3, 5 and 6. Total feed flow rate was in the range of 85-160 ml/min. In serial OSR-PROX and OSR-WGS-PROX reaction tests, the absence and presence of additional O_2 stream fed to the PROX reactor was also investigated.

The individual propane OSR reaction tests were conducted in the temperature range of 623-773 K for the feed and operating conditions given in Table 3.6. The serial OSR-WGS reaction tests were conducted at a fixed temperature of OSR reactor (723 K) and at different WGS reaction temperatures in the range of 523-623 K for the experimental conditions given in Table 3.7. The serial OSR-PROX reaction tests were conducted at a fixed temperature of OSR reactor (723 K) and at different PROX reaction temperatures in the range of 383-388 K and also for additional O_2 stream fed to the PROX reactor for the experimental conditions given in Table 3.8. The serial OSR-WGS-PROX reaction tests were conducted at fixed temperatures of OSR reactor (723 K), WGS reactor (623 K) and PROX reactor (383 K) for different S/C ratios and additional O_2 stream fed to the PROX reactor for the experimental conditions given in Table 3.9. In the performance tests, product analysis was performed for ca. two hours TOS guaranteeing that steady state product composition was achieved.

In the reaction tests, 150 mg of fresh OSR catalyst (0.2wt.%Pt-10wt.%Ni/δ-Al_2O_3), 75 mg of fresh WGS catalyst (1wt.%Pt-0.5wt.%Re-1wt.%V/CeO_2) and 250 mg of fresh PROX catalyst (1wt.%Pt-0.25wt.%Sn/AC3) were placed into the constant temperature zones of OSR, WGS and PROX microreactors, respectively. In individual OSR, serial OSR-WGS, OSR-PROX and OSR-WGS-PROX tests, OSR catalyst and weight were the same. The OSR catalyst was pretreated through reduction under 20 ml/min pure H_2 flow at 773 K for 4 hours (Figure 3.12). The WGS catalyst was pretreated through reduction under 15% H_2-He flow at 648 K for 2 hours (Figure 3.15). The PROX catalyst was calcined *in situ* under 50 ml/min He flow at 673 K for 2 hours and then reduced under 50 ml/min H_2 flow at 673 K for 10 hours in order to enable the surface stabilization prior to the reaction tests (Figure 3.16).

Table 3.6. Experimental conditions used in individual propane OSR reaction tests.

		Flow rate (ml/min)					
Exp. #	**T_{OSR} (K)**	**C_3H_8**	**O_2**	**H_2O**	**He**	**S/C**	**O/C**
A1	623	6.6	7.3	44.7	26.5	2.25	0.74
A2	623	6.6	7.3	59.6	26.5	3	0.74
A3	623	6.6	7.3	99.5	26.5	5	0.74
A4	623	6.6	7.3	119.2	26.5	6	0.74
A5	673	6.6	7.3	44.7	26.5	2.25	0.74
A6	673	6.6	7.3	59.6	26.5	3	0.74
A7	673	6.6	7.3	99.5	26.5	5	0.74
A8	673	6.6	7.3	119.2	26.5	6	0.74
A9	723	6.6	7.3	44.7	26.5	2.25	0.74
A10	723	6.6	7.3	59.6	26.5	3	0.74
A11	723	6.6	7.3	99.5	26.5	5	0.74
A12	723	6.6	7.3	119.2	26.5	6	0.74
A13	773	6.6	7.3	44.7	26.5	2.25	0.74
A14	773	6.6	7.3	59.6	26.5	3	0.74
A15	773	6.6	7.3	99.5	26.5	5	0.74
A16	773	6.6	7.3	119.2	26.5	6	0.74

Table 3.7. Experimental conditions used in serial propane OSR-WGS reaction tests.

			Flow rate (ml/min)					
Exp. #	**T_{OSR} (K)**	**T_{WGS} (K)**	**C_3H_8**	**O_2**	**H_2O**	**He**	**S/C**	**O/C**
B1	723	523	6.6	7.3	44.7	26.5	2.25	0.74
B2	723	523	6.6	7.3	59.6	26.5	3	0.74
B3	723	523	6.6	7.3	99.5	26.5	5	0.74
B4	723	523	6.6	7.3	119.2	26.5	6	0.74
B5	723	573	6.6	7.3	44.7	26.5	2.25	0.74
B6	723	573	6.6	7.3	59.6	26.5	3	0.74
B7	723	573	6.6	7.3	99.5	26.5	5	0.74
B8	723	573	6.6	7.3	119.2	26.5	6	0.74
B9	723	623	6.6	7.3	44.7	26.5	2.25	0.74
B10	723	623	6.6	7.3	59.6	26.5	3	0.74
B11	723	623	6.6	7.3	99.5	26.5	5	0.74
B12	723	623	6.6	7.3	119.2	26.5	6	0.74

Table 3.8. Experimental conditions used in serial propane OSR-PROX reaction tests.

			Flow rate (ml/min)				
Exp. #	**T_{OSR} (K)**	**T_{PROX} (K)**	**C_3H_8**	**O_2**	**H_2O**	**He**	**Additional O_2**
C1	723	383	6.6	7.3	59.6	26.5	0
C2	723	383	6.6	7.3	59.6	26.5	0.5
C3	723	383	6.6	7.3	59.6	26.5	1
C4	723	383	6.6	7.3	59.6	26.5	2
C5	723	383	6.6	7.3	59.6	26.5	4
C6	723	388	6.6	7.3	59.6	26.5	0
C7	723	388	6.6	7.3	59.6	26.5	0.5
C8	723	388	6.6	7.3	59.6	26.5	1
C9	723	388	6.6	7.3	59.6	26.5	2
C10	723	388	6.6	7.3	59.6	26.5	4

Table 3.9. Experimental conditions used in serial propane OSR-WGS-PROX reaction tests.

				Flow rate (ml/min)					
Exp. #	**T_{OSR} (K)**	**T_{WGS} (K)**	**T_{PROX} (K)**	**C_3H_8**	**O_2**	**H_2O**	**He**	**O_2**	**S/C**
D1	723	623	383	6.6	7.3	44.7	26.5	0	2.25
D2	723	623	383	6.6	7.3	59.6	26.5	0	3
D3	723	623	383	6.6	7.3	99.5	26.5	0	5
D4	723	623	383	6.6	7.3	119.2	26.5	4	5
D5	723	623	383	6.6	7.3	119.2	26.5	2	5
D6	723	623	383	6.6	7.3	119.2	26.5	2	6
D7	723	623	383	6.6	7.3	119.2	26.5	0	6

3.4.3. Methane OSR and Serial OSR-WGS Reaction Tests over Pt-Ni/δ-Al_2O_3 and Pt-Re-V/CeO_2 Catalysts

In this section, the FPP was used for individual methane OSR and serial OSR-WGS reaction tests. The reaction conditions and catalysts were based on the former studies conducted by our group for methane OSR (Gökaliler, 2012; Erdinç, 2014) and WGS (Özer, 2016; Kesim, 2016) reactions. OSR of methane reaction tests over Pt-Ni/δ-Al_2O_3 catalyst was formerly investigated for the effects of metal loadings in catalyst, C/O_2 ratio in the feed stream and temperature for the feed conditions given in Table 3.10.

Table 3.10. Experimental conditions used in formerly conducted individual methane OSR reaction tests (Gökaliler, 2012; Erdinç, 2014).

Set #	**Feed Flow rates (ml/min)**					**Feed Conditions**		
	CH_4	**O_2**	**H_2O**	**N_2**	**Total**	**S/C**	**C/O_2**	**W/F (mg-cat.min/ml)**
1	29.8	14.0	89.6	52.6	186.0	3	2.12	0.80
2	21.5	10.1	63.8	38.1	133.5	3	2.12	1.12
3	40.1	27.4	123.5	102.8	293.8	3	1.50	0.51
4	51.0	18.9	152.1	71.1	293.1	3	2.70	0.51
5	47.1	22.2	139.8	83.5	292.6	3	2.12	0.51

The experimental sets used in the current study were given in Table 3.1. Determination of new set values was explained in detail in Section 4.3.

Table 3.11. Experimental conditions used in individual methane OSR and serial OSR-WGS reaction tests in the current study.

Set #	Feed Flow rates (ml/min)					Feed Conditions		
	CH_4	O_2	H_2O	He	Total	S/C	C/O_2	W/F (mg-cat.min/ml)
6	13.7	9.3	42.0	35.0	100.0	3	1.50	1.50
7	13.7	9.3	54.8	35.0	112.8	4	1.50	1.33
8	13.7	9.3	68.5	35.0	126.5	5	1.50	1.19
9	13.7	11.0	68.5	35.0	128.2	5	1.25	1.17

In all catalytic performance tests, the feed stream included fixed volumetric flow rates of CH_4 (13.7 ml/min) and He (35 ml/min). Changes were made in steam and oxygen flow rates and reaction temperatures in order to investigate the product composition via the changes in the extent of the contributing reactions. In the tests, C/O_2 ratio was in the range of 1.25-1.50 and S/C ratio was selected as 3, 4 and 5. Total feed flow rate was in the range of 100-128 ml/min. The individual methane OSR reaction tests were conducted in the temperature range of 673-723 K for the feed conditions given in Table 3.11. The serial OSR-WGS reaction tests were conducted at a fixed temperature of OSR reactor (723 K) and at a fixed temperature of WGS reactor for the feed conditions given in Table 3.11. In the performance tests, product analysis was performed for ca. 1.5 hours TOS guaranteeing that steady state product composition was achieved.

In the reaction tests, 150 mg of fresh OSR catalyst (0.2wt.%Pt-10wt.%Ni/δ-Al_2O_3) and 75 mg of fresh WGS catalyst (1wt.%Pt-0.5wt.%Re-1wt.%V/CeO_2) were placed into the constant temperature zones of OSR and WGS microreactors, respectively. In individual OSR and serial OSR-WGS reaction tests, OSR catalyst and weight were the same. The OSR catalyst was pretreated through reduction under 20 ml/min pure H_2 flow at 773 K for 4 hours (Figure 3.12). The WGS catalyst was pretreated through reduction under 15% H_2-He flow at 648 K for 2 hours (Figure 3.15).

3.4.4. Adsorption Tests

The adsorption and desorption tests of activated carbon based adsorbents were conducted by using the gravimetric analyzer in the upstream for collecting pressure versus change in the adsorbent weight data and the mass spectrometer in the downstream for analyzing the gases leaving the adsorption unit, i.e., unadsorbed gas streams (Figures 3.10 and 3.11).

The adsorption and desorption isotherms were obtained for 70-75 mg AC-based samples within 0-1000 mbar pressure range for each 100 mbar step, 0-5000 mbar pressure range for each 500 mbar step, at room temperature and at 393 K. Four different feed streams were used in the adsorption studies, which are namely; 50 ml/min CO_2 (pure CO_2), 50 ml/min CH_4 (pure CH_4), 5 ml/min CO_2-45 ml/min CH_4 (10% CO_2-90% CH_4) and 25 ml/min CO_2-25 ml/min CH_4 (50% CO_2-50% CH_4). Prior to the adsorption tests, samples were outgassed overnight at RT to eliminate humidity and trapped gases. The adsorption performance of the adsorbents were tested and compared on the basis of their adsorption capacity (mg adsorbed/g adsorbent), mass uptake values (%) and selective adsorption ability of CO_2 over CH_4.

4. RESULTS AND DISCUSSION

The aim of this research study is to design and construct a fuel processor prototype (FPP), to determine its optimum steady state operation conditions, to model its dynamic/transient performance, and to design and develop high performance AC based adsorbents for selective CO_2 capture in order to reduce its CO_2 emission. In this context, the results of this study will be presented and discussed in five sections:

- Steady state performance analysis of propane OSR and serial OSR-WGS reactors over Pt-Ni/δ-Al_2O_3 and Au-Re/ZrO_2 catalysts,
- Steady state performance analysis of propane OSR, serial OSR-WGS, OSR-PROX, OSR-WGS-PROX reactors over Pt-Ni/δ-Al_2O_3, Pt-Re-V/CeO_2 and Pt-Sn/AC3 catalysts,
- Steady state performance analysis of methane OSR and serial OSR-WGS reactors over Pt-Ni/δ-Al_2O_3 and Pt-Re-V/CeO_2 catalysts,
- Modeling and transient performance analysis of the fuel processor,
- Adsorption studies over modified activated carbon based adsorbents

4.1. Steady State Performance Analysis of OSR and Serial OSR-WGS Reactors

The aim of this section is to determine the reaction conditions, i.e. OSR feed composition and the temperature combination of OSR and WGS reactors, yielding product having the highest H_2/CO ratio with the lowest CO concentration in serial OSR-WGS operation. Additionally, the response of the FPP system to the changes in OSR feed composition, which will form a basis to a heuristic for FP operation, was obtained. Individual and serial tests were performed at different OSR-WGS reactors' temperature combinations for different concentrations of oxygen, propane and steam in the OSR feed. Novel Pt-Ni/δ-Al_2O_3 and Au-Re/ZrO_2 catalysts were used in OSR and WGS reactors, respectively. It should be noted that small part of the work presented in this section includes the results of the studies conducted in M.Sc. thesis by Melek Selcen Başar (Başar, 2010), and the whole work in this section was published as a research paper (Başar *et al*., 2016).

4.1.1. Individual OSR Reaction Tests for Steady State Performance Analysis

In propane OSR over Pt-Ni catalyst, beside the desired reactions, such as steam reforming (CO and/or CO_2 producing SR), total and/or partial oxidation of propane (TOX and/or POX) and water gas shift reactions (WGS); undesired reactions, such as methanation (CO_2 and/or CO methanation), occur. The extent of those reactions highly depends on the type of the catalyst, operating conditions and feed gas composition (Gökaliler *et al*., 2012) (Table 4.1). TOX reaction is primarily catalyzed on Pt sites, while SR is primarily catalyzed on Ni sites of the bimetallic Pt-Ni/δ-Al_2O_3 catalysts. As Pt and Ni sites are present in closed vicinity, the heat produced at Pt sites by TOX can be easily transferred to Ni sites providing heat necessary for endothermic SR. The mentioned heat transfer can occur even at atomic distance as Pt-Ni surface alloy(s) is also formed on the catalyst surface. The Pt-Ni system and their active sites have been well characterized and their functions have been studied previously (Çağlayan *et al*., 2005a). As it is known, autothermal condition is achieved when highly exothermic TOX provides energy enough for endothermic SR reactions to proceed without any need for external heating. In our performance tests, upon the reaction temperature is reached, the heat input, which was monitored by the temperature controller, to the OSR reactor during time-on-stream (TOS) tests is very limited, sometimes close to zero, indicating the autothermal conditions were achieved though the heat insulation of the reactor is not perfect. In a previous paper (Çağlayan *et al*., 2005a) of our group, the temperature levels for which OSR reactor reaches autothermal conditions under the feed compositions used in the current study were specifically analyzed. As the exothermicity of TOX reaction is an order of magnitude higher than that of POX, the oxidation reactions cannot provide enough heat necessary for CO and/or CO_2 producing steam reforming reaction(s) thermodynamically when TOX is not the primary oxidation reaction; one cannot come even close to autothermal regime during time-on-stream tests without the dominance of TOX. Considering also the limited amount of O_2 in the feed stream and its complete conversion, the extent of POX should not be significant.

Lowered reformer temperature by using OSR as the reaction leads to a near-autothermal operation of the unit, which significantly reduces the energy demand of the reforming process, and decreases operational temperature range of the FP system, i.e. temperature difference between its reformer and PROX units. By this way, the crucial

requirements of an on-board FP system, which are increased energy efficiency, rapid start-up, quick response to transient changes in the operational parameters, and easy temperature control, can be satisfied.

In the analysis of product stream, which is a mixture of He, H_2, CH_4, CO, O_2, CO_2 and C_3H_8, possible miscalculations due to peak overlaps were prevented through the use of Matrix Inversion Method. As the method utilizes detailed calibration data indicating primary/secondary peaks of each component and fragmentation, the triple overlap of CO-C_3H_8-CO_2 and double overlap of C_3H_8-CH_4 and CH_4-H_2 gases were also overcome in MS analysis (Hatton and Southward, 2003).

The OSR reaction tests were conducted in the temperature interval of 623-723 K over 150 mg 0.2wt.%Pt-10wt.%Ni/δ-Al_2O_3 bimetallic catalyst for the feed compositions and conditions given in Table 3.4. The feed stream having 7.3 ml/min O_2, 6.6 ml/min C_3H_8 and 59.6 ml/min H_2O and balanced He was taken as the reference feed. Changes were made in O_2, C_3H_8 and H_2O flow rates in order to investigate the effect of changes in O_2, C_3H_8 and H_2O concentrations at the OSR inlet on the product composition and selectivity, which is defined as H_2/CO ratio in the product stream.

Table 4.1. Possible reactions in a propane oxidative steam reformer.

Reaction No	**Reaction Formula**	**Reaction Type**	ΔH°_{298} (kJ/mol)
1	$C_3H_8 + 3\,H_2O \rightarrow 3\,CO + 7\,H_2$	CO producing steam reforming	497
2	$C_3H_8 + 6\,H_2O \rightarrow 3\,CO_2 + 10\,H_2$	CO_2 producing steam reforming	376
3	$C_3H_8 + 5\,O_2 \rightarrow 3\,CO_2 + 4\,H_2O$	Total oxidation	-2046
4	$C_3H_8 + 3/2\,O_2 \rightarrow 3\,CO + 4\,H_2$	Partial oxidation	-229
5	$CO_2 + 4\,H_2 \rightarrow CH_4 + 2\,H_2O$	CO_2 methanation	-165
6	$CO + 3\,H_2 \rightarrow CH_4 + H_2O$	CO methanation	-206
7	$CO + H_2O \leftrightarrow CO_2 + H_2$	Water gas shift	-41

It was observed during the performance tests that there were only trace amounts of propane and oxygen in the product stream indicating nearly 100% propane conversion in the OSR unit. Therefore, in presenting the results of the performance tests, propane and oxygen concentrations are not given. Due to the high endothermicity of steam reforming reactions (CO and/or CO_2 producing SR) and the exothermicity of WGS and undesirable methanation reactions (CO_2 and/or CO methanation), higher temperatures favor higher hydrogen and lower methane production. Therefore, increasing OSR reaction temperature resulted in an overall increase in steady state H_2, CO and CO_2 concentrations, and a decrease in steady state CH_4 concentration. The effect of feed composition on OSR performance was analyzed in terms of concentration of each reactant in the feed stream.

4.1.1.1. Effect of Oxygen Concentration. The OSR product gas concentrations (dry basis, inert free), namely those of H_2, CH_4, CO and CO_2, and H_2/CO product ratio as well are given in Figure 4.1 for the experiments during which O_2 flow rate in the feed stream was changed from 7.3 ml/min to 8.4 ml/min and 10.3 ml/min (Table 3.4, O1-3, O7-9, O13-15), while the flow rates of other reactants were kept fixed. While keeping S/C ratio in the feed constant at 3, increasing oxygen concentration and O/C ratio in the feed stream directly affected TOX reaction, resulting in an increase in steady state CO_2 concentration from 30% to 33% in the product stream at 723 K. The increase in H_2, CO_2 and CO concentrations can also be explained by the decrease in CH_4 concentration (21%→15%), which is an indicator of suppressed CO_2 and/or CO methanation reactions. The percentage increase in CO concentration, 16%, in the OSR product at 723 K is almost two folds higher than that of CO_2, 9%, in response to the increase in O_2 flow, i.e. O/C ratio from 0.74 to 1.04, which shows that CO producing SR surpassed CO_2 producing SR and/or reverse WGS. The RWGS reaction was also responsible for the decrease in H_2/CO product ratio, since rate of increase in CO concentration was greater than the rate of increase in H_2 concentration (~6%), as can be seen in Figure 4.1. On the other hand, there was a significant decrease in H_2 concentration, followed by an increase in CH_4 concentration due to the enhanced methanation, when the reaction temperature was decreased to 623 K for the same feed composition.

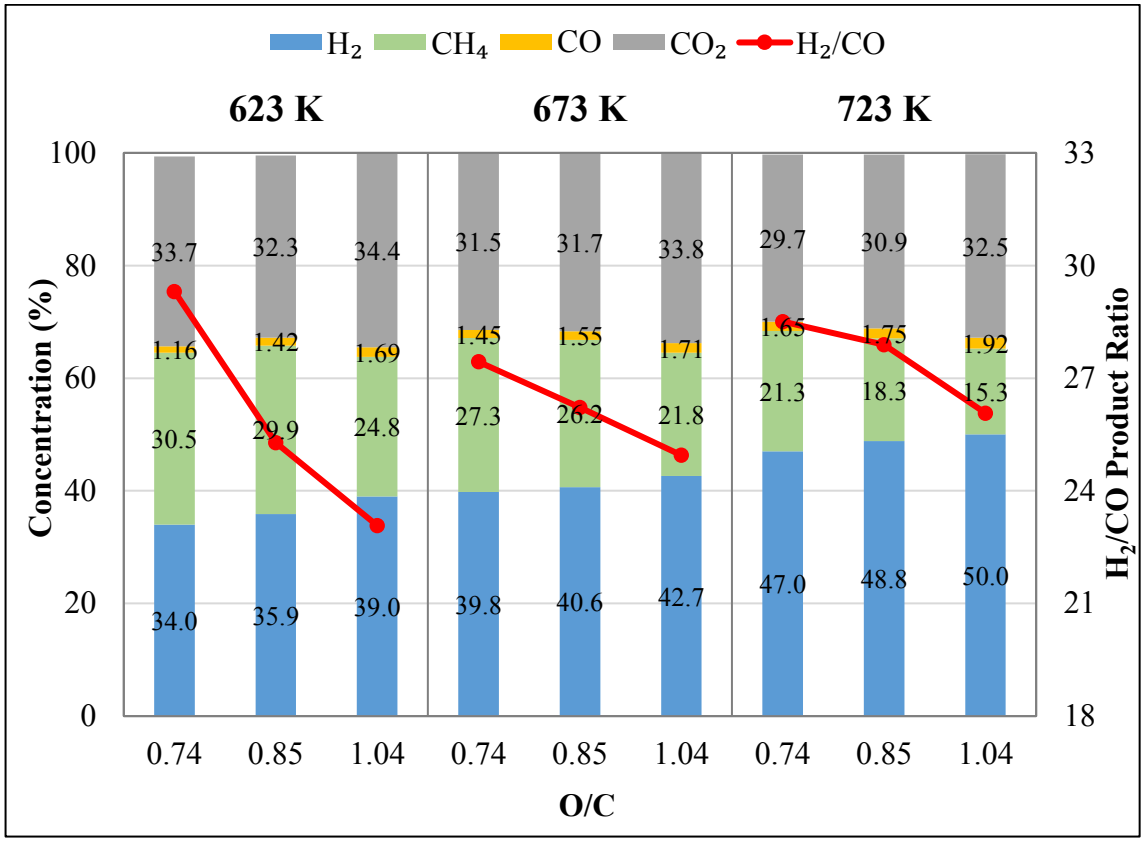

Figure 4.1. Steady state performance results for different oxygen concentrations in OSR feed at 623 K (O1-3), 673 K (O7-9) and 723 K (O13-15).

4.1.1.2. Effect of Propane Concentration. The OSR product gas concentrations (dry basis, inert free), namely those of H_2, CH_4, CO and CO_2, and H_2/CO product ratio as well are given in Figure 4.2 for the experiments during which C_3H_8 concentration in the feed stream was changed in the range of 5.1-7.3 ml/min (Table 3.4, O1, O4-5, O7, O10-11, O-13, O16-17), while flows of other reactants were kept fixed. Increasing C_3H_8 concentration in the feed stream caused decreased steam concentration in the feed stream, which shifted the equilibrium of the methanation reactions towards the products steam and methane. The C_3H_8 concentrations in the feed were chosen such as to keep S/C ratio in 2-3 range aiming to prevent coke formation. Decreasing S/C ratio in that range via increasing C_3H_8 concentration suppressed WGS reaction in the presence of limited steam, which resulted in increased CO and decreased CO_2 concentrations in the OSR product. Increased C_3H_8 concentration in the feed led to decreased H_2 (37%→30%) and increased CO product concentrations (1.2%→1.3%) lowering H_2/CO product ratio at 623 K. The rise in reaction temperature from 623 K to 723 K led to a significant increase in H_2 concentration from 30% up to 50%.

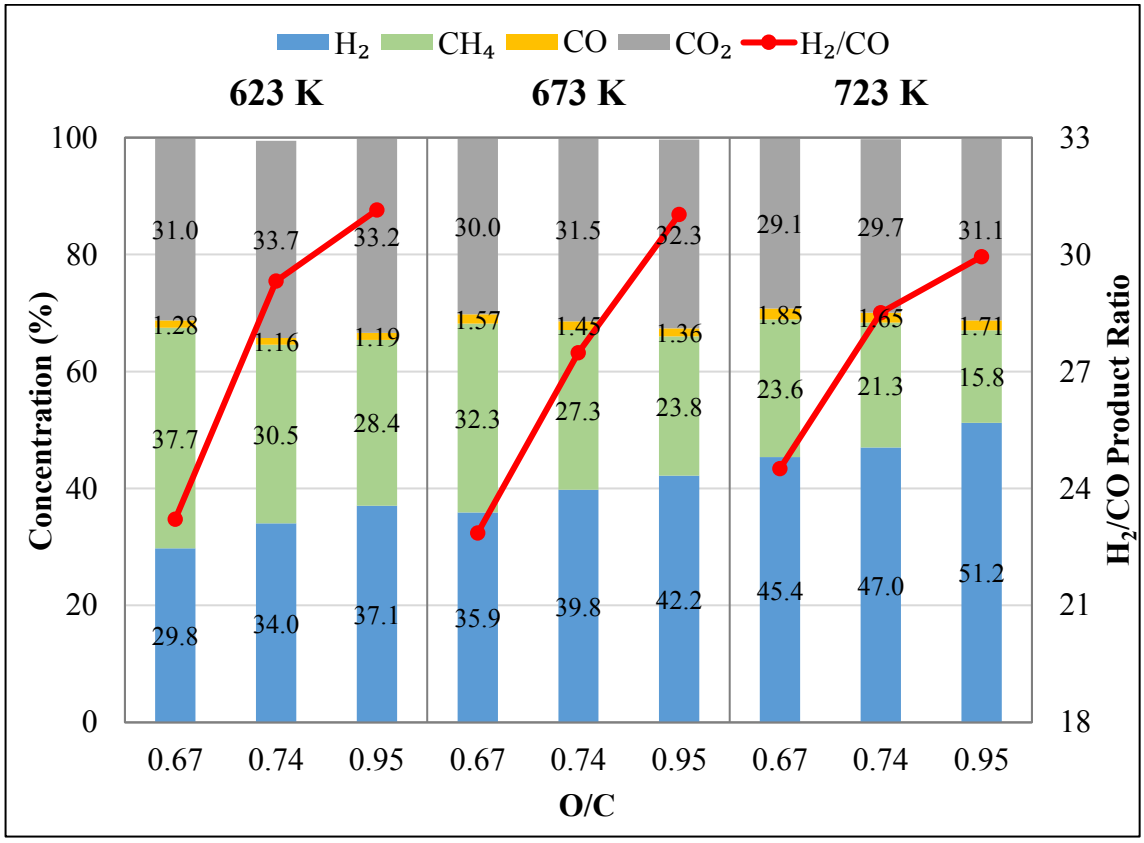

Figure 4.2. Steady state performance results for different propane concentrations in OSR feed at 623 K (O1, O4, O5), 673 K (O7, O10, O11) and 723 K (O13, O16, O17).

4.1.1.3. Effect of Steam Concentration. Experimental steady state results in terms of OSR product gas concentrations (dry basis, inert free) namely H_2, CH_4, CO and CO_2, and H_2/CO product ratio as well for different steam concentrations in the feed stream are given in Figure 4.3 for the experiments listed in Table 3.4 as O1, O6, O7, O12, O13 and O18. SR and WGS reactions, which contribute mostly to the H_2 amount produced, are directly related to the amount of water fed to the system. This is the reason why, the decrease in steam flow rate from 59.6 ml/min to 44.7 ml/min in the feed stream led to decreased steady state H_2 (34%→28%) and CO_2 (34%→32%) concentrations while increased steady state CH_4 (30%→38%) and CO (1.2%→1.4%) concentrations in the product stream at 623 K. All of these findings indicated decreased contribution of steam reforming reactions and enhanced methanation activity in the presence of limited steam. The decrease in steam concentration also shifted the WGS reaction in reverse direction resulting in increased steady state CO and decreased steady state CO_2 concentrations. Decreased H_2 and increased CO concentrations together led to a decreased H_2/CO product ratio.

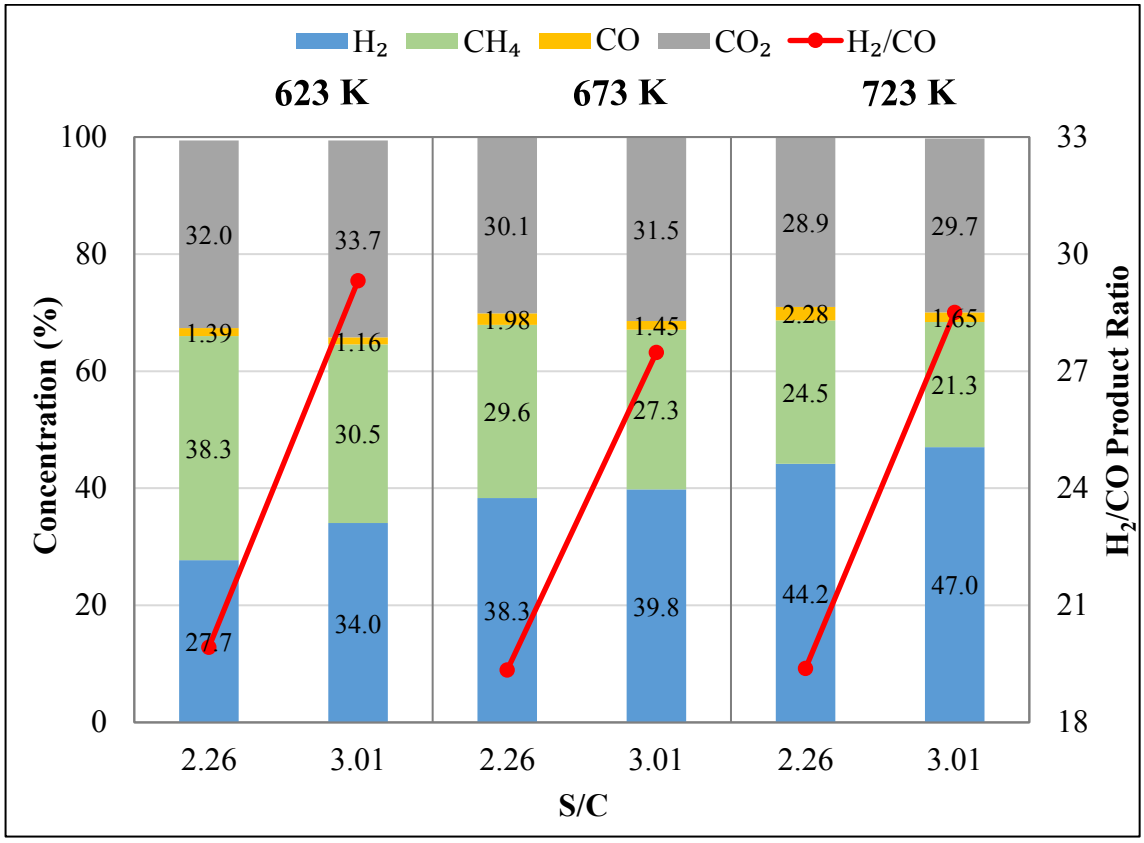

Figure 4.3. Steady state performance results for different steam concentrations in OSR feed at 623 K (O1, O6), 673 K (O7, O12) and 723 K (O13, O18).

4.1.2. Serial OSR-WGS Reaction Tests for Steady State Performance Analysis

In the steady state serial OSR-WGS reaction tests, the composition of the reactant stream fed to OSR reactor and temperature combinations of the OSR-WGS reactors were considered as the experimental parameters. The feed compositions of the OSR reactor and OSR reactor temperatures were used as the same as what had been applied in individual steady state OSR performance tests allowing clear understanding of the benefit of combining OSR with WGS. Thirty experiments were performed for five temperature combinations of serial OSR-WGS reactions. In the tests, 150 mg 0.2wt.%Pt-10wt.%Ni/δ-Al_2O_3 bimetallic OSR and 170 mg 2wt.%Au-1wt.%Re/ZrO_2 bimetallic WGS catalysts were loaded to the OSR and WGS reactors, respectively. The experimental parameters used are given in Table 3.5. In the reaction tests, two temperature levels, 673 and 723 K, for the OSR, and three temperature levels, 523, 573 and 623 K, for the WGS reactor were used. Hydrocarbon and oxygen conversions were calculated as nearly 100% throughout the serial experiments, as in

the individual OSR performance tests. It was found through comparative analysis of the inert flow rate and/or inert concentration in the OSR inlet, WGS inlet and WGS outlet that there is no significant difference in volumetric flow rate of the outlet streams of OSR and WGS units, which is an expected result as WGS reaction has 1:1 overall stoichiometry and is assumed to proceed with no significant side reaction. The results of the initial serial performance tests; the steady state concentrations of H_2, CH_4, CO and CO_2 gases (dry basis, inert free) at the exit of the WGS reactor for the reference feed composition (i.e. the feed stream having 7.3 ml/min O_2, 6.6 ml/min C_3H_8 and 59.6 ml/min H_2O and balanced He) for five OSR-WGS temperature combinations at the end of two hours, are given in Figure 4.4. The experiments are denoted by S1, S7, S13, S19 and S25, as given in Table 3.5.

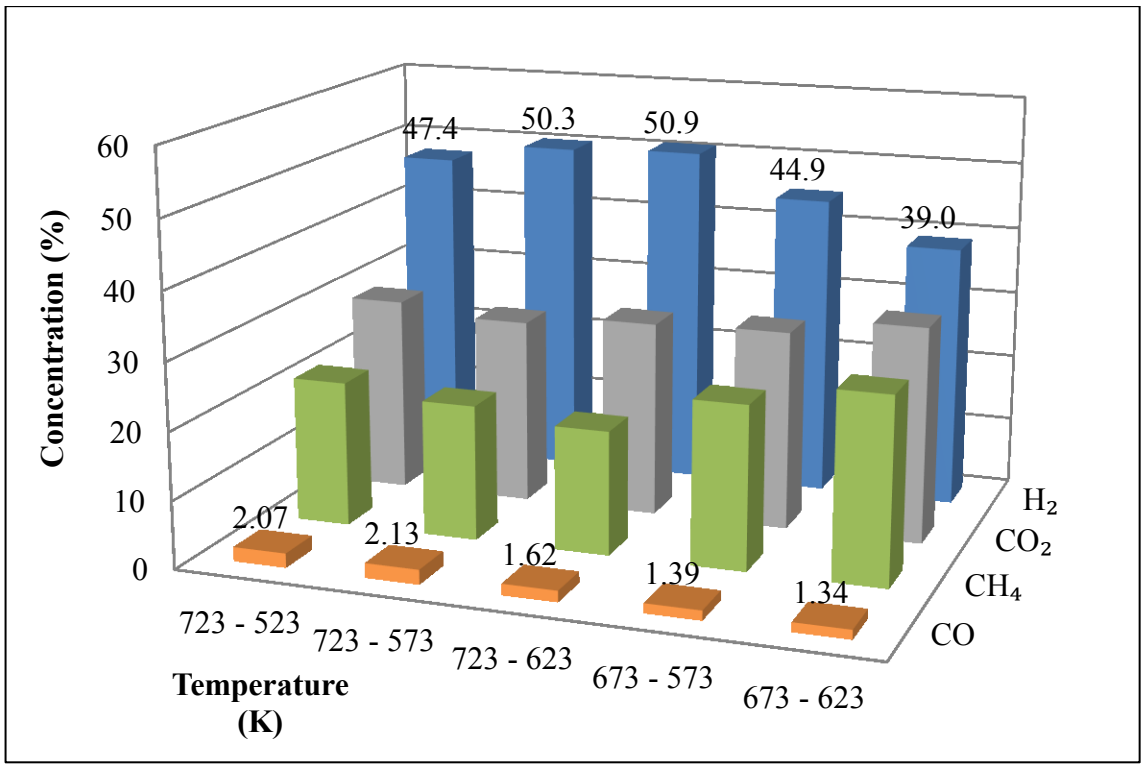

Figure 4.4. Steady state H_2, CO_2, CH_4 and CO concentrations at the WGS outlet for different temperature combinations (Table 3.5, S1, S7, S13, S19, S25).

Figure 4.4 clearly shows the positive effect of higher temperatures on H_2 and CO concentrations, especially when OSR reaction was conducted at 723 K. Increasing OSR reaction temperature definitely increases H_2 production, while decreases CO production. It should be also kept in mind that the use of lower temperatures in OSR favors the undesired

methanation reactions. Therefore, the results of the initial combined OSR-WGS tests show that conducting the serial tests at OSR-WGS temperature combinations having high OSR reaction temperature (723 K) is beneficial in suppressing undesired methanation reactions. Similarly, higher WGS temperature leads to lower CH_4 concentrations in the product stream. In serial operation, keeping OSR reaction temperature constant at 673 K or 723 K while increasing WGS reaction temperature in the temperature range of 523-623 K resulted in increased steady state H_2/CO product ratios; the enhanced activity thereby higher CO conversions (40-50%) achieved over WGS catalyst at higher temperatures favor higher H_2 selectivity. The comparison between the results of the sets indicated that the highest H_2/CO product ratio (~32-33) was obtained at 723-623 K and 673-573 K OSR-WGS temperature combinations. The highest achieved H_2 concentration was measured as 53.4% in Exp. S21 and S28, and the lowest achieved CO concentration was measured as 1.19% in Exp. S6 (Table 3.5).

The effect of oxygen concentration in the OSR feed stream on the steady state performance of serial OSR-WGS reactors was investigated through comparing the results of the experiments S1-3, S7-9, S13-15, S19-21 and S-25-27, which are listed in Table 3.5. As in the individual OSR reaction tests, an increase in O_2 concentration led to increased steady state H_2, CO_2 and CO, while decreased CH_4 concentrations at the exit stream of WGS reactor, all of which resulted in decreased H_2/CO product ratio values. A comparison of the results of the serial OSR-WGS tests, S13-15, S19-21 and S25-27, with those of the corresponding individual OSR experiments conducted at the same OSR temperature and feed composition, O13-15, clearly showed that when the temperature of the WGS unit was decreased, the WGS reaction occurred in the reverse direction yielding lower steady state CO_2 and higher steady state CO concentrations in the product stream of the serial OSR-WGS reactors (Figure 4.5).

OSR feed with lower S/C and O/C was obtained by increasing C_3H_8 flow rate from 6.6 ml/min to 7.3 ml/min while keeping steam and oxygen flow rates constant. As in the individual OSR reaction tests, an increase in C_3H_8 concentration in the OSR feed of the OSR-WGS system led to increased steady state CH_4 and CO, and decreased H_2 and CO_2 concentrations at the exit of WGS reactor resulting in lowered H_2/CO product ratio. A comparative analysis of the results obtained from serial OSR-WGS and individual OSR tests

show that the serial OSR-WGS system yielded higher H_2/CO product ratios for the same OSR temperature and feed composition.

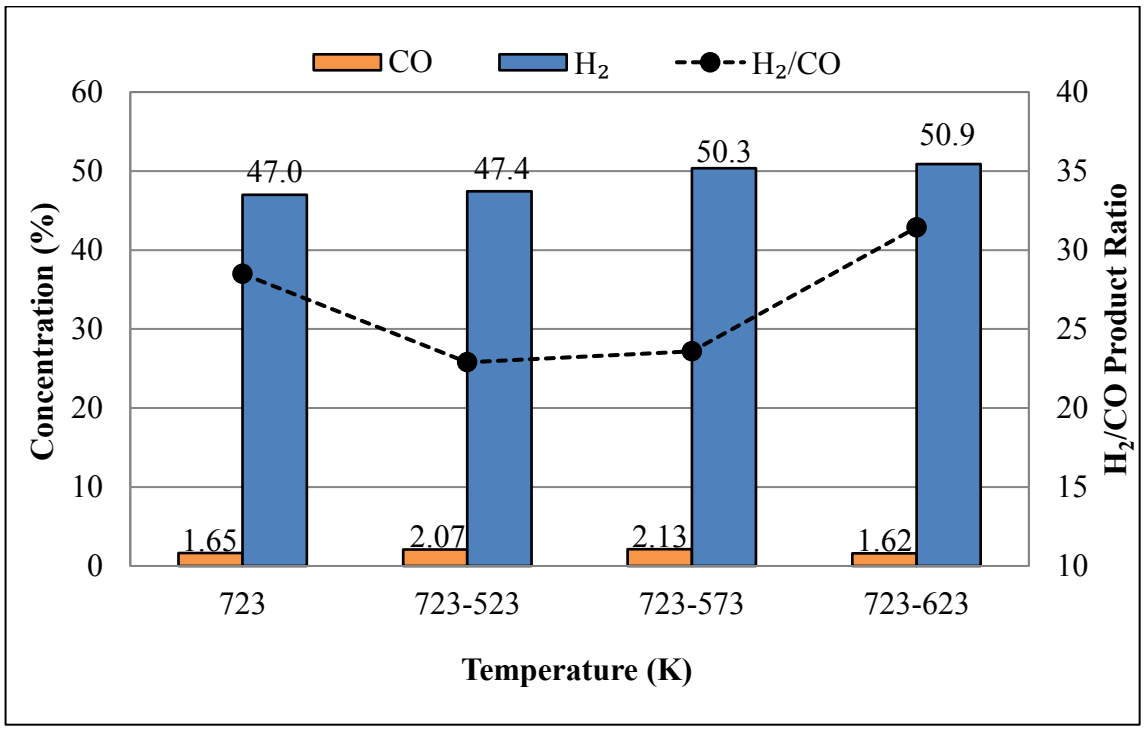

Figure 4.5. Steady state H_2 and CO concentrations, and H_2/CO product ratio at the OSR and WGS outlets as a function of OSR and OSR-WGS temperature combination at O/C=0.74 and S/C=3 (Table 3.5, O13 and Table 2 for S13, S19, S25).

Steam is the component having crucial importance in serial OSR-WGS tests as it is used both in steam reforming and water gas shift reactions. As in the individual OSR reaction tests, a decrease in steam concentration in the OSR feed led to increased steady state CH_4 and CO, and decreased H_2 and CO_2 concentrations in the product stream of WGS reactor. Consequently, decrease in steam concentration in the OSR feed led to a decreased H_2/CO product ratio of the serial OSR-WGS system.

A summary of the response of the FPP system to the changes in flow rate (concentration) of the reactants in the OSR feed, as the positive or negative variations in the concentrations of product gases at the WGS exit, are presented in Table 4.2. Steady state analysis of the FPP units both individually and in a serial fashion is the preliminary step in the determination of upper and lower bounds of a fuel processor with a target of high H_2/CO

ratio at the FPP exit stream to be used in a PEM-FC. These data can be used as guidance in the determination and prediction of the direction and composition of the outlet streams in both kinetic and dynamic tests with response to different feed conditions, e.g. step type perturbations given to the feed gases during FPP operation. The results given in Table 4.2 will form a basis to a heuristic for FP operation in our future studies.

Table 4.2. Response of FPP system against changes in the concentration of the reactants.

Reactant	**Change of Concentration in the Feed Stream**	**H_2**	**CH_4**	**CO**	**CO_2**	**H_2/CO**
Oxygen	Decrease	Decrease	Increase	Decrease	Decrease	Increase
Propane	Decrease	Increase	Decrease	Decrease	Increase	Increase
Steam	Increase	Increase	Decrease	Decrease	Increase	Increase

4.1.3. Thermodynamic Consistency Analysis of the Experimental Results

Equilibrium composition of propane OSR products was calculated by utilizing HSC Chemistry 5.11 software which uses minimization of Gibbs free energy method. Similar calculations were also performed by other groups (Wang *et al*., 2011; Faria *et al*., 2008; Pino *et al*., 2006; Wang *et al*., 2010). In calculations, the inlet gases C_3H_8, O_2, H_2O, He, and products H_2, CH_4, CO, CO_2 were included as species, and all the reactions that are listed in Table 4.1 were considered. The composition of the reference feed, used in sets O1, O7 and O13, was used in the calculations. The results of the simulations, which were reported in dry and inert free basis in Figure 4.6, confirmed that the experimental results of the current study were consistent with the thermodynamic trends, i.e. there were trace amounts of propane and oxygen in the product stream, indicating nearly 100% propane and oxygen conversions, and higher hydrogen and lower methane production with the increase in temperature. The calculated H_2 and CO product concentrations at 723 K, which are ca. 50% and 1.5%, respectively (Figure 4.6), are both above the concentration levels of both gases measured during the stability test (Figure 4.7).

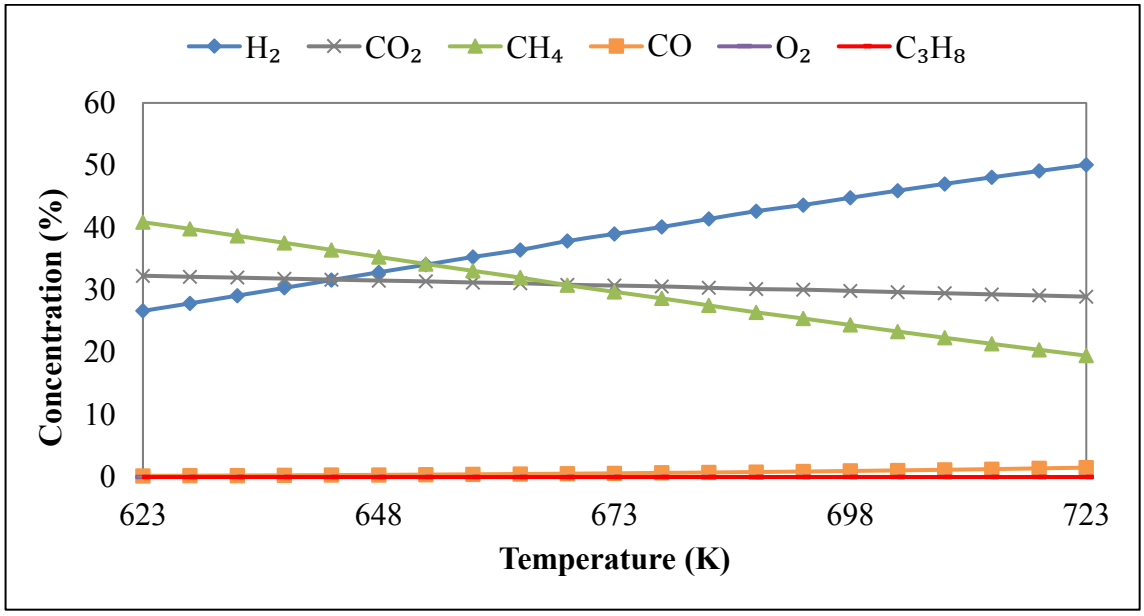

Figure 4.6. Dry based inert free equilibrium composition profile of the propane OSR predicted by thermodynamic simulation for the reference feed and OSR temperature range.

It should be noted that the published papers (Wang *et al*., 2011; Faria *et al*., 2008; Pino *et al*., 2006; Wang *et al*., 2010), in which the product compositions from the reformer have been proposed suitable for GTL and FT processes, reported equilibrium compositions having H_2/CO product ratio of ca. 1-2; whereas in the current study H_2/CO product ratio of ca. 30 was obtained both in the thermodynamic simulations and catalytic performance tests.

4.1.4. Performance Stability of OSR-WGS System

The stability test was performed on serial OSR-WGS system operating at 723 K and 623 K, respectively, for the OSR feed composition of 7.3% O_2, 6.6% C_3H_8, 59.6% H_2O and balanced He with a space velocity (GHSV) of 40000 ml/(h.g-cat). During the test, conversions of C_3H_8 and O_2 in the OSR unit were nearly 100% yielding concentrations less than 0.01% for both gases in the WGS product stream. Both catalysts showed no deactivation during 75 hours TOS test (Figure 4.7) guaranteeing promising stability characteristics.

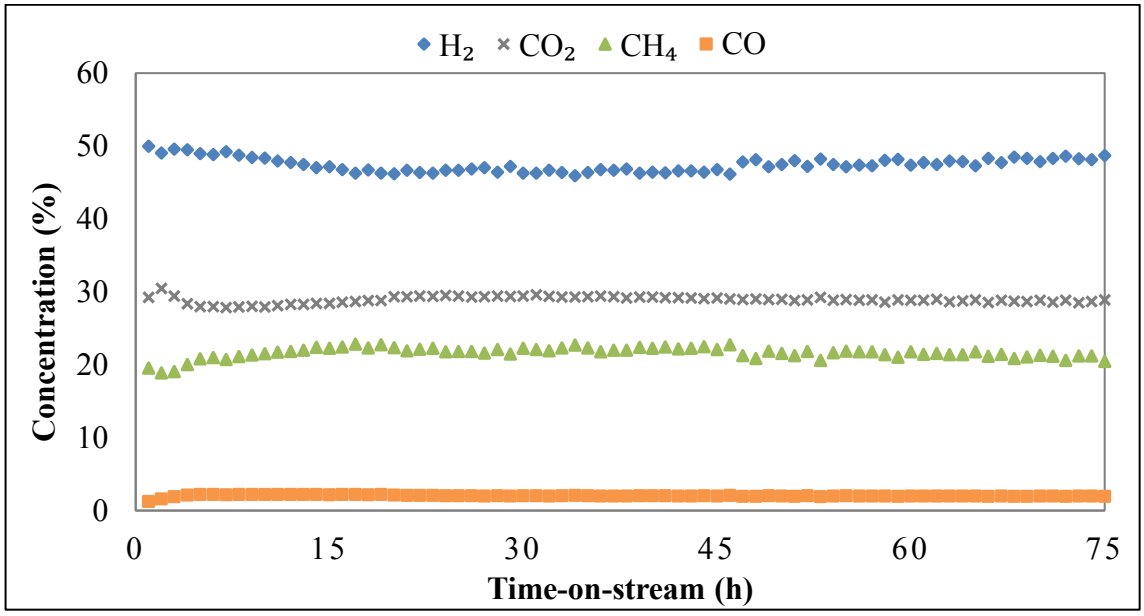

Figure 4.7. The result of the stability test conducted on serial OSR-WGS system as time-on stream concentration profiles (T_{OSR}=723 K; T_{WGS}=623 K; S/C=3, O/C=0.74; GHSV=40000 ml/(h.g-cat)).

The Pt-Ni bimetallic system has been characterized in our previous work (Çağlayan *et al*., 2005a). In the current study, SEM-EDX analyses were performed on both Pt-Ni and Au-Re catalysts in their freshly reduced and spent forms aiming to confirm the stability of catalyst surfaces during stability test.

The coke formation was found insignificant on 0.2wt.%Pt-10wt.%Ni/δ-Al_2O_3 catalyst at the end of the stability test (Figure 4.8). A comparative analysis of SEM-EDX mappings of freshly reduced and spent samples confirmed high dispersion of Pt and Ni particles and the stability of their dispersion at the end of stability test as well. In the fresh samples, Ni average wt.% was found to be 9.66% from three different locations. Since Pt content was very low (0.2 wt.%), it could not be detected quantitatively. In the spent samples, Ni average wt.% was found to be 9.33%.

Raman analysis was used to see whether there is coke deposition formed on the spent OSR catalyst sample, which was used in the stability test. The Raman spectra of the spent Pt-Ni/δ-Al_2O_3 catalyst showed no characteristic modes at ca. 1344 and ca. 1580 cm^{-1} wavelengths (Figure 4.9a), which correspond to the D band (disordered structural mode of

crystalline carbon species, defect mode) and the G band (graphitic carbon with high degree of symmetry, graphite mode), confirming no carbon deposited on the OSR catalyst during the stability test.

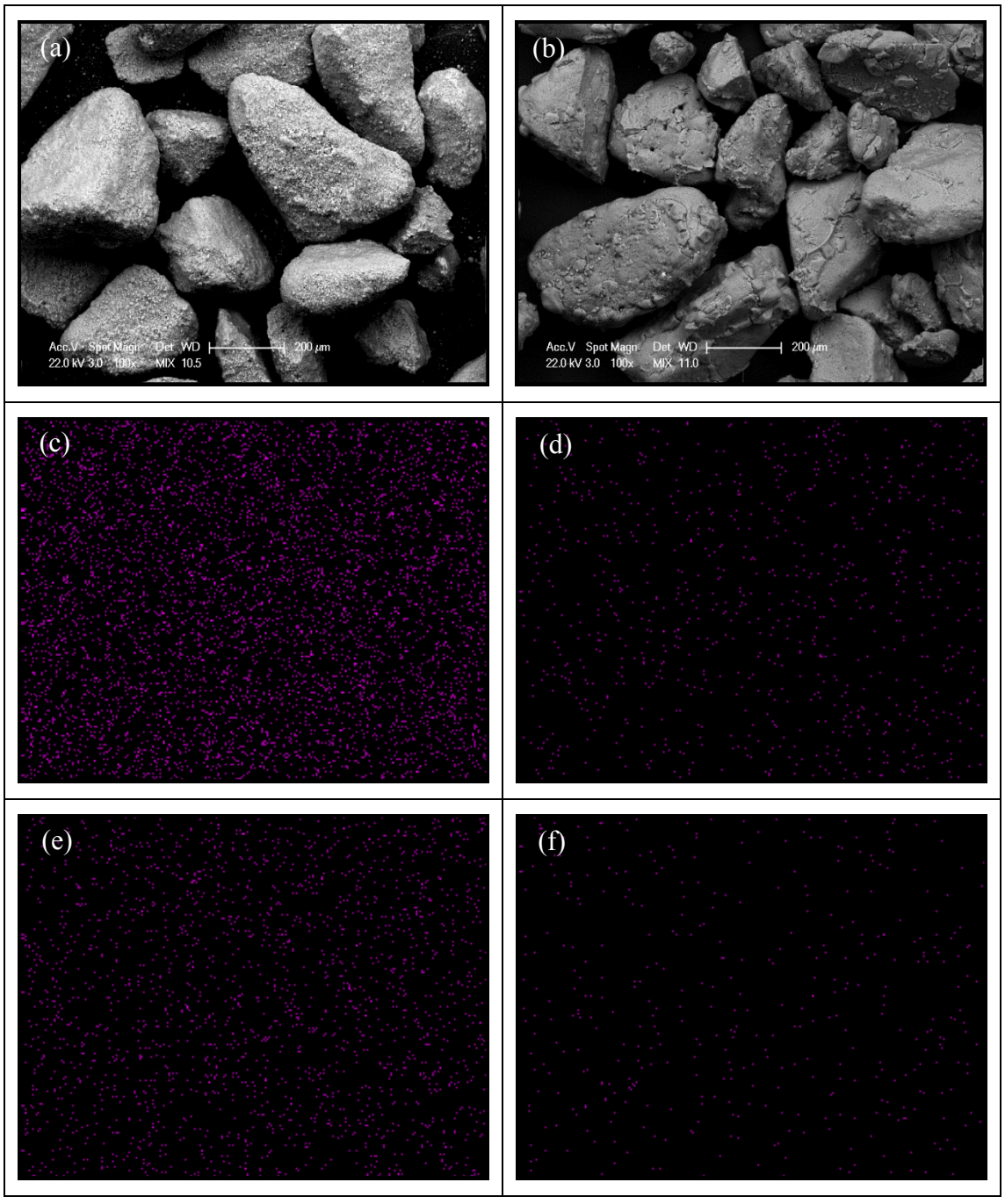

Figure 4.8. SEM images of the OSR catalyst samples; (a) freshly reduced, (b) spent catalyst, mapping of freshly reduced catalyst; (c) Ni, (d) Pt, mapping of spent catalyst; (e) Ni, (f) Pt.

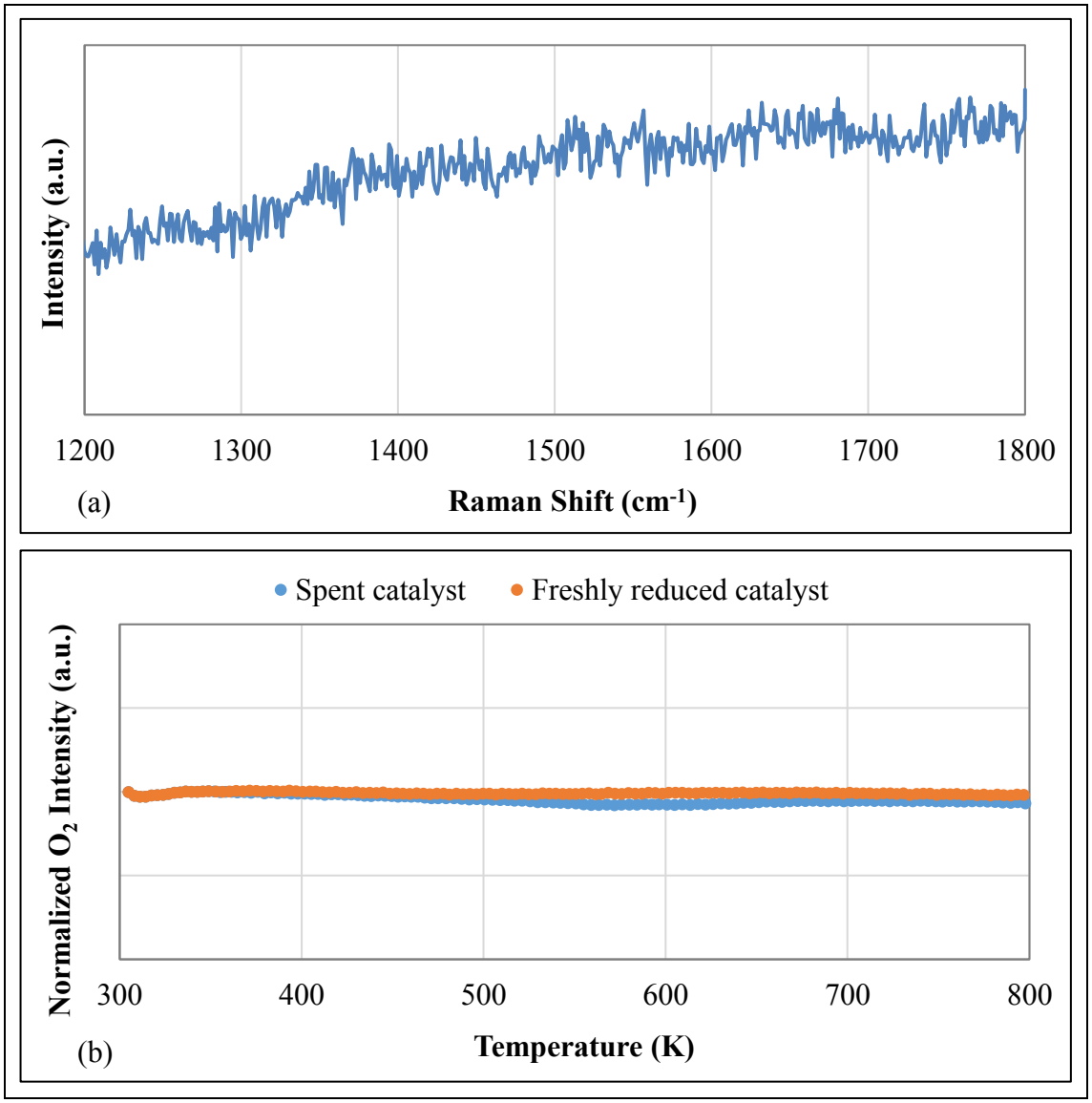

Figure 4.9. Raman and TPO spectra of Pt-Ni/δ-Al_2O_3 catalyst at the end of the stability test; (a) Raman spectra (T=723 K; S/C=3, O/C=0.74; GHSV=40000 ml/(h.g-cat)), (b) TPO spectra of freshly reduced and spent catalyst under 1 vol.% O_2/He flow.

Absence of coke formation was also confirmed by temperature programmed oxidation tests. Figure 4.9b shows the TPO profile of the freshly reduced and spent Pt-Ni/δ-Al_2O_3 catalyst, in terms of normalized O_2 intensity (concentration) change at the effluent, under a 1 vol.% O_2/He flow with a heating rate of 5 K/min in the temperature range of 300-800 K. It should be noted that there were no distinctive peaks, i.e. combustion products (CO_2 and/or CO) in the tested temperature range as well (not shown); during the tests, the change in O_2 concentration, and in CO_2 and CO concentrations analyzed by MS were insignificant.

The SEM-EDX mapping image of the WGS catalyst shows well dispersed metal particles, Au and Re, on the freshly reduced bimetallic 2wt.%Au-1wt.%Re/ZrO_2 catalyst sample (Figure 4.10). The crystalline phases of Au and Re were not detected by XRD confirming high dispersion of both metals yielding orderly clusters having size less than the detection limit of the instrument (Figure 4.11).

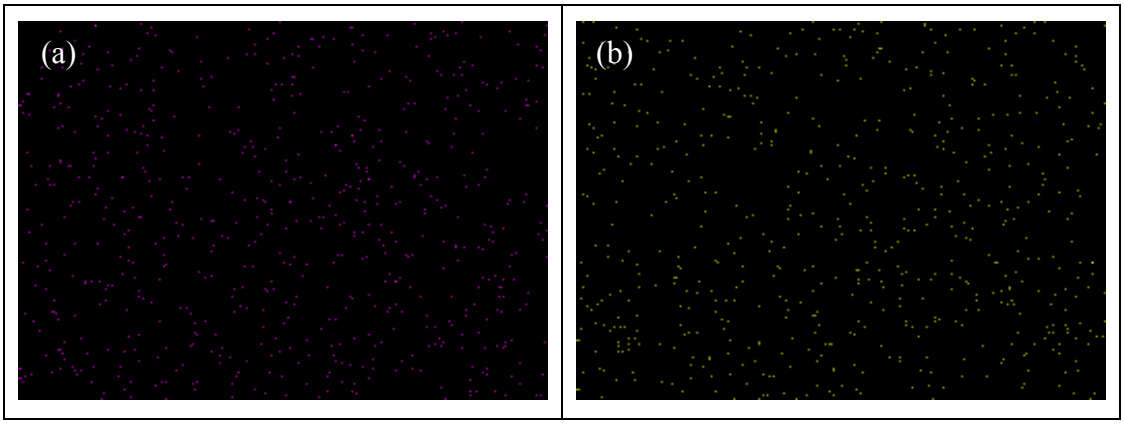

Figure 4.10. Mapping of freshly reduced 2wt.%Au-1wt.%Re/ZrO_2 WGS catalyst sample; (a) Au, (b) Re.

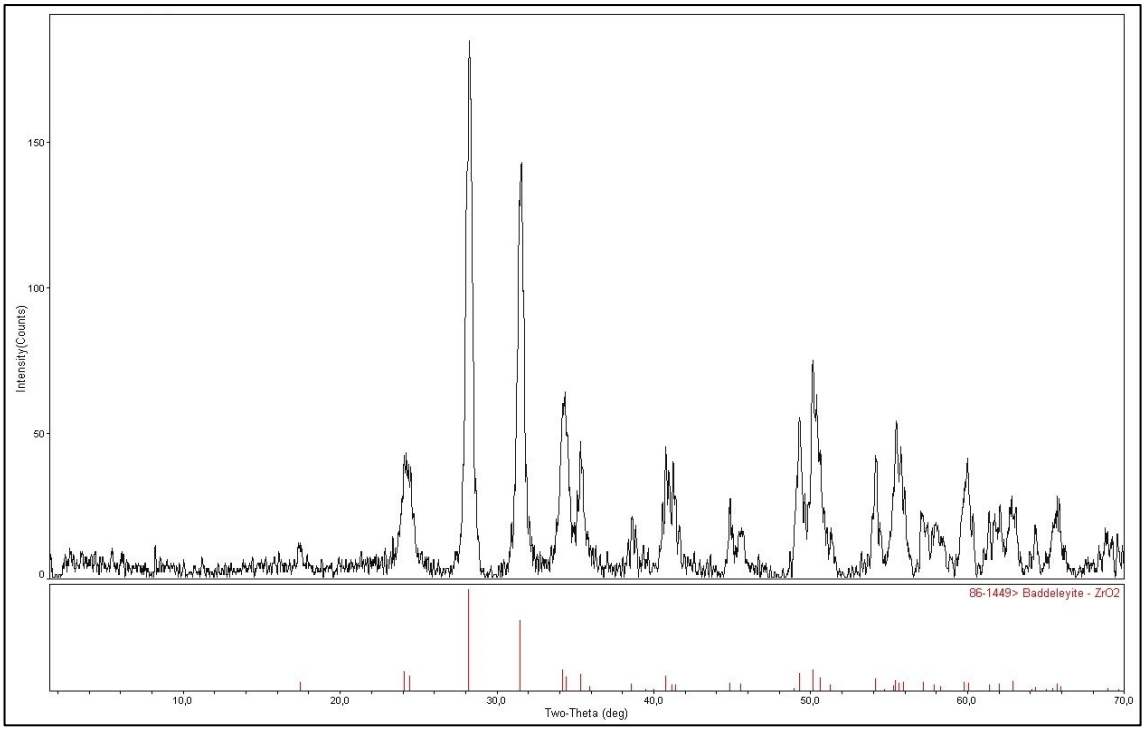

Figure 4.11. XRD profile of freshly reduced 2wt.%Au-1wt.%Re/ZrO_2 WGS sample.

4.2. Steady State Performance Analysis of Propane OSR, Serial OSR-WGS, OSR-PROX and OSR-WGS-PROX Reactors

The aim of this section is to determine the reaction conditions, i.e. propane OSR feed composition and the temperature combinations of OSR, WGS and PROX reactors, yielding a product stream having the highest H_2 concentration and the lowest CO, CH_4 and CO_2 concentrations in serial operations.

In this context, trimetallic WGS catalyst, Pt-Re-V/CeO_2, that had been determined having higher performance than Au-Re/ZrO_2, was utilized in the serial tests aiming to determine both its real performance under the flow of the OSR outlet as the feed, and its effect on overall performance of the serial OSR-WGS and OSR-WGS-PROX systems. In the tests, the effect of a larger S/C feed ratio range, 2.25-6, than that studied in the previous section, on the performance of individual OSR and of serial reactors was investigated, and the performance of OSR-PROX system, aiming to observe the possibility of using a simpler serial system that benefits from implicit HTS activity of the OSR catalyst, was analyzed and discussed. Additionally, the effect of absence and presence of additional oxygen stream fed to the PROX reactor in the performance of serial OSR-WGS-PROX system was also studied.

4.2.1. Individual OSR Reaction Tests for Steady State Performance Analysis

In propane OSR reaction over Pt-Ni catalyst, the desired reactions, such as CO and/or CO_2 producing SR, total and/or partial oxidation of propane and WGS reactions occur as mentioned above in Section 4.1.1. However, CO_2 and CO can undergo undesired methanation reactions under certain circumstances. Owing to the strong exothermic nature of the methanation reactions, these equilibrium reactions are thermodynamically favored at relatively low temperatures. Thus, conducting OSR at elevated temperatures or at higher steam to carbon ratios in the feed stream of the OSR unit shifts the equilibrium of methanation reactions in reverse direction and suppresses their extents.

4.2.1.1. Effect of Temperature. In OSR reactor, temperature plays an essential role in the extents of highly endothermic SR reactions (CO and/or CO_2 producing SR), highly exothermic methanation (CO_2 and/or CO methanation) and oxidation reactions (TOX and/or

POX) and also mildly exothermic WGS reaction (Table 4.1). Dry based inert free steady state H_2, CO, CH_4 and CO_2 concentrations at OSR outlet as a function of temperature for different S/C feed ratios in propane OSR are given in Figures 4.12, 4.13, 4.14 and 4.15, respectively, for the experiments listed in Table 3.6. In the determination of temperature levels of OSR reaction, first thermodynamic equilibrium calculations were performed by using HSC Chemistry 5.11 software over 473-1073 K temperature interval; the results of the thermodynamic study are discussed in Section 4.2.1.3. Based on thermodynamic calculations, four temperature levels, 623 K, 673 K, 723 K and 773 K, were used as OSR reactor temperature aiming to have relatively high H_2 concentrations and low CO, CH_4 and CO_2 concentrations. Significantly low, ppm level, C_3H_8 and O_2 concentrations in the product stream indicated almost 100% conversions of C_3H_8 and O_2 in the OSR reactor. Therefore, similar to Section 4.1, C_3H_8 and O_2 concentrations are not given in presenting the results of the performance tests.

The beneficial effect of temperature increase can be clearly seen as increased steady state H_2 concentrations, and decreased CH_4 and CO_2 concentrations given in Figures 4.12, 4.14 and 4.15, respectively, due to the increased extents of CO and/or CO_2 producing SRs and decreased CO_2 and/or CO methanation and TOX and/or POX reactions. Increasing OSR temperature from 623 K to 773 K increased dry based inert free steady state H_2 concentration from 41% up to 57% at S/C ratio of 6 (Table 3.6, A4 and A16). It should be noted that the highest achieved H_2 concentration in individual OSR reaction tests mentioned before in Section 4.1.1 was 51.2% at 723 K for Exp. O16 (Table 3.4) (Başar *et al.*, 2016), which was shown as a red straight line in Figure 4.12. At 723 K and 773 K for S/C of 5 and 6, higher H_2 concentrations were achieved for Exp. A11-12 and A15-16 (see Table 3.6).

Another reason for the increase in CO concentration and the decrease in CO_2 concentration might be the shift of WGS reaction in reverse direction at elevated temperatures, which was an expected trend from thermodynamic calculations given in Section 4.2.1.3. The effect of temperature on CO_2 outlet concentration change (Figure 4.15) were much limited than on the other species, however it had a positive impact as a decreased CO_2 concentrations down to 26% (Table 3.6, A16). Conducting OSR at 773 K resulted in relatively higher CO concentrations (~3-4%, Table 3.6, A13-14), therefore it would be more effective to perform the OSR reaction at lower temperatures, i.e. 673 K or 723 K (Figure

4.13). Methane formation can be halved by increasing the OSR temperature from 623 K up to 773 K. Even in dry based inert free form, CH_4 concentrations as low as 14% were obtained (Table 3.6, A16).

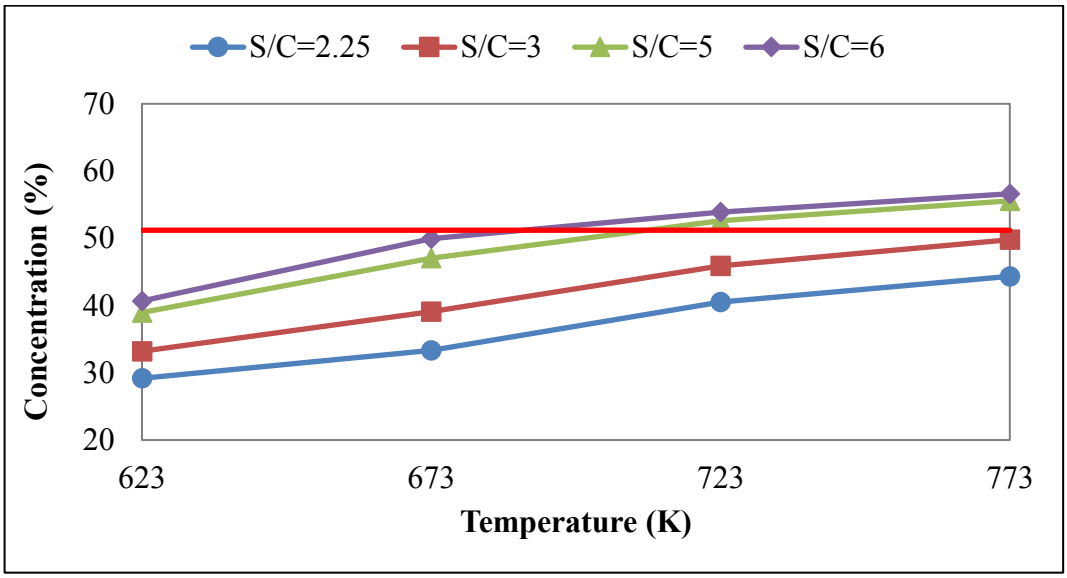

Figure 4.12. Dry based inert free steady state H_2 concentrations as a function of temperature at different S/C ratios in propane OSR (Table 3.6, A1-16).

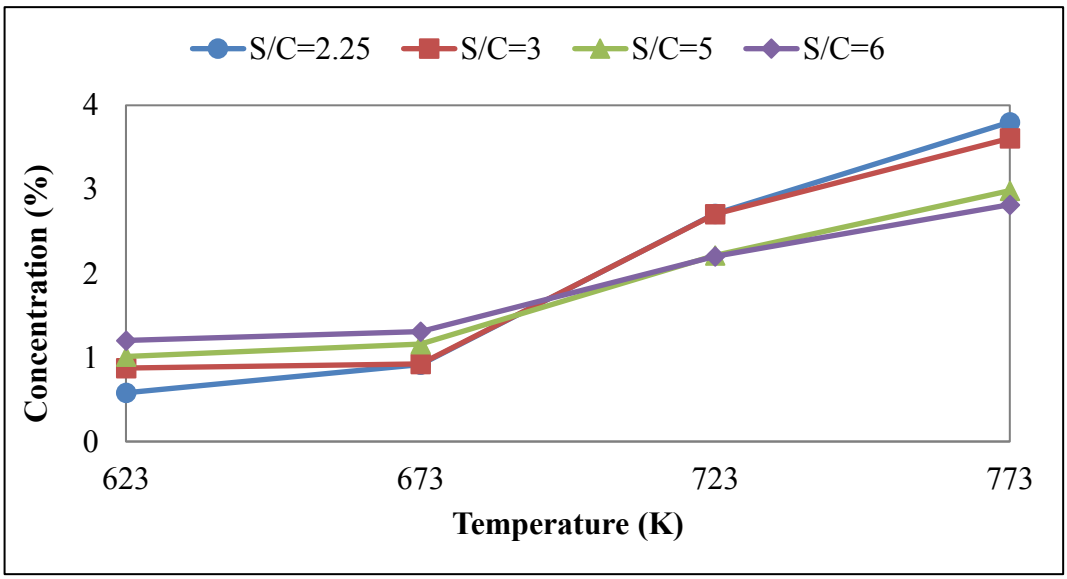

Figure 4.13. Dry based inert free steady state CO concentrations as a function of temperature at different S/C ratios in propane OSR (Table 3.6, A1-16).

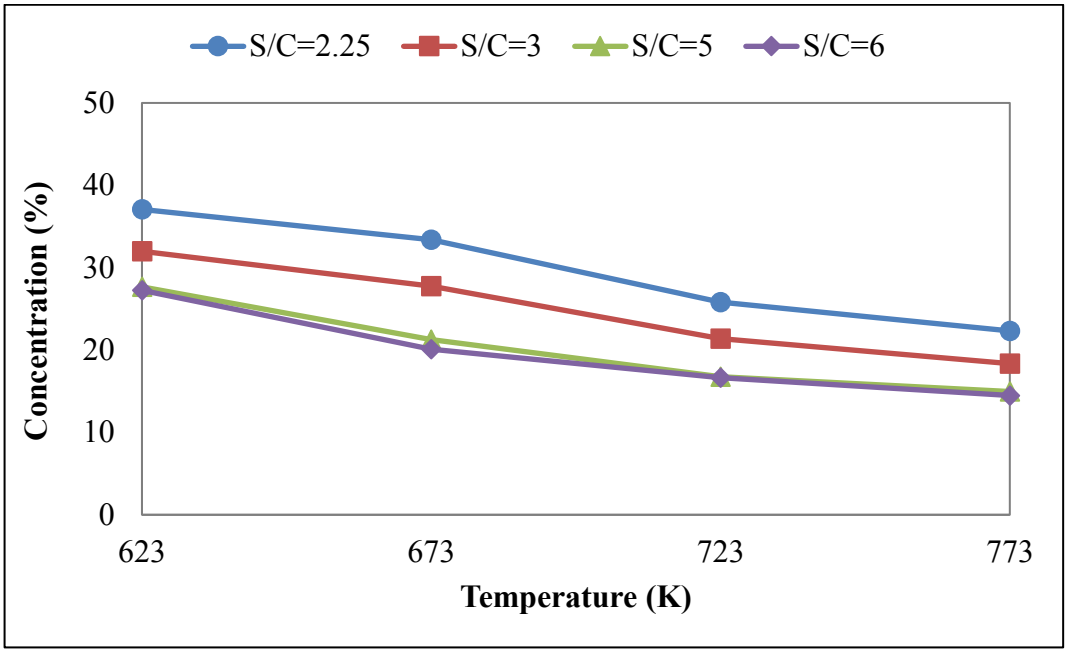

Figure 4.14. Dry based inert free steady state CH_4 concentrations as a function of temperature at different S/C ratios in propane OSR (Table 3.6, A1-16).

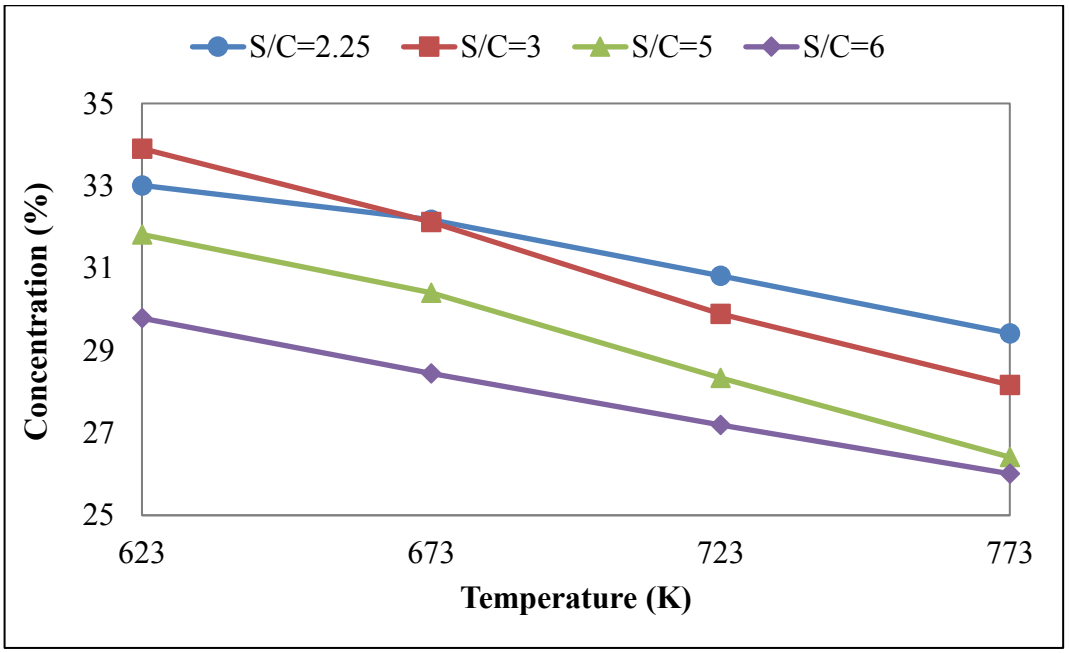

Figure 4.15. Dry based inert free steady state CO_2 concentrations as a function of temperature for different S/C ratios in propane OSR (Table 3.6, A1-16).

4.2.1.2. Effect of Steam to Carbon Ratio. Steam plays a vital role in fuel processing reactions owing to the fact that it is one of the species both used as a reactant and produced as an intermediate product. In order to investigate the contribution of additional steam fed to the OSR unit, S/C ratio was increased from 2.25 to 3, 5 and 6 via varying the steam concentration of the feed gas mixture while O/C ratio in the feed was kept fixed at 0.74 (Table 3.6). The extents of CO and/or CO_2 producing SR and WGS reactions, which use steam as the reactant and thereby contribute mostly to the H_2 production, are directly related to the amount of steam fed to the OSR unit. For this reason, the increase in steam flow rate, i.e. S/C ratio in the feed stream (2.25→6), led to increased steady state H_2 concentrations (Figure 4.12) and decreased CO (Figure 4.13) and CO_2 (Figure 4.15) concentrations in the product stream. Increased S/C feed ratio also suppressed methanation activity of the catalyst and resulted in a 30-35% decrease in CH_4 concentrations at 723 K (Figure 4.14). As shown in Figure 4.12, increasing S/C ratio up to 6 resulted in 20% increase of the H_2 concentration level at S/C feed ratio of 2.25. The highest achieved H_2 concentration was ~57% at S/C ratio of 6 (Table 3.6, A16) as mentioned before in Section 4.2.1.1. Figure 4.13 indicates that there is a trend change in CO outlet concentration in response to changes in S/C ratio at ca. 693 K. Higher S/C ratios in OSR feed led to increased CO concentrations at lower temperatures, while it leads to suppressed CO concentrations at elevated temperatures. One possible explanation for this might be the increase in the extent of highly endothermic CO producing SR reaction at elevated temperatures; simultaneous use of higher S/C feed ratios (i.e. 5 and 6) and high temperatures superposably contributes SR yielding high CO production rates than the secondary reactions. There wasn't also very remarkable difference between the results of the tests conducted with S/C ratio of 5 and 6 (Figure 4.12 and 4.16), therefore keeping S/C ratio at 5 would be an optimum condition in future studies.

Simultaneous use of high temperature and S/C feed ratio led to increased H_2, decreased CH_4 and CO_2 concentrations, and relatively lower CO concentrations in OSR product, which are in accordance with the fuel processing targets (Table 4.3). The highest achieved H_2 concentration was ~57% for S/C ratio of 6 at 723 K (Table 3.6, A16), while the lowest CO concentration was 0.58% at S/C ratio of 2.25 at 623 K. An overall evaluation of the results, through additionally considering the high rates at high temperatures, pointing out 723 K and 5 as the optimal combination of temperature and S/C feed ratio, respectively.

Table 4.3. Response of OSR unit with respect to temperature and steam to carbon ratio.

Parameter	Type of Change	H_2	CO	CH_4	CO_2
Temperature	Increase	Increase	Increase	Decrease	Decrease
S/C ratio	Increase	Increase	Decrease	Decrease	Decrease

4.2.1.3. Thermodynamic Validation of the Experimental Results. In this section, a comprehensive thermodynamic analysis aiming to find equilibrium compositions of propane OSR reactants and products was carried out by utilizing HSC Chemistry 5.11 software. The equilibrium compositions of all eight species (C_3H_8, O_2, H_2O, He, H_2, CO, CH_4 and CO_2) involved in the reactions listed in Table 4.1 were calculated at a temperature range of 473 K-1073 K at S/C feed ratio values of 2.25, 3, 5 and 6.

Dry based inert free equilibrium concentrations as a function of temperature and S/C ratio in propane OSR predicted by thermodynamic calculations for H_2 (Figure 4.16), CO (Figure 4.17), CH_4 (Figure 4.18) and CO_2 (Figure 4.19) species are given below. The boundaries of the temperature range used in the current experimental study, 623-773 K, were indicated by vertical red lines. Equilibrium H_2 concentration profiles resembling S-shaped curves are given in Figure 4.16; according to the calculations, H_2 concentration reaches a maximum value of ca. 71% at temperatures higher than 873 K independent of S/C ratio. The highest equilibrium H_2 concentration at 773 K and S/C ratio of 6 was calculated as 67%. Equilibrium CO concentration profiles show gradual increase at temperatures higher than 773 K, and the effect of S/C ratio on CO concentration is more distinct that temperature level. The highest equilibrium CO concentration is at 773 K for S/C ratio of 2.25, and was calculated as 3.74% (Figure 4.17).

The negative effect of elevated temperatures and high S/C ratios on the undesired by-product CH_4 can be clearly seen in Figure 4.18. The results indicated that it is possible to decrease CH_4 concentration down to 1% at temperatures higher than 873 K. In agreement with the experimental results in Sections 4.2.1.1 and 4.2.1.2, elevated temperatures and higher S/C ratios favored lower CO_2 production up to 773 K. However, the equilibrium CO_2 concentration profiles have an inflection point at 773 K, as given in Figure 4.19, and at higher

temperatures, high S/C ratio becomes comparatively beneficial for CO_2; the lowest equilibrium CO_2 concentration at 773 K for all S/C ratios was calculated as ~26.7%.

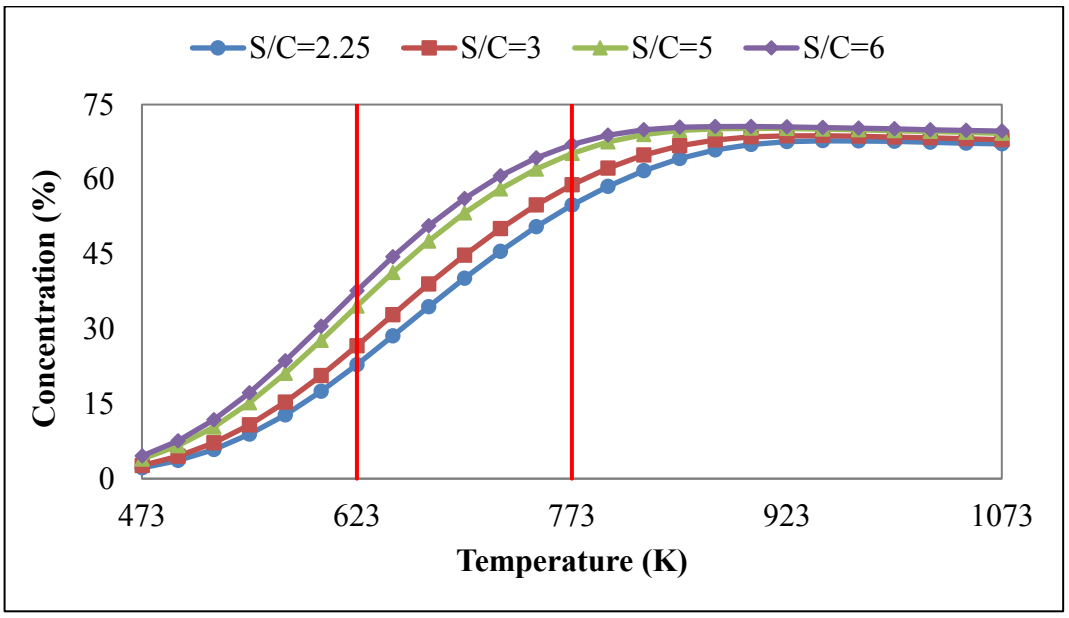

Figure 4.16. Dry based inert free equilibrium H_2 concentrations as a function of temperature and S/C ratio in propane OSR predicted by thermodynamic calculations.

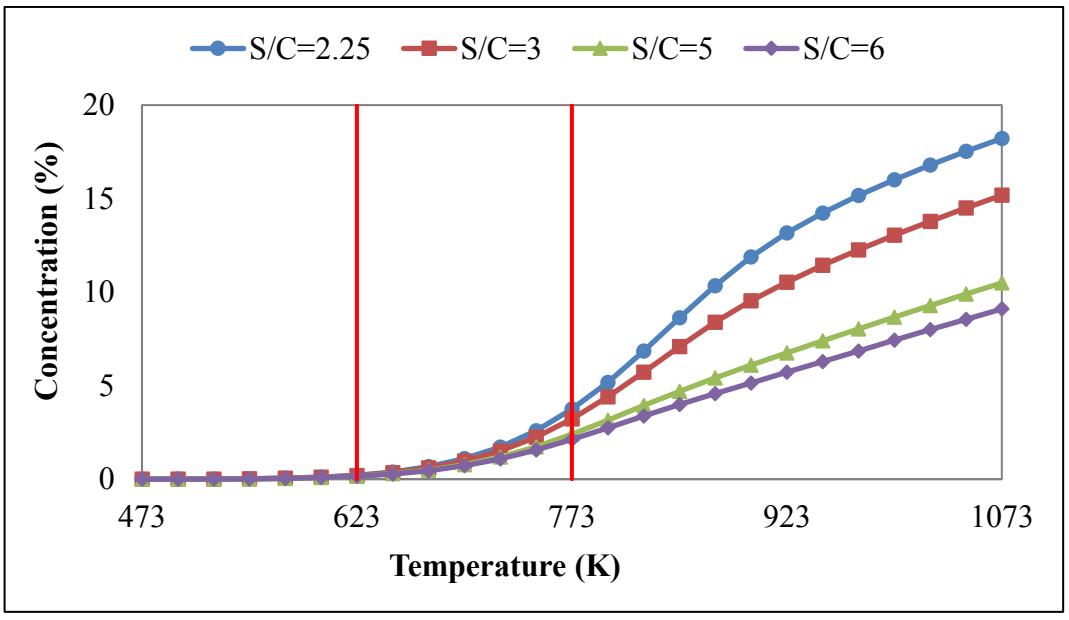

Figure 4.17. Dry based inert free equilibrium CO concentrations as a function of temperature and S/C ratio in propane OSR predicted by thermodynamic calculations.

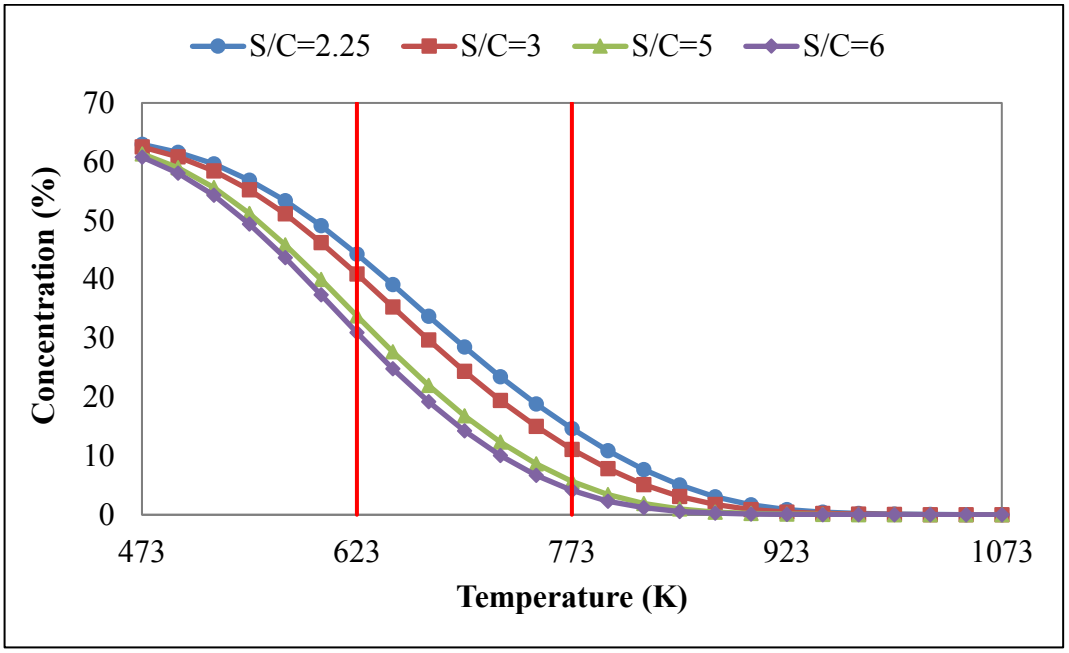

Figure 4.18. Dry based inert free equilibrium CH_4 concentrations as a function of temperature and S/C ratio in propane OSR predicted by thermodynamic calculations.

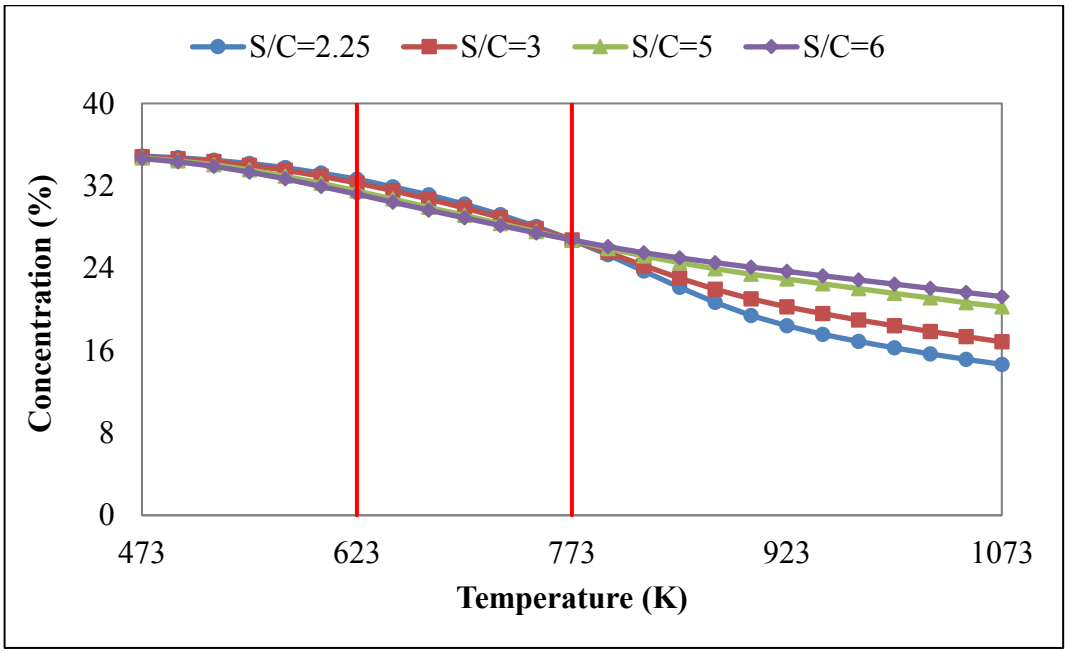

Figure 4.19. Dry based inert free equilibrium CO_2 concentrations as a function of temperature and S/C ratio in propane OSR predicted by thermodynamic calculations.

It should be noted that the thermodynamic calculations gave the results as equilibrium concentrations, i.e. as if the reaction would go to infinity. On the other hand, the experimental concentrations were measured for a finite residence time (W/F) value of 1.5 mg-cat.min/ml, which may result in a few inconsistencies between the thermodynamic calculations and experimental results. One another explanation would be the fact that some species have been involved in the reactions as both reactants and products, and simultaneous consumption and/or production might change the concentration of the species at the time of the data were measured. Additionally, the possibility of having reactions in addition to the ones listed in Table 4.1.

Comparison of the thermodynamic equilibrium calculations results with the experimental results revealed that the Gibbs free energy minimization method is an effective tool for understanding the reactions occurring in OSR unit and predicting the effects of the parameters such as temperature and feed composition on the performance of the catalysts for the given operating conditions. It can be concluded that the experimental product distributions and trends (Table 4.3) are consistent with the results of the thermodynamic calculations.

4.2.2. Serial OSR-WGS Reaction Tests for Steady State Performance Analysis

In the serial propane OSR-WGS performance tests, the S/C ratio of the feed stream into the OSR reactor (2.25, 3, 5 and 6) and temperature combinations of the OSR-WGS reactors (723-523 K, 723-573 K and 723-623 K) were considered as the experimental parameters. The feed composition and temperature of the OSR reactor were used as the same as what had been applied in individual steady state propane OSR performance tests (Section 4.2.1). These serial reaction tests were carried out aiming to define the benefit of combining OSR with WGS. In the current tests, Au-Re/ZrO2 previously used in OSR-WGS tests explained in Section 4.1 was replaced by a recently designed and developed trimetallic WGS catalyst, Pt-Re-V/CeO_2. The tests performed by our group (Özer, 2016; Kesim 2016) showed that CO conversions up to 65% were obtained in the catalytic performance tests were obtained over Pt-Re-V/CeO_2 for real feed streams containing 2-5% CO (wet basis with inert) and steam to carbon ratios of 6.7 and 16.2 over the temperature range of 573-673 K, (Özer, 2016; Kesim, 2016).

A comparison of the results of the serial OSR-WGS tests B1-4, B5-8 and B9-12 (Table 3.7) with those of the corresponding individual OSR experiments A9-12 (Table 3.6) conducted at the same OSR temperature and feed compositions is presented in Figure 4.20. It is clear from the results that combining OSR with WGS is an effective way to decrease the CO concentration, which was ca. 2.7% at the exit of the individual OSR unit, down to ca. 0.57% and 0.90% at the exit of OSR-WGS serial reactors for which WGS was conducted at 523 K and 623 K, respectively. For all tested S/C ratio of the OSR inlet and OSR-WGS temperature combinations, CO concentrations lower than those measured in individual OSR tests conducted at 723 K were obtained. The solid red line in Figure 4.29 demonstrates the minimum CO concentration value (1.62%) obtained in the previous serial OSR-WGS test conducted under S25 conditions in Section 4.1.2 (Table 3.2), where Au-Re/ZrO_2 was used as the WGS catalyst (Başar *et al*., 2016). An important conclusion drawn from these findings is that in the serial OSR-WGS tests, the new WGS catalyst, Pt-Re-V/CeO_2, led to higher CO conversion values (55-60%) than those obtained under the same conditions where Au-Re/ZrO_2 had been used as the WGS catalyst (45-50%).

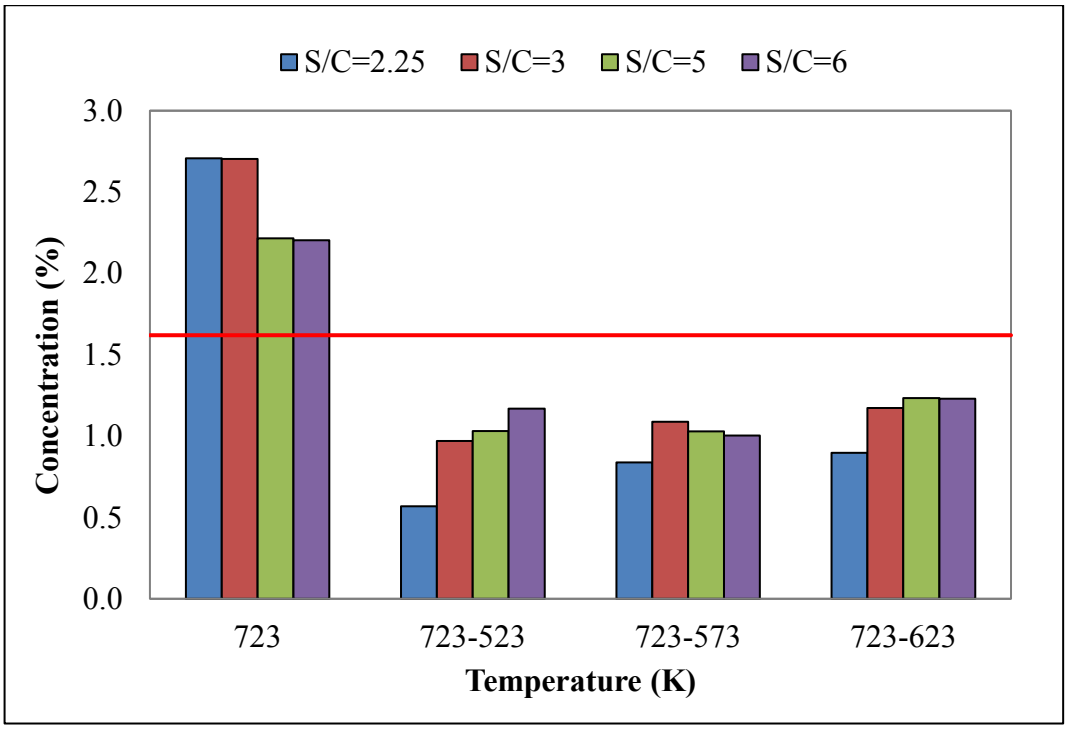

Figure 4.20. Steady state CO concentrations at the OSR and WGS outlets as a function of OSR and OSR-WGS temperature combination and S/C ratio in propane OSR (Table 3.6, A9-12, Table 3.7, B1-12).

WGS reaction has 1:1 overall stoichiometry and is assumed to proceed with no significant side reaction, as mentioned in Section 4.1.2. Conversions around 60% over WGS catalyst for such low CO feed concentrations, 1-2%, resulted in distinctive differences in CO trends (Figure 4.20). However, the observed changes in H_2 and CO_2 concentrations in WGS product were small, ca. 1%, for all WGS temperature levels (Figure 4.21). Elevated WGS temperatures led to decreased CO conversions (Figure 4.20) due to the exothermic nature of the WGS reaction, whilst the effect of WGS temperature on H_2 and CO_2 concentrations were better observed at higher S/C ratios (5-6). The increase of H_2 concentration and activity with increased S/C ratios at elevated temperatures can be explained by the shift of WGS reaction in forward direction in the presence of high steam. Both CO_2 and CH_4 concentrations decreased with increased temperature at higher S/C ratios. Similar trends in response of OSR-WGS unit with respect to temperature and S/C ratio were observed as in the individual OSR tests, which were summarized in Table 4.3. When the results of OSR-WGS serial operations conducted for different OSR-WGS temperature combinations were comparatively analyzed, the optimum combination would be 723-623 K case, for which higher H_2 concentrations (~53%) and comparatively low CO concentrations (~0.9%) were obtained (Table 3.7, B1-12, Figure 4.21) with no methanation activity.

WGS reaction is a mildly exothermic and reversible, i.e. equilibrium-limited, reaction that exhibits decreasing CO conversion with increasing temperature. Temperature dependence of equilibrium conversions of CO predicted by thermodynamic calculations were shown in Figure 4.22. In calculations, the real OSR outlet compositions obtained in experiments A9-12 (Table 3.6) were used as WGS feed including CO, CO_2, H_2, H_2O, He and also CH_4. Though propane and oxygen concentrations were in ppm levels, t they were also included in the thermodynamic calculations. The minimum equilibrium conversion was 93.3% in the temperature range of the current study, which was shown between the red lines in Figure 4.22. A gradual decrease in CO conversion was observed at temperatures higher than 673 K. Negative CO conversions were obtained at temperatures higher than 723 K (not shown), which was caused by the RWGS. The increase of S/C ratio in the feed stream of OSR resulted in WGS feed having high steam content and, consequently, higher WGS equilibrium conversions at elevated temperatures due to suppressed RWGS. Figure 4.22 clearly showed the thermodynamically favorable temperature range and maximum attainable CO conversion values. The attained experimental CO conversions are in 55-60%

range remained below the thermodynamic equilibrium conversion within the entire temperature and GHSV range.

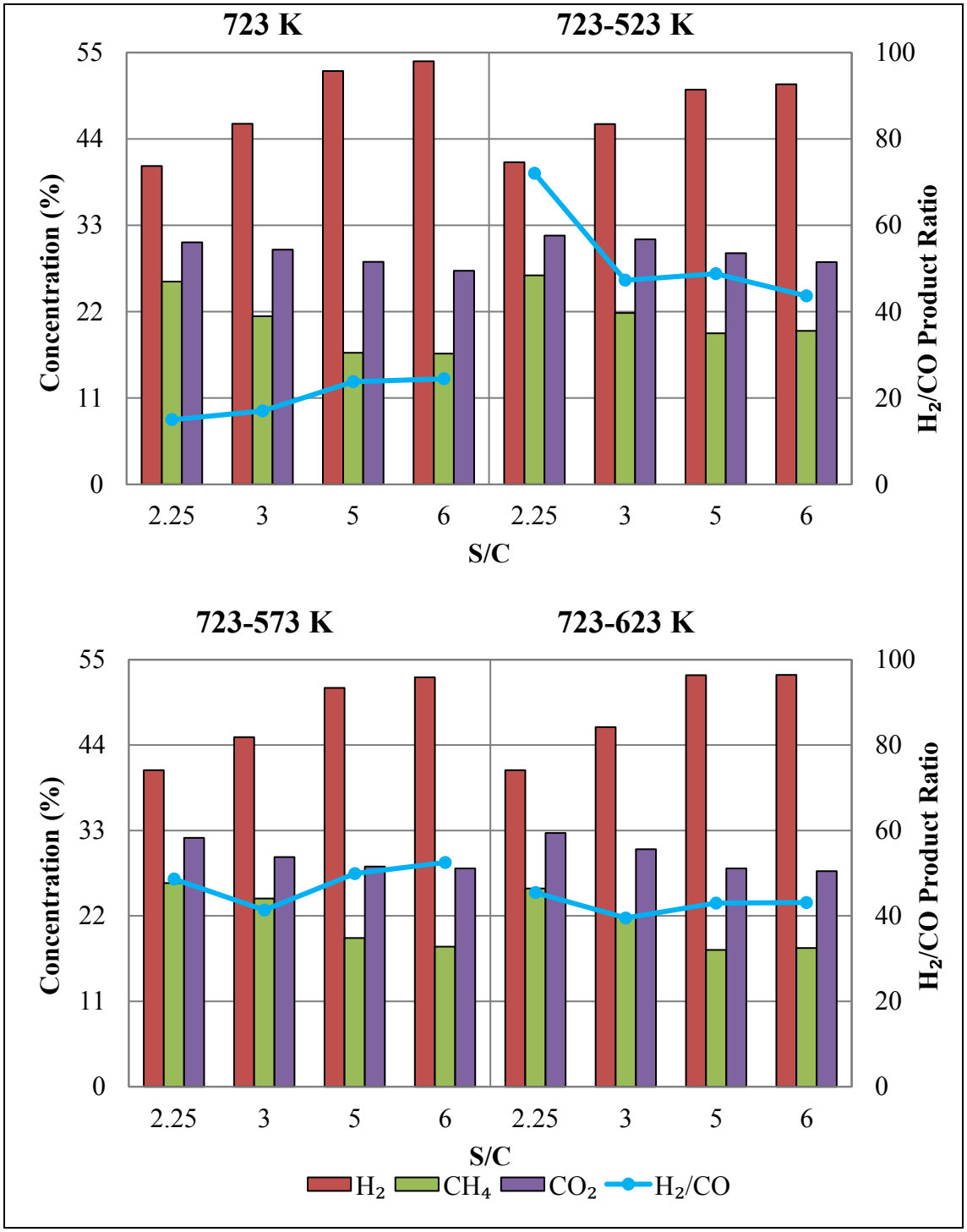

Figure 4.21. Steady state H_2, CH_4 and CO_2 concentrations and H_2/CO product ratio at the OSR and WGS outlets as a function of OSR and OSR-WGS temperature combination and S/C ratio in propane OSR (Table 3.6, A9-12, Table 3.7, B1-12).

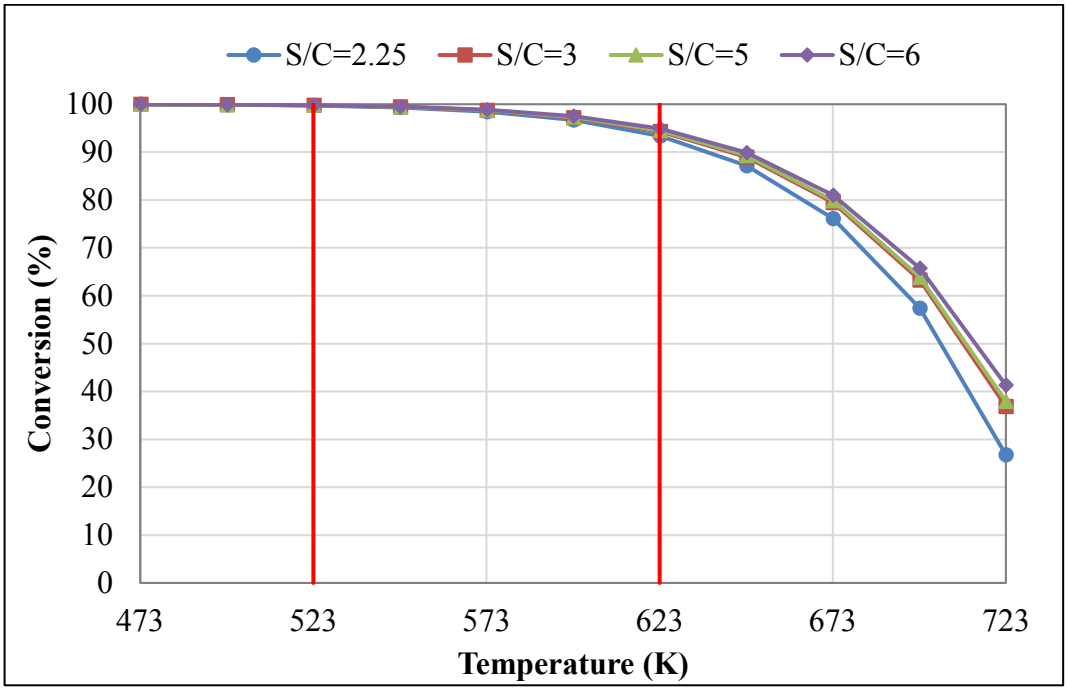

Figure 4.22. Equilibrium conversion of CO predicted by thermodynamic calculations for real compositions of OSR exit streams (Table 3.6, A9-12).

4.2.3. Serial OSR-PROX Reaction Tests for Steady State Performance Analysis

The results of our previous studies (Çağlayan *et al*., 2005a; Gökaliler *et al*., 2012) and the current study clearly reveal HTS activity of the OSR catalyst for the above tested temperature and S/C feed ratio ranges leading very low CO concentrations in the OSR product. Çağlayan et al. studied PROX of CO over Pt-Sn/AC catalyst through tests for 383-408 K range under the flow of ideal and realistic feeds having 1% CO and O_2/CO ratios in 1-1.25 range (Çağlayan *et al*., 2011b), and reached CO conversions ca. 97%. On the basis of those findings, this part of the current study is devoted to find out whether the use of a very simple, two reactor OSR-PROX system has a potential to be used in CO-free hydrogen production from propane. In the tests, the feed composition and temperature of the OSR reactor were used as the same as what had been applied in individual steady state propane OSR performance tests (Table 3.6, A10), and the additional oxygen flow rate fed to the PROX reactor (0, 0.5, 1, 2 and 4) and temperature combinations of OSR-PROX reactors (723-383 K and 723-388 K) were considered as the experimental parameters in accordance with Çağlayan's study.

Steady state H_2 and CO concentrations and H_2/CO product ratio at the PROX outlet as a function of additional O_2 flow rate fed to the PROX reactor for OSR-PROX temperature combination 723 K-383 K were given in Figure 4.23. With a starting value of ~2.7% CO, feeding an additional O_2 stream of 4 ml/min clearly decreased CO concentration to one third of its initial value (~0.9%) and increased H_2/CO product ratio up to 55 (Table 3.8, C5). One important finding was that as the additional O_2 flow rate was increased, H_2 concentration was decreased from ~55% down to ~47% due to H_2 oxidation side reaction. However, the increase H_2/CO product ratio can be explained by the fact that the rate of CO oxidation was greater than the rate of H_2 oxidation side reaction in the PROX unit (Figure 4.23).

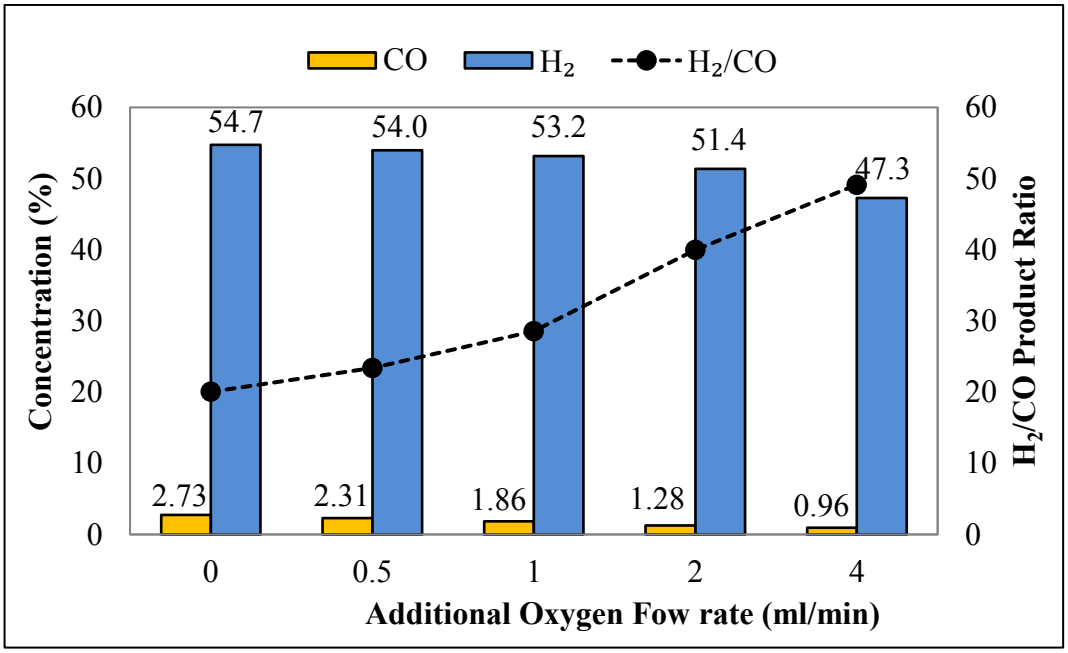

Figure 4.23. Steady state H_2 and CO concentrations and H_2/CO product ratio at the PROX outlet as a function of additional O_2 flow rate fed to the PROX reactor (T_{OSR}=723 K, T_{PROX}=383 K, S/C=3, Table 3.8, C1-5).

Dry based inert free steady state H_2 and CO concentrations as a function of temperature at different S/C feed ratios in individual propane OSR reactions tests were given before in Figures 4.12 and 4.13 in Section 4.2.1.1. The maximum achieved H_2 concentration for S/C feed ratio of 3 at 723 K was ~46% and minimum CO concentration obtained was 2.7% for the same operating and feed conditions, which were given in the first columns in Figures 4.24 and 4.25, respectively, as the reference CO levels.

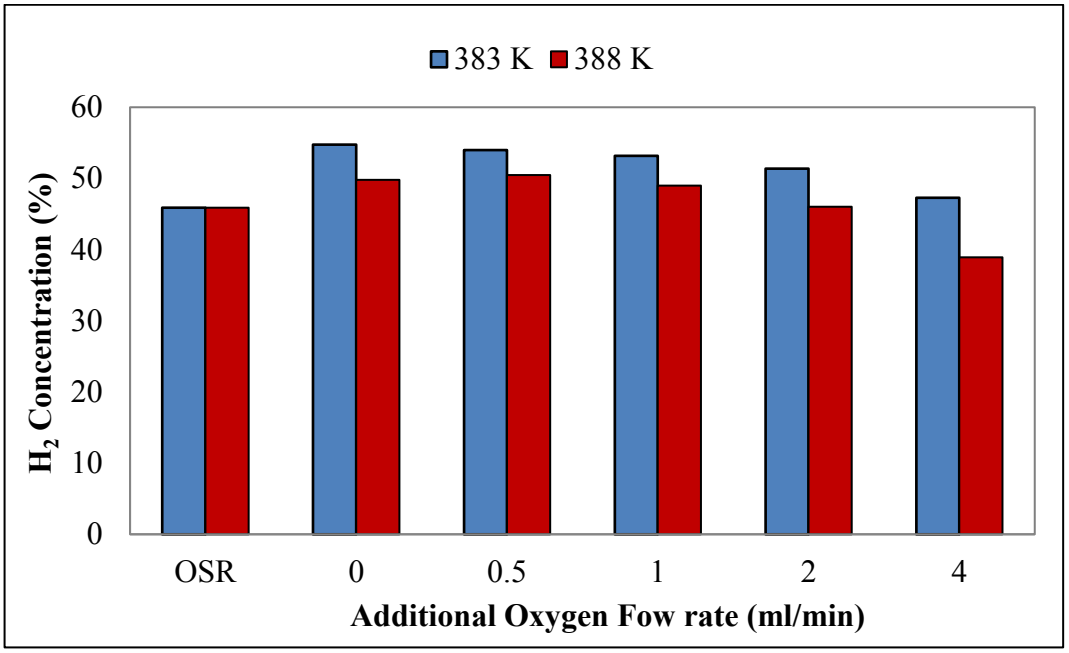

Figure 4.24. Steady state H_2 concentrations at the OSR and PROX outlets as a function of additional O_2 flow rate fed to the PROX reactor and PROX operating temperature (Table 3.6, A10, Table 3.8, C1-10).

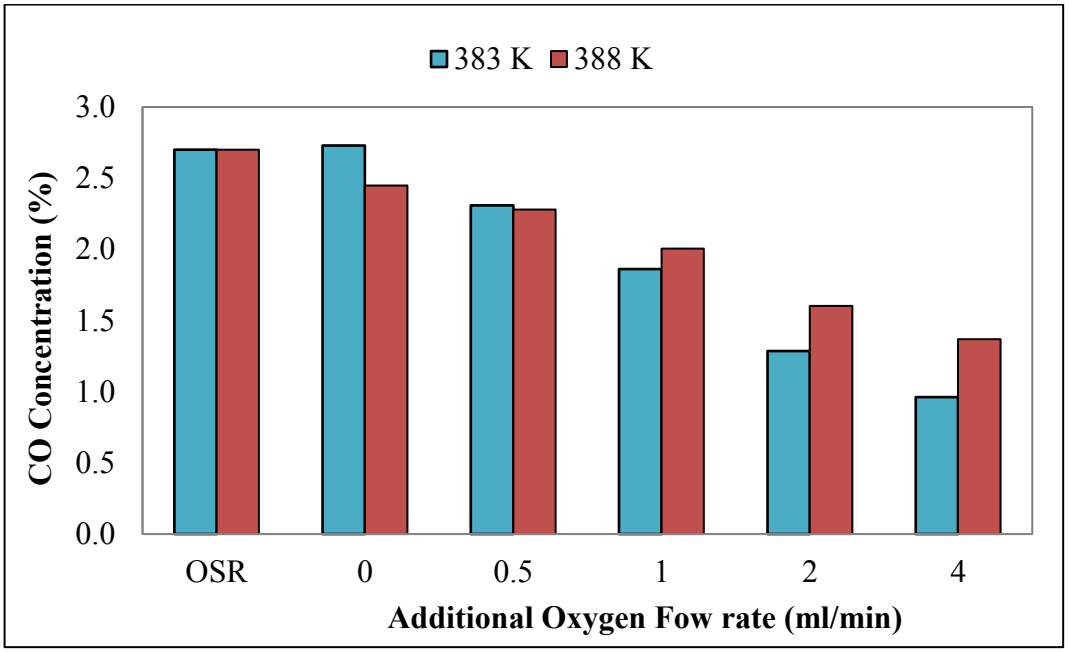

Figure 4.25. Steady state CO concentrations at the OSR and PROX outlets as a function of additional O_2 flow rate fed to the PROX reactor and PROX operating temperature (Table 3.6, A10, Table 3.8, C1-10).

Figure 4.24 shows the steady state H_2 concentration at the PROX outlet as functions of additional oxygen flow rate and PROX temperature. For the tested range of oxygen flow rate (0-4 ml/min), higher H_2 concentrations were obtained at PROX outlet when PROX conducted at lower temperature (383 K). Another positive outcome was that the serial addition of PROX reactor to OSR reactor definitely increased H_2 concentration at the outlet even in case of no additional oxygen stream. Due to the exothermic nature of PROX reaction, decreasing conversions with increasing temperature can be better seen at additional oxygen flow rates of 1-4 ml/min; for example, CO concentration as low as 0.96% (dry based inert free) was obtained for 4 ml/min oxygen addition. It should be noted that PROX reaction was performed at temperatures higher than 383 K in order to guarantee complete vaporization of steam in the feed mixture and to avoid condensation of water vapor in PROX reactor in real performance tests. The flow rates of additional oxygen stream and the PROX temperatures were selected such as to suppress unwanted oxidation of high concentration hydrogen present in the PROX feed. CO concentrations as low as ca. 0.9% obtained in serial OSR-PROX tests seems promising considering the CO concentrations (min 0.5%) obtained in the serial OSR-WGS performance tests.

4.2.4. Serial OSR-WGS-PROX Reaction Tests for Steady State Performance Analysis

In propane fuel processing through serial OSR-WGS-PROX, the performance of the serial process is analyzed in the tests for which the S/C ratio of the feed stream into the OSR reactor (2.25, 3, 5 and 6) and the additional oxygen flow rate fed to the PROX reactor (0, 0.5, 1, 2 and 4) were considered as the experimental parameters. The feed compositions and temperature of the OSR (723 K) and WGS (623 K) reactors were used as the same as what had been applied in individual and serial propane OSR and OSR-WGS performance tests (Table 3.6, A9-12 and Section 4.2.1, Table 3.7, B9-12 and Section 4.2.2). The PROX feed has very high H_2 but very low CO concentrations; thus enhancing CO oxidation while not triggering/supporting H_2 oxidation is of crucial importance. This is the reason why the temperature of the PROX reactor was kept at 383 K, which had been found the optimal temperature for the highest possible PROX selectivity for realistic feed conditions without leading water vapor condensation in PROX reactor and transfer lines. Figure 4.26 represents the dry based inert free concentrations of H_2, CH_4, CO and CO_2 species and H_2/CO product

ratio at the PROX outlet as a function of S/C ratio at the OSR inlet and additional O_2 flow rate fed to the PROX reactor for the experimental conditions given in Table 3.9.

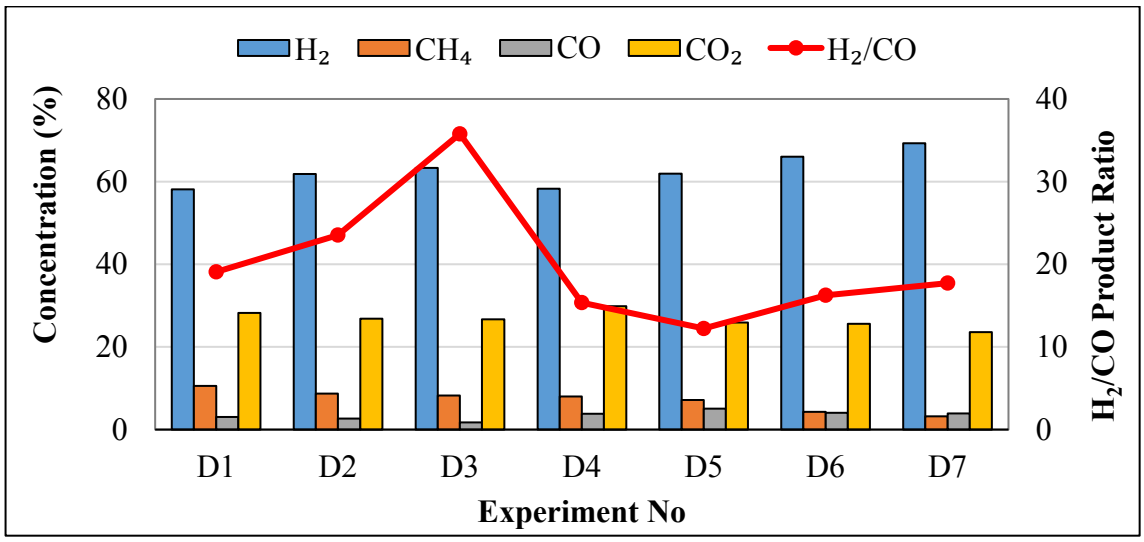

Figure 4.26. Steady state H_2, CH_4, CO and CO_2 concentrations and H_2/CO product ratio at the PROX outlet as a function of S/C ratio at the OSR inlet and additional O_2 flow rate and fed to the PROX reactor (T_{OSR}=723 K, T_{PROX}=383 K, Table 3.9, D1-7).

The results show that increasing S/C ratio at the inlet of the OSR reactor from 2.25 to 5 increased H_2 concentration from 58% up to 63% (D1-3). Addition of steam also suppressed CH_4, CO_2 and CO formations; CO concentration at PROX exit reduced to its half (~1.7%) though CH_4 and CO_2 concentrations decreased slightly. At S/C feed ratio of 5, addition of O_2 to PROX reactor with a flow rate of 4 ml/min (D4) surprisingly increased CO concentration up to ~3.8%, while decreasing CH_4 and H_2 concentrations and increasing CO_2 concentration. In order to handle this situation, additional oxygen flow rate was decreased to 2 ml/min (D5), which resulted in a decrease in CO_2 concentration, but could not prevent the increase in CO concentration. As the next step, oxygen addition to PROX reactor was kept fixed at 2 ml/min, while S/C ratio was increased to 6 (D6); under these conditions, CO concentration decreased 20% down of its former, i.e. D5, value. Keeping S/C ratio at 6 and decreasing O_2 flow rate, D7 conditions, resulted in H_2 concentrations at the PROX outlet as high as ~70%. In these serial tests, CO concentrations higher than the values obtained in OSR-WGS reactions tests were obtained. An interesting finding was much lower CH_4 concentrations obtained in OSR-WGS-PROX (3-10%) tests those obtained in OSR-WGS

tests for the same conditions (18-25%). As a general evaluation, the results indicate that the serial OSR-WGS-PROX fuel processing should involve a recycle stream, and its operating/reaction conditions should be meticulously optimized through using an experimental design procedure, which additionally involves W/F values for all three reactors, and fraction of the PROX outlet sent back and mixes with the fresh OSR feed (i.e. recycle ratio) besides all the experimental parameters used in the current study.

4.3. Steady State Performance Analysis of Methane OSR and Serial OSR-WGS Reactors

Methane OSR over Pt-Ni/δ-Al_2O_3 catalysts had been formerly investigated by our group in several studies for which the effects of metal loadings of the catalyst, C/O_2 ratio in the feed stream and temperature were considered as experimental parameters (Gökaliler, 2012; Erdinç, 2014). As product stream of in those studies had been analyzed by a gas chromatograph, there experienced sensitivity problems in measuring CO concentration in the product stream especially when CO concentration is low, i.e. below 1%. In this section of the current study, both individual methane OSR and serial OSR-WGS performance of the catalysts were investigated. In the tests, 0.2wt.%Pt-10wt.%Ni/δ-Al_2O_3 and 1wt.%Pt-0.5wt.%Re-1wt.%V/CeO_2 were used as the OSR and WGS catalysts, respectively. In the tests, S/C ratio of the OSR feed, and OSR temperature/OSR-WGS temperature combination were used as the experimental parameters. OSR product in individual OSR tests, and WGS product in serial OSR-WGS tests were analyzed on line real time by using a mass spectrometer. In the current study, thermodynamic analysis of the reaction sets of both former (Table 3.10) and current studies (Table 3.11) including different feed compositions and temperatures was also conducted.

Experimental conditions used in the former studies (Gökaliler, 2012; Erdinç, 2014), i.e. steam-to-carbon (S/C) and carbon-to-oxygen (C/O_2) feed ratios, catalyst weight-to-total flow rate ratio (W/F) and corresponding total feed flow rates are given in Table 3.10. The experiments were carried out in a total flow rate range of 133-294 ml/min. In all those performance tests, catalyst weight was 150 mg, and the residence time values (W/F) were between 0.51-1.12 mgcat.min/ml. The C/O_2 feed ratio was varied in 1.50-2.70 range, while S/C feed ratio was kept constant as 3 (Gökaliler, 2012; Erdinç, 2014). Methane conversion

levels and hydrogen production rates for both performance tests and equilibrium conditions were calculated according to Equation 4.1 and 4.2. Since stoichiometry of methane OSR is not 1:1 leading different total flow rates for reactant and product streams, the exit concentrations of other species involved in the reactions were calculated by taking the inert concentration/flow as the reference basis.

$$Conversion\ of\ CH_4\ (\%) = \frac{C_{CH_4,in} - C_{CH_4,out}}{C_{CH_4,in}} \tag{4.1}$$

$$H_2\ production\ rate\ (\mu mol.\ gcat^{-1}.s^{-1}) = \frac{F_{H_2,out}}{W_{catalyst}} \tag{4.2}$$

Table 3.10. Experimental conditions used in formerly conducted individual methane OSR reaction tests (Gökaliler, 2012; Erdinç, 2014).

Set #	Feed Flow rates (ml/min)					Feed Conditions		
	CH_4	**O_2**	**H_2O**	**N_2**	**Total**	**S/C**	**C/O_2**	**W/F (mg-cat.min/ml)**
1	29.8	14.0	89.6	52.6	186.0	3	2.12	0.80
2	21.5	10.1	63.8	38.1	133.5	3	2.12	1.12
3	40.1	27.4	123.5	102.8	293.8	3	1.50	0.51
4	51.0	18.9	152.1	71.1	293.1	3	2.70	0.51
5	47.1	22.2	139.8	83.5	292.6	3	2.12	0.51

In order to determine the best experimental conditions for the new performance tests, first the thermodynamic trends were determined for the feed flow rates and conditions used in the previous studies (see Table 3.10). Figure 4.27 shows the equilibrium conversions of CH_4 predicted by thermodynamic calculations for those feed conditions for the temperature range of 523-1023 K. It should be noted that as the same feed compositions had been used in Sets 1, 2 and 5 for which the effect of residence time, W/F, on OSR performance had been analyzed, the equilibrium conversion profiles calculated for those sets are overlapped The temperature range used in the former studies (Gökaliler, 2012; Erdinç, 2014) is indicated between the red lines in Figure 4.27; the calculation results showed that Set 3 yields the

highest equilibrium conversions, whereas the conversions predicted for Set 4 were almost half of the conversion levels of Set 3. The results presented by Erdinç for the above mentioned five set of experiments conducted at 723 K (Erdinç, 2014) are consistent with the results of the thermodynamic calculations conducted in the current study; the highest conversion levels was reached under Set 3 conditions, whereas Set 4 yielded the lowest conversions, and the conversion levels obtained for Sets 1, 2 and 5 were very close to each other. Therefore, in the current study "Set 3" was selected as the reference feed composition for methane OSR performance tests; for feed ratios S/C=3 and C/O_2=1.50 (Set 6), which are the same as those used in Set 3, the flow rate of reactant species were arranged for the total flow rate of 100 ml/min, and in Sets 7-9, the total flow rate was only affected by the changes in water vapor and oxygen flow rates for having different S/C and C/O_2 feed ratios, respectively (Table 3.11).

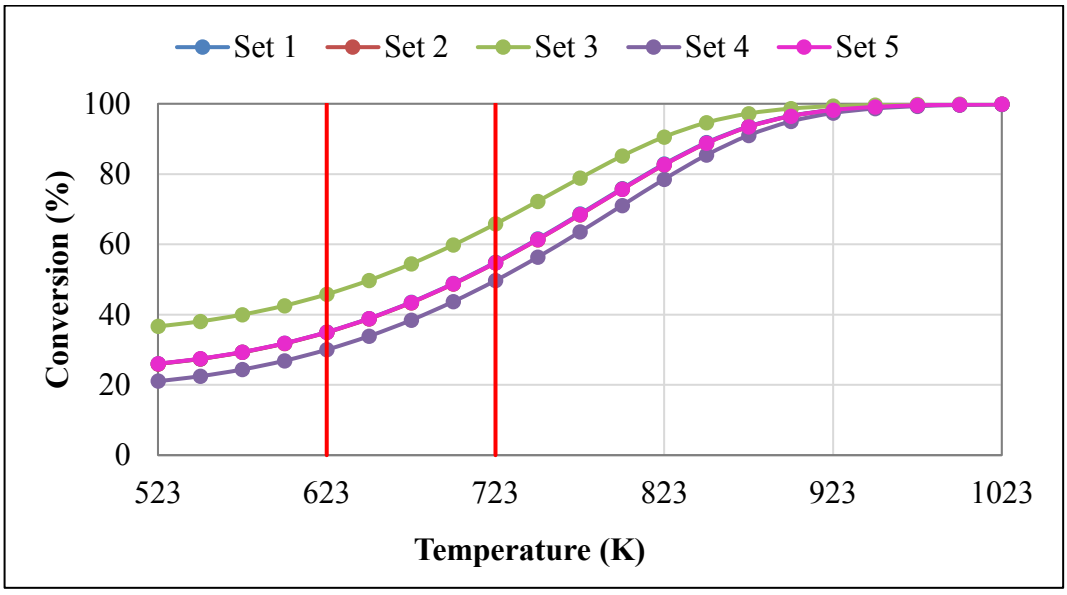

Figure 4.27. Equilibrium conversions of CH_4 in OSR unit predicted by thermodynamic calculations for different feed compositions given in Table 3.10.

Five experiments were conducted for each temperature level of OSR (673 K and 723 K) by using the given feed conditions in Table 3.11; in individual OSR reaction tests, Sets 6, 7 and 8 were used as the experimental conditions, whereas in serial OSR-WGS reaction tests, Sets 8 and 9 conditions were used. Time on stream dry based concentration profiles of the species at the exit of OSR unit for the feed conditions of Set 6 were given in Figure 4.28

for OSR temperature of 723 K. It can be clearly seen that oxygen in the feed stream was completely consumed, however it took approximately 20 minutes to reach the steady state value, which was ppm levels. On the contrary, in propane OSR reaction tests, complete consumptions of propane and oxygen were observed just in seconds after the reaction was started. This situation can be explained by the speed of oxidation reactions. It was clear that methane TOX reaction was slower than that of propane. Compared to propane OSR tests, other species reached their steady state values much more quickly in methane OSR tests.

Table 3.11. Experimental conditions used in individual methane OSR and serial OSR-WGS reaction tests in the current study.

Set #	Feed Flow rates (ml/min)					Feed Conditions		
	CH_4	O_2	H_2O	He	Total	S/C	C/O_2	W/F (mg-cat.min/ml)
6	13.7	9.3	42.0	35.0	100.0	3	1.50	1.50
7	13.7	9.3	54.8	35.0	112.8	4	1.50	1.33
8	13.7	9.3	68.5	35.0	126.5	5	1.50	1.19
9	13.7	11.0	68.5	35.0	128.2	5	1.25	1.17

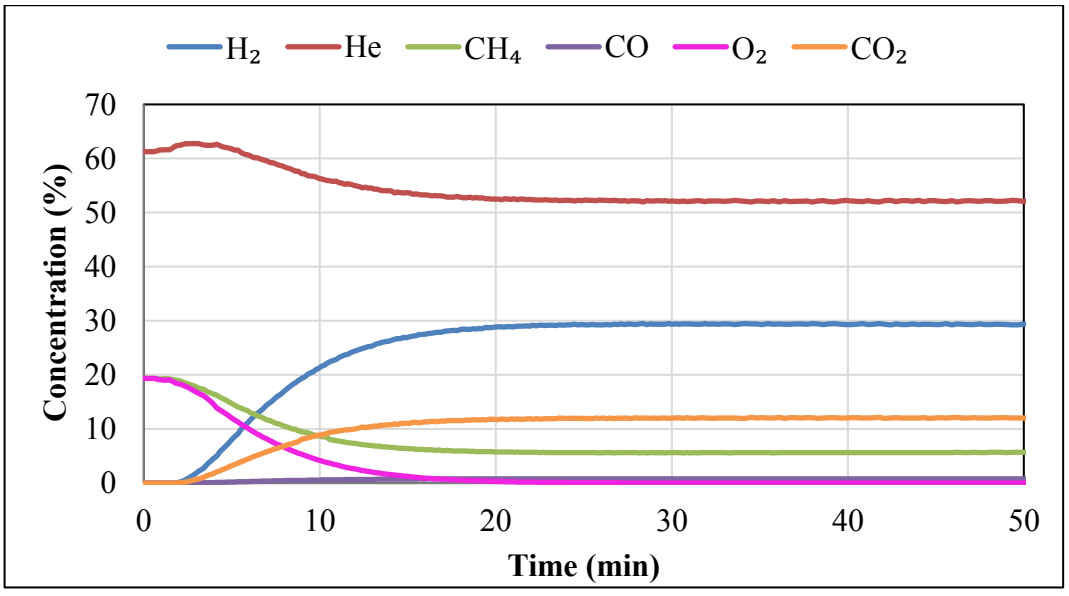

Figure 4.28. Dry and time based concentration profiles of the species at the exit of OSR unit for the feed conditions of Set 6 given in Table 3.11 (T_{OSR}=723 K).

Dry based inert free steady state H_2, CO_2, CH_4 and CO product concentrations and CH_4 conversions obtained in individual OSR (OSR feed conditions: Sets 6-8) and serial OSR-WGS tests (OSR feed conditions: Sets 8 & 9) are given for OSR temperatures of 673 K and 723 K in Figure 4.29 and 4.30, respectively, for a fixed WGS temperature of 623 K in serial tests. The results show that the increase in steam concentration in the feed (Sets 6→7→8) resulted in an increase in CH_4 conversion and, consequently, in a parallel rise in H_2 product concentration; a comparison of the results of Sets 6 and 8 reveals that H_2 concentration increased from 58% to 61% at T_{OSR}=673 K and from 61% to 65% at T_{OSR}=723 K. Since O_2 was totally consumed, addition of steam in the feed stream resulted in increased conversion levels of CH_4 from 61% to 67% at T_{OSR}=673 K and from 66% to 73% at T_{OSR}=723 K, whereas the changes observed in CO_2 concentration were almost 1%. The benefit of combining OSR with WGS can be seen from the increase in H_2 concentrations up to 62% at T_{OSR}=673 K and 67% at T_{OSR}=723 K (Figure 4.29 and 4.30) and the decrease in CO concentrations (Figure 4.31) between Set 8 and Set8-WGS experiments, which will be explained later. In the serial operation, the increase in O_2 concentration in the feed stream of OSR unit (from 9.3% to 11%, i.e. Sets 7→8), led to an increase in CH_4 conversion levels up to 71% and 77% at T_{OSR}=673 K and T_{OSR}=723 K, respectively.

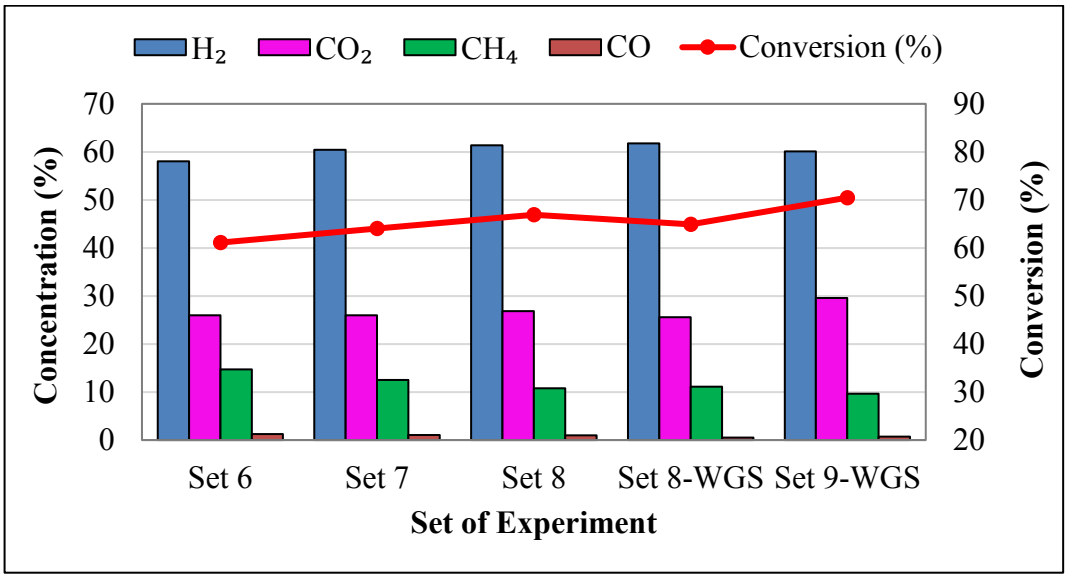

Figure 4.29. Dry based inert free steady state H_2, CO_2, CH_4 and CO concentrations and CH_4 conversions for different feed compositions (T_{OSR}=673 K, T_{WGS}=623 K).

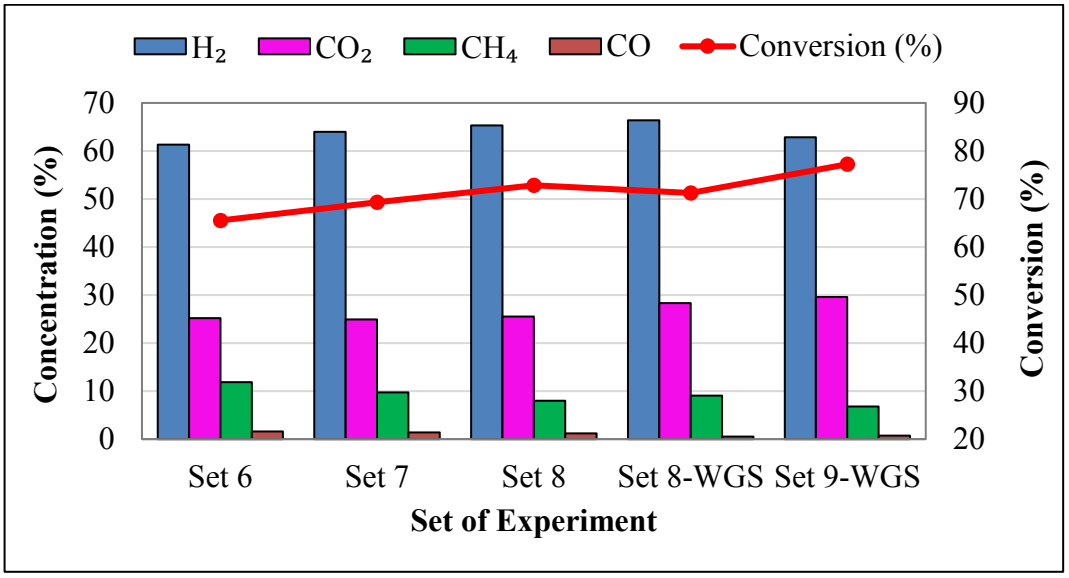

Figure 4.30. Dry based inert free steady state H_2, CO_2, CH_4 and CO concentrations and CH_4 conversions for different feed compositions (T_{OSR}=723 K, T_{WGS}=623 K).

Dry based inert free steady state CO product concentrations and H_2 production rates were given in Figure 4.31 and 4.32, respectively, for OSR temperatures of 673 and 723 K with Sets 6-9 feed conditions. The results show that increasing steam concentration in the feed stream led to decreased CO product concentrations; and increasing OSR temperature resulted in both higher CO concentrations and higher H_2 production rates. It should be noted that CO concentration increase in response to the rise in OSR temperature is diminished for OSR-WGS serial operation compared to those observed in individual OSR tests.

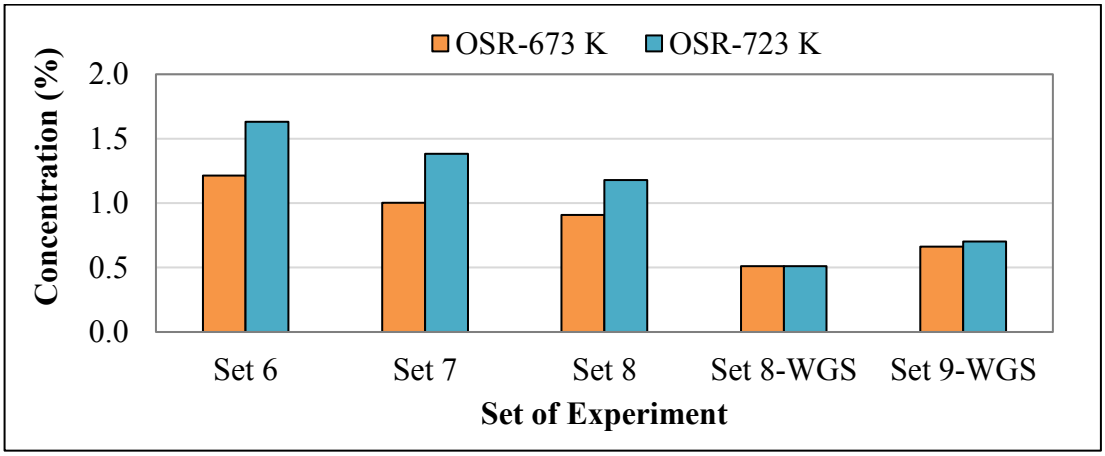

Figure 4.31. Dry based inert free steady state CO concentrations for different feed compositions (T_{WGS}=623 K for sets 8 and 9).

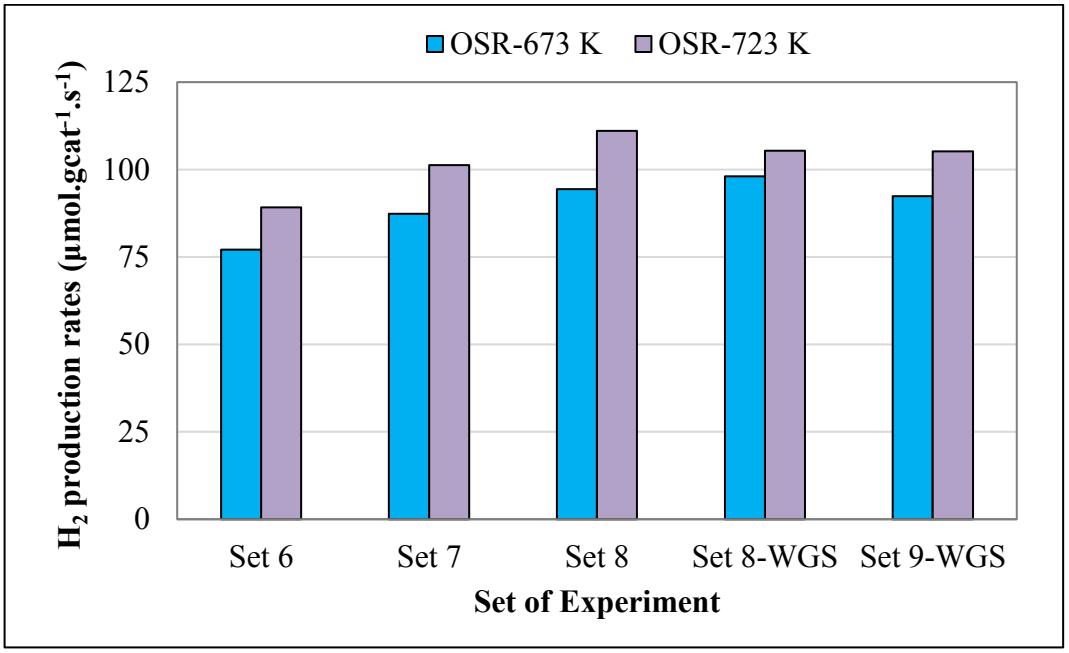

Figure 4.32. Hydrogen production rates for different feed compositions (T_{WGS}=623 K for Sets 8 and 9).

Although CO was the product of both incomplete oxidation and reforming reactions, and increasing steam amount resulted in enhanced reforming, the decrease in CO concentration can be explained by the secondary HTS activity of the Pt-Ni/Al_2O_3 catalyst, which was encountered before also in propane OSR reaction tests. Comparative analysis of the results of Set 6 and Set 9-WGS reveals that upon increasing steam concentration and adding a serial WGS reactor, CO concentration was decreased from 1.21% down to 0.66% at T_{OSR}=673 K, and H_2 production rates were obtained close to 105 µmol/gcat/s. Increase in OSR temperature to 723 K was resulted in the increased rates of steam reforming. Comparing the results of the Set 8-WGS and Set 9-WGS reveals that the increase in O_2 concentration in the OSR feed (i.e. lowered C/O_2 feed ratio) resulted in an increased conversion levels from 65% to 71% at T_{OSR}=673 K and from 71% to 77% at T_{OSR}=723 K. This can be explained by the fact that higher O_2 concentrations in OSR feed triggered TOX directly and, at the same time, supports SR indirectly via additional heat supplied from TOX sites to the SR sites of the catalyst, both of which resulted in higher methane conversions (Figure 4.29 and 4.30).

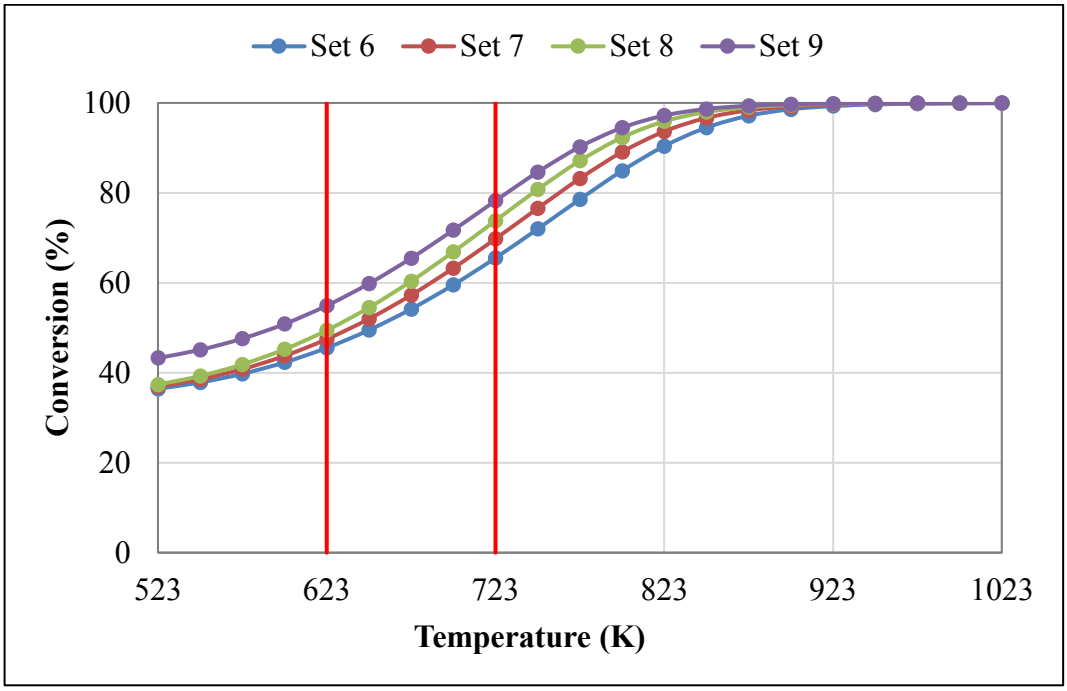

Figure 4.33. Equilibrium conversions of CH_4 in OSR unit predicted by thermodynamic calculations for different feed compositions given in Table 3.11.

Equilibrium conversions of methane in OSR reaction with respect to temperature predicted by thermodynamic calculations for different feed compositions in Sets 6-9 are given in Figure 4.33. A comparative analysis of the experimental data and thermodynamic calculation results reveals that most of the data are consistent with the thermodynamics, especially for the experiments conducted at 723 K. The possible reasons of the slight deviations are explained in Section 4.2.1.3. By observing the trends in Figure 4.34, 4.35, 4.36 and 4.37 for dry based inert free equilibrium H_2, CO, CH_4 and CO_2 concentrations, respectively, it can be concluded that the experimental product distributions and trends (Table 4.4) were also consistent with the results of the thermodynamic calculations.

Table 4.4. Response of methane OSR unit with respect to temperature and S/C ratio.

Parameter	**Type of Change**	**H_2**	**CO**	**CH_4**	**CO_2**
Temperature	Increase	Increase	Increase	Decrease	Decrease
S/C ratio	Increase	Increase	Decrease	Decrease	Decrease

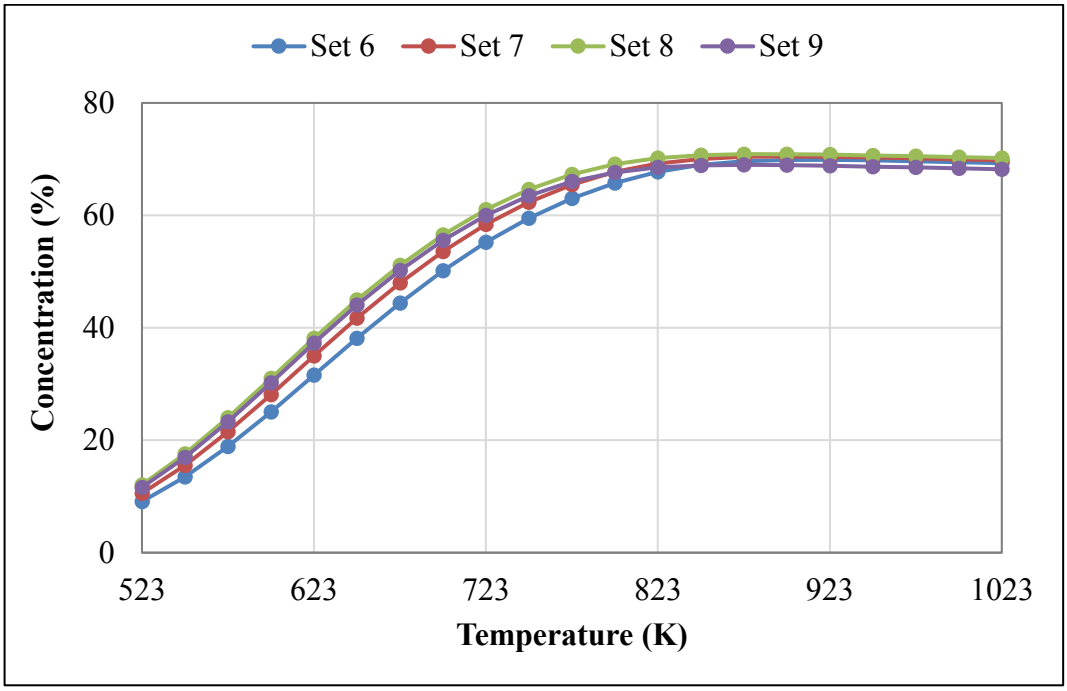

Figure 4.34. Dry based inert free equilibrium H_2 concentrations as a function of temperature in methane OSR predicted by thermodynamic calculations.

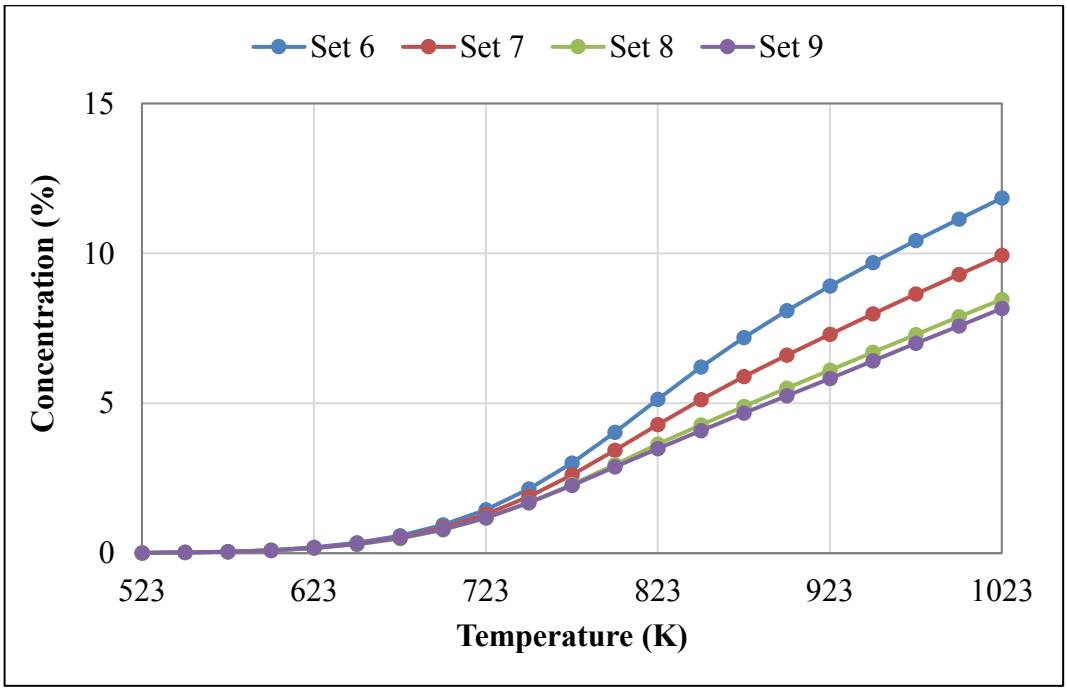

Figure 4.35. Dry based inert free equilibrium CO concentrations as a function of temperature in methane OSR predicted by thermodynamic calculations.

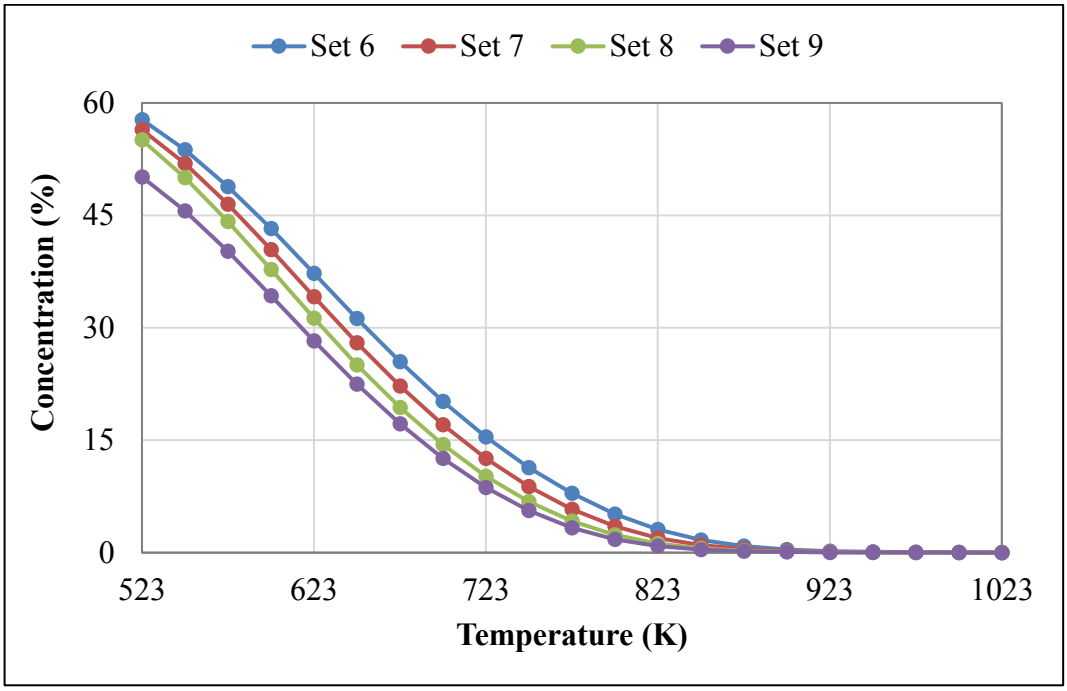

Figure 4.36. Dry based inert free equilibrium CH_4 concentrations as a function of temperature in methane OSR predicted by thermodynamic calculations.

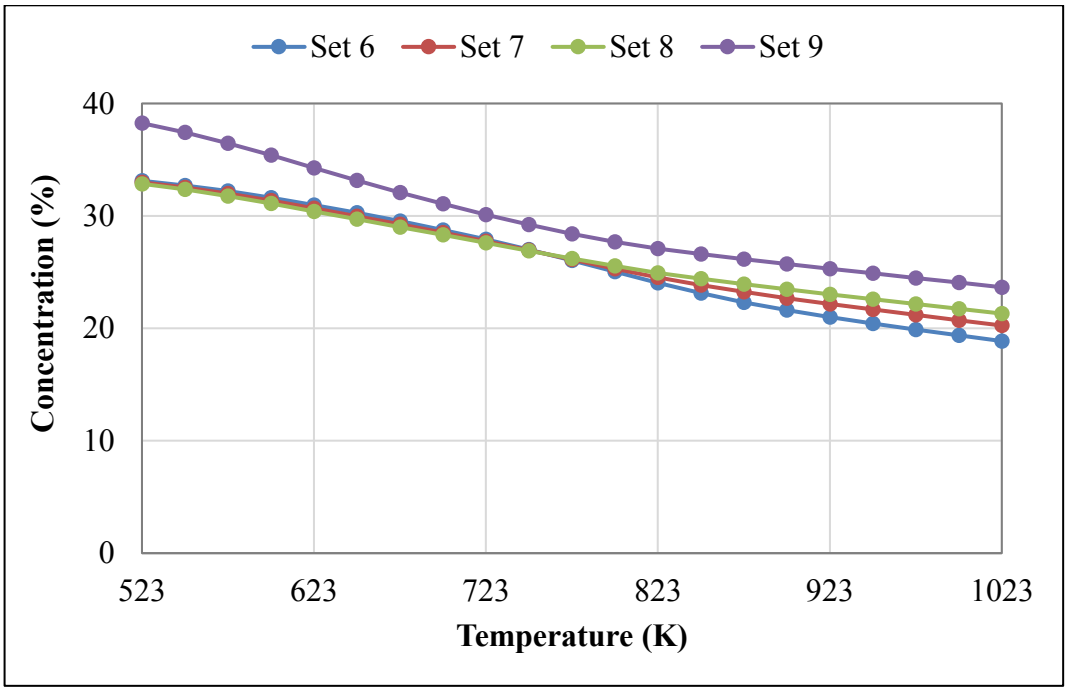

Figure 4.37. Dry based inert free equilibrium CO_2 concentrations as a function of temperature in methane OSR predicted by thermodynamic calculations.

4.4. Modeling and Transient Performance Analysis of the Fuel Processor

The aim of this section is to model the dynamic/transient performance of the FPP. In this context, (i) the dynamic/transient performance of the FPP was pre-modeled through the use of formerly obtained power-law type kinetics of reactions, which were corrected further based on the response of the units/FPP to step changes in process variables, and (ii) a suitable control-oriented full system dynamic model for the FPP with reliable and consistent control parameters was obtained.

4.4.1. Modeling of the Fuel Processor Units

Kinetic studies conducted at realistic feed conditions are essential in reactor design and modeling. Obtaining kinetic model through the use of feed conditions including both the reactants and products play an important role in reliability of the rate expressions especially in serial operations. For this reason, formerly obtained power-law type rate expressions, by using realistic feeds and mixed feeds close to the conditions to be encountered in a FP, for OSR reaction over 0.2%Pt-10%Ni/δ-Al_2O_3 catalyst (Gökaliler *et al*., 2012), for WGS reaction over 1wt.%Au-0.5wt.%Re/CeO_2 catalyst (Gökaliler *et al*., 2013) and for PROX reaction over 1wt.%Pt-0.25wt.%Sn/AC3 catalyst (Eropak and Aksoylu, 2016) were used in modeling of the FPP units. The power-law type rate expressions, i.e. the rate orders and specific rate constants, were formerly estimated by non-linear regression analysis in MATLAB environment. The non-linear regression analysis was carried out on the conversion vs residence time data obtained through parametric studies covering up to 40 experiments.

4.4.1.1. Modeling of the OSR Reactor. A complex series of reactions take place in an OSR unit, which have their own intrinsic kinetic dependence on the temperature and feed conditions, as explained in Section 4.1.1. Among these reactions some are denoted as primary reactions such as SR, TOX and WGS, whose extents are an order of magnitude greater than the secondary reactions, such as methanation and POX (Table 4.1). For this reason, OSR can be named as the net sum of all these reactions occurring between the various chemical species (Shekhawat *et al*., 2011). A lumped power-law type propane OSR rate expression was obtained for 0.2%Pt-10%Ni/δ-Al_2O_3 catalyst by our group as the simplified

kinetic model of the reaction for realistic conditions as S/C feed ratio range of 2-3 and C/O_2 feed ratio range of 3.0-5.4 for the temperature interval of 653-693 K (Gökaliler *et al*., 2012). The estimated parameters were given in Table 4.5 for the power-law type rate expression in Equation 4.3, where P represents the partial pressure of the species involved.

Table 4.1. Possible reactions in a propane oxidative steam reformer.

Reaction No	**Reaction Formula**	**Reaction Type**	ΔH°_{298} (kJ/mol)
1	$C_3H_8 + 3\,H_2O \rightarrow 3\,CO + 7\,H_2$	CO producing steam reforming	497
2	$C_3H_8 + 6\,H_2O \rightarrow 3\,CO_2 + 10\,H_2$	CO_2 producing steam reforming	376
3	$C_3H_8 + 5\,O_2 \rightarrow 3\,CO_2 + 4\,H_2O$	Total oxidation	-2046
4	$C_3H_8 + 3/2\,O_2 \rightarrow 3\,CO + 4\,H_2$	Partial oxidation	-229
5	$CO_2 + 4\,H_2 \rightarrow CH_4 + 2\,H_2O$	CO_2 methanation	-165
6	$CO + 3\,H_2 \rightarrow CH_4 + H_2O$	CO methanation	-206
7	$CO + H_2O \leftrightarrow CO_2 + H_2$	Water gas shift	-41

$$-r_{C_3H_8} = \left[k_0 exp\left(\frac{-E_A}{RT}\right)\right] P^{\alpha}_{C_3H_8} P^{\beta}_{O_2} P^{\gamma}_{H_2O} \tag{4.3}$$

Table 4.5. Estimated kinetic parameters and reaction orders for the OSR reaction of propane over 0.2wt.%Pt-10wt.%Ni/δ-Al_2O_3 catalyst (Gökaliler *et al*., 2012).

Parameter	**Estimate**	**Unit**
k_0	5.51	$\mu mol.mgcat^{-1}.s^{-1}.kPa^{-3.49}$
E_A	46.19	$kJ.gmol^{-1}$
α	1.64	-
β	2.44	-
γ	-0.59	-

The differential form of the packed bed reactor design equation (Equation 4.4) was used in the calculation of the rate data, where change in molar flow rate of propane (F) can be rewritten in terms of conversion.

$$-r_{C_3H_8} = -\frac{dF_{C_3H_8}}{dW_{cat}} = F_{0_{C_3H_8}} \frac{dX_{C_3H_8}}{dW_{cat}} \tag{4.4}$$

The partial pressure terms were replaced with concentrations by using ideal gas law relation via inserting Equation 4.5 into Equation 4.3.

$$P = CRT \tag{4.5}$$

$$F_{0_{C_3H_8}} = C_{0_{C_3H_8}} v_0 \tag{4.6}$$

Substituting the rate term in Equation 4.3 into Equation 4.4 and rewriting initial propane molar flow rate in terms initial concentration and total volumetric flow rate (Equation 4.6) yields the model equation given in Equation 4.7.

$$C_{0_{C_3H_8}} v_0 \frac{dX_{C_3H_8}}{dW_{cat}} = \left[k_0 exp\left(\frac{-E_A}{RT}\right)\right] (RT)^{\alpha+\beta+\gamma} C_{C_3H_8}^{\alpha} C_{O_2}^{\beta} C_{H_2O}^{\gamma} \tag{4.7}$$

The right hand side of Equation 4.7 required denoting the concentration of each species in terms of the concentration of the limiting reactant (propane) and its conversion. The *extent of reaction* approach was used to solve the multiple reaction system with a general formulation. The extent of a reaction, shown as ξ, satisfies Equation 4.8 and gives information about to what extent a reaction proceeds. It can be calculated from known inlet and outlet molar flow rates and stoichiometric coefficient of the species shown as φ in Equation 4.8, where *i* and *j* represent species and reactions, respectively.

$$F_i - F_{0_i} = \sum_{j}^{reactions} \varphi_{i,j} \xi_j \tag{4.8}$$

By using the stoichiometric coefficients of the seven species for the seven reactions given in Table 4.1 (- for reactants, + for products), Equation 4.8 can be written in matrix form:

$$\begin{bmatrix} F_{C_3H_8} - F_{0_{C_3H_8}} \\ F_{O_2} - F_{0_{O_2}} \\ F_{H_2O} - F_{0_{H_2O}} \\ F_{CO} - F_{0_{CO}} \\ F_{CO_2} - F_{0_{CO_2}} \\ F_{H_2} - F_{0_{H_2}} \\ F_{CH_4} - F_{0_{CH_4}} \end{bmatrix} = \begin{bmatrix} -1 & -1 & -1 & -1 & 0 & 0 & 0 \\ 0 & 0 & -5 & -1.5 & 0 & 0 & 0 \\ -3 & -6 & 4 & 0 & 2 & 1 & -1 \\ 3 & 0 & 0 & 3 & 0 & -1 & -1 \\ 0 & 3 & 3 & 0 & -1 & 0 & 1 \\ 7 & 7 & 10 & 0 & 4 & -3 & 1 \\ 0 & 0 & 0 & 0 & 1 & 1 & 0 \end{bmatrix} . \begin{bmatrix} \xi_1 \\ \xi_2 \\ \xi_3 \\ \xi_4 \\ \xi_5 \\ \xi_6 \\ \xi_7 \end{bmatrix} \quad (4.9)$$

The system given in Equation 4.9 including 7 unknowns and 7 equations were solved for the extent of reactions via using the information of feed and exit molar flow rates of the OSR experiments given in Table 4.7. The coefficient matrix was square, but close to singular, therefore the pseudoinverse function was used to solve for the unknowns. The computation was based on treating any singular value less than tolerance value as zero. The use of computed extents in the back calculation of exit molar flow rates gave a max of 10% deviation.

The change in total volumetric flow rate due to the changing total molar flow rate during the reactions *due to stoichiometry differences between reactant and product sides* was taken into account by using Equations 4.10 and 4.11, where ϵ represents the ratio of change in total number of moles for complete conversion to the total moles fed, δ represents change in total number of moles per propane reacted and x denotes the feed mole fraction.

$$\epsilon = \delta_{C_3H_8} x_{0_{C_3H_8}} \quad (4.10)$$

$$\delta_{C_3H_8} = \sum_{j}^{reactions} \delta_j \xi_j \quad (4.11)$$

By using the simplifications and arrangements mentioned above, concentration of each species was defined by Equation 4.12, which considers the multiple reaction system as one lumped reaction, and the consumption and production rates were normalized with respect to propane consumption.

$$C_j = C_{0_{C_3H_8}} \frac{\frac{\nu_{0\,j}}{\nu_{0\,C_3H_8}} - \frac{\sum_j^{reactions}(\varphi_{i,j}\xi_j)}{\sum_j^{reactions}(\varphi_{C_3H_8,j}\xi_j)} X_{C_3H_8}}{1 + \varepsilon X_{C_3H_8}} \tag{4.12}$$

At this stage, by rewriting the concentrations of propane, oxygen and steam with respect to Equation 4.12 and then by inserting them into the rate expression given in Equation 4.7, the design equation can be solved for the only unknown, which is conversion level, with respect to the catalyst weight. Conversion vs catalyst weight data were obtained as the output of the model for the inputs of initial concentration of the species in the feed stream, temperature, pressure, estimated kinetic parameters and reaction orders.

After constructing and modifying the kinetic model, the results of the model were compared with the results of a former experimental study conducted in our group (Gökaliler *et al*., 2012) on the basis of propane conversion. Figure 4.38 shows the results of the kinetic experiments formerly conducted at 673 K (Gökaliler *et al*., 2012) and the results obtained through modeling in the current study in terms of propane conversion. The experimental conditions used in the kinetic experiments and modeling calculations are listed in Appendix A as Table A.1.

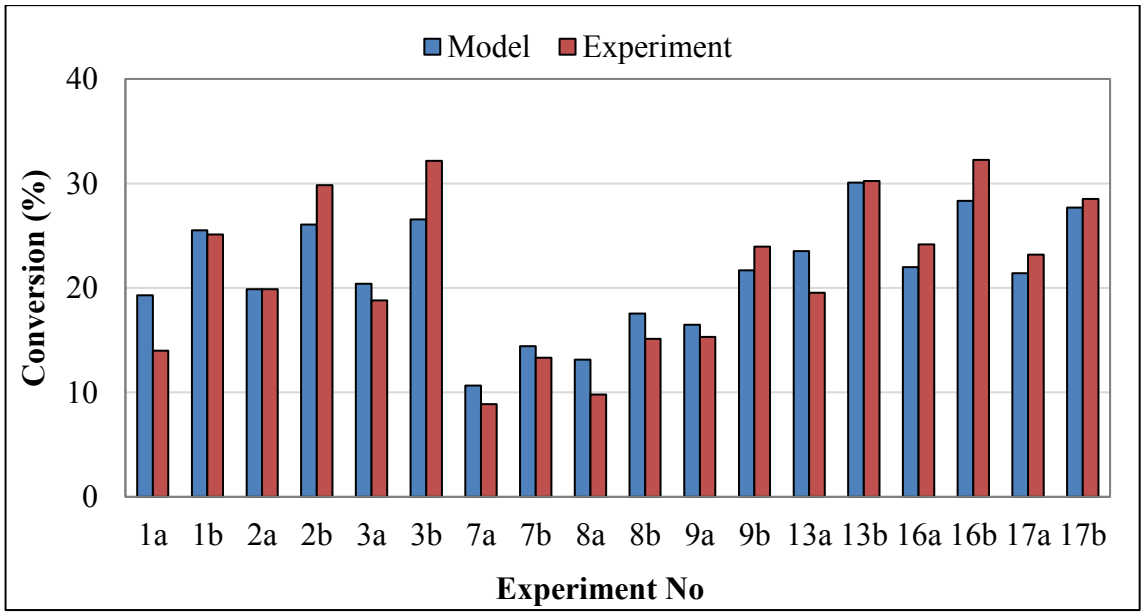

Figure 4.38. Comparison of the C_3H_8 conversions obtained through the kinetic experiments (Gökaliler *et al*., 2012) and modeling for the experimental conditions given in Table A.1.

The feed conditions used in the kinetic experiments (Gökaliler *et al*., 2012) were close to the experimental conditions used in the performance tests conducted in the current study for experiments A9 and A10 in Table 4.6. The extent values, which were calculated for the performance tests with almost complete conversion over 150 mg catalyst, were used in the modeling calculations. The conversion values in Figure 4.38 were in good agreement with each other and the average of the errors in conversions between the experimental and modelling results was calculated as 12.5%.

The experimental C_3H_8 conversion values obtained in the current study and conversion values obtained through modeling were given in Table 4.6. In cases, where the feed conditions (Exp. A9 and A10) were very similar to the kinetic tests' operation conditions, the findings were agreed with each other within 2-6% error margin in conversion values, which was quite acceptable. However, increasing the S/C ratio (5-6) in the feed stream led to the deviations from the conversion values indicating the possible changes of the reaction kinetics with the change in S/C ratio and also indirectly supporting the validity of the rate expression obtained for the S/C ratios used in both performance and kinetic tests (2-3).

Table 4.6. Comparison of the conversion of propane values obtained experimentally in the current study and through modeling for the given feed conditions.

		Flow rate (ml/min)						
Exp. #	**T_{OSR} (K)**	**C_3H_8**	**O_2**	**H_2O**	**He**	**S/C**	**$X_{exp.}$ (%)**	**X_{model} (%)**
A9	723	6.6	7.3	44.7	26.5	2.25	99.38	97.11
A10	723	6.6	7.3	59.6	26.5	3	99.46	93.68
A11	723	6.6	7.3	99.5	26.5	5	99.53	79.70
A12	723	6.6	7.3	119.2	26.5	6	99.56	71.37

Output of OSR modeling algorithm in terms of conversion vs catalyst weight for the experiments A9 and A10 (Table 4.6), for the kinetic experiments given in Gökaliler *et al*., 2012, and output of exit concentration of the species vs catalyst weight for the experiments A9 and A10 (Table 4.6) were given in Figure 4.39, 4.40 and 4.41, respectively. The red and blue dots represent the conversion values for experiment A9 (0.9938) and A10 (0.9946),

respectively. Up to 100% conversions were obtained with 150 mg of catalyst, modeling and experimental results were quite consistent. The outlet concentration profiles of each species involved in OSR reaction for a given catalyst weight for experiment A9 in Table 4.6 were given in Figure 4.41. Figure 4.40 shows conversion vs catalyst weight curves obtained through modeling for the formerly conducted kinetic experiments and red dots represent experimental conversion values obtained with 10 mg catalyst, whereas blue dots represent experimental conversion values obtained with 15 mg catalyst. One can safely say that the data obtained through modeling are broadly consistent with the major trends and the model is able to predict overall propane conversion rates quantitatively within ca. 12.5% error margin.

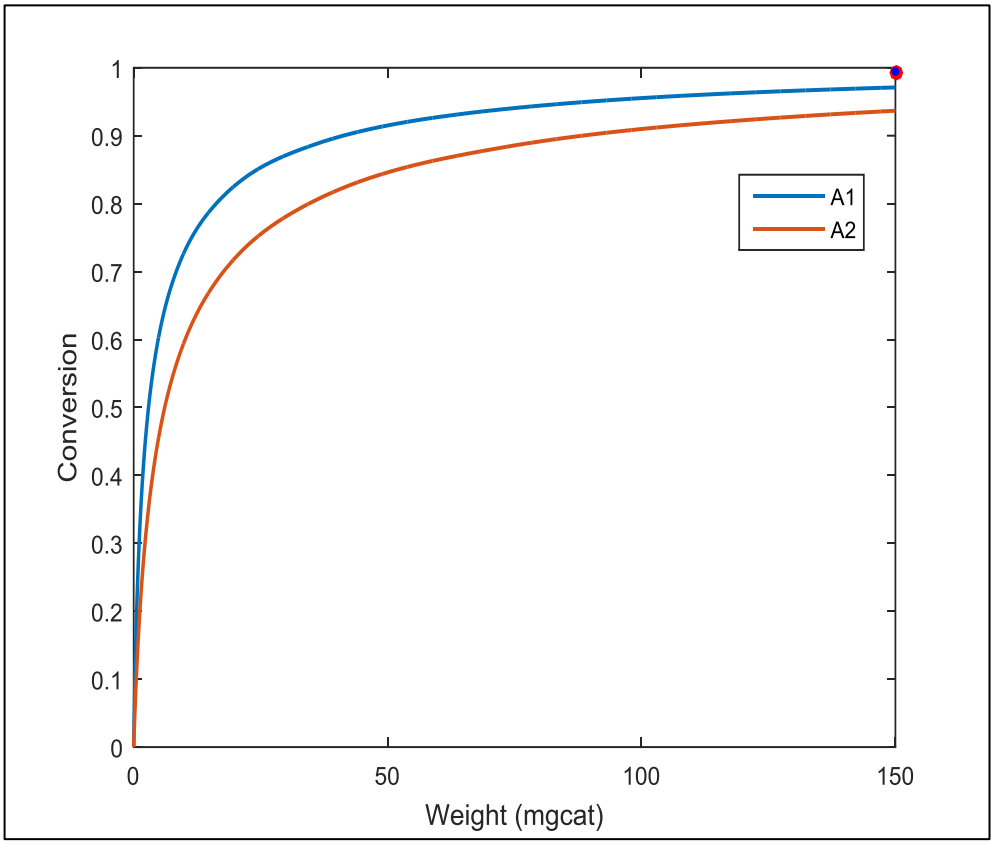

Figure 4.39. Output of OSR modeling algorithm in terms of conversion vs catalyst weight for exp. A1 and A2 given in Table 4.6. (Blue and red dots represent experimental data)

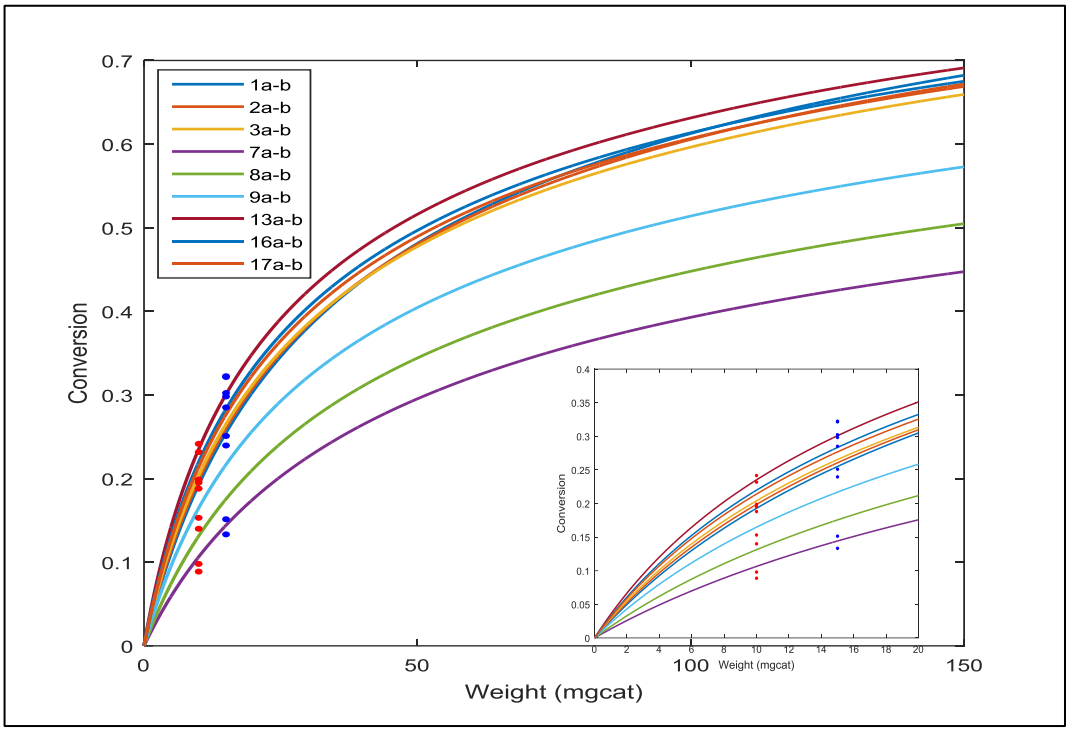

Figure 4.40. Output of OSR modeling algorithm in terms of conversion vs catalyst weight for the kinetic experiments given in Gökaliler *et al*., 2012 (Blue and red dots represent experimental data for 10 and 15 mg catalysts, respectively).

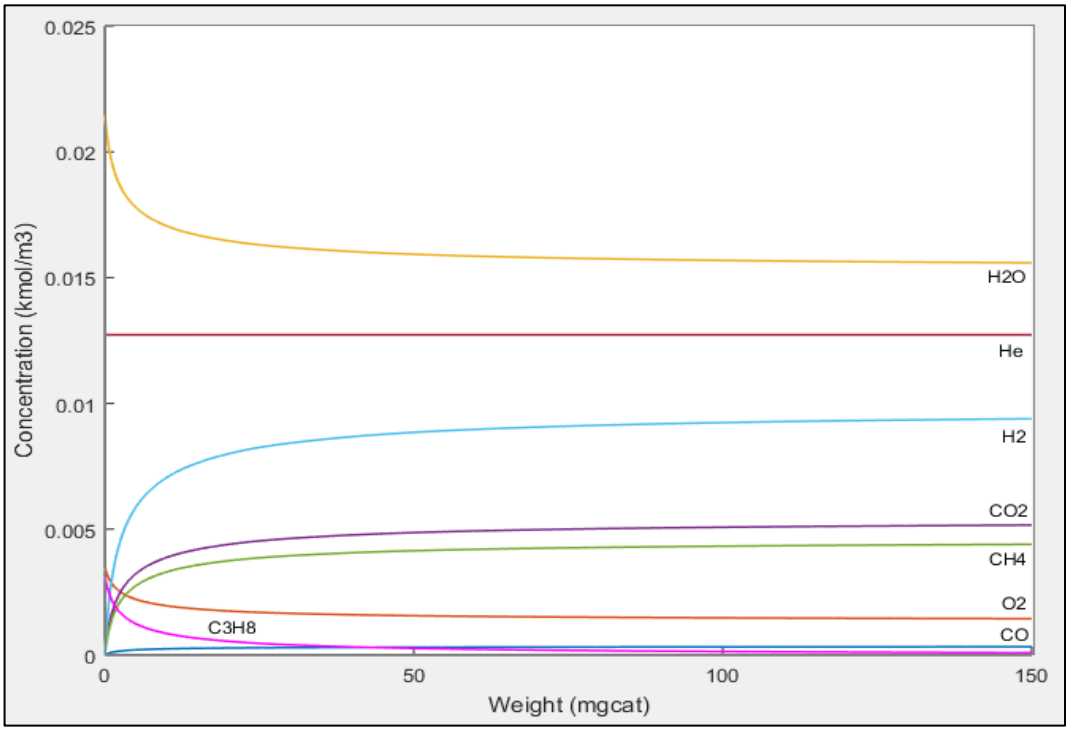

Figure 4.41. Output of OSR modeling algorithm in terms of exit concentration of the species vs catalyst weight for experiment A1 (Table 4.6).

4.4.1.2. Modeling of the WGS Reactor. A power-law type WGS rate expression was obtained for 1%Au-0.5%Re/CeO_2 catalyst by our group as the simplified kinetic model of the reaction (Equation 2.15) for realistic conditions as H_2O/CO feed ratio range of 3-7 for the temperature interval of 553-598 K (Gökaliler *et al*., 2013). The estimated parameters were given in Table 4.7 for the power-law type rate expression in Equation 4.13.

$$CO + H_2O \leftrightarrow CO_2 + H_2 \tag{2.15}$$

$$-r_{CO} = \left[k_0 exp\left(\frac{-E_A}{RT}\right)\right] P_{CO}^a P_{H_2O}^b P_{CO_2}^c P_{H_2}^d (1-\beta') \tag{4.13}$$

$$\beta' = \frac{1}{K_{eq}} \frac{P_{CO_2} P_{H_2}}{P_{CO} P_{H_2O}} \tag{4.14}$$

$$K_{eq} = \exp\left(\frac{4577.8}{T} - 4.33\right) \tag{4.15}$$

Table 4.7. Estimated kinetic parameters and reaction orders for the WGS reaction over 1wt.%Au-0.5wt.%Re/CeO_2 catalyst (Gökaliler *et al*., 2013).

Parameter	Unit	Estimate
k_0	μmol.gcat^{-1}.s^{-1}.kPa$^{-1.83}$	84.62
E_A	kJ.gmol^{-1}	29.44
a	-	0.75
b	-	2.02
c	-	-0.34
d	-	-0.60

The starting point in the modeling was the differential form of the packed bed reactor design equation (Equation 4.16) and similar approach was used in the modifications and simplifications of the rate expression (Equation 4.13) as explained in Section 4.4.1.1. Since CO is the limiting reactant, all modeling calculations and conversion values were based on CO and the rate equation (Equation 4.13) can be written in the form of Equation 4.17.

$$-r_{CO} = -\frac{dF_{CO}}{dW_{cat}} = F_{CO_0}\frac{dX_{CO}}{dW_{cat}} \tag{4.16}$$

$$C_{CO_0}v_0\frac{dX_{CO}}{dW_{cat}} = \left[k_0 exp\left(\frac{-E_A}{RT}\right)\right](RT)^{a+b+c+d}$$
$$C_{CO}^a C_{H_2O}^b C_{CO_2}^c C_{H_2}^d\left(1 - \frac{1}{\exp\left(\frac{4577.8}{T} - 4.33\right)}\frac{C_{CO_2}C_{H_2}}{C_{CO}C_{H_2O}}\right) \tag{4.17}$$

Since WGS reaction has 1:1 overall stoichiometry and is assumed to proceed with no significant side reaction, thus no change in the total volumetric/molar flow rate was observed. Concentration of each species in terms of conversion were given in Equations 4.18-4.21.

$$C_{CO} = C_{CO_0}(1 - X_{CO}) \tag{4.18}$$

$$C_{H_2O} = C_{CO_0}\left(\frac{\nu_{0_{H_2O}}}{\nu_{0_{CO}}} - X_{CO}\right) \tag{4.19}$$

$$C_{CO_2} = C_{CO_0}\left(\frac{\nu_{0_{CO_2}}}{\nu_{0_{CO}}} + X_{CO}\right) \tag{4.20}$$

$$C_{H_2} = C_{CO_0}\left(\frac{\nu_{0_{H_2}}}{\nu_{0_{CO}}} + X_{CO}\right) \tag{4.21}$$

As WGS is a reversible exothermic reaction, CO conversion is thermodynamically limited, and the equilibrium conversion was calculated by Equation 4.22 in each simulation for any temperature and feed conditions including only the reactants (ideal) and the reactants and the products together (realistic). The bisection method was used in order to find the roots (i.e. conversion values) of Equation 4.22 in the defined subinterval 0-1 for further processing.

$$K_{eq} = \exp\left(\frac{4577.8}{T} - 4.33\right) = \frac{C_{CO_2}C_{H_2}}{C_{CO}C_{H_2O}} \tag{4.22}$$

The results of the kinetic experiments formerly conducted at 573 K (Gökaliler *et al*., 2013) and the results obtained through the current model in terms of CO conversion were given in Figure 4.42. (The experimental conditions used in the kinetic experiments and modeling calculations are listed in Appendix A as Table A.2.) Firstly, the results indicated that the kinetic experiments and the reactions were carried out far from equilibrium. Since there were no multiple/side reactions occurring and no volumetric flow rate change due to the 1:1 stoichiometry, the conversion values in Figure 4.42 are in good agreement with each other and the average of the errors in conversions between the experimental and modelling results was calculated as 16.3%.

Figure 4.43 summarizes the results of the formerly conducted performance tests with 75 mg catalyst (Çağlayan *et al*., 2011a) and the modeling results for the experimental conditions given in Appendix as Table A.3. Considering the fact that the rate expression used in modeling was obtained for a H_2O/CO feed ratio range of 3-7, modeling studies with higher H_2O/CO ratios (~5) were in better match with the experimental results giving the average of errors as 7.5% (Exp. 9-14).

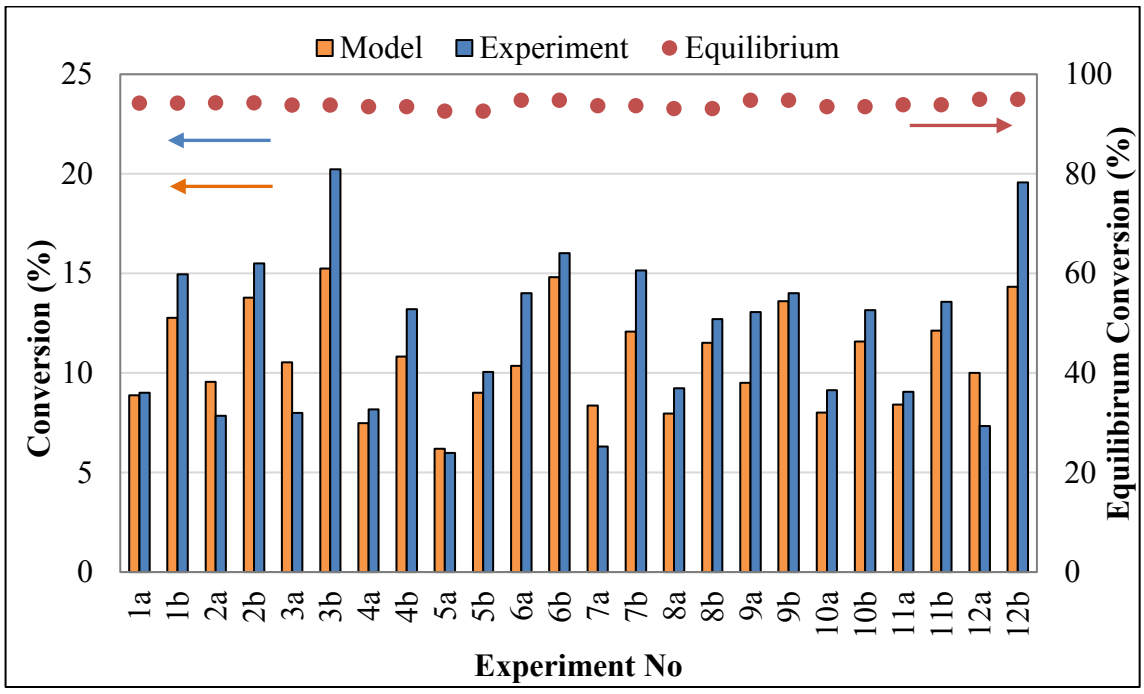

Figure 4.42. Comparison of the CO conversions obtained through the kinetic experiments (Gökaliler *et al*., 2013) and modeling for the experimental conditions given in Table A.2.

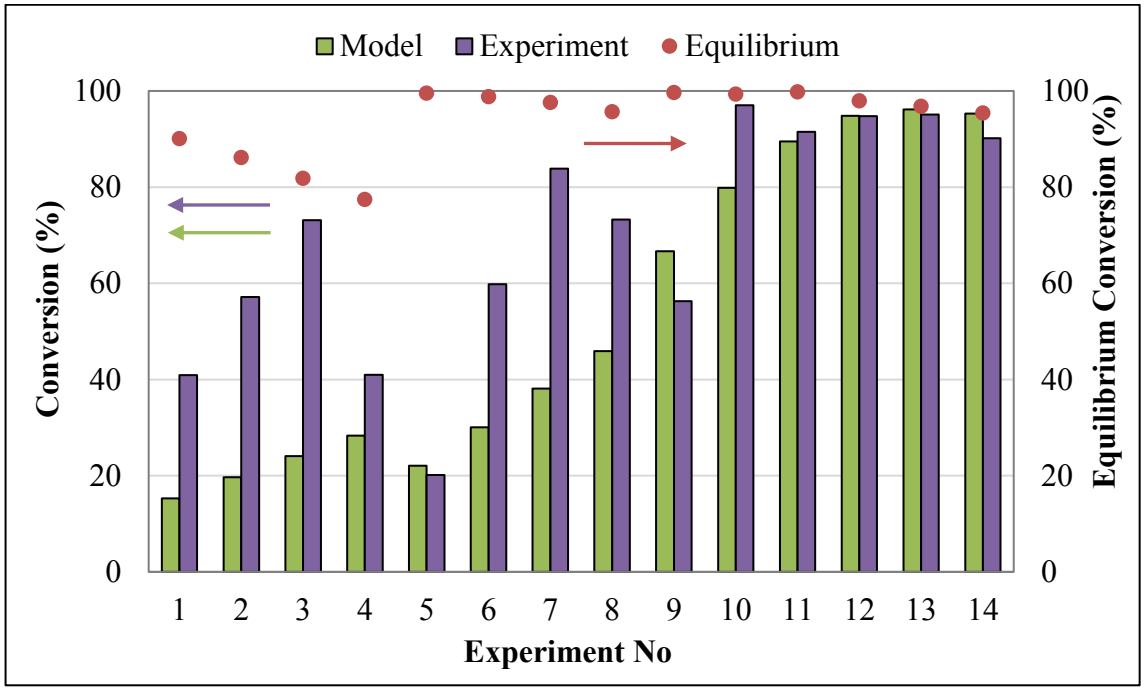

Figure 4.43. Comparison of the CO conversions obtained through the performance tests (Çağlayan *et al*., 2011a) and modeling for the experimental conditions given in Table A.3.

Output of WGS modeling algorithm in terms of conversion vs catalyst weight for 12 different feed compositions as well as results of the corresponding kinetic tests (Gökaliler *et al*., 2013) are given in Figure 4.44. The output profiles as exit concentration of the species vs catalyst weight by the model for experiment 3b (Gökaliler *et al*., 2013) is given in Figure 4.45. Considering the equilibrium conversions given in Figure 4.42 for the same experimental conditions, conversions obtained through modeling were below thermodynamic limits. The model can provide information for determining experimental conditions for the future performance tests for which process parameters-catalyst weight combinations lead higher conversions.

Figure 4.45 shows a sample output of WGS modeling algorithm in terms of concentration of the species as a function of the catalyst weight for the conditions used in a kinetic experiment had yielded 20% conversion over 15 mg catalyst (Gökaliler *et al*., 2013). Regarding WGS reaction, slight decreases in CO and H_2O concentrations, and increases in H_2 and CO_2 concentrations are in accordance with the expectations. Due to the 1:1 stoichiometry of the reaction, there wasn't any change in the He concentration.

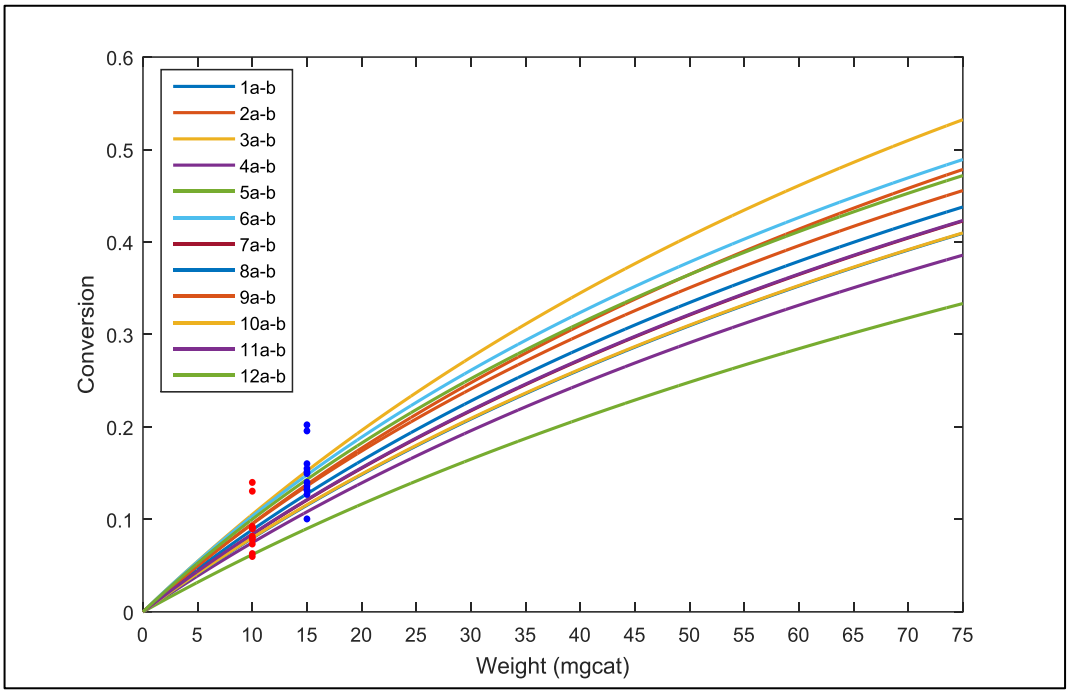

Figure 4.44. Output of WGS modeling algorithm in terms of conversion vs catalyst weight for the kinetic experiments given in Gökaliler *et al*., 2013 (Blue and red dots represent experimental data for 10 and 15 mg catalysts, respectively).

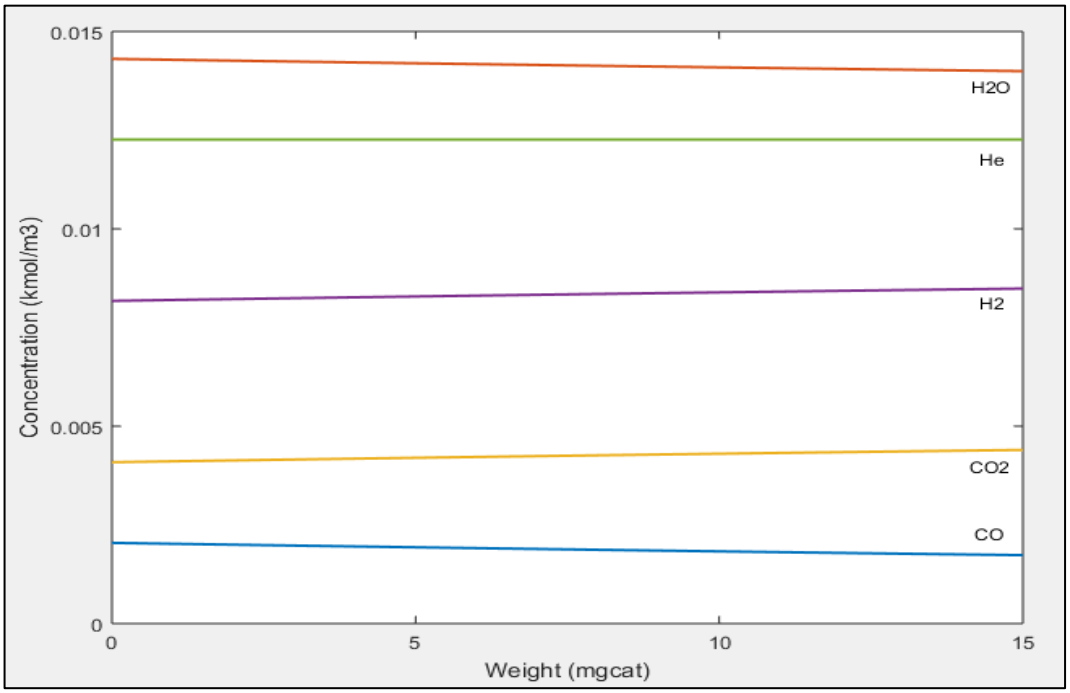

Figure 4.45. Output of WGS modeling algorithm in terms of exit concentration of the species vs catalyst weight for experiment 3b (Gökaliler *et al*., 2013).

4.4.1.3. Modeling of the PROX Reactor. A power-law type rate expression was obtained by our group in the kinetic modeling of PROX reaction (Equation 2.16) over 1wt.%Pt-0.25wt.%Sn/AC3 catalyst in the C/O_2 feed ratio range of 0.5-1.5 in the temperature interval of 383-408 K (Eropak and Aksoylu, 2016) for H_2-rich, fully realistic feed conditions. The estimated parameters are given in Table 4.8 for the power-law type rate expression in Equation 4.23.

$$CO + \frac{1}{2}O_2 \rightarrow CO_2 \tag{2.16}$$

$$-r_{CO} = \left[k_0 exp\left(\frac{-E_A}{RT}\right)\right] P_{CO}^{\alpha} P_{O_2}^{\beta} \tag{4.23}$$

Table 4.8. Estimated kinetic parameters and reaction orders for the PROX reaction over 1wt.%Pt-0.25wt.%Sn/AC3 catalyst (Eropak and Aksoylu, 2016).

Parameter	**Unit**	**Estimate**
k_0	mmol.mgcat^{-1}.min^{-1}.kPa$^{0.1}$	315
E_A	kJ.gmol^{-1}	45.3
α	-	0.47
β	-	0.57

The starting point in the modeling was the differential form of the packed bed reactor design equation (Equation 4.15) and similar approach was used in the modifications and simplifications of the rate expression (Equation 4.23) as explained in Section 4.4.1.1. Since CO is the limiting reactant, all modeling calculations and conversion values were based on CO, and the rate equation (Equation 4.23) can be written in the form of Equation 4.24.

$$-r_{CO} = -\frac{dF_{CO}}{dW_{cat}} = F_{CO_0}\frac{dX_{CO}}{dW_{cat}} \tag{4.16}$$

$$C_{CO_0} v_0 \frac{dX_{CO}}{dW_{cat}} = \left[k_0 exp\left(\frac{-E_A}{RT}\right)\right] (RT)^{\alpha+\beta} C_{CO}^{\alpha} C_{O_2}^{\beta} \tag{4.24}$$

Since PROX reaction has 1:1.5 overall stoichiometry, the change in the total volumetric/molar flow rate has been also taken into account. The slight extent of the H_2 oxidation side reaction was ignored, and PROX reaction was assumed to proceed with no other significant side reaction. Concentration of each species in terms of conversion were given in Equations 4.25-4.29.

$$C_{CO} = C_{CO_0} \frac{(1 - X_{CO})}{1 + \varepsilon X_{CO}} \tag{4.25}$$

$$C_{O_2} = C_{CO_0} \frac{\left(\frac{v_{O_2}}{v_{CO}} - 0.5X_{CO}\right)}{1 + \varepsilon X_{CO}} \tag{4.26}$$

$$C_{CO_2} = C_{CO_0} \frac{\left(\frac{v_{CO_2}}{v_{CO}} + X_{CO}\right)}{1 + \varepsilon X_{CO}} \tag{4.27}$$

$$C_{H_2} = C_{CO_0} \frac{\left(\frac{v_{H_2}}{v_{CO}}\right)}{1 + \varepsilon X_{CO}} \tag{4.28}$$

$$C_{He} = C_{CO_0} \frac{\left(\frac{v_{He}}{v_{CO}}\right)}{1 + \varepsilon X_{CO}} \tag{4.29}$$

The results of the kinetic experiments formerly conducted at 383 K (Eropak and Aksoylu, 2016) and the results obtained through the current model in terms of CO conversion are given in Figure 4.46. (The experimental conditions used in the kinetic experiments and modeling calculations are listed in Appendix A as Table A.4.) The results indicated that the conversion levels obtained through modeling are in good agreement with the kinetic experiments except some experimental errors (4b), the average of the errors in conversions between the experimental and modelling results was calculated as ~20%.

Figure 4.47 shows the results of the formerly conducted performance tests with 250 mg catalyst (Çağlayan *et al*., 2011b) and the results obtained through the current model. (The experimental conditions used in the performance experiments and modeling calculations are listed in Appendix A as Table A.5.) The average of the errors in conversions between the experimental and modeling results for all 8 cases was calculated as ~17%.

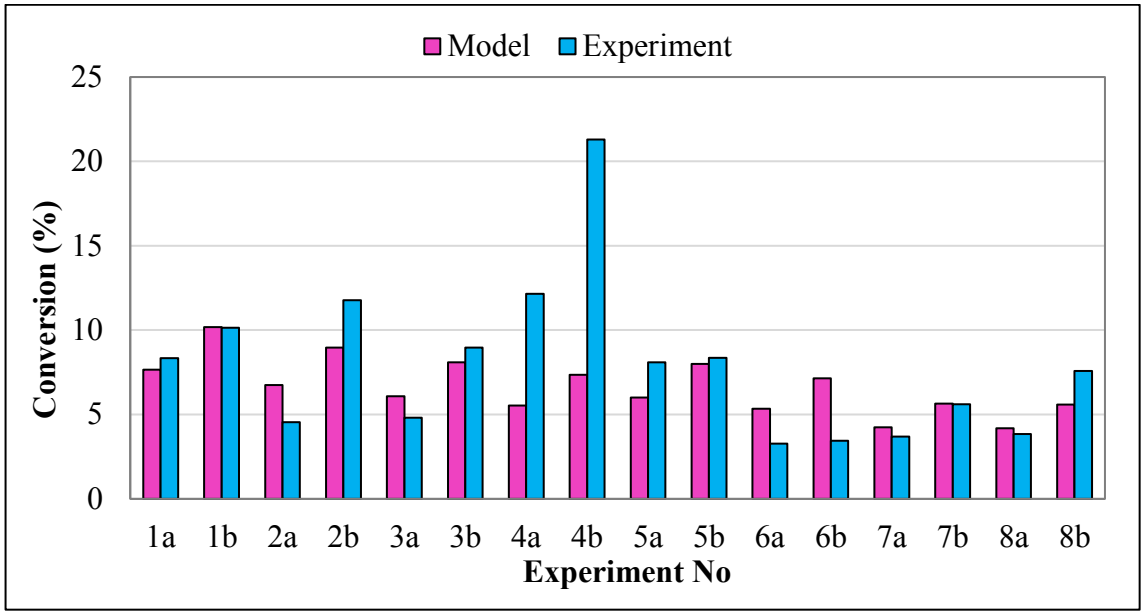

Figure 4.46. Comparison of the CO conversions obtained through the kinetic experiments (Eropak and Aksoylu, 2016) and modeling for the feed conditions given in Table A.4.

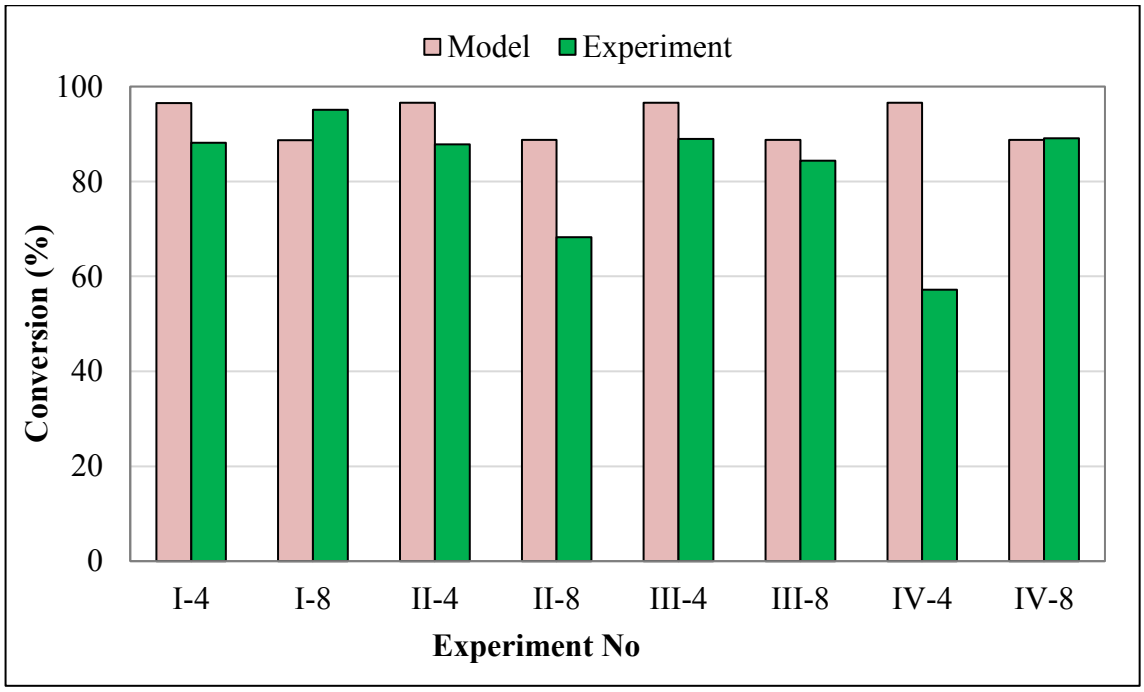

Figure 4.47. Comparison of the CO conversions obtained through the performance tests (Çağlayan *et al*., 2011b) and modeling for the experimental conditions given in Table A.5.

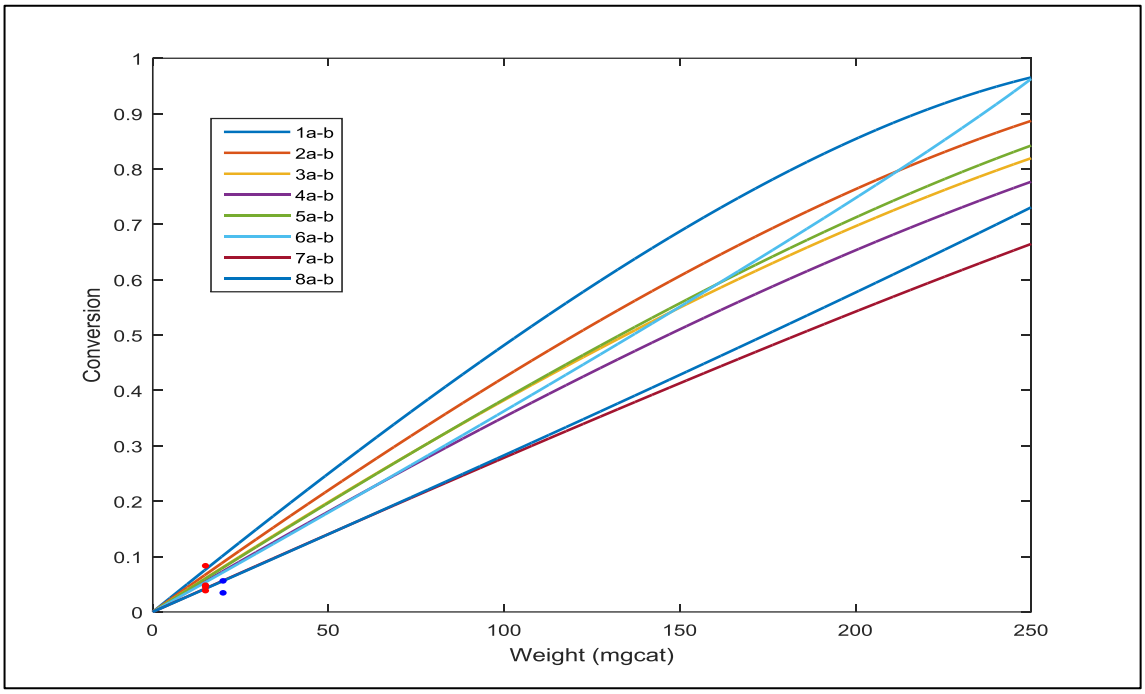

Figure 4.48. Output of PROX modeling algorithm in terms of conversion vs catalyst weight for the kinetic experiments given in Eropak and Aksoylu (2016).

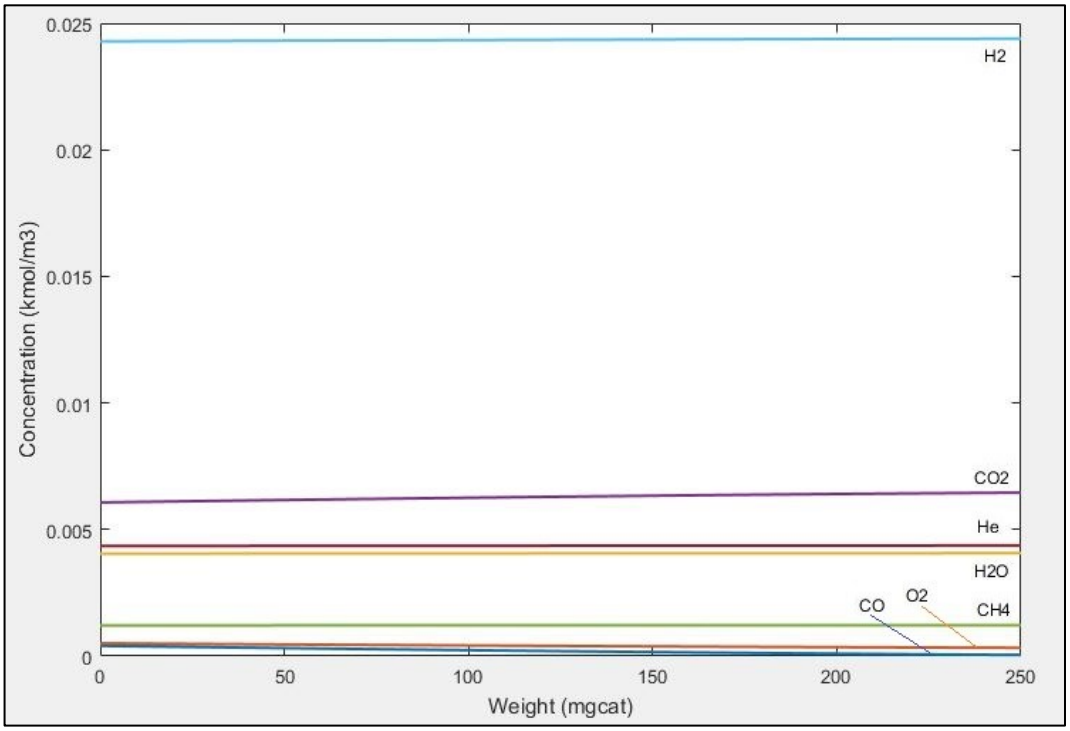

Figure 4.49. Output of PROX modeling algorithm in terms of exit concentration of the species vs catalyst weight for experiment IV-8 (Çağlayan *et al*., 2011b).

Sample output of PROX modeling algorithm in terms of conversion vs catalyst weight, and sample output of exit concentration of the species vs catalyst weight for the operation conditions of Exp. IV-8 (Çağlayan *et al*., 2011b) were given in Figures 4.48 and 4.49, respectively. Since the CO and O_2 concentrations in the feed stream and thereby the conversion levels were very low (~10), the change in the total flow rate cannot be seen clearly, but it was taken into consideration.

4.4.2. Inertia Tests

Modeling of system inertia is the essential element of system dynamics analysis. Inertia tests were conducted to observe *when* and *how* the system responds (*i.e. timely response*) to step changes in the concentrations of C_3H_8 and O_2 in the FPP feed stream under "no reaction" condition. During the tests the reactors were filled with unreduced δ-alumina support in order to create/imitate the effect of possible pressure drop, i.e. velocity change, which may occur through the catalyst bed. As it is mentioned before, there are a lot of transfer lines with changing diameters and lengths in the FPP. Inertia tests helped to determine the time that took MS to sense any change in the feed stream -after the gas mixture passed through all reactors, transfer lines and condensers- and also the time for reaching steady state under no reaction condition.

The tests were performed on the FPP attached to a condenser, whose volume was far larger than the total volume of the reactors and transfer lines that the gas stream travels in FPP. The condenser was used for guaranteeing complete removal of water vapor from the product stream sent to MS for analysis during the performance tests. The tests were conducted in four parts of the FPP, which were only condenser, OSR unit followed by condenser, serial OSR-WGS units followed by condenser and serial OSR-WGS-PROX units followed by condenser. Temperatures of the OSR, WGS and PROX reactors were kept constant at 723 K, 623 K and 383 K, respectively, while the temperature of the main oven and transfer lines were kept at 393 K. The concentrations of C_3H_8, O_2 and H_2O in OSR feed were chosen such as to keep S/C close to 3.0 and C/O_2 close to 2.7, which were the feed ratios of the reference feed used in the catalytic performance tests in Section 4.1.

In general, response time is defined as the time required for a system to reach a new steady state upon a perturbation given to a process variable(s). In the current work, the perturbation was given to the concentration of a species in the feed stream as a step change and the concentration of that species is monitored at the system outlet. As the outlet concentration never reached the level set by the step change in the feed, the response time was defined as the time necessary for the outlet to recover 99.5% of the concentration gap between consecutive concentrations of the species in the feed before and after the step change. In each test, after the gas mixture with the reference feed reached steady state, the system response was observed against positive or negative step changes in either C_3H_8 or O_2 concentrations in the feed stream of OSR unit. As O_2 flow rate in the reference feed was 7.3 ml/min, a positive step with a magnitude of 41.1% (7.3 ml/min→10.3 ml/min) followed by a negative step with a magnitude of 18.4% (10.3 ml/min→8.4 ml/min) were applied in the tests, for which O_2 was the manipulated variable. As C_3H_8 flow rate in the reference feed was 6.6 ml/min, a positive step with a magnitude of 10.6% (6.6 ml/min→7.3 ml/min) followed by a negative step with a magnitude of 30.1% (7.3 ml/min→5.1 ml/min) were applied in the tests, for which C_3H_8 was the manipulated variable. As water must be removed before MS analysis, water (vapor) concentration was not used as the manipulated variable.

Figure 4.50 shows the timely response of the system at the condenser exit against a positive step change (7.3 ml/min→10.3 ml/min) in the O_2 concentration in the FPP feed stream under "no reaction" condition. Though the figure can be used to approximate the response time, online and real time data analysis allowed determining the exact time for a precise analysis. The positive step change was given at t=61 min and the steady state concentration profile of the former/original set was disturbed after 2 minutes and 45 seconds, and the new steady state was reached after 36 minutes.

The real time response of the system at the condenser exit against a negative step change (7.3 ml/min→5.1 ml/min) in the C_3H_8 concentration in the FPP feed stream was given in Figure 4.51. The negative step change was given at t=20 min and similarly the steady state concentration profile of the former set was disturbed after 2 minutes and 45 seconds, and the steady state was reached after 36 minutes.

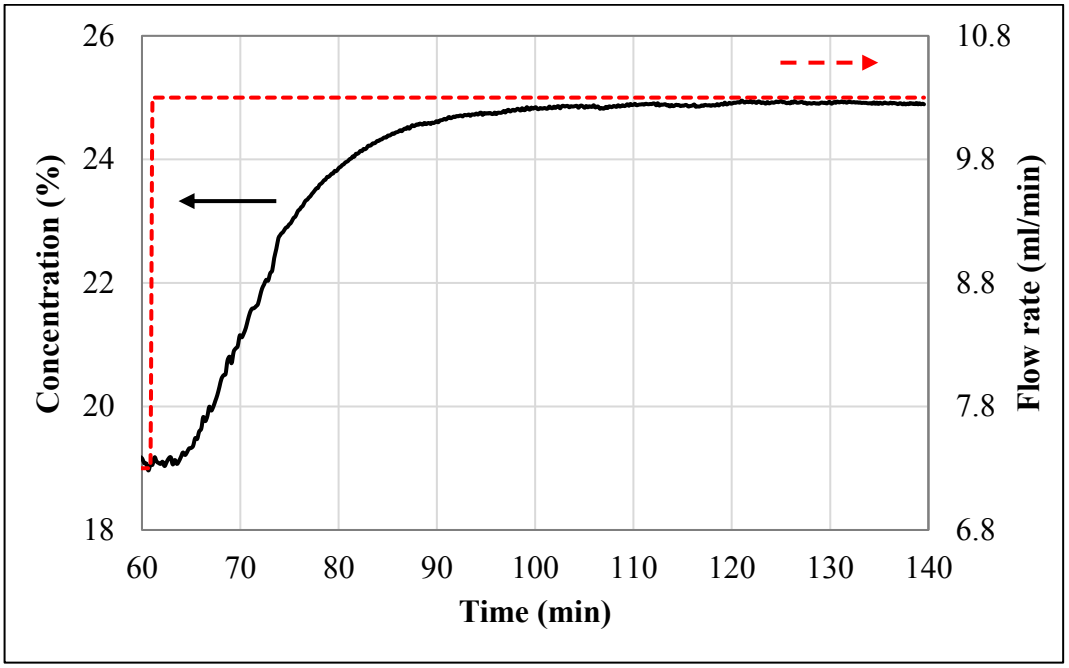

Figure 4.50. Time response of the system at the condenser exit against a positive step change in the O_2 concentration in the FPP feed stream under "no reaction" condition.

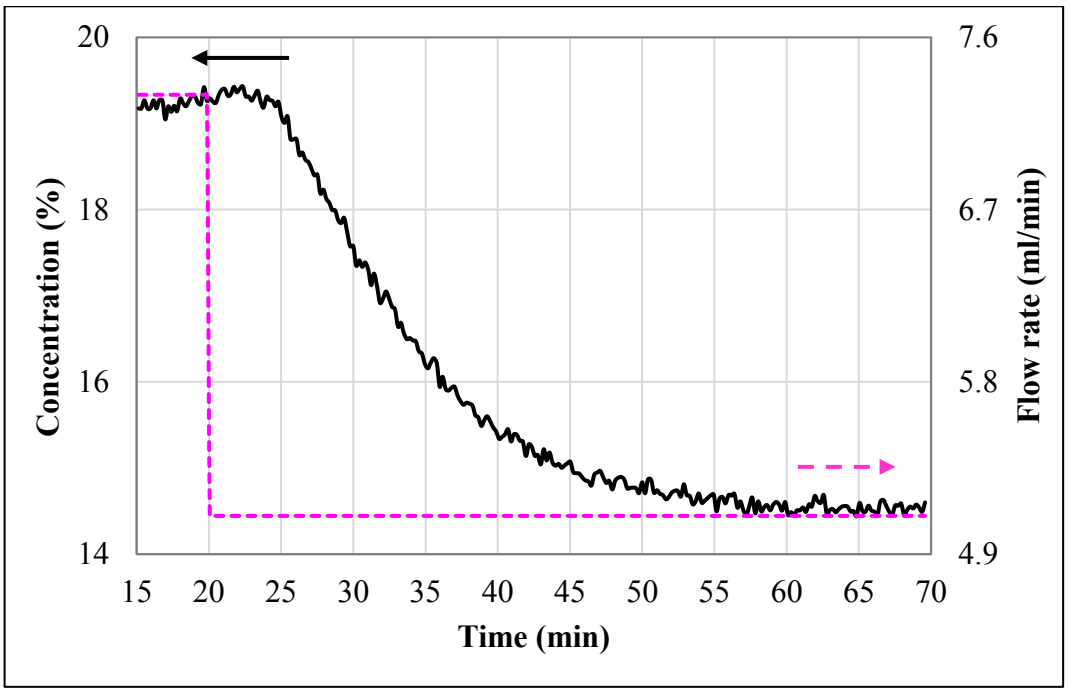

Figure 4.51. Time response of the system at the condenser exit against a negative step change in the C_3H_8 concentration in the FPP feed stream under "no reaction" condition.

The response of the system as normalized concentrations at the exit of different system parts against a positive step change in the O_2 concentration and a negative step change in the C_3H_8 concentration in the FPP feed stream under "no reaction" condition are given in Figure 4.52 and 4.53, respectively. The sensing time of a step change increased to 3.5 minutes at the OSR and condenser exit, to 4 minutes at the OSR-WGS and condenser exit and to 4.5 minutes at the OSR-WGS-PROX and condenser exit. The steady state concentrations before and after the step changes were the same. As it can be seen from the figures, since the system parts were added serially in the above mentioned tests, the volume that the gas mixture must travel through and fill increased and thus, longer times were required to sense any change in MS analysis, thereby to reach the new steady state. Inertia tests confirmed that sensing time of MS and the steepness of the normalized concentration profiles depended on the size of the step change and total volume of the system, but the difference was limited only to seconds. It can be said that in "no reaction" condition, a positive or negative step change given to the whole FPP system sensed after ≈4.5 minutes, and approximately 36 minutes was required for reaching a new steady state after a step change in the feed was made. Similar results were obtained, when a negative step change was applied to the oxygen concentration or positive step change to the propane concentration under "no reaction" condition.

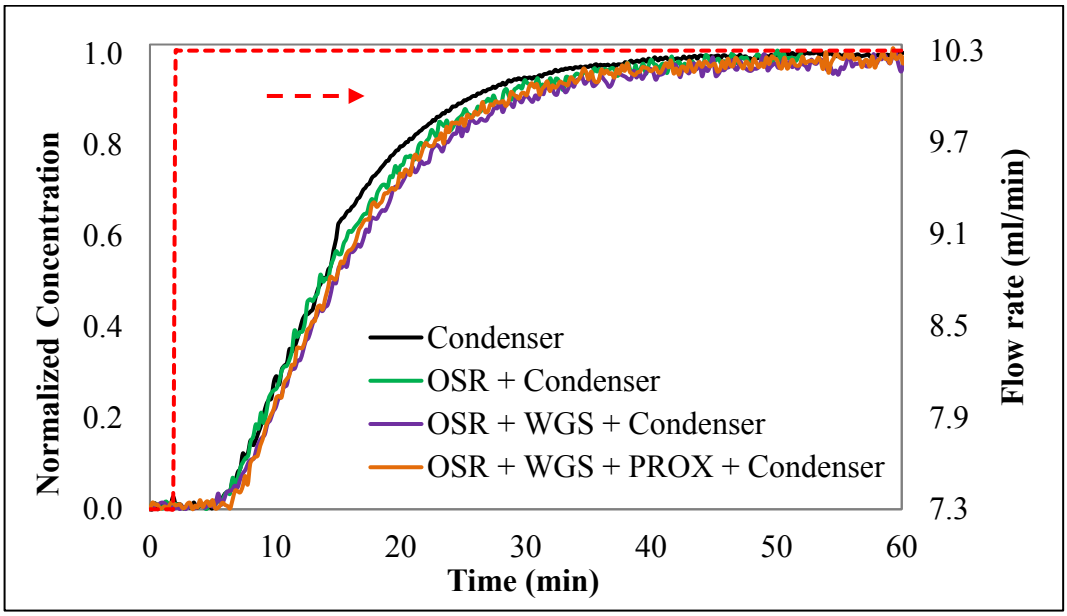

Figure 4.52. Response of the system at different exits against a positive step change in the O_2 concentration in the FPP feed stream under "no reaction" condition.

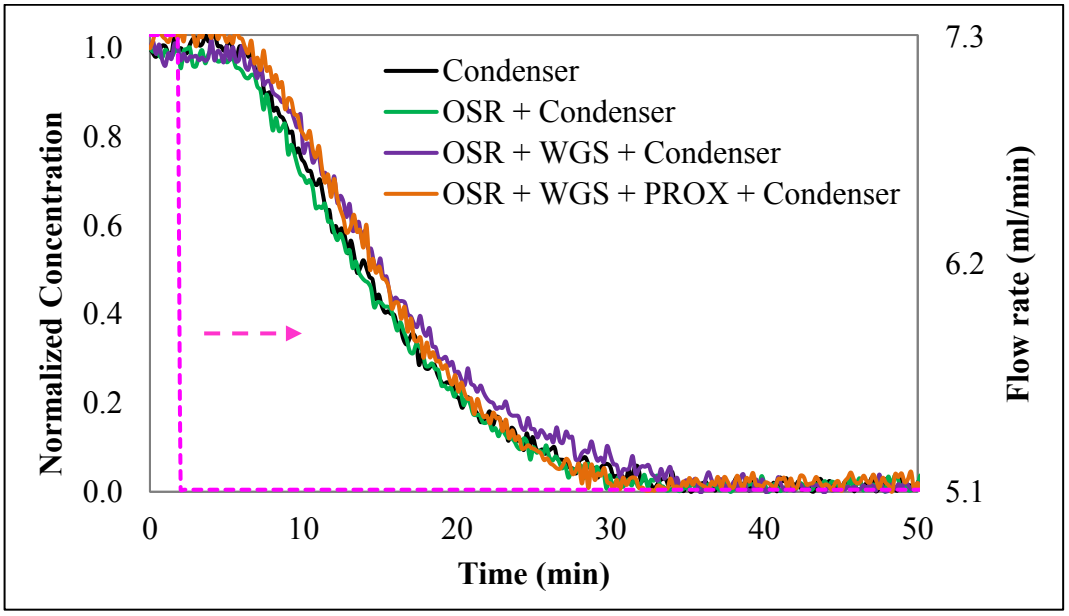

Figure 4.53. Response of the system at different exits against a negative step change in the C_3H_8 concentration in the FPP feed stream under "no reaction" condition.

The rate of change in molar fraction of incoming and outgoing gas streams with different gas compositions in a *particular* volume can be written as:

$$\frac{dx_j}{dt} = \frac{F_{total}}{n_{total}}\left(x_{j,inlet} - x_j\right) = \frac{F_{total}RT}{PV}\left(x_{j,inlet} - x_j\right) \tag{4.30}$$

$$x_j(t_0) = x_{j,0} \tag{4.31}$$

where x_j is the molar fraction of the gas species j in the exit of the system, F_{total} is the total inlet molar flow rate in kmol/min, n_{total} is the total number of moles in kmol in a particular volume V. The initial value of the mole fraction at time t_0 is $x_{j,0}$. $x_{j,inlet}$ is the new value of the process variable with the step change, and x_0 is the former steady state value at the particular volume.

Inertia modeling algorithm covered comparison of both experimental data obtained during the inertia test against step changes and also modeling of different parts of the system by using Equation 4.30 and 4.31, i.e. by knowing initial and final (steady state) values of the

molar fractions. The aim of the algorithm is to minimize the error between the experimental data and modeling data for a volume in a specified interval. The optimum volume corresponding to minimum error, i.e. residual sum of squares (RSS) was compared to the real volume of the different parts of the system as given in Table 4.9. Residual sum of squares was calculated by the Equation 4.32 and was used to predict deviations from the experimental data and to measure the difference between the experimental data and the model estimation.

$$RSS = \sum_{i=1}^{n} \left(x_{exp,i} - x_{model,i}\right)^2 \tag{4.32}$$

where $x_{exp,i}$ is the value of the mole fraction to be predicted (experimental) and $x_{model,i}$ is the predicted value of x_i obtained through modeling for the same time values of experimental data. The different parts of the FPP includes cylinder condensers (0.2 L each), spiral condenser (2 m - 1/4" stainless steel tubing), 1/4" stainless steel tubings (0.3167 cm^2 cross section), 1/8'' stainless steel tubings (0.079 cm^2 cross section), reactors (37 cm - 1/4" stainless steel tubing), reducing unions, etc. The calculated real volumes were given in Table 4.9. Close results were obtained with respect to the actual volumes with an average of 2-4% error in optimum volume values.

Table 4.9. Comparison of the real volume and optimum volume obtained through modeling of the different parts of the FPP.

Part of the FPP	$\boldsymbol{V_{real}\ (L)}$	$\boldsymbol{V_{optimum}\ (L)}$	**RSS**
Condenser	0.487	0.475	0.000118
OSR + Condenser	0.510	0.490	0.000108
OSR + WGS + Condenser	0.543	0.521	0.000118
OSR + WGS + PROX + Condenser	0.560	0.542	0.000123

Minimization of the residual sum of square/error with respect to volume in condenser for a negative step change in C_3H_8 concentration is given in Figure 4.54. The optimum volume giving the minimum error was found as ~0.475 L, as given in Table 4.9. Similar

optimization procedure was carried out for all parts of the FPP system. Since the actual volume was known, the interval was selected on the basis of the expected volume interval. Figure 4.55, 4.56 and 4.57 show the comparison of experimental and predicted mole fractions with respect to time for oxygen, helium and propane species, respectively, in OSR-WGS-condenser system for a positive step change in O_2 concentration. The results showed that the model fitted experimental data very well.

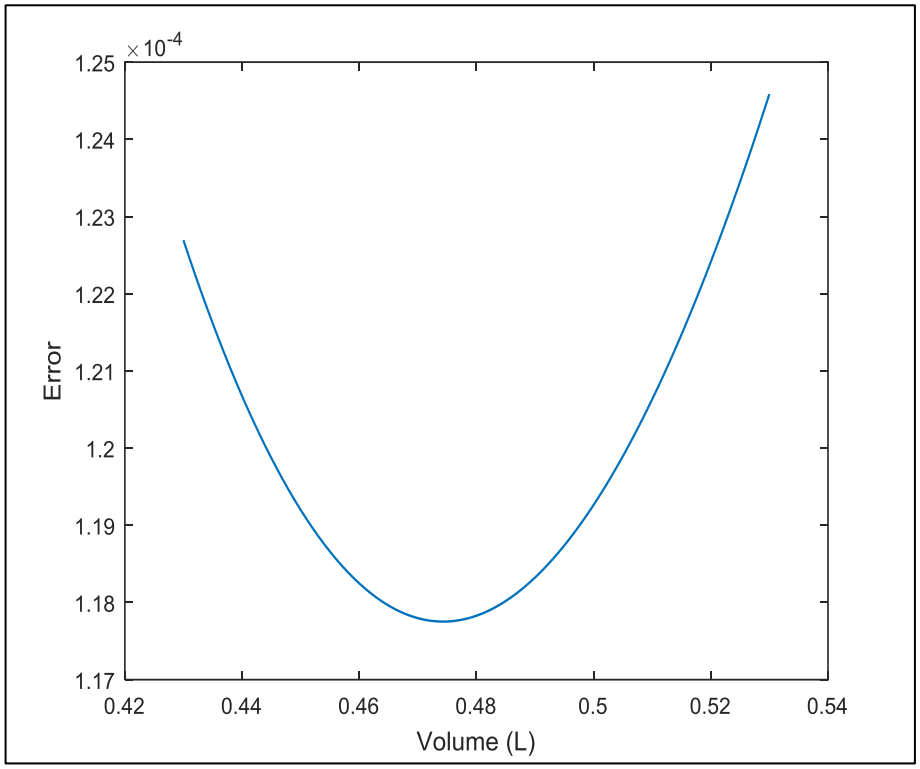

Figure 4.54. Minimization of the residual sum of square/error for O_2 mole fractions with respect to volume in condenser for a negative step change in C_3H_8 concentration.

It can be predicted that in dynamic tests reaching a new steady state will take longer than 36 minutes because of the time required to bring all reactors, in which many side reactions occur beside the main reaction, to the new steady state. Knowing the inertia of the system, one can study the dynamic response of the system to any step change in a detailed fashion and can model the system response. The inertia test models can be used in analyzing the system dynamics during real operation helping to form the control structure.

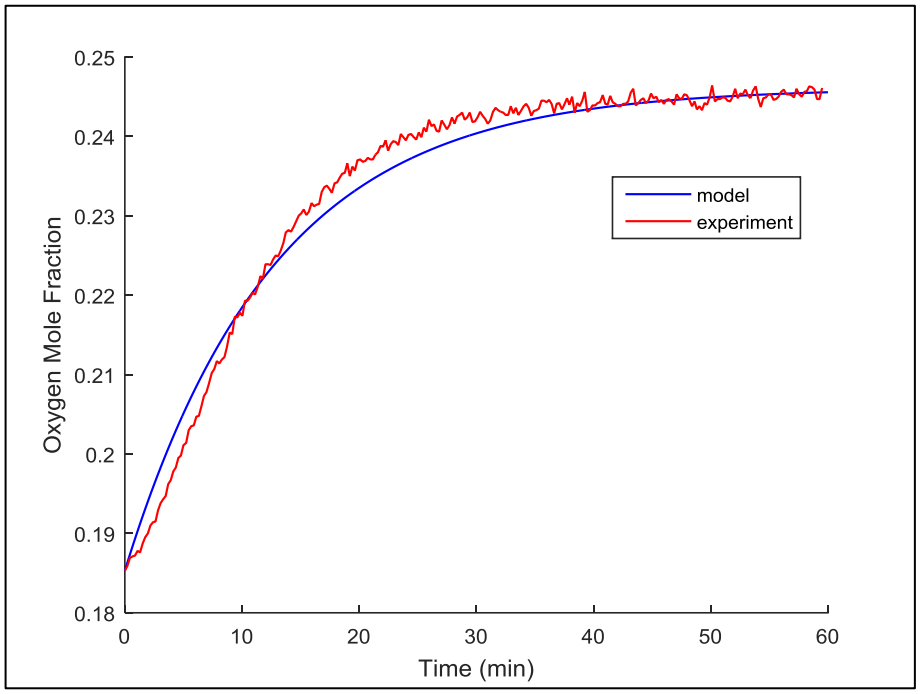

Figure 4.55. Experimental and predicted oxygen mole fractions with respect to time in OSR-WGS-condenser system for a positive step change in O_2 concentration.

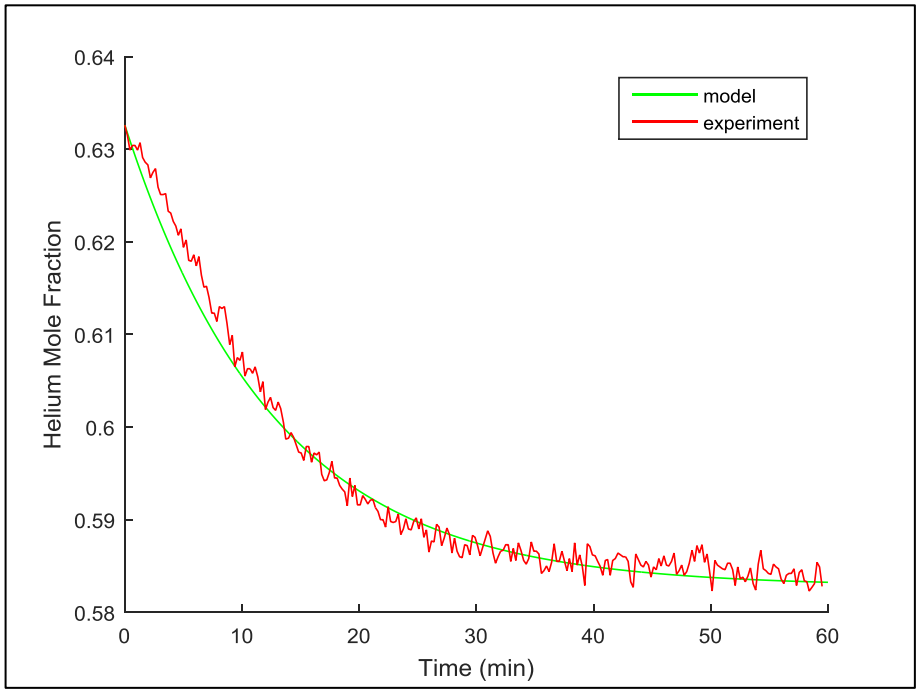

Figure 4.56. Experimental and predicted helium mole fractions with respect to time in OSR-WGS-condenser system for a positive step change in O_2 concentration.

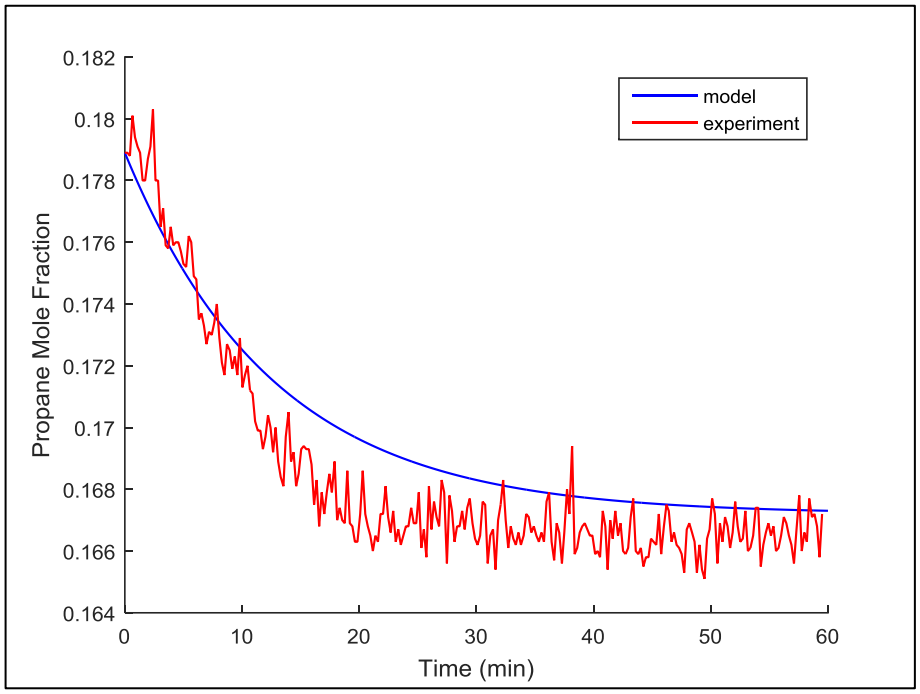

Figure 4.57. Experimental and predicted propane mole fractions with respect to time in OSR-WGS-condenser system for a positive step change in O_2 concentration.

4.4.3. Dynamic Tests

Determination of the dynamic response of the FPP system against step changes in the concentrations of the feed gases, e.g. O_2, C_3H_8 and H_2O required the analysis of the exit concentration profiles till the new steady state is reached under reactive conditions. Current preliminary analysis in this section focuses on the determination of the reliable system control parameters under dynamic operation. As the results of the performance tests showed C_3H_8 and O_2 species were totally converted in the OSR unit, H_2, CH_4, CO and CO_2 concentrations are the only candidates to be used as the control parameter(s). Due to the fact that H_2 and CO gases are simultaneously consumed and produced in all reactors, it was harder to observe steady state concentration profiles for those species. However, CO_2 and CH_4 concentrations showed much more stable steady state profiles with higher signal-to-noise ratios and thus are considered the most reliable and consistent system control parameters during real operation and reactive conditions.

Figure 4.58, 4.59 and 4.60 show the dynamic response of the OSR unit against step changes in the process variables during reaction. H_2, CH_4, CO and CO_2 concentration profiles obtained resemble S-shaped curves as the profiles of C_3H_8, O_2, and He observed in the inertia tests. Dynamic tests enabled to explain the system *and* the catalyst performances, in terms of increasing or decreasing extents of the contributing reactions, through observing increased or decreased concentrations of the species in the product stream (Figure 4.58, 4.59 and 4.60). It became possible to compare, and *sense*, the size of the step change given to the feed concentrations of the manipulated variables through the resultant amounts (%) of increased or decreased concentrations in the product stream.

Dynamic tests formed a basis that allows combining transient and kinetic modeling of the FPP system. The experimental data obtained during dynamic tests were compared to the time based product concentration data, which were estimated through the system model(s) utilizing corrected kinetic expressions. The FPP system allows to perform 3 to 5 separate experiments within 6-8 hour TOS by giving step changes to the species in the feed concentrations. Experimental results discussed in Section 4.1, 4.2 and 4.3 were obtained through this method and the stability of the catalysts were confirmed in a 75 hour TOS performance test given in Section 4.1.4.

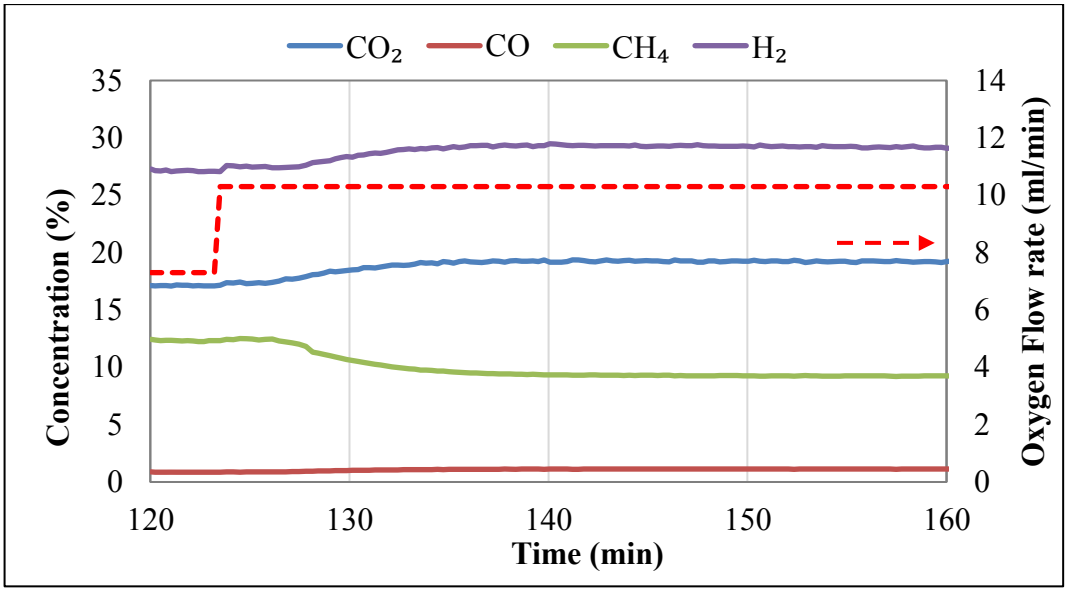

Figure 4.58. Dynamic response of the OSR unit against a positive step change (7.3 ml/min→10.3 ml/min) in the O_2 concentration in the FPP feed stream under reactive conditions at 723 K (dry based with inert).

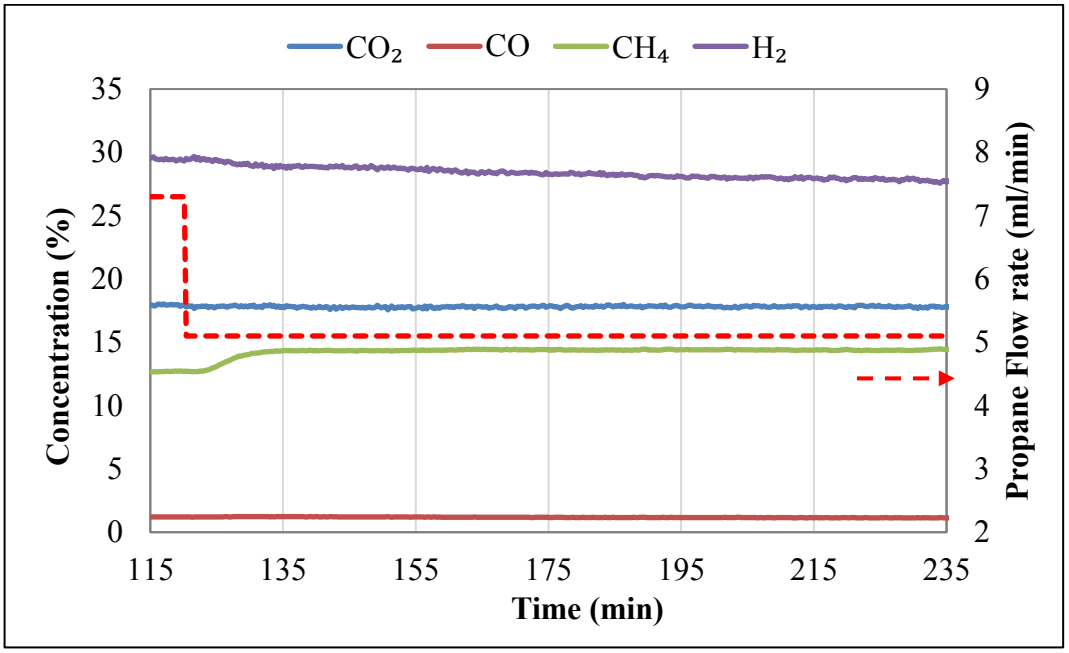

Figure 4.59. Dynamic response of the OSR unit against a negative step change (7.3 ml/min→5.1 ml/min) in the C_3H_8 concentration in the FPP feed stream under reactive conditions at 723 K (dry based with inert).

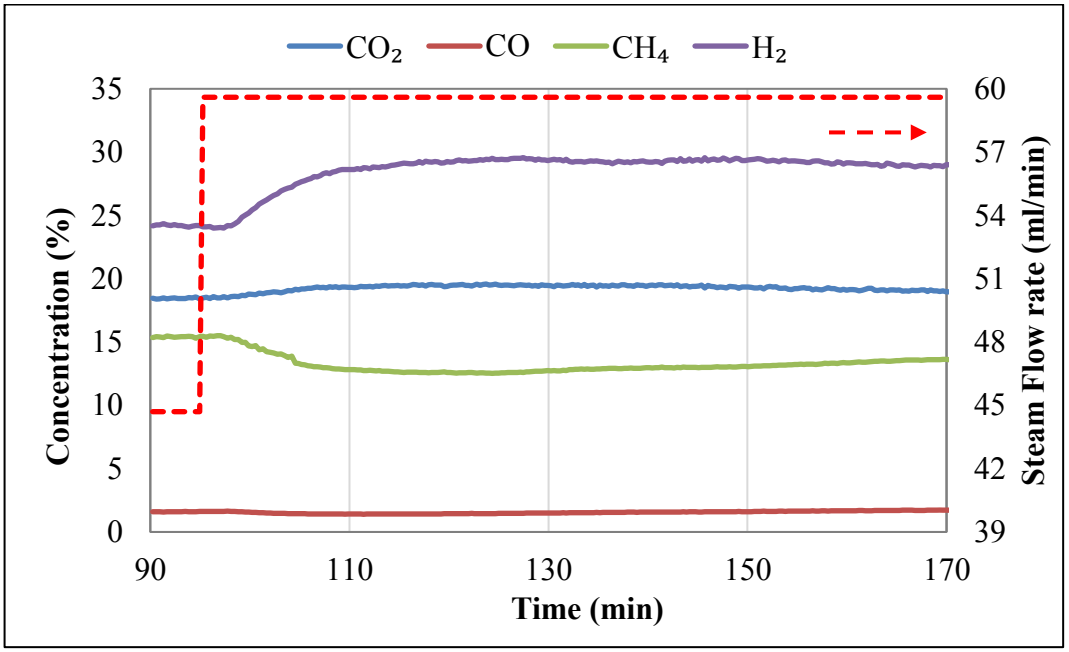

Figure 4.60. Dynamic response of the OSR unit against a positive step change (44.7 ml/min→59.6 ml/min) in the H_2O concentration in the FPP feed stream under reactive conditions at 723 K (dry based with inert).

As stated before, steady state profiles were achieved in 36 minutes during inertia tests conducted for “no reaction” condition. As it is expected, steady state in the presence of the catalysts/reactions (i.e. for “reactive” condition) was achieved in a longer TOS; approximately 1 hour and 20 minutes was needed to reach ~99.5% of the steady state value, as the time lengths necessary to reach steady state under reactive conditions differed from reactor to reactor. As an example, TOX occurs very fast, however WGS occurs rather slowly due to its reversibility; thereby, reaching a steady state required a longer TOS when WGS is involved. In any case, 2 hour TOS was found enough to observe steady state profiles, as given in Figure 4.58, 4.59 and 4.60.

4.4.4. Combined Transient and Kinetic Modeling of the FPP System

The aim of this section is to compare the experimental data obtained during the catalytic performance tests in the FPP system with the time based concentration data estimated through dynamic modeling and corrected kinetic rate expressions. Figure 4.24 shows the structure of the modeling algorithm including all inlet and outlet streams of the reactor blocks. In the FPP system, the first assumption was that each reactor was composed of two sections; (i) catalyst bed, where the reaction actually occurs and kinetic rate expressions were used for (K), (ii) the volume, which was considered as a tank (T) that had to be filled by the gas mixture in order to reach a steady state value.

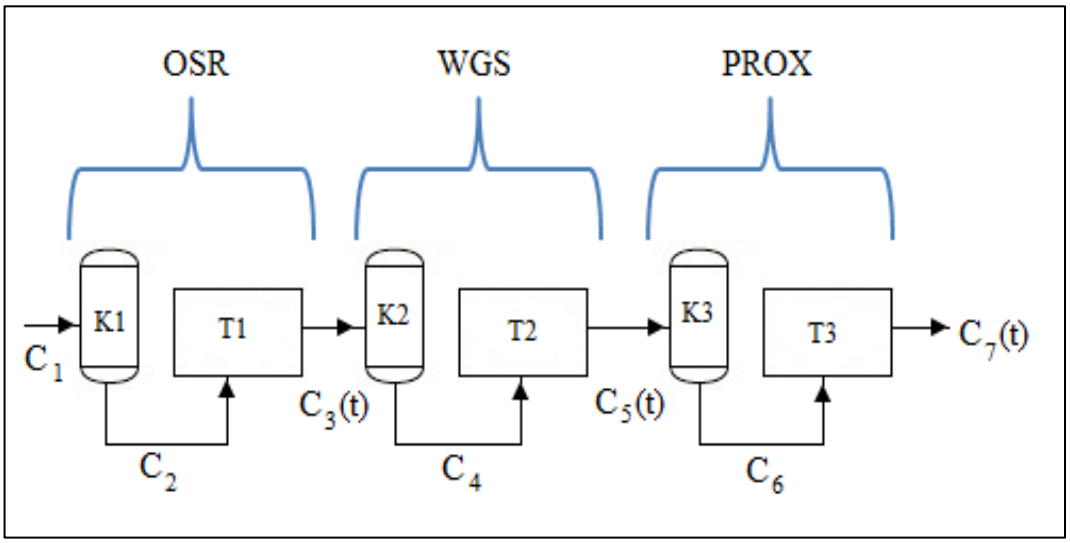

Figure 4.61. Structure of the modeling algorithm.

There were several reasons for analyzing each reaction in two separate sections. The first reason was the occurrence of the reactions were so fast that it became extremely hard to define the concentrations throughout the catalyst bed with respect to time. The second reason was the results of the inertia tests showing time-based concentrations of the species were mostly dependent on the volume that should be travelled.

In a more detailed way, e.g. for the OSR reaction, the first part of the algorithm (K1) calculated the output variables, conversion and concentrations of each species, by *excluding* time for the given input parameters, temperature, OSR kinetic rate expression, feed composition (C1) and catalyst weight. This algorithm was used above in Section 4.1, where sample output of OSR modeling algorithm in terms of conversion vs catalyst weight and exit concentration of the species (C2) vs catalyst weight were given in Figure 4.39 and 4.41, respectively. The algorithm enabled both to observe the linear region *(indicating the kinetically controlled region)* and also the thermodynamically controlled region. It was also possible to observe the maximum achievable conversion under the operation conditions of the kinetic regime for higher catalyst weights. The second part of the algorithm used the concentrations of the species (C2) just after the reaction as the feed composition, which were used as the *inlet* conditions in the first order differential equation given below. The form of the equation was very similar to the one used in inertia tests (Equation 4.30) except the initial and inlet conditions. The rate of change in the concentrations of each species for the inlet stream, $C_{j,inlet}$ and the initial condition corresponding to a former steady state value, $C_{j,ss}$ in a *particular* volume V_i can be written as Equation 4.32.

$$\frac{dC_j}{dt} = \frac{F_{total}}{V_i}\left(C_{j,inlet} - C_{j,ss}\right) \tag{4.32}$$

Figure 4.62 shows a sample output of the time-dependent OSR outlet concentrations (C3(t)) estimated through the second part of the modeling for a 1-h TOS and a particular volume (~0.51 L) filled with helium before, representing the condenser, for the experimental conditions given as A9 in Table 3.6. The decrease in helium concentration and the increase in the other species' concentrations due to the reactions can be clearly seen. The algorithm

gave a propane conversion of 97.11%. S-shaped concentration profiles were observed similar to those obtained in the inertia tests for the given particular volume.

In the modeling of WGS reaction (Section 4.1.2), the feed compositions including only the species involved in the reaction (CO, H_2O, CO_2, H_2 and He) were given *by the user* as the inputs. In this part, all species (CO, H_2O, CO_2, H_2, He, CH_4, C_3H_8, O_2) with real concentrations were used as the feed stream sent to the WGS reactor. Continuing with the same experiment A9, the algorithm gave a CO conversion of 45.1% for OSR feed having S/C ratio of 2.25, which were very close to the experimental conversion level (C4 concentrations). Figure 4.63 shows a sample output of the time-dependent WGS outlet concentrations (C5(t)) estimated through the second part of the modeling for a 1-h TOS and a particular volume (~0.54 L) filled with helium before, representing the condenser.

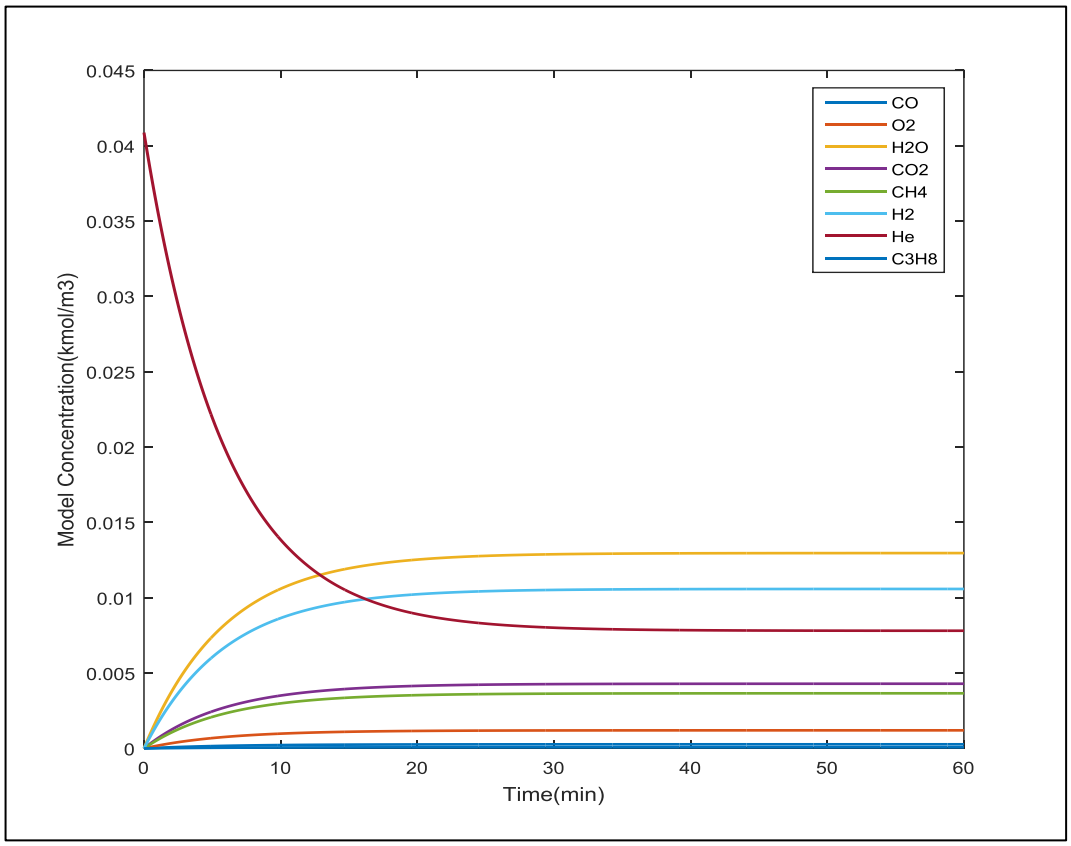

Figure 4.62. Output of the second part of the modeling in terms of time-dependent concentrations (C3(t)) of the species in the exit of the OSR block (T1).

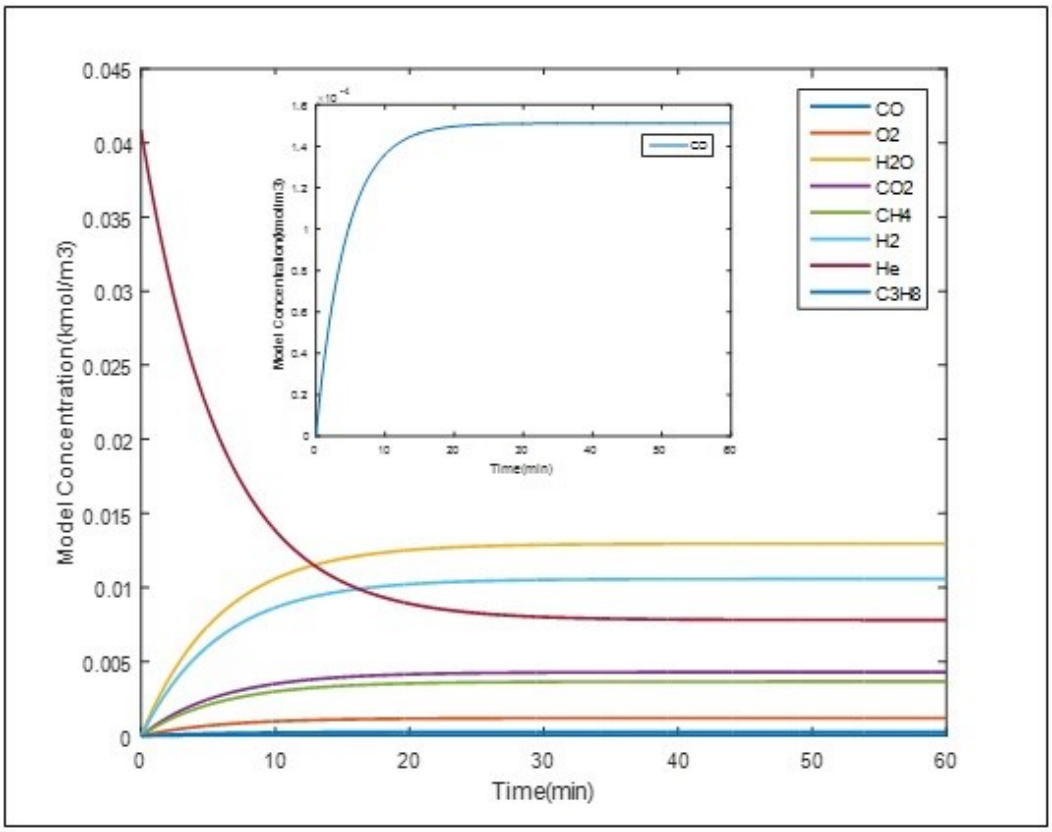

Figure 4.63. Output of the second part of the modeling in terms of time-dependent concentrations (C5(t)) of the species in the exit of the WGS block (T2).

In the modeling of PROX reaction (Section 4.1.3), the feed compositions, i.e. concentrations of the species involved in the reaction, CO, H_2O, CO_2, H_2, He, CH_4 and O_2, were given *by the user* as inputs. In this part, the unconverted C_3H_8 in OSR unit was transferred to the PROX unit and used in the modeling calculations as well. Continuing with the same experiment A9, the algorithm gave a CO conversion in the PROX reactor of 44.6% for no additional O_2 (C6 concentrations). Finally, the considering the volume of the whole FPP system, the time-dependent PROX outlet concentrations (C7(t)) were estimated through the second part of the modeling for a 1-h TOS and a particular volume (~0.56 L) filled with helium before, representing the condenser.

The next part of the modeling covered comparison of experimental concentration data with the data obtained via the combination of dynamic modeling utilizing rate expressions. Before comparison, the first step was to get rid of the time delay in the experimental data, which was determined as 2 minutes and 45 second for the condenser exit, 3 minutes and 30

seconds for the exit of OSR-condenser system, 4 minutes for the exit of OSR-WGS-condenser system, and 4 minutes and 30 seconds for the exit of OSR-WGS-PROX-condenser system. As data acquisition time range and corresponding number of data points were different between experimental and dynamic model data sets, an interpolation scheme was applied to the dynamic model output data such as to synchronize the sampling times. In this way, for each time level in the experiments, a dynamic modeling data was obtained including all concentrations, volumes, etc. The next step was to calculate residual sum of squares or error between the measured and estimated concentrations of all the species per number of sampling time (n_s) for the interested time period, as given in Equation 4.33.

$$E = \frac{1}{n_s}\left(\sum_{species}\sum_{exp}\sum_{time}\left(\left(C_{model}(t) - C_{exp}(t)\right)^2\right)\right) \qquad (4.33)$$

The exit concentration of each species was given as a function of both time and the parameters used in the kinetic rate expressions. In order to correct the kinetic rate expressions, the error was calculated as a function of the rate orders and they were changed parametrically in ±10% of the published values given in Table 4.5 (Gökaliler *et al*., 2012) for Equation 4.3. The function E must be minimized with respect to all orders. The calculated errors as a function of the rate order combinations (Table 4.10) were given in Figure 4.64.

Table 4.5. Estimated kinetic parameters and reaction orders for the OSR reaction of propane over 0.2wt.%Pt-10wt.%Ni/δ-Al_2O_3 catalyst (Gökaliler *et al*., 2012).

Parameter	**Estimate**	**Unit**
k_0	5.51	μmol.mgcat^{-1}.s^{-1}.kPa$^{-3.49}$
E_A	46.19	kJ.gmol^{-1}
α	1.64	-
β	2.44	-
γ	-0.59	-

$$-r_{C_3H_8} = \left[k_0 exp\left(\frac{-E_A}{RT}\right)\right] P_{C_3H_8}^{\alpha} P_{O_2}^{\beta} P_{H_2O}^{\gamma} \qquad (4.3)$$

As the first step, the ranges of the reaction orders to be tested were determined for the basis of RSS calculations. Three values of α, β, γ were selected as given in Table 4.10 by keeping the range in ±10% of the published values, resulting in a total of 27 combinations. Considering the validity of the rate expression for the S/C feed ratio range of 2-3 used in the kinetic tests (Gökaliler *et al*., 2012), experiments both fitting that range and out of that range were selected for a better comparison. The selected experiments were conducted in the S/C ratio range of 2.25-6 and at 723 K, which were given in Table 3.6. The maximum measured concentration values in the experiments were in the 0.005-0.01 kmol/m^3 range, similar to the estimated data. Therefore, RSS values with ~0.0001 values showed very small discrepancies between the experimental data and the estimation model. Note that the reaction order values presented in combination number 14 in Table 4.10 are the orders determined by our group based on the kinetic data (Gökaliler *et al*., 2012). As it can be seen in Figure 4.64, the combinations corresponding to lower limits of the reaction orders resulted in lower error values. The blue square points in Figure 4.64 denote the total error values for the experiments conducted. In the minimization of the error, the combination giving the lowest total error value should be considered. When the upper limits of the reaction orders were observed, the gradual increase in the error values can be clearly seen in Figure 4.64. At higher reaction orders of α and β the sensitivity to S/C feed ratio increased and higher error values were observed, while decreasing the γ value resulted in lower error values. Considering these trends, combination number 3 would be the most appropriate selection giving the minimum error in the tested range.

The concentration data measured during the experiment A9 at 90 min TOS are given in Table 3.6, and data obtained by dynamic modeling are given in Figures 4.65 and 4.66, respectively. CO_2, CH_4, CO and C_3H_8 concentration profiles fitted perfectly, and their steady state values were nearly the same.

The combination of dynamic modeling and correction of kinetic rate expressions requires an extensive parametric study covering hundreds of experimental data by excluding time delays, since the concentrations were affected not only by the reaction orders but also the activation energy and specific rate constant; thus, the optimization schemes can be extended such as to include optimization through activation energy and specific rate constant for ±10% range of their experimental values.

Table 4.10. Combinations of reaction orders in the correction of OSR rate expression

Combination Number	α	β	γ
1	1.46	2.19	-0.50
2	1.46	2.19	-0.56
3	1.46	2.19	-0.60
4	1.46	2.43	-0.50
5	1.46	2.43	-0.56
6	1.46	2.43	-0.60
7	1.46	2.67	-0.50
8	1.46	2.67	-0.56
9	1.46	2.67	-0.60
10	1.62	2.19	-0.50
11	1.62	2.19	-0.56
12	1.62	2.19	-0.60
13	1.62	2.43	-0.50
14	1.62	2.43	-0.56
15	1.62	2.43	-0.60
16	1.62	2.67	-0.50
17	1.62	2.67	-0.56
18	1.62	2.67	-0.60
19	1.78	2.19	-0.50
20	1.78	2.19	-0.56
21	1.78	2.19	-0.60
22	1.78	2.43	-0.50
23	1.78	2.43	-0.56
24	1.78	2.43	-0.60
25	1.78	2.67	-0.50
26	1.78	2.67	-0.56
27	1.78	2.67	-0.60

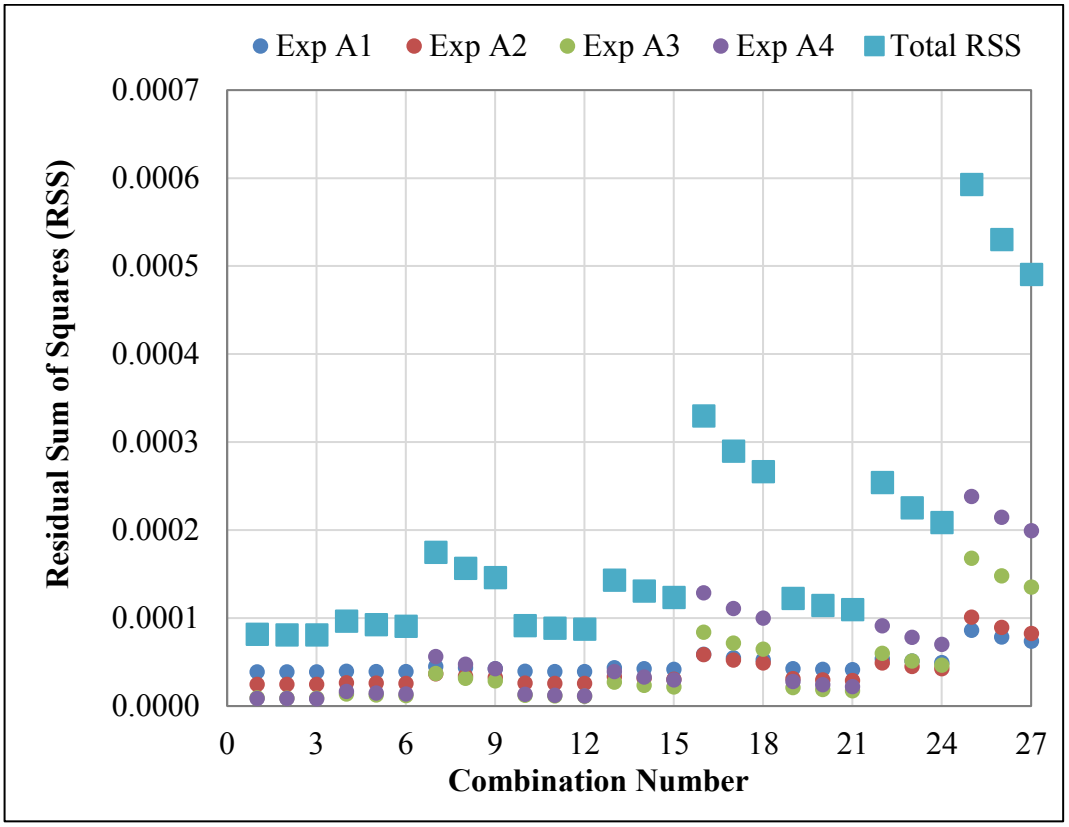

Figure 4.64. Residual sum of squares as a function of the combinations of reaction orders in the exit of the OSR block (T1).

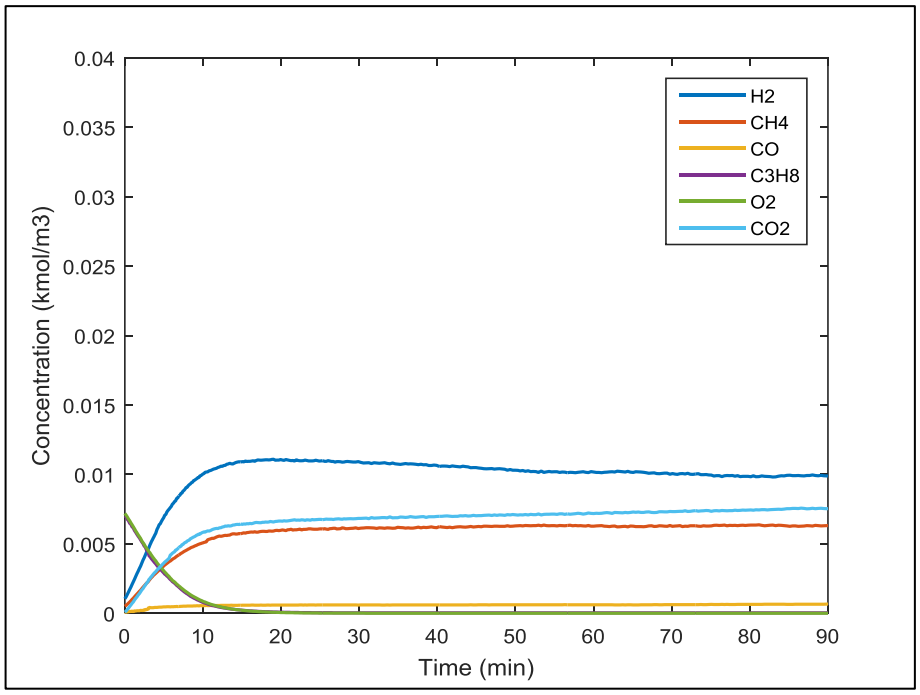

Figure 4.65. Experimental time based concentration data for exp. A9 given in Table 3.6.

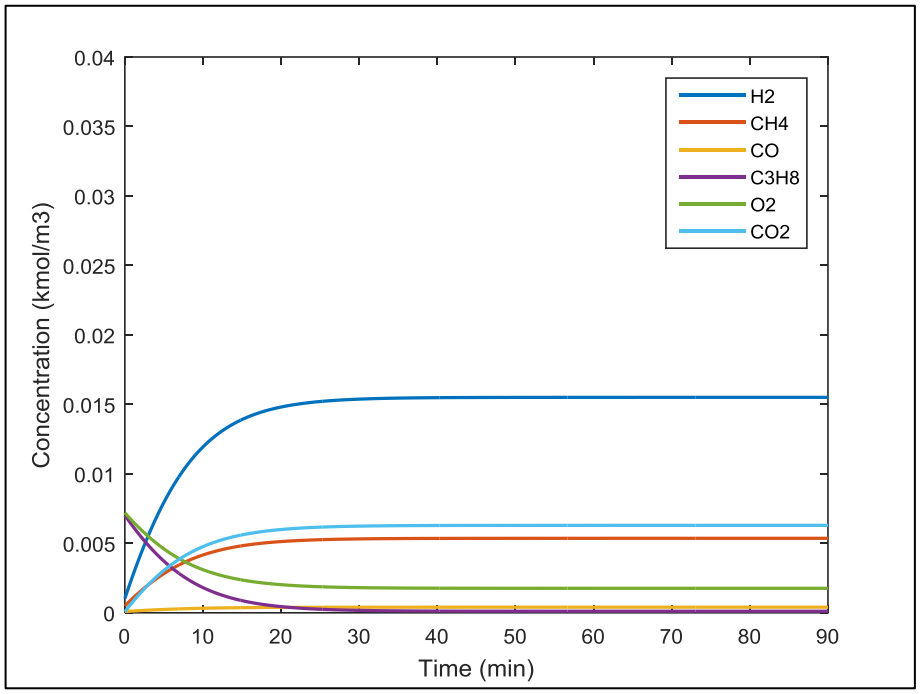

Figure 4.66. Concentration data obtained through modeling and kinetic rate expression for the feed conditions of exp. A9 given in Table 3.6.

4.5. Adsorption Studies over Modified Activated Carbon Based Adsorbents

The aim of the current work is to design and develop high performance AC based adsorbents for selective CO_2 adsorption. In this context, basic N-containing surface groups were introduced to AC samples in an experimentally designed fashion through liquid and gaseous ammonia treatment methods to increase both their CO_2 adsorption capacity under pure CO_2, and their selective adsorption ability under CO_2-involved gas mixture atmospheres.

In adsorbent preparation, a commercial activated carbon, Norit ROX, was subjected to different oxidative, alkali, thermal, amination and ammoxidation treatments as given in Table 3.3. The adsorbents were characterized by Scanning Electron Microscopy/Electron dispersive X-Ray (SEM-EDX) for studying microstructural properties. The adsorption performance of the adsorbents were tested and measured by using IGA-DSMS system, and comparatively analyzed on the basis of their adsorption capacity, in terms of mg adsorbed/g

adsorbent or percentage mass uptake, and of their selective CO_2 adsorption ability from CO_2-CH_4 mixture.

A new methodology for the determination of selective adsorption capacity of the adsorbent under multicomponent gas mixture atmosphere/flow was developed and proposed (for the detailed procedure see Section 4.5.1). The methodology utilizes IGA-DSMS data, and makes both the calculation of adsorption capacity and adsorption kinetics parameters of an adsorbent possible for each species under binary, tertiary and multicomponent atmospheres/flows.

4.5.1. Determination of Selective Adsorption Capacities in Multicomponent Mixtures

The integrated gravimetric analyzer-mass spectrometer (IGA-MS) system is designed in such a way that; (i) gases are supplied by pressurized cylinders through gas pressure regulators and mass flow controllers at constant pressure and flow rate, and (ii) changes in *total* adsorbent weight are acquired by the gas sorption analyzer in real time with respect to the ramp type changes in pressure followed by data acquisition at the specified pressure set point, and (iii) the composition of the unadsorbed gas stream exiting the adsorption chamber is analyzed via dynamic sampling mass spectrometer. The combined use of gravimetric sorption measurements by dynamic mixed gas sorption analyzer, and unadsorbed/effluent gas analysis results by dynamic sampling mass spectrometer is the basis of a reliable methodology that can be used in determination of the adsorption capacity of the adsorbent for each species in multicomponent sorption studies.

As the first step of the calculation procedure, blank experiments are carried out at RT for the multicomponent gas mixtures to be tested, i.e. 50% CO_2-50% CH_4 and 10% CO_2-90% CH_4 mixtures in the current study, without using any adsorbent material in the sample container. Blank tests are conducted in order to observe the effect of ramp type pressure increase by the gas sorption analyzer and corresponding partial pressure signals of the studied gases for each set pressure level on the mass spectrometer analysis. The output data of mass spectrometer resemble S-shaped curve between each successive pressure set points, e.g. 500-600 mbar, as given in Figure 4.67. The partial pressure signal at time t_1, which belongs to the former set point, i.e. 500 mbar, is subtracted from all the partial pressure

signals in the current pressure range studied. Then, these data are divided by the steady state pressure signal belonging to the latter set point, i.e. 600 mbar, which results in normalized partial pressure levels for each species. Finally, time vs. normalized pressures are used to approximate the area under the solid curve from t_1 to t_3 via trapezoidal rule (Figure 4.67).

As the second step of the calculation procedure, S-shaped curve obtained in adsorption tests is investigated as two consecutive regions; in Region (i), pressure is ramp-wise increased, and adsorption of both species occur on the adsorbent material from t_1 to t_2; and in Region (ii), pressure set point is reached in the adsorption chamber, however the adsorption process continues at constant pressure till adsorbent surface is saturated with related species from t_2 to t_3 (Figure 4.67). The slight decrease in partial pressure signal in the mass spectrometer and the increase in the weight of the adsorbent with respect to the time due to *ongoing adsorption* in gas sorption analyzer can be clearly seen in Figure 4.67 and Figure 4.68, respectively. Therefore, normalization procedure for the adsorption tests is based on the partial pressure signal corresponding to time t_2 (the time, at which the pressure set point is reached) instead of steady state partial pressure signal used in the blank tests. Then, the area under the dashed curve in normalized pressure vs time graph is approximated from t_1 to t_3 by using trapezoidal rule.

As the next step, the area under the adsorption curve (dashed) is subtracted from the area under the blank curve (solid), which is related to the amount of *adsorption* (Figure 4.30). Volume of each sent gas is calculated by using the volumetric flow rate of each species (ν_j) in the feed stream and the time range (t_1-t_3). The area, which corresponds to the amount of the sent gas that reached mass spectrometer shown as rectangular area in Figure 4.30, is used to relate the volume of each sent gas to the volume of the adsorbed gas, i.e. the ratio of areas are related to the ratio of the volume of the gases as given in Equation 4.34. Since $P^*_{b,1}$ and $P^*_{b,3}$ are lower and upper limits of the normalized partial pressure data of blank tests, Equation 4.34 can be simplified into Equation 4.35.

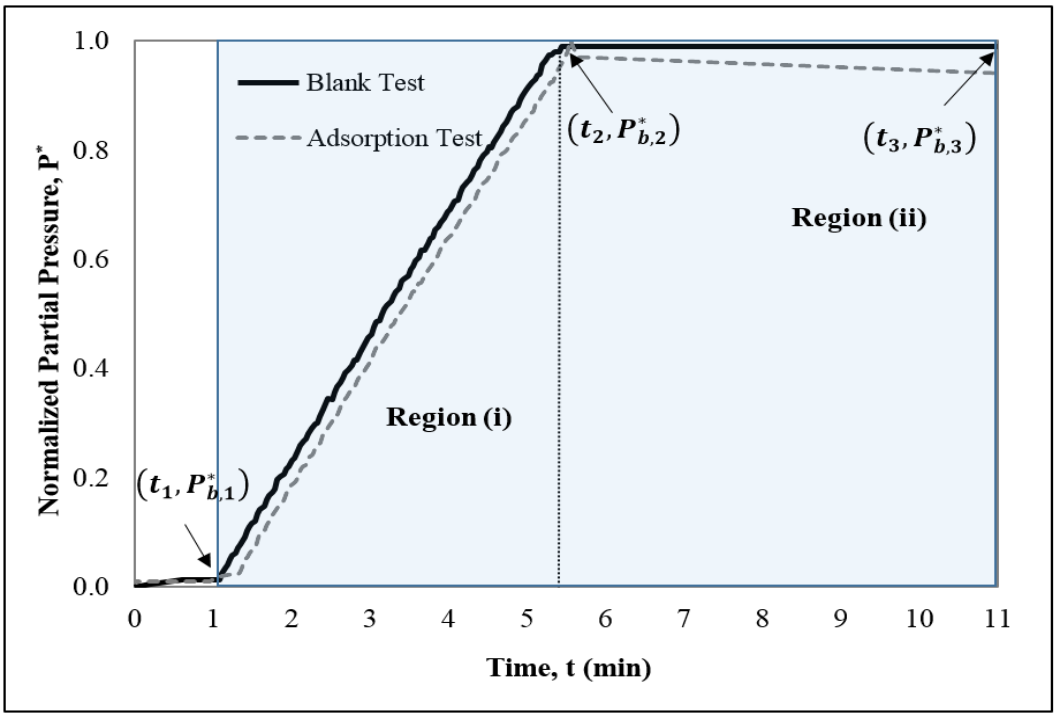

Figure 4.67. Comparison of normalized MS partial pressures in blank and adsorption tests at RT for 500-600 mbar pressure range with 50% CO_2-50% CH_4 mixture.

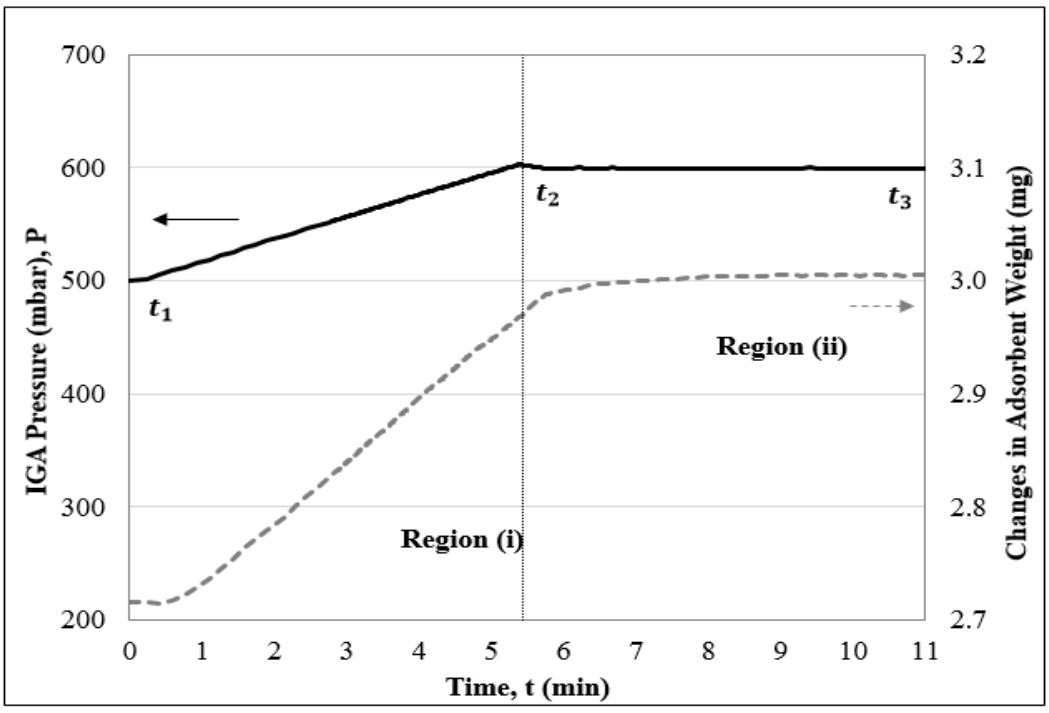

Figure 4.68. Change of IGA pressure and adsorbent weight with respect to time for the adsorption test conducted at RT for 500-600 mbar pressure range with 50% CO_2-50% CH_4 mixture.

$$\frac{\int_{t_1}^{t_3} P^*_{blank}(t)dt - \int_{t_1}^{t_3} P^*_{ads}(t)dt}{(t_3 - t_1) \times (P^*_{b,3} - P^*_{b,1})} = \frac{V_{adsorbed\ gas}}{\nu_j \times (t_3 - t_1)} \quad (4.34)$$

$$\nu_j \times \left[\int_{t_1}^{t_3} P^*_{blank}(t)dt - \int_{t_1}^{t_3} P^*_{ads}(t)dt\right] = V_{adsorbed\ gas} \quad (4.35)$$

By using the information of the molar volume of an ideal gas at atmospheric conditions (1 atm and 25 °C) as 24.5 liters; adsorbed volumes, moles and weights of each species in the multicomponent mixture are calculated successively. The *total* weight change data due to adsorption directly acquired from the gas sorption analyzer and those calculated by using the current methodology differ due to the purge of a big portion of the feed gas in Region (ii), i.e. at constant pressure region, by the vacuum pump before and after the adsorption chamber. Thereby, this methodology combines *total* weight change and MS data, i.e. weight ratio of the adsorbed species. Finally, by using this weight ratio, the calculated adsorbed amounts are normalized with respect to the *total* weight change in gas sorption analyzer.

4.5.2. Pure and Selective Carbon Dioxide Adsorption Studies

Four different feed streams were used in pure and selective adsorption/desorption studies, which are namely; pure CO_2 (50 ml/min CO_2), pure CH_4 (50 ml/min CH_4), 10% CO_2-90% CH_4 (5 ml/min CO_2-45 ml/min CH_4) and 50% CO_2-50% CH_4 (25 ml/min CO_2-25 ml/min CH_4), for 0-1000 mbar and 0-5000 mbar pressure ranges.

The adsorption/desorption isotherms in pure CO_2, pure CH_4 and CO_2-CH_4 mixture were obtained in order to investigate the changes in adsorption behavior of the activated carbon based adsorbents upon modifications, heat/chemical treatments and/or alkali impregnations applied. When adsorption/desorption isotherms of pure gases at room temperature are compared, it was observed that the mass uptake values of pure CO_2 indicated by the isotherms (~9.8%) were six folds that of the pure CH_4 (~1.66%) for AC1-25NH3w sample at 1000 mbar (Figure 4.69). The results also reveal that as the concentration of CH_4 in the feed stream increased, the mass uptake values showing total amount of adsorbed gas decreased. A maximum of 100 mg CO_2 and 17 mg CH_4 gases were adsorbed per gram of

adsorbent at 1000 mbar and RT. When the adsorption capacity of the adsorbents for gas mixtures were compared, in case of 50% CH_4-50% CO_2 feed mixture the total adsorption capacity were almost two folds, 65 mg adsorbed/g adsorbent, compared to that measured for 90% CH_4-10% CO_2 feed mixture, 31 mg adsorbed/g adsorbent (Figure 4.69).

In order to investigate the reason for this further, the changes in the adsorbed CO_2 and CH_4 amounts as a function of total pressure under 25 ml/min CO_2-25 ml/min CH_4 (50% CO_2-50% CH_4) flow are presented in Figure 4.70. The adsorbed amount of each adsorbate, CO_2 and CH_4, and the selectivity, as the ratio of m_{CO_2}/m_{CH_4}, were calculated through using the methodology explained in Section 4.5.1. The adsorbed CO_2 and CH_4 amounts were calculated as ~48 mg/g adsorbent and ~17 mg/g adsorbent, respectively, at 1000 mbar total pressure showing that AC1-25NH3w had a slight tendency to adsorb CO_2 selectively; the mass feed ratio of CO_2:CH_4 mixture for equimolar composition was 2.75, and the mass ratio of the adsorbed amounts was calculated as 2.82 (Figure 4.70).

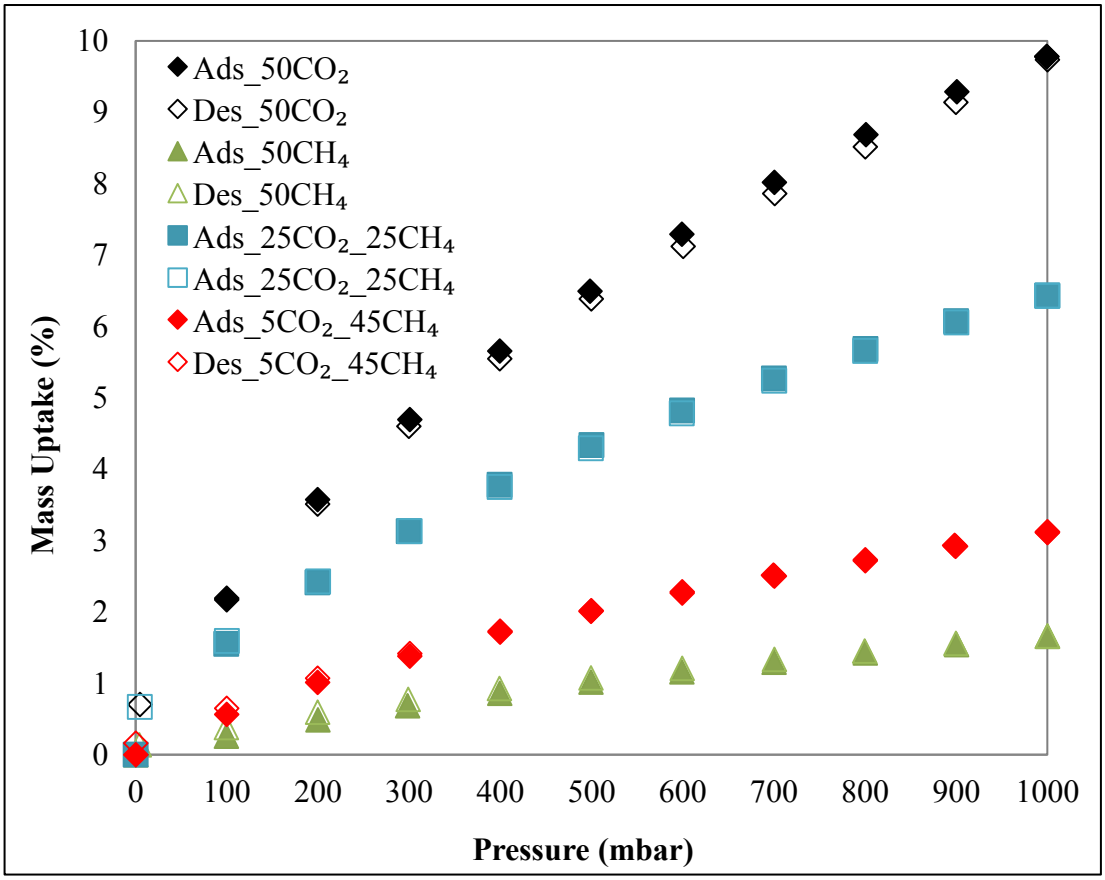

Figure 4.69. Mass uptakes of AC1-25NH3w sample under different flow compositions.

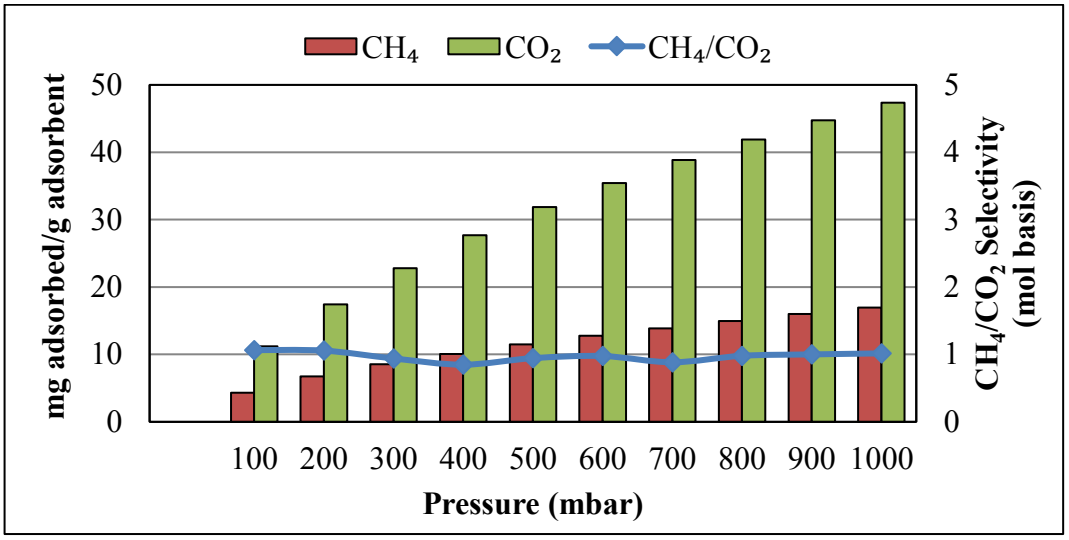

Figure 4.70. Adsorption capacity of AC1-25NH3w sample under 25 ml/min CO_2-25 ml/min CH_4 flow.

The change in the CO_2 and CH_4 adsorption capacities of AC1-25NH3w at room temperature under 10% CO_2-90% CH_4 atmosphere (i.e. 5 ml/min CO_2-45 ml/min CH_4 flow) as a function of pressure is given in Figure 4.71. In the total of 31 mg/g adsorbent weight increase, shares of CO_2 and CH_4 were calculated as 9 mg/g adsorbent and 22 mg/g adsorbent, respectively. The weight-based CO_2:CH_4 ratio in the feed was calculated as 0.3, while the adsorbed CO_2:CH_4 ratio was found as 0.41 at 1000 mbar. The results revealed that as the weight-based CO_2:CH_4 feed ratio was decreased from 2.75 to 0.3, the ratio of CO_2:CH_4 in the adsorbed state was decreased from 2.8 to 0.41. The mole based adsorbed CH_4:CO_2 selectivity values were presented in Figures 4.70 and 4.71, the results indicated that while mole based CH_4:CO_2 feed ratio was increased from 1 to 9, the ratio of adsorbed CH_4:CO_2 was only increased from 1 to 8, clearly showing the adsorbent AC1-25NH3w has a tendency to adsorb CO_2 selectively.

Almost 80% of the CO_2 adsorption capacity was lost in response to the increase in adsorption temperature from RT to 120 °C, and the mass uptake values for pure CO_2 gas dropped down to 2% on AC1-10NH3w (Figure 4.72). The corresponding CH_4 adsorption capacity loss with temperature rise was 77%; the mass uptake values for pure CH_4 decreased down to 0.4%, as given in Figure 4.73. It can be deduced that CH_4 was adsorbed more strongly than CO_2 at elevated temperatures. It was also observed that the adsorbed amounts

decreased with temperature on all samples. A perfect overlap of adsorption and desorption profiles was observed in pure CO_2 tests indicating complete reversibility of CO_2 adsorption with pressure. However, the difference between adsorption and desorption profiles observed in CH_4 tests at both temperatures, especially for low pressure values, shows there is no complete reversibility in CH_4 adsorption (Figure 4.73).

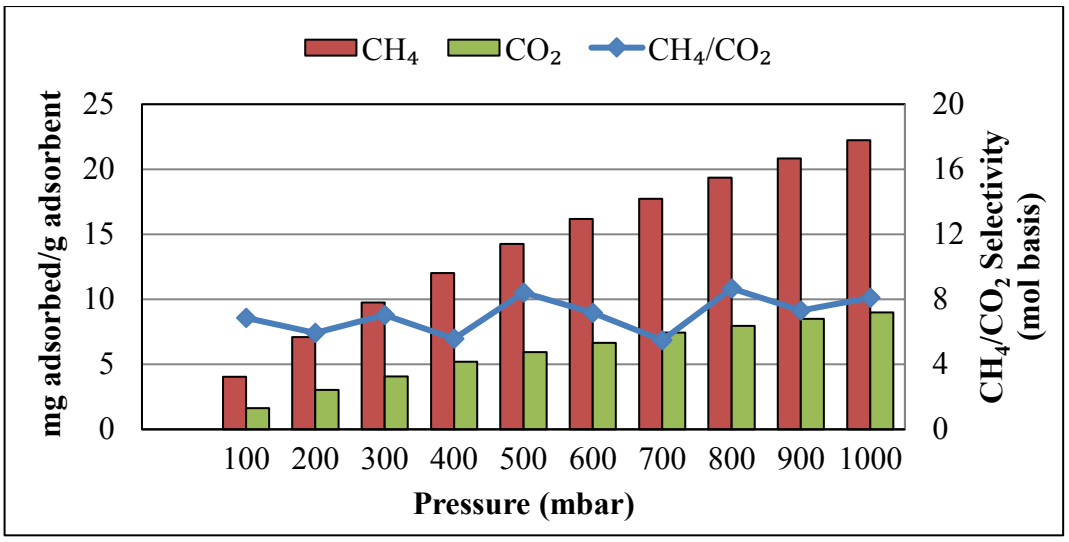

Figure 4.71. Adsorption capacity of AC1-25NH3w sample under 5 ml/min CO_2-45 ml/min CH_4 flow.

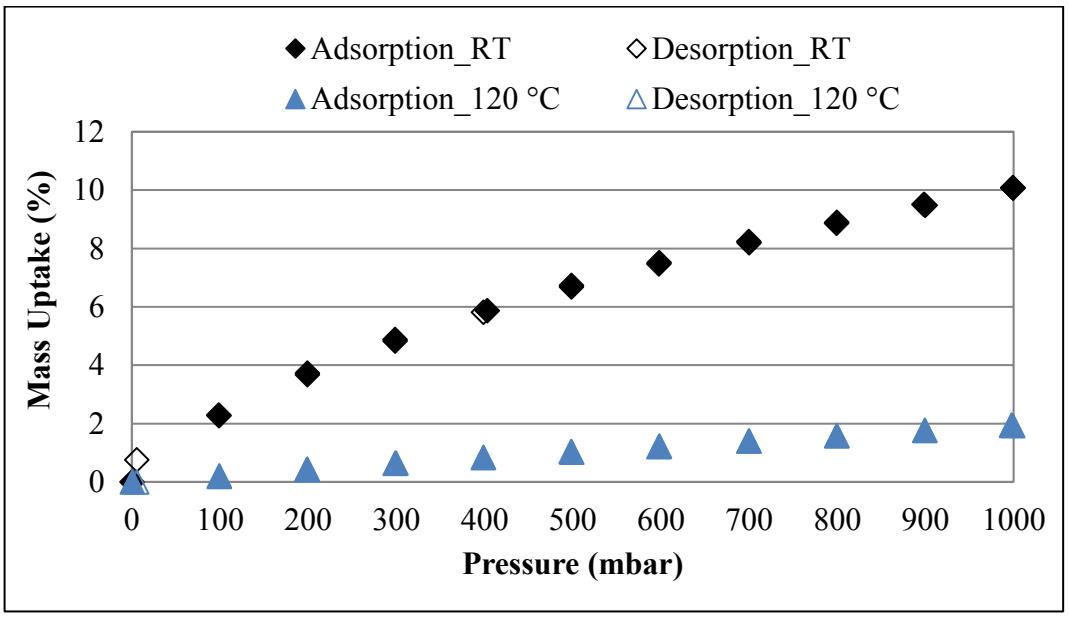

Figure 4.72. Mass uptakes of AC1-10NH3w sample under 50 ml/min CO_2 flow.

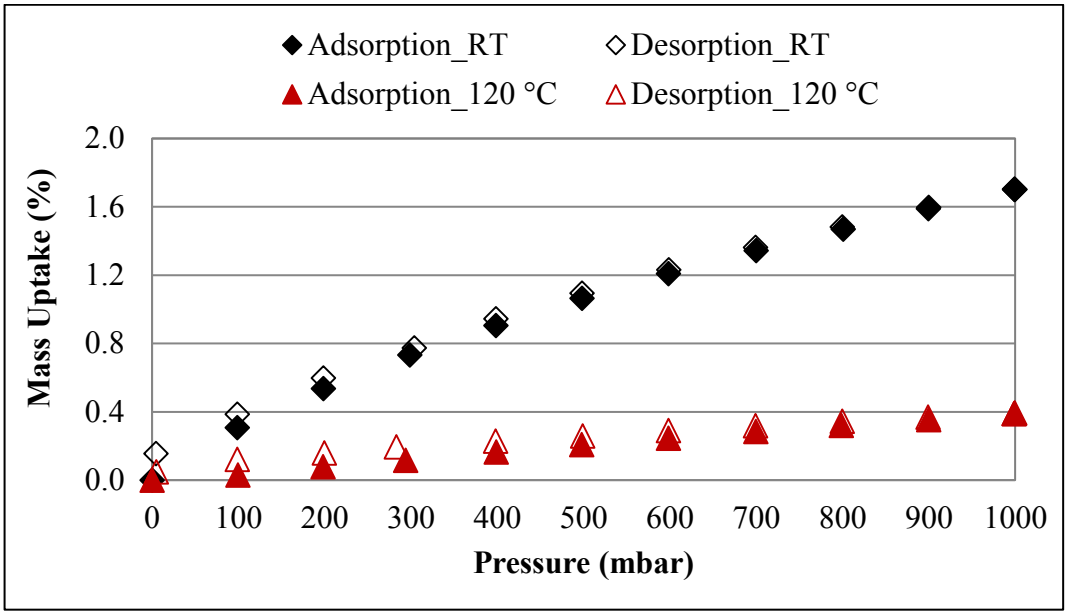

Figure 4.73. Mass uptakes of AC1-10NH3w sample under 50 ml/min CH_4 flow.

Table 4.11. Results of adsorption experiments on the samples prepared by wet-ammonia.

Sample	Flow Type	Mass Uptake (%)
AC1-10NH3w	50 CO_2	10.080
	50 CH_4	1.701
	5 CO_2 & 45 CH_4	3.179
	25 CO_2 & 25 CH_4	6.479
	50 CO_2 (120 °C)	1.937
	50 CH_4 (120 °C)	0.389
AC1-25NH3w	50 CO_2	9.785
	50 CH_4	1.659
	5 CO_2 & 45 CH_4	3.121
	25 CO_2 & 25 CH_4	6.433
AC1-10NH3i-250	50 CO_2	10.162
	50 CO_2 (120 °C)	2.024
AC1-25NH3i-250	50 CO_2	9.818
	50 CH_4	1.644
	5 CO_2 & 45 CH_4	3.157
	25 CO_2 & 25 CH_4	7.114
AC1-25NH3w-600He	50 CO_2	10.056
	50 CO_2 (120 °C)	2.024

The results revel that pure and selective CO_2 adsorption capacities of AC1-10NH3w was found slightly higher than those of AC1-25NH3w (Table 4.11). High temperature treatment under He-flow applied in preparation of AC1-25NH3w-600He increased its CO_2 adsorption capacity for both at RT and 120 °C. It was also found that samples prepared through incipient-to-wetness-impregnation method, like AC1-25NH3i-250 had slightly higher pure and selective CO_2 adsorption capacities compared to those of the samples prepared through solution treatment and filtration, like AC1-25NH3w (Table 4.11).

Adsorbed CO_2 amounts on the samples pretreated with gaseous ammonia, measured under pure CO_2 flow at 1000 mbar and RT, are given in Figure 4.74 in terms of mass uptake values. In the figure, the adsorption capacities of AC1-3 are given as reference basis. The measurements reveal that CO_2 adsorption capacity of nitric acid oxidized adsorbent AC3 is significantly lower than that of air oxidized AC2, while air oxidation procedure (AC2) increased the CO_2 adsorption capacity of the AC1 slightly by 1.65%. The highest CO_2 adsorption capacity was measured on AC1-N-600 sample, while AC3 sample exhibited the lowest CO_2 adsorption capacity. A comparison of the adsorption capacities of AC1-N-600 and AC1-N-800 shows amination temperature higher than a limit led to a lower adsorption capacity. In order to observe the effect of alkali impregnation on CO_2 adsorption performance of the samples prepared by amination, an adsorption test on AC1-N-600i-250, which was prepared by impregnating 10% Na_2CO_3 on AC1-N-600 sample followed by calcination at 250 °C, was performed. Na impregnated AC1-N-600i-250 exhibited lower CO_2 adsorption capacity than that of AC1-N-600. There may be a few reasons behind this outcome: (i) the addition of Na_2CO_3 to the surface might block the micropores preventing CO_2 diffusion through/inside the pores, (ii) the surface of the adsorbent might already been saturated before the impregnation process, thus the additional calcination might lead to loss of the oxygen bearing surface groups.

The adsorption tests were also conducted at higher pressures in 0-5000 mbar range under pure CO_2 and CH_4 atmospheres. The system described in detail in Section 3.2.4 allows performing high pressure adsorption/desorption tests under pure gas or gas mixture atmospheres in flow mode via controlling flow rate and partial pressure of each species. The similarity in mass uptake profiles observed in pure gas, CO_2 and CH_4, adsorption tests in 0-5000 mbar pressure range and the profiles had been obtained in the tests performed for 0-

1000 mbar range confirms the reliability of high pressure adsorption measurements (Figure 4.75 and 4.76). The deviation of the data up to 1000 mbar level of 0-5000 mbar range from those previously obtained for 0-1000 mbar range is lower than 10%, which might be caused from the difference in waiting time for reaching equilibrium at the given pressure level; since adsorption process continues at the set point of the pressure, and the retention time were different, it was possible to see such deviations. The results clearly show that the CO_2 mass uptake of the AC1-10NH3w at 5000 mbar is 6.2 times higher than its CH_4 mass uptake.

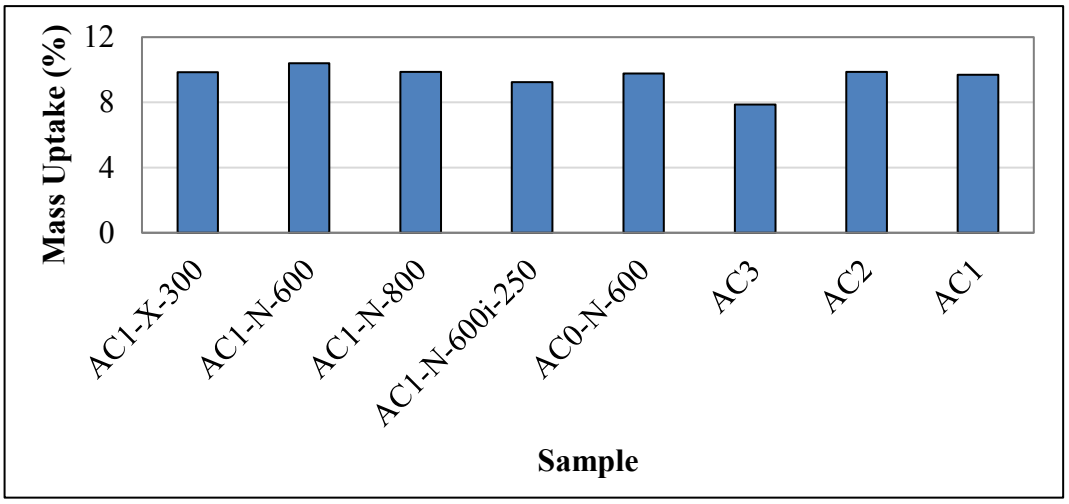

Figure 4.74. Comparison of mass uptakes of samples prepared by gaseous ammonia under 50 ml/min CO_2 flow.

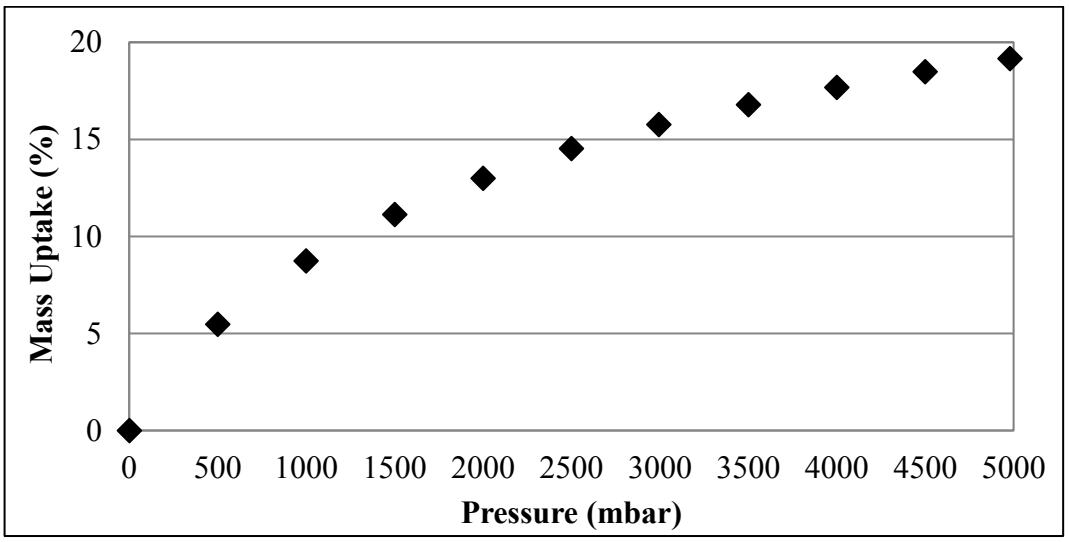

Figure 4.75. Mass uptakes of AC1-10NH3w sample under 50 ml/min CO_2 flow at room temperature and high pressure.

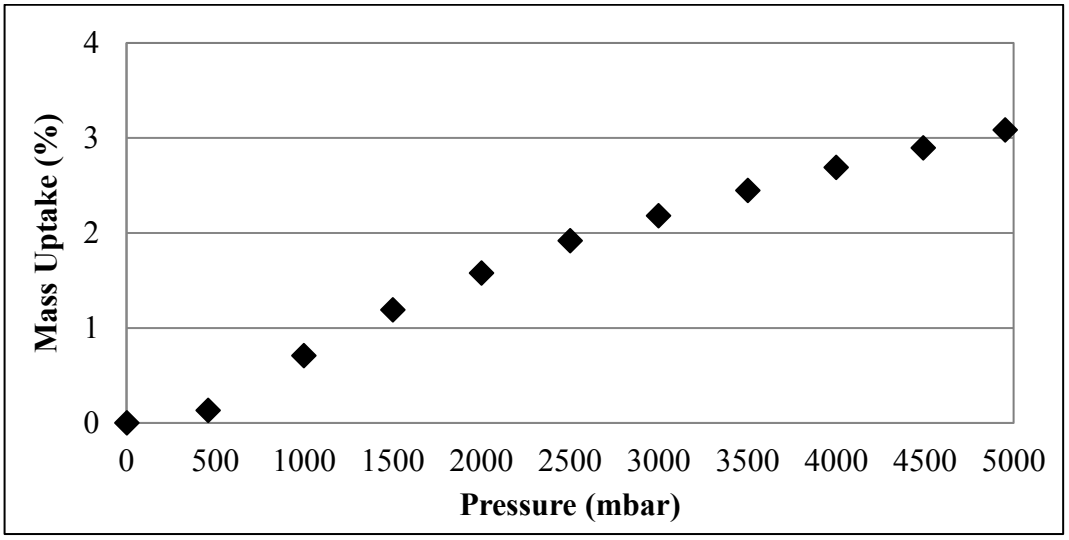

Figure 4.76. Mass uptakes of AC1-10NH3w sample under 50 ml/min CH_4 flow at room temperature and high pressure.

4.5.3. Adsorption Modeling Studies

As a part of the ongoing adsorption modelling studies in our group, CO_2 isotherms on four samples (Table 4.12) obtained at RT and at 120 °C in pure CO_2 atmosphere were fitted to Langmuir, Freundlich and Dubinin-Radushkevich (D-R) models as in our previous study (Çağlayan and Aksoylu, 2016) to obtain information on the adsorption mechanism, strength of adsorption and surface properties of the adsorbent as well.

The simplest theoretical model that can be used to describe monolayer adsorption quantitatively is the Langmuir equation, which assumes a uniform surface, a single layer of adsorbed material and constant temperature. The Langmuir equation may be written as follows:

$$\frac{P}{Q} = \frac{1}{Q_m} P + \frac{1}{bQ_m} \tag{4.36}$$

where Q is the amount adsorbed (mmol/g adsorbent), P is the pressure (mmHg), Q_m is the theoretical monolayer saturation capacity and b is the Langmuir isotherm constant.

Langmuir model gave theoretical monolayer saturation capacity of the adsorbents in a very close, 3.94-4.01 mmol/g adsorbent range, and Langmuir isotherm constants in the range of 0.00159-0.00259 $mmHg^{-1}$. In all calculations, the correlation coefficients were greater than 0.99. In accordance with the fact that the adsorption rate is negatively affected from temperature rise, the increase in temperature led to a drastic decrease in both Langmuir model parameters calculated (Table 4.12). It should be noted that significantly higher Langmuir constant b, which is adsorption equilibrium constant defined by the ratio of adsorption and desorption specific rate constants for the adsorbent-adsorbate combination, indicate that adsorption on AC1-25NH3w-600He is significantly faster than desorption compared to those of the other samples.

Table 4.12. Langmuir isotherm parameters for CO_2 adsorption.

Sample	**Langmuir constants (298 K)**			**Langmuir constants (393 K)**		
	Q_m	**b**	**R^2**	**Q_m**	**b**	**R^2**
AC1-25NH3w	4.037	0.00159	0.932			
AC1-25NH3i-250	3.942	0.00168	0.993			
AC1-10NH3w	4.049	0.00168	0.992	2.966	0.00023	0.932
AC1-25NH3w-600He	4.117	0.00293	0.993	2.076	0.00040	0.959

The Freundlich equation is an empirical formula which provides a very reasonable description of non-linear adsorption isotherms involving heterogeneous surfaces (multilayer adsorption) can be written in the form:

$$Q = kP^{1/n} \tag{4.37}$$

where k and n are Freundlich constants, which represent adsorption capacity and adsorption intensity, respectively. Fitting Freundlich model to experimental CO_2 adsorption data yielded k value ca. in 0.034-0.036 range. On the other hand, 1/n constants calculated for the adsorbents are very close, ca. 0.64 at RT. The increase in temperature to 393 K resulted in higher 1/n values, which are very close to 1, indicating relatively uniform surfaces (Table 4.13).

Table 4.13. Freundlich isotherm parameters for CO_2 adsorption.

Sample	Freundlich constants (298 K)			Freundlich constants (393 K)		
	k	1/n	R^2	k	1/n	R^2
AC1-25NH3w	0.03127	0.648	0.9986			
AC1-25NH3i-250	0.03403	0.636	0.9986			
AC1-10NH3w	0.03477	0.636	0.9986	0.00080	0.9563	0.9986
AC1-25NH3w-600He	0.03252	0.646	0.9986	0.00144	0.8795	0.9997

Dubinin and Radushkevich describes the adsorption of gases and vapors on microporous adsorbents such as carbons. The Dubinin-Radushkevich (D-R) equation may be written as:

$$\frac{W}{W_0} = exp\left[-\left(\frac{RT}{E} ln\left(\frac{P}{P_0}\right)\right)^2\right] \tag{4.38}$$

where W is the amount of gas adsorbed per unit mass of adsorbent (g/g catalyst), W_0 is micropore capacity (g/g catalyst), R is the universal gas constant (8.315 J/mol K), T is the temperature (K), E is the characteristic energy (J/mol) and P_0 is the saturation pressure (mmHg). In the current study, the best fit was obtained in Dubinin-Radushkevich model with correlation coefficients greater than 0.999. This model was used to estimate the characteristic porosity of the adsorbent and the apparent energy of adsorption. The micropore capacity was found to be 0.221 and the obtained characteristic energy of the adsorbents with an average of 7.48 kJ/mol, which is less than 8 kJ/mol, confirmed the adsorption process to be a physical one in this study (Table 4.14).

Table 4.14. Dubinin-Radushkevich isotherm parameters for CO_2 adsorption.

Sample	D-R constants (298 K)			D-R constants (393 K)		
	Wo (cc/g)	E (J/mol)	R^2	Wo (cc/g)	E (J/mol)	R^2
AC1-25NH3w	0.22322	7404	0.9997			
AC1-25NH3i-250	0.21647	7482	0.9997			
AC1-10NH3w	0.22218	7478	0.9997	0.08843	6099	0.9996
AC1-25NH3w-600He	0.22693	7421	0.9997	0.08000	6363	0.9984

5. CONCLUSION

5.1. Conclusions

The aim of this research study was to design and construct a fuel processor prototype (FPP), to determine its optimum steady state operation conditions, to model its dynamic or transient performance, and to design and develop high performance AC based adsorbents for selective CO_2 capture in order to reduce its CO_2 emission.

In this context, a fuel processor prototype (FPP) consisting of OSR, WGS and PROX units was designed and constructed; individual (OSR, WGS, PROX) and serial (OSR-WGS-PROX) performance tests were performed by using propane/methane as the hydrocarbon fuel over novel OSR, WGS and PROX catalysts by utilizing Pt-Ni/δ-Al_2O_3 as OSR, Au-Re/ZrO_2, Au-Re/CeO_2 and Pt-Re-V/CeO_2 as WGS, and Pt-Sn/AC as PROX catalysts.

The first part covered steady state performance analysis of propane OSR and serial OSR-WGS reactions over Pt-Ni/δ-Al_2O_3 and Au-Re/ZrO_2 catalysts, respectively. Reaction tests were performed at different OSR-WGS reactors' temperature combinations for different concentrations of oxygen, propane and steam in the OSR feed. The major conclusions that can be drawn from this part of the study can be given as follows:

- Almost 100% propane and up to 50% CO conversions were achieved in the OSR and WGS units, respectively.
- The highest achieved H_2/CO product ratio was ~33, which was obtained for OSR-WGS temperature combinations of 723-623 K and 673-573 K with S/C ratio of 3 and O/C ratio of 0.74. Increasing both OSR and WGS reaction temperatures suppressed methanation and thereby increased H_2/CO product ratio in serial OSR-WGS operation.
- Dry basis, inert free H_2 and CO concentrations at the WGS exit were obtained as ~53% and ~1%, respectively.
- The stability of both catalysts were confirmed during 75 hours TOS test performed on OSR-WGS system and by microstructural characterization of the catalysts as well.

The second part covered steady state performance analysis of propane OSR, serial OSR-WGS, OSR-PROX and OSR-WGS-PROX reactions over Pt-Ni/δ-Al_2O_3, Pt-Re-V/CeO_2 and Pt-Sn/AC3 catalysts, respectively, at different reactors' temperature combinations for a larger S/C feed ratio range, 2.25-6, than that studied in the first part. The major conclusions that can be drawn from this part of the study can be given as follows:

- Simultaneous use of high temperature and S/C feed ratio led to increased H_2, decreased CH_4 and CO_2 concentrations, and relatively lower CO concentrations in OSR product, which were in accordance with the fuel processing targets. The highest achieved H_2 concentration was ~57% for S/C ratio of 6 at 723 K, while the lowest CO concentration was 0.58% at S/C ratio of 2.25 at 623 K.
- Increased S/C feed ratio also suppressed methanation activity of the catalyst and resulted in a 30-35% decrease in CH_4 concentrations at 723 K.
- An overall evaluation of the results pointed out 723 K and 5 as the optimal combination of temperature and S/C feed ratio in individual OSR reaction tests, respectively.
- The experimental product distributions and trends were consistent with the results of the thermodynamic calculations.
- In the serial OSR-WGS tests, the new WGS catalyst, Pt-Re-V/CeO_2, led to higher CO conversion values (55-60%) than those obtained under the same conditions where Au-Re/ZrO_2 had been used as the WGS catalyst (45-50%).
- The optimum combination in OSR-WGS serial operation was 723-623 K case, for which higher H_2 concentrations (~53%) and comparatively low CO concentrations (~0.9%) were obtained with no methanation activity.
- In the serial OSR-PROX tests, CO concentration as low as 0.96% (dry based inert free) for 4 ml/min oxygen addition seems promising considering the CO concentrations (min 0.5%) obtained in the serial OSR-WGS performance tests.
- In the serial OSR-WGS-PROX tests, keeping S/C ratio at 6 and decreasing O_2 flow rate resulted in H_2 concentrations as high as ~70% at the PROX outlet.

The third part covered steady state performance analysis of methane OSR and serial OSR-WGS reactions over Pt-Ni/δ-Al_2O_3 and Pt-Re-V/CeO_2 catalysts, respectively. S/C ratio of the OSR feed, and OSR temperature/OSR-WGS temperature combinations were used as

the experimental parameters. The major conclusions that can be drawn from this part of the study can be given as follows:

- Increased S/C ratio in the feed (3→5) led to increased H_2 concentrations from 58% to 61% at T_{OSR}=673 K and from 61% to 65% at T_{OSR}=723 K and increased conversion levels of CH_4 from 61% to 67% at T_{OSR}=673 K and from 66% to 73% at T_{OSR}=723 K.
- Oxygen was totally consumed, whereas maximum achieved CH_4 conversion levels were 71% and 77% at T_{OSR}=673 K and at T_{OSR}=723 K, respectively.
- Upon increasing steam concentration and adding a serial WGS reactor, CO concentration was decreased from 1.21% down to 0.66% at T_{OSR}=673 K, and H_2 production rates were obtained close to 105 μmol/gcat/s.
- Compared to C_3H_8 OSR tests, CH_4 TOX reaction was much slower than that of C_3H_8.

The fourth part covered pre-modeling of the dynamic performance of the FPP through the use of formerly obtained power-law type kinetics of reactions, which were corrected further based on the response of the units/FPP to step changes in process variables. The section also included the determination of the most reliable and consistent control parameters and construction of a suitable control-oriented full system dynamic model for the FPP. The major conclusions that can be drawn from this part of the study can be given as follows:

- Comparison of the propane conversion values obtained through the kinetic experiments (Gökaliler *et al*., 2012) and modeling calculations through the use of formerly obtained power-law type kinetics in the current study gave the average of the errors as ~12.5% in the OSR unit for 0.2%Pt-10%Ni/δ-Al_2O_3 catalyst.
- Comparison of the CO conversion values obtained through the kinetic experiments (Gökaliler *et al*., 2013) and modeling calculations through the use of formerly obtained power-law type kinetics in the current study gave the average of the errors as ~16.3% in the WGS unit for 1wt.%Au-0.5wt.%Re/CeO_2 catalyst.
- Comparison of the CO conversion values obtained through the kinetic experiments (Eropak and Aksoylu, 2016) and modeling calculations through the use of formerly obtained power-law type kinetics in the current study gave the average of the errors as ~20% in the PROX unit for 1wt.%Pt-0.25wt.%Sn/AC3 catalyst.

- The inertia tests revealed that the sensing time of a step change by the mass spectrometer was 2.75 minutes at the condenser exit, increased to 3.5 minutes at the OSR and condenser exit, to 4 minutes at the OSR-WGS and condenser exit and to 4.5 minutes at the OSR-WGS-PROX and condenser exit. The volume of the FPP system was found to be ~0.6 L.
- The dynamic tests revealed that CO_2 and CH_4 concentrations showed much more stable steady state profiles with higher signal-to-noise ratios and thus were considered the most reliable and consistent system control parameters during real operation and reactive conditions.
- In order to correct the OSR kinetic rate expression, the error was calculated as a function of the rate orders and they were changed parametrically in ±10% of the published values (Gökaliler *et al*., 2012). 1.46, 2.19 and -0.60 values as propane, oxygen and steam rate orders were obtained as the most appropriate selections giving the minimum error in the tested range.

The fifth part covered the design and development of high performance activated carbon based, chemically modified adsorbents for selective CO_2 capture through an experimental design procedure having AC pretreatment types, type and loading of additives, temperature and adsorbate gas composition as the parameters. The major conclusions that can be drawn from this part of the study can be given as follows:

- A new methodology for the determination of selective adsorption capacity of the adsorbent under multicomponent gas mixture atmosphere/flow was developed.
- The mass uptake values under pure CO_2 flow (~9.8%) were six folds that of the pure CH_4 (~1.66%) for AC1-25NH3w sample at 1000 mbar and at RT.
- AC1-25NH3w had a slight tendency to adsorb CO_2 selectively, the mass feed ratio of CO_2:CH_4 mixture for equimolar composition was 2.75, and the mass ratio of the adsorbed amounts was calculated as 2.82 under 25 ml/min CO_2-25 ml/min CH_4 flow at 1000 mbar and at RT.
- While mole based CH_4:CO_2 feed ratio was increased from 1 to 9, the ratio of adsorbed CH_4:CO_2 was only increased from 1 to 8, clearly showing the adsorbent AC1-25NH3w had a tendency to adsorb CO_2 selectively.

- Almost 80% of the CO_2 adsorption capacity was lost in response to the increase in adsorption temperature from RT to 120 °C.
- The highest CO_2 adsorption capacity was measured on AC1-N-600 sample (~10.4%), while AC3 sample (~7.9%) exhibited the lowest CO_2 adsorption capacity.
- By conducting the adsorption tests at higher pressures in 0-5000 mbar range, the mass uptake values under pure CO_2 flow increased up to ~20%.
- The best fit in the adsorption isotherm models was obtained in Dubinin-Radushkevich model with correlation coefficients greater than 0.999.

5.2. Recommendations

Considering the results of the present study, the following points are thought to be beneficial for the future studies:

- The serial OSR-WGS-PROX fuel processing should involve a recycle stream, and its operating/reaction conditions should be meticulously optimized through using an experimental design procedure, which additionally involves W/F values for all three reactors, and fraction of the PROX outlet sent back and mixes with the fresh OSR feed (i.e. recycle ratio) besides all the experimental parameters used in the current study.
- The combination of dynamic modeling and correction of kinetic rate expressions requires an extensive parametric study covering hundreds of experimental data by excluding time delays, since the concentrations were affected not only by the reaction orders, but also the activation energy and specific rate constant; thus, the optimization schemes can be extended such as to include optimization through activation energy and specific rate constant for ±10% range of their experimental values.
- Keeping S/C ratio at 5 would be an optimum condition to obtain lower CO concentrations in future studies.
- Effect of oxygen concentration in the feed stream of OSR unit can be studied in methane OSR and serial reactions. Thermodynamic calculations should also be carried out to confirm the experimental trends.

REFERENCES

Acar, B., 2016, *An Experimental Study on Design and Characterization of CO_2 Adsorbents*, M. S. Thesis, Boğaziçi University.

Adelodun, A. A., K. Kim, J. C. Ngila and J. Szulejko, 2015, "A Review on the Effect of Amination Pretreatment for the Selective Separation of CO_2", *Applied Energy*, Vol. 158, pp. 631-642.

Ahmed, S., R. Ahluwalia, S. H. D. Lee and S. Lottes, 2006, "A Gasoline Fuel Processor Designed to Study Quick-start Performance", *Journal of Power Sources*, Vol. 154, pp. 214-222.

Aicher, T., J. Full and A. Schaadt, 2009, "A Portable Fuel Processor for Hydrogen Production from Ethanol in a 250 W Fuel Cell System", *International Journal of Hydrogen Energy*, Vol. 34, pp. 8006-8015.

Aksoylu, A. E., M. Madalena, A. Freitas and J. L. Figueiredo, 2000, "Bimetallic Pt-Sn Catalysts Supported on Activated Carbon. II. CO Oxidation", *Catalysis Today*, Vol. 62, pp. 337-346.

Aroua, M. K., W. M. A. Daud, C. Y. Yin and D. Adinata, 2008, "Adsorption Capacities of Carbon Dioxide, Oxygen, Nitrogen and Methane on Carbon Molecular Basket Derived from Polyethyleneimine Impregnation on Microporous Palm Shell Activated Carbon", *Separation and Purification Technology,* Vol. 62, pp. 609-613.

Aschenbrenner, O., P. McGuire, S. Alsamaq, J. Wang, S. Supasitmongkol, B. Al-Duri, P. Styring and J. Wood, 2011, "Adsorption of Carbon Dioxide on Hydrotalcite-like Compounds of Different Compositions", *Chemical Engineering Research and Design,* Vol. 89, pp. 1711-1721.

Aslanzadeh, S., A. Gorzin and M. Kazeminejad, 2014, *Indian Journal of Scientific Research*, Distributed Generation in Electrical Networks, Vol. 2, No.1, pp. 1-4.

Avcı, A. K., 2003, "*Computational and Experimental Investigation of Catalytic Hydrocarbon Fuel Processing for Autothermal Hydrogen Production*", Ph.D. Dissertation, Bogazici University.

Avcı, A. K., Z. I. Önsan and D. L. Trimm, 2001, "On-board Fuel Conversion for Hydrogen Fuel Cells: Comparison of Different Fuels by Computer Simulations", *Applied Catalysis A: General*, Vol. 216, pp. 243-256.

Ayabe, S., H. Omoto, T. Utaka, R. Kikuchi, K. Sasaki, Y. Teraoka and K. Eguchi, 2003, "Catalytic Autothermal Reforming of Methane and Propane over Supported Metal Catalysts", *Applied Catalysis A: General*, Vol. 241, pp. 261-269.

Baltrusaitis, J., J. Schuttlefieldb, E. Zeitler and V. H. Grassian, 2011, "Carbon Dioxide Adsorption on Oxide Nanoparticle Surfaces", *Chemical Engineering Journal*, Vol. 170, pp. 471-481.

Başar, M. S., 2010, *Design, Construction and Testing of a Lab-Scale Fuel Processor Prototype for Dynamic Performance Studies*, M. S. Thesis, Boğaziçi University.

Başar, M. S., H. Bedir and A. E. Aksoylu, 2016, "Steady State Performance Analysis of OSR and Serial OSR-WGS Reactors", *Fuel Processing Technology*, Vol. 152, pp. 240-249.

Beckhaus, P., A. Heinzel, J. Mathiak and J. Roes, 2004, "Dynamics of H_2 Production by Steam Reforming", *Journal of Power Sources*, Vol. 127, pp. 294-299.

Ben, T., Y. Li, L. Zhu, D. Zhang, D. Cao, Z. Xiang, X. Yao and S. Qiu, 2012, "Selective Adsorption of Carbon Dioxide by Carbonized Porous Aromatic Framework", *Energy and Environmental Science*, Vol. 5, pp. 8370-8376.

Bi, Y., H. Xu, W. Li and A. Goldbach, 2009, "Water Gas Shift Reaction in a Pd Membrane Reactor over $Pt/Ce_{0.6}Zr_{0.4}O_2$ Catalyst", *International Journal of Hydrogen Energy*, Vol. 34, pp. 2965-2971.

Boaro, M., M. Vicario, J. Llorca, C. Leitenburg, G. Dolcetti and A. Trovarelli, 2009, "A Comparative Study of Water Gas Shift Reaction over Gold and Platinum Supported on ZrO_2 and CeO_2-ZrO_2", *Applied Catalysis B: Environmental*, Vol. 88, pp. 272-282.

Boehme, T. R., C. H. Onder and L. Guzzella, 2008, "Dynamic Model of an Autothermal Gasoline Fuel Processor", *International Journal of Hydrogen Energy*, Vol. 33, pp. 6150-6164.

Brandon, N. P. and D. Thompsett, 2005, *Fuel Cells Compendium,* Elsevier, Great Britain.

Calgon Carbon Cooperation, 2007, *Activated Carbon Principles*, Pittsburgh, USA.

Chan, S. H. and H. M. Wang, 2001, "Carbon Monoxide Yield in Natural Gas Autothermal Reforming Process", *Journal of Power Sources*, Vol. 101, pp. 188-195.

Chen, Y. H., C. C. Yu, Y. C. Liu and C. H. Lee, 2006, "Start-up Strategies of an Experimental Fuel Processor", *Journal of Power Sources*, Vol. 160, pp. 1275-1286.

Chen, C., J. Kim, D. Yang and W. Ahn, 2011, "Carbon Dioxide Adsorption over Zeolite-like Metal Organic Frameworks (ZMOFs) Having a Sod Topology: Structure and Ion-exchange Effect", *Chemical Engineering Journal*, Vol. 168, pp. 1134-1139.

Cipiti, F., L. Pino, A. Vita, M. Lagana and V. Recupero, 2013, "Experimental Investigation on a Methane Fuel Processor for Polymer Electrolyte Fuel Cells", *International Journal of Hydrogen Energy*, Vol. 38, pp. 2387-2397.

Çağlayan, B. S., A. K. Avcı, Z. I. Önsan and A. E. Aksoylu, 2005a, "Production of Hydrogen over Bimetallic Pt-Ni/δ-Al_2O_3: I. Indirect Partial Oxidation of Propane", *Applied Catalysis*, Vol. 280, pp. 181-188.

Çağlayan, B. S., Z. I. Önsan and A. E. Aksoylu, 2005b, "Production of Hydrogen over Bimetallic Pt-Ni/δ-Al_2O_3: II. Indirect Partial Oxidation of LPG", *Catalysis Letters*, Vol. 102, No. 1-2, pp. 63-67.

Çağlayan, B. S., 2011, *Design and Development of Catalysts and Adsorbents for CO_x Free H_2 Production*, Ph. D. Dissertation, Boğaziçi University.

Çağlayan, B. S. and A. E. Aksoylu, 2011a, "Water Gas Shift Activity of Ceria Supported Au-Re Catalysts", *Catalysis Communications*, Vol. 12, pp. 1206-1211.

Çağlayan, B. S., I. I. Soykal and A. E. Aksoylu, 2011b, "Preferential Oxidation of CO over Pt-Sn/AC Catalyst: Adsorption, Performance and DRIFTS Studies", *Applied Catalysis B: Environmental*, Vol. 106, pp. 540-549.

Çağlayan, B. S. and A. E. Aksoylu, 2013, "CO_2 Adsorption on Chemically Modified Activated Carbon", *Journal of Hazardous Materials*, Vol. 252-253, pp. 19-28.

Çağlayan, B. S. and A. E. Aksoylu, 2016, "CO_2 Adsorption Behavior and Kinetics on Chemically Modified Activated Carbons", *Turkish Journal of Chemistry*, Vol. 40, pp. 576-587.

Dali, A. M., A. S. Ibrahem and A. Hadi, 2012, "General Study about Activated Carbon for Adsorption Carbon Dioxide", *Journal of Purity*, Vol. 1, No.5, pp. 206-221.

Dantas, T. L. P., S. M. Amorim, F. M. T. Luna, I. J. Silva Jr., D. C. S. de Azevedo, A. E. Rodrigues and R. F. P. M. Moreira, 2010, "Adsorption of Carbon Dioxide onto Activated Carbon and Nitrogen-Enriched Activated Carbon: Surface Changes, Equilibrium, and Modeling of Fixed-Bed Adsorption", *Separation Science and Technology*, Vol. 45, pp. 73-84.

Demirhan, C. D., 2015, *Design and Development of WGS Catalysts for Small Scale Hydrogen Production Units*, M. S. Thesis, Boğaziçi University.

Diez, N., P. Alvarez, M. Granda, C. Blanco, R. Santamaria and R. Menendez, 2015, "CO_2 Adsorption Capacity and Kinetics in Nitrogen-enriched Activated Carbon Fibers Prepared by Different Methods, *Chemical Engineering Journal*, Vol. 281, 704-712.

Djeridi, W., A. Ouederni, N. B. Mansour, P. L. Llewellyn, A. Alyamani, L. El Mir, 2016, "Effect of the Both Texture and Electrical Properties of Activated Carbon on the CO_2 Adsorption Capacity", *Materials Research Bulletin,* Vol. 73, pp. 130-139.

Dokupil, M., C. Spitta, J. Mathiak, P. Beckhaus and A. Heinzel, 2006, "Compact Propane Fuel Processor for Auxiliary Power Unit Application", *Journal of Power Sources,* Vol. 157, pp. 906-913.

El-Moemen, A. A., A. Karpenko, Y. Denkwitz and R. J. Behm, 2009, "Activity, Stability and Deactivation Behavior of Au/CeO_2 Catalysts in the Water Gas Shift Reaction at Increased Reaction Temperature (300 °C)", *Journal of Power Sources*, Vol. 190, pp. 64-75.

Erdinç, E., 2014, *A Study on Kinetics of Methane Oxidative Steam Reforming (OSR) over Pt-Ni/δ-Al_2O_3 Bimetallic Catalysts*, M. S. Thesis, Boğaziçi University.

Eropak, B. M. and A. E. Aksoylu, 2016, "A Reliable Power-Law Type Kinetic Expression for PROX over Pt-Sn/AC under Fully Realistic Conditions", *Catalysis Communications*, submitted.

Faria, W. L. S., L. C. Dieguez and M. Schmal, 2008, "Autothermal Reforming of Propane for Hydrogen Production over Pd/CeO_2/Al_2O_3 Catalysts", *Applied Catalysis B: Environmental*, Vol. 85, pp. 77-85.

Faro, M. L., V. Modafferi, P. Frontera, P. Antonucci and A. S. Arico, 2013, "Catalytic Behavior of Ni-modified Perovskite and Doped Ceria Composite Catalyst for the Conversion of Odorized Propane to Syngas", *Fuel Processing Technology*, Vol. 113, pp. 28-33.

Fenrong, L., Y. Honghong, T. Xiaolong, N. Ping, Y. Qiongfen and K. Dongjuan, 2010, "Adsorption of Carbon Dioxide by Coconut Activated Carbon Modified with Cu/Ce", *Journal of Rare Earths*, Vol. 28, pp. 334-337.

Fu, Q., W. Deng, H. Saltsburg and M. Flytzani-Stephanopoulos, 2005, "Activity and Stability of Low Content Gold-cerium Oxide Catalysts for the Water Gas Shift Reaction", *Applied Catalysis B: Environmental*, Vol. 56, pp. 57-68.

Goel, C., H. Bhunia and P. K. Bajpai, 2016, "Novel Nitrogen Enriched Porous Carbon Adsorbents for CO_2 Capture: Breakthrough Adsorption Study", *Journal of Environmental Chemical Engineering*, Vol. 4, pp. 346-356.

Goetz, V., O. Pupier and A. Guillot, 2006, "Carbon Dioxide-Methane Mixture Adsorption on Activated Carbon", *Adsorption*, Vol. 12, pp. 55-63.

Gonzalez, I. D., R. M. Navarro, W. Wen, N. Marinkovic, J. A. Rodriguez, F. Rosa and J. L. G. Fierro, 2010, "A Comparative Study of the Water Gas Shift Reaction over Platinum Catalysts Supported on CeO_2, TiO_2 and Ce-modified TiO_2", *Catalysis Today*, Vol. 149, pp. 372-379.

Gosavi, P. V. and R. B. Biniwale, 2013, "Catalytic Preferential Oxidation of Carbon Monoxide over Platinum Supported on Lanthanum Ferrite-ceria Catalysts for Cleaning of Hydrogen", *Journal of Power Sources*, Vol. 222, pp. 1-9.

Gou, B., W. K. Na and B. Diong, 2010, *Fuel Cells Modeling, Control and Applications, CRC Press*, Florida.

Gökaliler, F., B. S. Çağlayan, Z. I. Önsan and A. E. Aksoylu, 2008a, "Hydrogen Production by Autothermal Reforming of LPG for PEM Fuel Cell Applications", *International Journal of Hydrogen Energy,* Vol. 33, pp. 1383-1391.

Gökaliler, F., B. A. Göçmen and A. E. Aksoylu, 2008b, "The Effect of Ni:Pt Ratio on Oxidative Steam Reforming Performance of Pt-Ni/Al_2O_3 Catalyst", *International Journal of Hydrogen Energy,* Vol. 33, pp. 4358-4366.

Gökaliler, F., Z. I. Önsan and A. E. Aksoylu, 2012, "Power Law Type Rate Equation for Propane ATR over Pt-Ni/Al_2O_3 Catalyst", *International Journal of Hydrogen Energy*, Vol. 37, pp. 10425-10429.

Gökaliler, F., Z. I. Önsan and A. E. Aksoylu, 2013, "Power Law Type Rate Expression for WGS Reaction over Au-Re/CeO_2 Catalyst under Realistic Fuel Processor Conditions", *Catalysis Communications*, Vol. 39, pp. 70-73.

Guo, B., L. Chang and K. Xie, 2006, "Adsorption of Carbon Dioxide on Activated Carbon", *Journal of Natural Gas Chemistry,* Vol. 15, pp. 223-229.

Gupta, R. B., 2009, *Hydrogen Fuel: Production, Transport, and Storage,* CRC Press, Florida.

Güven, S., 2009, *A Study on Bimetallic Water Gas Shift Catalysts to be Used in Fuel Processing,* M. S. Thesis, Boğaziçi University.

Hatton, P. J. and B. W. L. Southward, 2003, "Optimization of the Connection between TA-MS Systems together with Improved Data Interpretation for TA-MS Applications", *Journal of Thermal Analysis and Calorimetry*, Vol. 72, pp. 83-92.

Hessel, V., H. Löwe, A. Müller and G. Kolb, 2005, *Chemical Micro Process Engineering Processing and Plants*, Wiley, Weinheim, Germany.

Hilaire, S., X. Wang, T. Luo, R. J. Gorte and J. Wagner, 2004, "A Comparative Study of Water Gas Shift Reaction over Ceria-supported Metallic Catalysts", *Applied Catalysis A: General*, Vol. 258, pp. 271-276.

Hordeski, M. F., 2008, *Alternative Fuels the Future of Hydrogen*, Fairmont Press, Lilburn, Georgia, 2nd edition.

Hordeski, M. F., 2009, *Hydrogen and Fuel Cells: Advances in Transportation and Power*, Fairmont Press, Lilburn, Georgia.

Hosseini, S., E. Marahel, I. Bayesti, A. Abbasi, L. C. Abdullah and T. S. Y. Choong, 2015, "CO_2 Adsorption on Modified Carbon Coated Monolith: Effect of Surface Modification by Using Alkaline Solutions", *Applied Surface Science*, Vol. 324, pp. 569-575.

Hu, Y. and E. Ruckenstein, 2004, "Catalytic Conversion of Methane to Synthesis Gas by Partial Oxidation and CO_2 Reforming", *Advances in Catalysis*, Vol. 48, pp. 297-345.

Hurtado-Juan, M. A., C. M. Y. Yeung and S. C. Tsang, 2008, "A Study of Co-precipitated Bimetallic Gold Catalysts for Water Gas Shift Reaction", *Catalysis Communications*, Vol. 9, pp. 1551-1557.

Jung, U. H., W. Kim, K. Y. Koo and W. L. Yoon, 2014, "Genuine Design of Compact Natural Gas Fuel Processor for 1 kW Class Residential Proton Exchange Membrane Fuel Cell Systems", *Fuel Processing Technology*, Vol. 121, pp. 32-37.

Kang, I. and J. Bae, 2006, "Autothermal Reforming Study of Diesel for Fuel Cell Application", *Journal of Power Sources*, Vol. 159, pp. 1283-1290.

Kesim, B., 2016, *An Experimental Study on Optimization of Pt-based Trimetallic WGS Catalysts*, M. S. Thesis, Boğaziçi University.

Kolb, G., 2008, *Fuel Processing for Fuel Cells*, Wiley, Weinheim, Germany.

Kolb, G., T. Baier, J. Schürer, D. Tiemann, A. Ziogas, H. Ehwald and P. Alphonse, 2008a, "A Microstructured 5 kW Complete Fuel Processor for Isooctane as Hydrogen Supply System for Mobile Auxiliary Power Units Part I. Development of Autothermal

Reforming Catalyst and Reactor", *Chemical Engineering Journal,* Vol. 137, pp. 653-663.

Kolb, G., T. Baier, J. Schürer, D. Tiemann, A. Ziogas, S. Specchia, C. Galletti, G. Germani and Y. Schuurman, 2008b, "A Microstructured 5 kW Complete Fuel Processor for Isooctane as Hydrogen Supply System for Mobile Auxiliary Power Units Part II. Development of Water Gas Shift and Preferential Oxidation Catalysts Reactors and Assembly of the Fuel Processor", *Chemical Engineering Journal,* Vol. 138, pp. 474-489.

Lee, I. C. and D. Chu, 2003, *Literature Review of Fuel Processing*, Army Research Laboratory.

Lee, D., H. C. Lee, K. H. Lee and S. Kim, 2007, "A Compact and Highly Efficient Natural Gas Fuel Processor for 1-kW Residential Polymer Electrolyte Membrane Fuel Cells", *Journal of Power Sources*, Vol. 165, pp. 337-341.

Lee, H., Y. Lim, N. Park and Y. Kim, 2009, "Catalytic Autothermal Reforming of Propane over the Noble Metal-doped Hydrotalcite-type Catalysts", *Chemical Engineering Journal*, Vol. 146, pp. 295-301.

Lee, T. S., J. N. Chung and Y. Chen, 2011, "Design and Optimization of a Combined Fuel Reforming and Solid Oxide Fuel Cell System with Anode Off-gas Recycling", *Energy Conversion and Management*, Vol. 52, pp. 3214-3226.

Li, F., H. Yi, X. Tang, P. Ning and Q. Yu, 2009, "Adsorption of Carbon Dioxide on Coconut Shell Activated Carbon"*, College of Environmental Science and Engineering Kunming University of Science and Technology*.

Li, J., J. Chen, W. Song, J. Liu and W. Shen, 2008, "Influence of Zirconia Crystal Phase on the Catalytic Performance of Au/ZrO_2 Catalysts for Low Temperature Water Gas Shift Reaction", *Applied Catalysis A: General*, Vol. 334, pp. 321-329.

Li, J., Y. Ma, M. C. McCarthy, J. Sculley, J. Yu, H. Jeong, P. B. Balbuena and H. Zhou, 2011, "Carbon Dioxide Capture-related Gas Adsorption and Separation in Metal-organic Frameworks", *Coordination Chemistry Reviews*, Vol. 255, pp. 1791-1823.

Lim, S., H. Lee, D. Moon, J. Kim, N. Park, J. Shin and Y. Kim, 2009, "Autothermal Reforming of Propane over Ce Modified Ni/$LaAlO_3$ Perovskite Type Catalysts", *Chemical Engineering Journal*, Vol. 152, pp. 220-226.

Lin, S. T., Y. H. Chen, C. C. Yu, Y. C. Liu and C. H. Lee, 2005, "Modeling an Experimental Methane Fuel Processor", *Journal of Power Sources*, Vol. 148, pp. 43-53.

Lin, S. T., Y. H. Chen, C. C. Yu, Y. C. Liu and C.H. Lee, 2006, "Dynamic Modeling and Control Structure Design of an Experimental Fuel Processor", *International Journal of Hydrogen Energy*, Vol. 31, pp. 413-426.

Luengnaruemitchai, A., S. Osuwan and E. Gulari, 2003, "Comparative Studies of Low Temperature Water Gas Shift Reaction over Pt/CeO_2, Au/CeO_2, and Au/Fe_2O_3 Catalysts", *Catalysis Communications*, Vol. 4, pp. 215-221.

Ma, L., 1995, *Hydrogen Production from Steam Reforming of Light Hydrocarbons in an Autothermic System*, Ph. D. Dissertation, University of New South Wales.

Maillet, T., J. Barbier Jr. and D. Duprez, 1996, "Reactivity of Steam in Exhaust Gas Catalysis. III. Steam and Oxygen/steam Conversions of Propane on a Pd/Al_2O_3 Catalyst", *Applied Catalysis B: Environmental*, Vol. 9, pp. 251-266.

Malaibari, Z. O., E. Croiset, A. Amin and W. Epling, 2015, "Effect of Interactions between Ni and Mo on Catalytic Properties of a Bimetallic Ni-Mo/Al_2O_3 Propane Reforming Catalyst", *Applied Catalysis A: General*, Vol. 490, pp. 80-92.

Mekhilef, S., R. Saidur and A. Safari, 2012, "Comparative Study of Different Fuel Cell Technologies", *Renewable and Sustainable Energy Reviews*, Vol. 16, pp. 981-989.

Mishra, A. and R. Prasad, 2011, "A Review on Preferential Oxidation of Carbon Monoxide in Hydrogen Rich Gases", *Bulletin of Chemical Reaction Engineering and Catalysis*, Vol. 6, No. 1, pp. 1-14.

Momirlan, M. and T. N. Veziroğlu, 2005, "The Properties of Hydrogen as a Fuel Tomorrow in Sustainable Energy System for a Cleaner Planet", *International Journal of Hydrogen Energy*, Vol. 30, pp. 795-802.

Nielsen, A., 1995, *Ammonia: Catalysis and Manufacture*, Springer, Berlin, Germany.

Ning, P., F. Li, H. Yi, X. Tang, J. Peng, Y. Li, D. He and H. Deng, 2012, "Adsorption Equilibrium of Methane and Carbon Dioxide on Microwave-activated Carbon", *Separation and Purification Technology,* Vol. 98, pp. 321-326.

Özer, Ö., 2016, *Design and Development of Pt-based Trimetallic WGS Catalysts*, M. S. Thesis, Boğaziçi University.

Özkara, Ş. and A. E. Aksoylu, 2003, "Selective Low Temperature Carbon Monoxide Oxidation in H_2-rich Gas Streams over Activated Carbon Supported Catalysts", *Applied Catalysis A: General*, Vol. 251, pp. 75-83.

Papadias, D., S. H. D. Lee and D. J. Chmielewski, 2006, "Autothermal Reforming of Gasoline for Fuel Cell Applications: A Transient Reactor Model", *Industrial and Engineering Chemistry Research,* Vol. 45, pp. 5841-5858.

Panagiotopoulou, P. and D. I. Kondarides, 2007, "A Comparative Study of the Water Gas Shift Activity of Pt Catalysts Supported on Single (MO_x) and Composite (MO_x/Al_2O_3, MO_x/TiO_2) Metal Oxide Carriers", *Catalysis Today*, Vol. 127, pp. 319-329.

Pastor-Perez, L., R. Buitrago-Sierra, A. Sepulveda-Escribano, 2014, "CeO_2-promoted Ni/Activated Carbon Catalysts for the Water Gas Shift (WGS) Reaction", *International Journal of Hydrogen Energy*, Vol. 39, pp. 17589-17599.

Pino, L., A. Vita, F. Cipiti, M. Lagana and V. Recupero, 2006, "Performance of Pt/CeO_2 Catalyst for Propane Oxidative Steam Reforming", *Applied Catalysis A: General*, Vol. 306, pp. 68-77.

Pino, L., A. Vita, F. Cipiti, M. Lagana and V. Recupero, 2008, "Catalytic Performance of $Ce_{1-x}Ni_xO_2$ Catalysts for Propane Oxidative Steam Reforming", *Catalysis Letters*, Vol.122, pp. 121-130.

Pires, J., M. Bestilleiro, M. Pinto and A. Gil, 2008, "Selective Adsorption of Carbon Dioxide, Methane and Ethane by Porous Clays Heterostructures", *Separation and Purification Technology*, Vol. 61, pp. 161-167.

Przepiorski, J., M. Skrodzewicz and A. W. Morawski, 2004, "High Temperature Ammonia Treatment of Activated Carbon for Enhancement of CO_2 Adsorption", *Applied Surface Science*, Vol. 225, No. 1-4, pp. 235-242.

Radhakrishnan, R., R. R. Willigan, Z. Dardas and T. H. Vanderspurt, 2006, "Water Gas Shift Activity and Kinetics of Pt/Re Catalysts Supported on Ceria-zirconia Oxides", *Applied Catalysis B: Environmental*, Vol. 66, pp. 23-28.

Ramaswamy, S., M. Sundaresan, A. Eggert and R.M. Moore, 2000, "System Dynamics and Efficiency of the Fuel Processor for an Indirect Methanol Fuel Cell Vehicle", *Proceedings of the 35th Intersociety Energy Conversion Engineering Conference*, American Institute of Aeronautics and Astronautics, Vol. 2, pp.1372-1377.

Recupero, V., L. Pino, A. Vita, F. Cipiti, M. Cordaro and M. Lagana, 2005, "Development of a LPG Fuel Processor for PEFC Systems: Laboratory Scale Evaluation of Autothermal Reforming and Preferential Oxidation Subunits", *International Journal of Hydrogen Energy,* Vol. 30, pp. 963-971.

Reddy, G. K. and P. Smirniotis, 2015, *Water Gas Shift Reaction: Research Developments and Applications*, Elsevier, China.

Reuse, P., A. Renken, K. Haas-Santo, O. Görke and K. Schubert, 2004, "Hydrogen Production for Fuel Cell Application in an Autothermal Microchannel Reactor", *Chemical Engineering Journal*, Vol. 101, pp 133-141.

Sa, J., 2015, *Fuel Production with Heterogeneous Catalysis*, CRC Press, Florida.

Sammes, N., 2006, *Fuel Cell Technology: Reaching towards Commercialization*, Springer, Germany.

Sato, Y., K. Terada, S. Hasegawa, T. Miyao and S. Naito, 2005, "Mechanistic Study of Water Gas Shift Reaction over TiO_2 Supported Pt-Re and Pd-Re Catalysts", *Applied Catalysis A: General*, Vol. 296, pp. 80-89.

Sato, Y., Y. Soma, T. Miyao and S. Naito, 2006, "The Water Gas Shift Reaction over Ir/TiO_2 and Ir-Re/TiO_2 Catalysts", *Applied Catalysis A: General*, Vol. 304, pp. 78-85.

Schadel, B. T., M. Duisberg and O. Deutschmann, 2009, "Steam Reforming of Methane, Ethane, Propane, Butane, and Natural Gas over a Rhodium-based Catalyst", *Catalysis Today*, Vol. 142, pp. 42-51.

Shaarani, F. W. and B. H. Hameed, 2011, "Ammonia-modified Activated Carbon for the Adsorption of 2,4-dichlorophenol", *Chemical Engineering Journal*, Vol. 169, pp. 180-185.

Shafeeyan, M. S., W. M. A. W. Daud, A. Houshmand and A. Shamiri, "A Review on Surface Modification of Activated Carbon for Carbon Dioxide Adsorption", 2010, *Journal of Analytical and Applied Pyrolysis*, Vol. 89, pp. 143-151.

Shafeeyan, M. S., W. M. A. W. Daud, A. Shamiri and N. Aghamohammadi, 2015, "Adsorption Equilibrium of Carbon Dioxide on Ammonia-modified Activated Carbon", *Chemical Enginnering Research and Design*, Vol. 104, pp. 42-52.

Shekhawat, D., J. J. Spivey and D. A. Berry, 2011, *Fuel Cells: Technologies for Fuel Processing*, Elsevier, Spain.

Shen, C., C. A. Grande, P. Li, J. Yu and A. E. Rodrigues, 2010, "Adsorption Equilibria and Kinetics of CO_2 and N_2 on Activated Carbon Beads", *Chemical Engineering Journal,* Vol. 160, pp. 398-407.

Siddle, A., K. D. Pointon, R. W. Judd and S. L. Jones, 2003, *Fuel Processing for Fuel Cells: A Status Review and Assessment of Prospects*, Advantica Ltd., Crown Press, Loughborough, United Kingdom.

Sommer, M., A. Lamm, A. Docter and D. Agar, 2004, "Modeling and Dynamic Simulation of a Fuel Cell System with an Autothermal Gasoline Reformer", *Journal of Power Sources*, Vol. 127, pp. 313-318.

Sopena, D., A. Melgar, Y. Briceno, R. M. Navarro, M. C. Alvarez-Galvan and F. Rosa, 2007, "Diesel Fuel Processor for Hydrogen Production for 5 kW Fuel Cell Application", *International Journal of Hydrogen Energy*, Vol. 32, pp. 1429-1436.

Specchia, S., 2011, "Hydrocarbons Valorisation to Cleaner Fuels: H_2-rich Gas Production via Fuel Processors", *Catalysis Today*, Vol. 176, pp. 191-196.

Şimşek, E., Ş. Özkara, A. E. Aksoylu and Z. I. Önsan, 2007, "Preferential CO Oxidation over Activated Carbon Supported Catalysts in H_2-rich Gas Streams Containing CO_2 and H_2O", *Applied Catalysis A: General*, Vol. 316, pp. 169-174.

Tabakova, T., F. Boccuzzi, M. Manzoli, J. W. Sobczak, V. Idakiev and D. Andreeva, 2004, "Effect of Synthesis Procedure on the Low Temperature WGS Activity of Au/ceria Catalysts", *Applied Catalysis B: Environmental*, Vol. 49, pp. 73-81.

Tang, Y., W. Yuan, M. Pan, Z. Li, G. Chen and Y. Li, 2010, "Experimental Investigation of Dynamic Performance and Transient Responses of a kW Class PEM Fuel Cell Stack under Various Load Changes", *Applied Energy*, Vol. 87, pp. 1410-1417.

Vadlamudi, V. K. and S. Palanki, 2011, "Modeling and Analysis of Miniaturized Methanol Reformer for Fuel Cell Powered Mobile Applications", *International Journal of Hydrogen Energy*, Vol. 36, No. 5, pp. 3364-3370.

Vaduva, M. and V. Stanciu, 2007, "Selective Carbon Dioxide Adsorption from N_2-CH_4-CO_2 Mixture on Carbon Molecular Sieves", *University Politehnica of Bucharest Scientific Bulletin Series B*, Vol. 67, No. 4, pp. 59-70.

Vanston, J. and H. Elliott, 2003, *Fuel Cells: A Technology Forecast*, Texas State Technical College, Texas.

Vita, A., L. Pino, F. Cipiti, M. Lagana and V. Recupero, 2010, "Structured Reactors as Alternative to Pellets Catalyst for Propane Oxidative Steam Reforming", *International Journal of Hydrogen Energy*, Vol. 35, No. 18, pp. 9810-9817.

Yong, Z., V. Mata and A. E. Rodrigues, 2002, "Adsorption of Carbon Dioxide at High Temperature - A Review", *Separation and Purification Technology,* Vol. 26, pp. 195-205.

Yoon, S. and J. Bae, 2010, "A Diesel Fuel Processor for Stable Operation of Solid Oxide Fuel Cells System: I. Introduction to Post-reforming for the Diesel Fuel Processor", *Catalysis Today*, Vol. 156, No. 1-2, pp. 49-57.

Yu, Q., W. Chen, Y. Li, M. Jin and Z. Suo, 2010, "The Action of Pt in Bimetallic Au-Pt/CeO_2 Catalyst for Water Gas Shift Reaction", *Catalysis Today*, Vol. 158, No. 3-4, pp. 324-328.

Wang, X., N. Wang, J. Zhao and L. Wang, 2010, "Thermodynamic Analysis of Propane Dry and Steam Reforming for Synthesis Gas or Hydrogen Production", *International Journal of Hydrogen Energy*, Vol. 35, pp. 12800-12807.

Wang, X., N. Wang and L. Wang, 2011, "Hydrogen Production by Sorption Enhanced Steam Reforming of Propane: A Thermodynamic Investigation", *International Journal of Hydrogen Energy*, Vol. 36, pp. 466-472.

Zhang, L., X. Wang, B. Tan and U. S. Özkan, 2009, "Effect of Preparation Method on Structural Characteristics and Propane Steam Reforming Performance of Ni-Al_2O_3 Catalysts", *Journal of Molecular Catalysis A: Chemical*, Vol. 297, pp. 26-34.

Zhang, Z., M. Xu, H. Wang and Z. Li, 2010, "Enhancement of CO_2 Adsorption on High Surface Area Activated Carbon Modified by N_2, H_2 and Ammonia", *Chemical Engineering Journal*, Vol. 160, pp. 571-577.

Zhao, Z., X. Cui, J. Ma and R. Li, 2007, "Adsorption of Carbon Dioxide on Alkali-Modified Zeolite 13X Adsorbents", *International of Greenhouse Gas Control*, Vol.1, pp. 355-359.

APPENDIX A: EXPERIMENTAL CONDITIONS USED IN THE FORMER STUDIES AND MODELING CALCULATIONS

Experimental conditions used in the OSR kinetic experiments (Gökaliler *et al*., 2012) over 0.2wt.%Pt-10wt.%Ni/δ-Al_2O_3 catalyst and modeling calculations are listed in Table A.1. 17 pairs of experiments were performed at 673 K with 10 and 15 mg catalyst each (denoted as Run a, Run b; respectively) for a constant total flow rate of 202 ml/min at atmospheric pressure.

Table A.1. Experimental conditions used in the OSR kinetic experiments (Gökaliler *et al*., 2012) and modeling calculations.

	Flow rate in the feed stream (ml/min)			
Exp.#	**C_3H_8**	**O_2**	**H_2O**	**He**
1	10.1	10.3	92.3	89.4
2	11.1	10.3	92.3	88.4
3	12.2	10.3	92.3	87.3
4	13.1	10.3	92.3	86.4
5	14.1	10.3	92.3	85.4
6	15.2	10.3	92.3	84.4
7	13.1	7.3	92.3	89.4
8	13.1	8.1	92.3	88.6
9	13.1	9.1	92.3	87.6
10	13.1	11.1	92.3	85.5
11	13.1	12.1	92.3	84.5
12	13.1	12.6	92.3	84.0
13	13.1	11.1	95.0	82.8
14	13.1	11.1	101.0	76.8
15	13.1	11.1	107.1	70.7
16	13.1	11.1	113.2	64.7
17	13.1	11.1	121.3	56.6

Experimental conditions used in the WGS kinetic experiments (Gökaliler *et al*., 2013) over 1wt.%Au-0.5wt.%Re/CeO_2 catalyst and modeling calculations are listed in Table A.2. 12 pairs of experiments were performed at 573 K with 10 and 15 mg catalyst each (denoted as Run a, Run b; respectively) for a constant total flow rate of 150 ml/min at atmospheric pressure.

Table A.2. Experimental conditions used in the WGS kinetic experiments (Gökaliler *et al*., 2013) and modeling calculations.

	Percentage in the feed stream (%)				
Exp.#	**CO**	**H_2O**	**CO_2**	**H_2**	**He**
1	10	35	10	20	25
2	7.5	35	10	20	27.5
3	5	35	10	20	30
4	10	32	10	20	28
5	10	29	10	20	31
6	10	38	10	20	22
7	10	35	12	20	23
8	10	35	14	20	21
9	10	35	8	20	27
10	10	35	10	24	21
11	10	35	10	22	23
12	10	35	10	16	29

Experimental conditions used in the WGS performance experiments (Çağlayan *et al*., 2011b) over 1wt.%Au-0.5wt.%Re/CeO_2 catalyst and modeling calculations are listed in Table A.3. 14 experiments were performed at different reaction temperatures with 75 mg catalyst for a constant total flow rate of 150 ml/min at atmospheric pressure for different ideal feed conditions.

Table A.3. Experimental conditions used in the WGS performance experiments (Çağlayan *et al*., 2011b) and modeling calculations.

			Percentage in the feed stream (%)		
Exp. #	**Temperature (K)**	**S/C**	**CO**	**H_2O**	**N_2**
1	523	1	3	3	94
2	573	1	3	3	94
3	623	1	3	3	94
4	673	1	3	3	94
5	473	2	3	6	91
6	523	2	3	6	91
7	573	2	3	6	91
8	623	2	3	6	91
9	523	5	3	15	82
10	573	5	3	15	82
11	623	5	3	15	82
12	673	5	3	15	82
13	723	5	3	15	82
14	773	5	3	15	82

Experimental conditions used in the PROX kinetic experiments (Eropak and Aksoylu, 2016) over 1wt.%Pt-0.25wt.%Sn/AC3 catalyst and modeling calculations are listed in Table A.4. 8 pairs of experiments were performed at 383 K with 15 and 20 mg catalyst each (denoted as Run a, Run b; respectively) for a constant total flow rate of 100 ml/min at atmospheric pressure.

Table A.4. Experimental conditions used in the PROX kinetic experiments (Eropak and Aksoylu, 2016) and modeling calculations.

	Percentage in the feed stream (%)						
Exp. #	**CO**	**O_2**	**H_2O**	**CO_2**	**CH_4**	**H_2**	**He**
1	1	1	10	15	3	60	10.00
2	1	1.25	10	15	3	60	9.75
3	1	1.5	10	15	3	60	9.50
4	1.2	1.5	10	15	3	60	9.30
5	1.25	1.25	10	15	3	60	9.50
6	2	1	10	15	3	60	9.00
7	2	1.5	10	15	3	60	8.50
8	2.5	1.25	10	15	3	60	8.25

Experimental conditions used in the PROX performance experiments (Çağlayan *et al*., 2011b) over 1wt.%Pt-0.25wt.%Sn/AC3 catalyst and modeling calculations are listed in Table A.5. 32 experiments were performed at different reaction temperatures with 250 mg catalyst for a constant total flow rate of 100 ml/min at atmospheric pressure.

Table A.5. Experimental conditions used in the PROX performance experiments (Çağlayan *et al*., 2011b) and modeling calculations.

		Flow rate in the feed stream (ml/min)						
Set #	**Exp. #**	**CO**	**O_2**	**H_2**	**He**	**CH_4**	**H_2O**	**CO_2**
I	**1**	1	1	60	38	0	0	0
	2	1	1	60	38	0	0	0
	3	1	1	60	38	0	0	0
	4	1	1	60	38	0	0	0
	5	1	1.25	60	37.75	0	0	0
	6	1	1.25	60	37.75	0	0	0
	7	1	1.25	60	37.75	0	0	0
	8	1	1.25	60	37.75	0	0	0
II	**1**	1	1	60	14	0	10	15
	2	1	1	60	14	0	10	15
	3	1	1	60	14	0	10	15
	4	1	1	60	14	0	10	15
	5	1	1.25	60	13.75	0	10	15
	6	1	1.25	60	13.75	0	10	15
	7	1	1.25	60	13.75	0	10	15
	8	1	1.25	60	13.75	0	10	15
III	**1**	1	1	60	36	3	0	0
	2	1	1	60	36	3	0	0
	3	1	1	60	36	3	0	0
	4	1	1	60	36	3	0	0
	5	1	1.25	60	35.75	3	0	0
	6	1	1.25	60	35.75	3	0	0
	7	1	1.25	60	35.75	3	0	0
	8	1	1.25	60	35.75	3	0	0
IV	**1**	1	1	60	11	3	10	15
	2	1	1	60	11	3	10	15
	3	1	1	60	11	3	10	15
	4	1	1	60	11	3	10	15
	5	1	1.25	60	10.75	3	10	15
	6	1	1.25	60	10.75	3	10	15
	7	1	1.25	60	10.75	3	10	15
	8	1	1.25	60	10.75	3	10	15